PHOTOPHYSICAL PROPERTIES AND REACTIVITY STUDIES OF PHOSPHINE-BORANE DONOR-ACCEPTOR COMPOUNDS

by

Yufei Li

A thesis submitted to the Department of Chemistry

In conformity with the requirements for

the degree of Doctor of Philosophy

Queen's University

Kingston, Ontario, Canada

(September, 2015)

Abstract

This thesis describes the preparation of several phosphine-borane species containing bulky aryl groups on the heteroatoms for steric protection. Depending on the system, they either exhibit interesting photophysical properties, unusual reactivity, or both, based on the environment around the heteroatoms as well as the linking unit connecting them.

A highly congested P-B donor-acceptor compound with a 1,8-naphthalene backbone has been synthesized. Despite the high degree of steric congestion, this molecule was found to possess a P-B dative bond which persistents in solution. The new P-B molecule is thermally and photochemically inert, displaying no reactivity toward some common small molecules with the exception of halogens. The high stability of the molecule is attributed to the crowded environment around P and B, as well as the highly rigid 1,8-naphthyl linker. The reaction of this new P-B molecule with halogens in the presence of water leads to the formation of a P-O-B compound.

An unbound U-shaped new phosphine-borane compound has been synthesized and displays distinct through-space CT transition and intense dual emission. The use of this new P-B compound in turn-on/switchable fluorescent sensing of fluoride has been demonstrated. The P-B compound was found to have a ratiometric response toward fluoride ions greater than that of the related N-B compounds.

Converting the unbound U-shaped donor-acceptor compound to its phosphonium salt greatly enhanced its fluoride binding affinity at the boron center by 2 orders of magnitude. Furthermore, despite the significant steric congestion present in the phosphine-borane species, it behaved as an effective ligand towards metal ions such as Au(I) and Pt(II) yielding their respective coordination complexes. In the case of the Pt(II) complex, it displayed interesting “turn-on” fluorescent to fluoride addition.

Finally, the cationic phosphonium-borane compound was found capable of effectively tearing apart an NHC molecule, yielding a vinyl-amine bridged P-B species. In addition to IMe which plays a key role in its self-destruction, a FLP-like ylide-borane and $IMeH^+$ salt have been identified as key species involved in this transformation. The balance of Lewis acidity/basicity and the cooperativity among the phosphonium/ylide, IMe, and borane appear to all be critical in this unprecedented fragmentation.

Acknowledgements

First of all, I would like to thank my supervisor Prof. Suning Wang for granting me the opportunity to work in her lab, as well as for providing plenty of support during my stay in Canada and studies at Queen's University. Her patient guidance, invaluable advice, and heart-warming encouragement have accompanied me for the past four years and will always be remembered.

Further, it has been a pleasure to work with all the excellent scientists in the Chemistry Department at Queen's University. In particular, I would like to thank my committee members Prof. Anne Petitjean and Prof. Gang Wu for their valuable suggestions and knowledge. I also want to show my appreciation to Dr. Ruiyao Wang and Dr. Gabriele Schatte for their help with X-ray Crystallographic analyses, Dr. Jiaxi Wang for his help with Mass Spectrometric analyses, and Dr. Françoise Sauriol for her help with NMR spectroscopic analyses.

I am also thankful for the wonderful and enjoyable time spent working with many talented chemists who were part of Prof. Wang's group. First, I would like to express my gratitude to Prof. Young-Jin Kang who provided me generous and patient guidance when I first came to this lab. Also, I sincerely appreciate the friendship, suggestions, and encouragement from all of the past and present group members I spent the last four years working alongside.

Lastly, I want to thank my family; my father and mother who have always been caring and supportive even though they are far away in China. I would also like to thank my husband Yu Wang who has been fully supportive and understanding throughout all the good and bad times. I love you all with my true heart.

Statement of Originality

I hereby certify that all of the work described within this thesis is the original work of the author carried out under the guidance and supervision of Prof. Suning Wang with the following exceptions:

Chapter 2: The dynamic NMR study of compound **2.1** was carried out by Dr. Françoise Sauriol. The DFT and TD-DFT calculations for compounds **2.1** and **2.2** were performed by Dr. Soo-Byung Ko and Dr. Yingli Rao.

Chapter 3: The synthesis of compound **3.1** was carried out with the help of Prof. Youngjin Kang. The calculation of fluoride binding constant of compound **3.1** was carried out by Dr. Ian Wyman. The DFT and TD-DFT calculations for compound **3.1** performed by Dr. Soo-Byung Ko.

Chapter 4: X-ray structure of compound **4.2** was solved by Dr. Jiasheng Lu. The calculation of fluoride binding constant of compound **4.1** and **4.3** was carried out by Dr. Ian Wyman. The DFT and TD-DFT calculations for compound **4.1**, **4.2** and **4.3** were performed by Dr. Soo-Byung Ko.

Chapter 5: *N,N'*-dimethylimidazol-2-ylidene (IMe) was synthesized by Dr. Yingli Rao. The DFT calculations for all compounds included in this chapter were performed by Soren K. Mellerup. The NMR analysis of compound **5.1** was carried out by Dr. Françoise Sauriol. X-ray structure of compound **5.2** was solved by Gabriele Schatte.

Any published (or unpublished) ideas and/or techniques from the work of others are fully acknowledged in accordance with the standard referencing practices.

(Yufei Li)

(September, 2015)

Table of Contents

List of Figures

List of Tables

List of Abbreviations

°	Degrees
δ	chemical shift
Δ	Delta, difference
ε	molar extinction coefficient
π	pi
σ	sigma
λ	lambda, wavelength
λ_{max}	absorption/emission maximum
λ_{em}	emission wavelength
λ_{ex}	excitation wavelength
μL	microliters, 10^{-6} L
Φ	quantum efficiency
6-31G(d)	type of basis set
Å	angstrom, 10^{-10} m
A	absorbance; acid
Anal	analytical
Ar	aromatic
atm	atmospheres
B	base
B3LYP	a type of DFT exchange-correlational functional
B3PW91	a type of DFT exchange-correlational functional
br	broad
C	Celsius
Calcd.	calculated

CD_2Cl_2	deuterated dichloromethane
C_6D_6	deuterated benzene
COSY	correlation spectroscopy
CT	charge transfer
Cy	cyclohexyl
d	doublet
dd	doublet of doublets
DFT	density functional theory
DMF	dimethylformamide
DMSO	dimethylsulfoxide
equiv.	equivalent
et al.	*et alia* (and others)
etc.	*et cetera*
Et	ethyl, C_2H_5
Et_2O	diethyl ether
FLP	frustrated Lewis pair
g	grams
h	hour
Hz	Hertz
HMBC	heteronuclear multiple-bond correlation spectroscopy
HOMO	highest occupied molecular orbital
HRMS	high resolution mass spectrometry
HSQC	heteronuclear single-quantum correlation spectroscopy
in vacuo	under vacuum
*i*Pr	isopropyl, $(CH_3)_2CH$
J	scalar coupling constant

K	Kelvin
kJ	kilojoules
kcal	kilocalories, 10^3 cal
LA	Lewis acid
LB	Lewis base
LC	ligand-centered
LMCT	ligand-to-metal charge transfer
LUMO	lowest unoccupied molecular orbital
m	meta
m	multiplet
M	mol/L
Me	methyl
Mes	mesityl, 2,3,6-$(CH_3)_3C_6H_2$
MHz	megahertz, 10^6 Hz
mg	milligram, 10^{-3} g
MLCT	metal-to-ligand charge-transfer
mL	millilitre, 10^{-3} L
mmol	millimol, 10^{-3} mol
mol	mol
Naph	naphthyl
NHC	*N*-heterocyclic carbene
NMR	Nuclear Magnetic Resonance
OLED	organic light-emitting diode
o	ortho
o-tol	*ortho*-tolyl, 2-$(CH_3)C_6H_4$
p	para

Ph	phenyl, C_6H_5
pH	measure of acidity and basicity (potential hydrogen)
ppm	parts per million, 10^{-6}
PR_3	tertiary phosphine
r.t.	room temperature, 25 °C
s	singlet
S_0	singlet ground state
S_n, (n>0)	n^{th} singlet excited state
SMe_2	dimethylsulfide, $S(CH_3)_2$
T	temperature; triplet
T_n (n > 0)	n^{th} triplet excited state
t	triplet
TBAF	tetrabutylammonium fluoride
TD-DFT	time-dependent density functional theory
THF	tetrahydrofuran, C_4H_8O
tol	toluene
*t*Bu	*tert*-butyl
q	quartet
UV	ultraviolet light
V	volume
Vis	visible

Chapter 1

Introduction

Triarylborane compounds have recently found broad applications in materials chemistry such as emitters in organic light emitting diodes (OLEDs),[1] highly selective sensors of small anions such as fluoride or cyanide,[2] and even as metal-free catalysts for small molecule activation as illustrated in the chemistry of "Frustrated Lewis Pairs" (FLPs).[3] This diverse range of functionality available to such systems is a direct result of the unique electronic, and structural features of the boron moiety. In its "natural" electronic configuration, the boron atom adopts sp^2-hybridization which results in three-fold coordination and trigonal planar geometry around boron. Further, this electronic configuration leaves an empty p_π orbital perpendicular to the trigonal plane (Figure 1.1a), indicating that the boron atom is inherently electron deficient (breaks the "octet" rule). It is this key contributing factor that allows triarylborane compounds to serve as excellent electron acceptors, which is the basis for the majority of their applications. Not surprisingly, this electron deficiency feature also causes triarylborane compounds to be reactive towards many nucleophiles such as oxygen, water, and small anions. For practical applications in material science, such vulnerable stability needs to be addressed. Conventionally, bulky groups such as mesityl or 2,4,6-triisopropylphenyl (Figure 1.1b) are introduced to the boron atom which greatly improves the kinetic stability of triarylborane compounds under air.

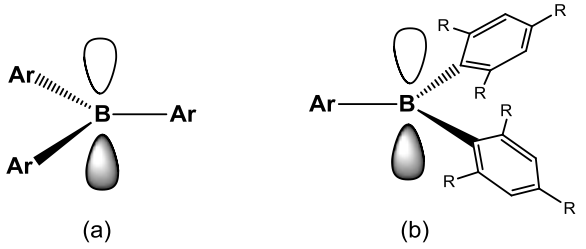

Figure 1.1. (a) Triarylborane compound; (b) Triarylborane compounds with bulky substituents.

This chapter will begin with a brief overview of basic luminescence principles. Next the introduction of Frustrated Lewis Pairs (FLPs) chemistry will be presented, followed by some examples of reactivity phosphine-triarylborane based FLPs. Applications of triarylborane systems as fluoride sensors will be shown later, especially mesityl substituted organoborane compounds. Lastly, the chemistry of N-heterocyclic carbene (NHC) degradation will be highlighted, particularly the work that is related to boron-containing systems.

1.1 Luminescence Principles

Luminescence is the emission of photons from a molecule in electronically excited states. Generally speaking, luminescence is classified into two different emission pathways - fluorescence and phosphorescence, where each refers to an electronic transition from different spin states. The electronic transitions available to chemical species are presented in Figure 1.2, where the various processes that determine a molecule's luminescent properties are outlined.[4] In the case of fluorescence, molecules are excited from the ground state to a singlet excited state ($S_0 \rightarrow S_1$, S_2, *etc*) meaning that the spin of the electron is not changed during the excitation. Normally, this process includes the internal conversion to reach the lowest singlet excited state (S_1). Non-radiative decay is a relaxation pathway whereby the various molecular vibration modes displace the excess energy as heat. The other pathway available is radiative relaxation which involves returning from the lowest singlet excited state to the ground state as shown Figure 1.2 ($S_1 \rightarrow S_0$). This transition is typically very fast with excited state lifetimes of $10^{-9} \sim 10^{-7}$ s. Conversely, during phosphorescence the spin multiplicity of a molecule changes following excitation as a result of intersystem crossing ($S \rightarrow T$). Radiative relaxation from the triplet excited state to the ground state is forbidden and, therefore, spin inversion must occur before the electron can relax to the ground state. The consequence of this is that $T_1 \rightarrow S_0$ is much slower than $S_1 \rightarrow S_0$, which is why excited state lifetimes for phosphorescence range from 10^{-6}s to seconds. Normally pure organic compounds do not display phosphorescence at room temperature because the $S_1 \rightarrow T_1$ process is spin-forbidden. However, the presence of a heavy metal center allows for spin-orbit coupling which induces the mixing of relevant

excited states. This ultimately allows for more efficient intersystem crossing and therefore a higher probability of phosphorescence occurring. Although the heavy atom effect allows phosphorescence to occur at room temperature, this effect is further enhanced in the solid state or by cooling to very low temperatures (*e.g.* 77 K), as radiationless decay pathways such as molecular vibration and energy transfer to solvent molecules through collisions is sufficiently minimized. Regardless of nature of the electronic transitions, not all of the energy gained *via* photon absorption is completely re-emitted as fluorescence or phosphorescence due to the involvement of the aforementioned non-radiative thermal decay pathways. This results in a loss of luminescence efficiency, which is generally described as the percentage of photons emitted *vs.* photons absorbed and simply known as luminescence quantum yield (Φ).

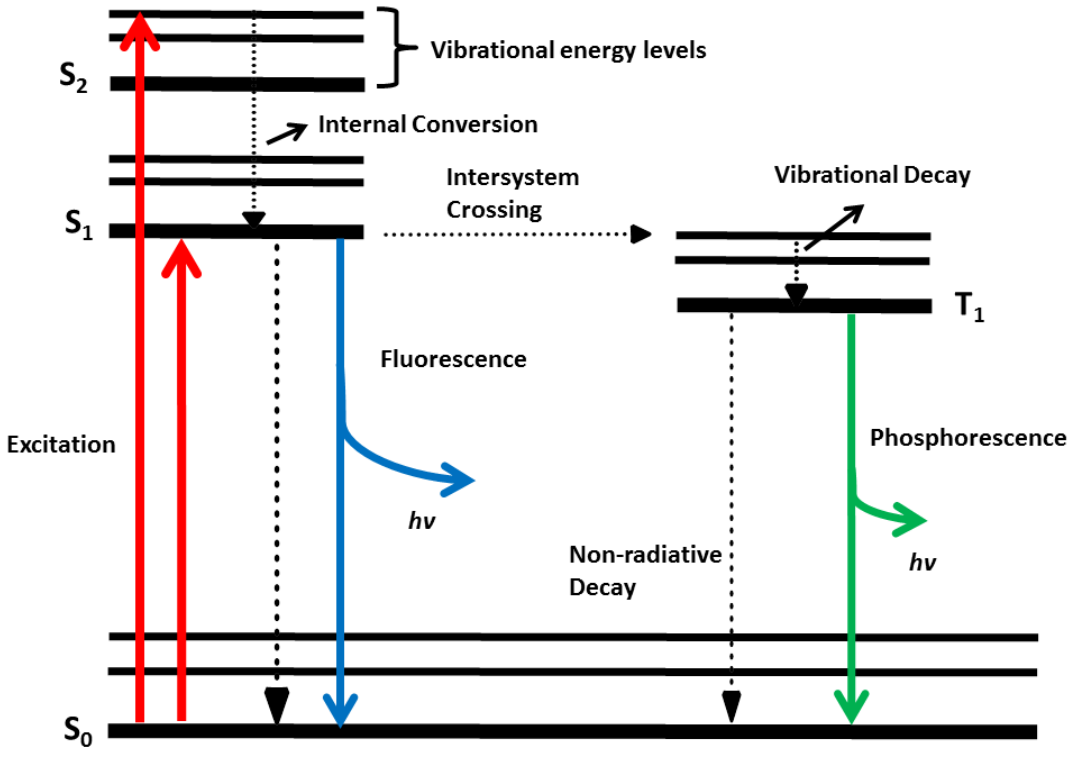

Figure 1.2. Jablonski diagram illustrating the processes involved in luminescence.

The luminescent properties of molecules vary depending on the orbitals involved in the electronic transition and their overall structural features. In the case of molecules bearing donor and acceptor groups,

intramolecular or through-space charge-transfer (CT) transitions from the highest occupied molecular orbital (HOMO) to the lowest unoccupied molecular orbital (LUMO) are most likely to occur. Following excitation, the electron density of the donor-acceptor system is redistributed which results in the CT transition. In solution, CT transitions are very sensitive to solvent polarity due to the large molecular dipole created as a result of the new electron density distribution. The consequence of this is that the S_1 excited state is stabilized with increasing solvent polarity which narrows the band gap of the molecular species and reduces the emission energy. Much more commonly observed transitions are known as π- π^*, in which an electron from the filled π orbital (HOMO) is promoted to a π antibonding orbital (LUMO). Due to the minimal change in the distribution of electron density following these transitions, they are relatively insensitive to external stimuli such as solvent polarity.

In transition-metal complexes, the possible electronic transitions are more complicated due to the participation of *d* orbitals. Depending on the frontier orbitals of the coordination complex, there are four possible electronic transitions. If the HOMO and LUMO are both from organic ligands, a molecule may exhibit ligand-centered (LC) emission. If the HOMO and LUMO both involve *d* orbitals of the transition-metal center, then the *d-d* transition is the lowest energy transition. However, this transition is non-emissive. The third situation is the ligand-to-metal charge-transfer (LMCT) transitions, which involve a HOMO and LUMO centered on the organic ligand and metal center, respectively. Should the two roles in the third case be reversed, the last possible transition is known as a metal-to-ligand charge-transfer (MLCT) transition.

1.2 Triarylborane Compounds in Frustrated Lewis Pairs

1.2.1 Introduction of FLPs

Since their inception in 1923 by Gilbert N. Lewis, the terms Lewis “acids” and “bases” have become ubiquitous in all fields of chemistry for describing the complementary electron accepting/donating nature

of chemical species and their mutual interactions.[5] With respect to a "classical" pair of Lewis acids and bases, their combination results in the formation of a single adduct comprised of the two initial components (Figure 1.3).

Figure 1.3. Normal Lewis acid and base reactivity.

The first observation of the behavior now commonly associated with FLPs was in 1942, when Herbert C. Brown *et al.* reported that bulky substituents on either the Lewis acid or the base could hinder their neutralization by not allowing the formation of a dative bond (Figure 1.4).[6] Although this example set the precedence for the trope of FLP chemistry, the potential applications did not get much attention until much later.

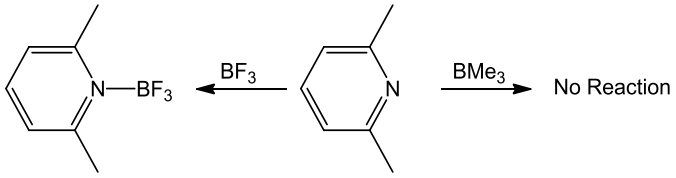

Figure 1.4. The distinct reactivity of lutidine with BMe_3 and BF_3.

More than 60 years following the initial report by Brown and co-workers, a new class of compounds was discovered and developed which contain sterically encumbered electron donors and acceptors (Lewis base and acid) within the same system. Due to steric effects, the Lewis base and acid cannot form a dative bond which results in an energetically strained system. As such, they are aptly named "Frustrated Lewis Pairs" (Figure 1.5). Such systems have been found to display new chemical reactivity such as the activation of small molecules and can even function as effective metal-free catalysts for chemical transformations.

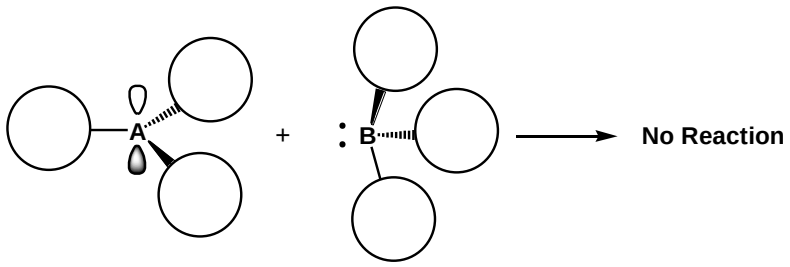

Figure 1.5. Frustrated Lewis Pairs.

Since the serendipitous discovery by Douglas Stephan *et al.* of a metal-free system capable of reversibly activating H_2 in 2006,[7] the field of FLPs chemistry has experienced an immense growth and expansion. In Stephan's first report, a phosphonium-borane compound $(C_6H_2Me_3)_2PH(C_6F_4)BH(C_6F_5)_2$ (**1.1**) was described to release hydrogen gas when heated to 150 °C, generating the phosphine-borane species **1.2** in the process (Figure 1.6). Remarkably, this phosphine-borane product was found to activate hydrogen gas in solution (THF) at room temperature, resulting in the reformation of the phosphonium-borane (**1.1**).

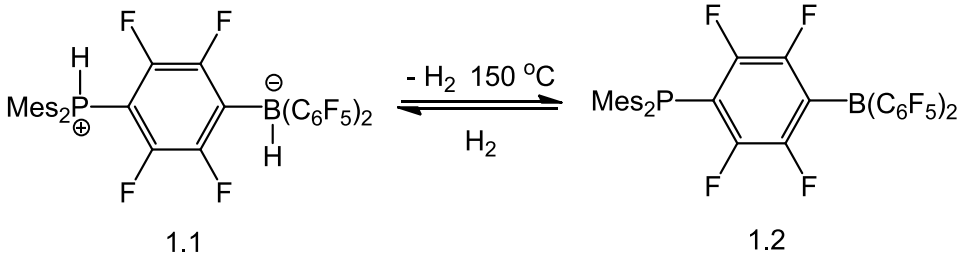

Figure 1.6. Reversible H_2 activation by **1.2**.

This unique discovery was the first example of a metal-free system capable of both releasing and capturing H_2, which has ultimately resulted in the birth and growth of the field known as FLP chemistry. In the following years, great research efforts were dedicated to the activation of several small molecules using FLP systems of both inter- and intramolecular variety. In 2007, Stephan's group examined simple combinations of individual phosphine and borane compounds.[8] From an NMR study of mixtures of R_3P (R=*t*Bu, $C_6H_2Me_3$) and $B(C_6F_5)_3$, no adduct formation was observed. Upon the introduction of 1 atm of H_2 to the samples, the phosphonium borate salts precipitated immediately (Figure 1.7). Different

combinations of Lewis acids and bases were also examined. The reaction of (tBu)$_3$P and BPh$_3$ in the presence of H$_2$ proceeded slowly, but did generate the expected phosphonium borate product. This decrease in reactivity is likely a result of the reduced Lewis acidity of the boron center compared to B(C$_6$F$_5$)$_3$. Interestingly, the combinations of (C$_6$H$_2$Me$_3$)$_3$P and BPh$_3$, (C$_6$F$_5$)$_3$P and B(C$_6$F$_5$)$_3$, or (tBu)$_3$P and B(C$_6$H$_2$Me$_3$)$_3$ did not react in the presence of H$_2$. Further, Ph$_3$P and Me$_3$P were found to readily form the classic Lewis acid-base adduct with B(C$_6$F$_5$)$_3$. Based on these results, it is clear that both electronic and steric factors are important for H$_2$ activation by FLPs. In addition, this work also established that H$_2$ activation could be performed by intermolecular FLPs under similar conditions. Unfortunately, these systems do have several limitations, such as the meticulous consideration of Lewis acidity, basicity, and steric restrictions. Neglecting any of these aspects will lead to species which do not behave in the desired fashion, such as the reversible H$_2$ activation by the intramolecular FLPs discussed previously (Figure 1.6).

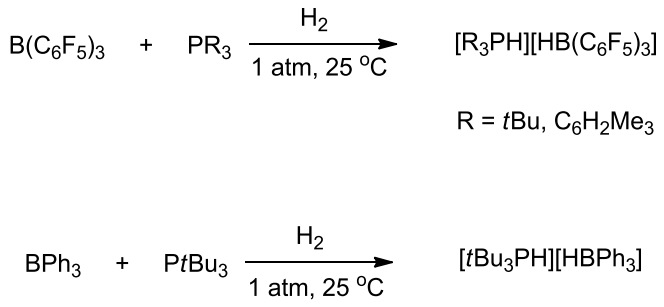

Figure 1.7. H$_2$ activation by intermolecular FLPs.

Following the preliminary work of Stephan and co-workers, an interesting ethylene bridged phosphine-borane system was synthesized and investigated by Gerhard Erker *et al.* for its reactivity with H$_2$.[9] The linked phosphine-borane compound (**1.3**) has a four-membered ring and exhibits a P-B interaction according to ^{11}B (δ 8.5 ppm) and ^{31}P NMR (δ 20.6 ppm) data. Although the crystal structure could not be obtained to confirm the proposed structure, DFT calculations suggested two isomeric open-forms (gauche and trans) which are likely responsible for the activation of H$_2$ at room temperature (Figure 1.8).

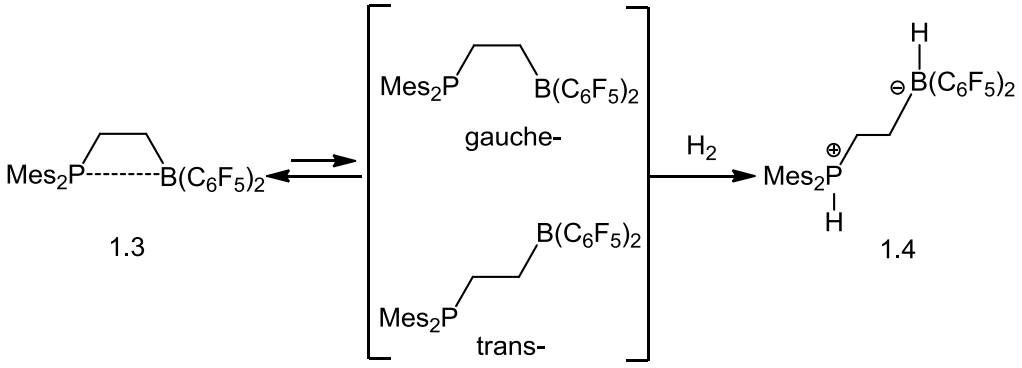

Figure 1.8. H_2 activation by **1.3**.

1.2.2 Metal-Free Hydrogenation by Phosphine-Borane Based FLPs

Due to the ever increasing number of FLPs that participate in the reversible uptake and release of H_2, many efforts have been put into developing these systems for catalytic hydrogenation of organic substrates which is the most promising application for such systems. In 2007, Stephan's group demonstrated the first example of such catalytic systems in the metal-free catalytic hydrogenation of imines which were obtained in high yields and under relatively mild reaction conditions.[10] The imines were reduced to the corresponding amines in toluene at temperatures ranging from 80-140 °C and 1-5 atm of H_2 in the presence of catalytic amounts phosphonium borate compounds. Initially, the imine is protonated by **1.1** resulting the formation of an iminium salt. Next, hydride transfer occurs from the hydridoborate to the iminium carbon, which results in a B-N intermediate. Release of the corresponding amine regenerates the active catalyst **1.2**, which is then free to perform subsequent hydrogenations following the uptake of 1 equiv. of H_2. The proposed catalytic cycle is shown in Figure 1.9.

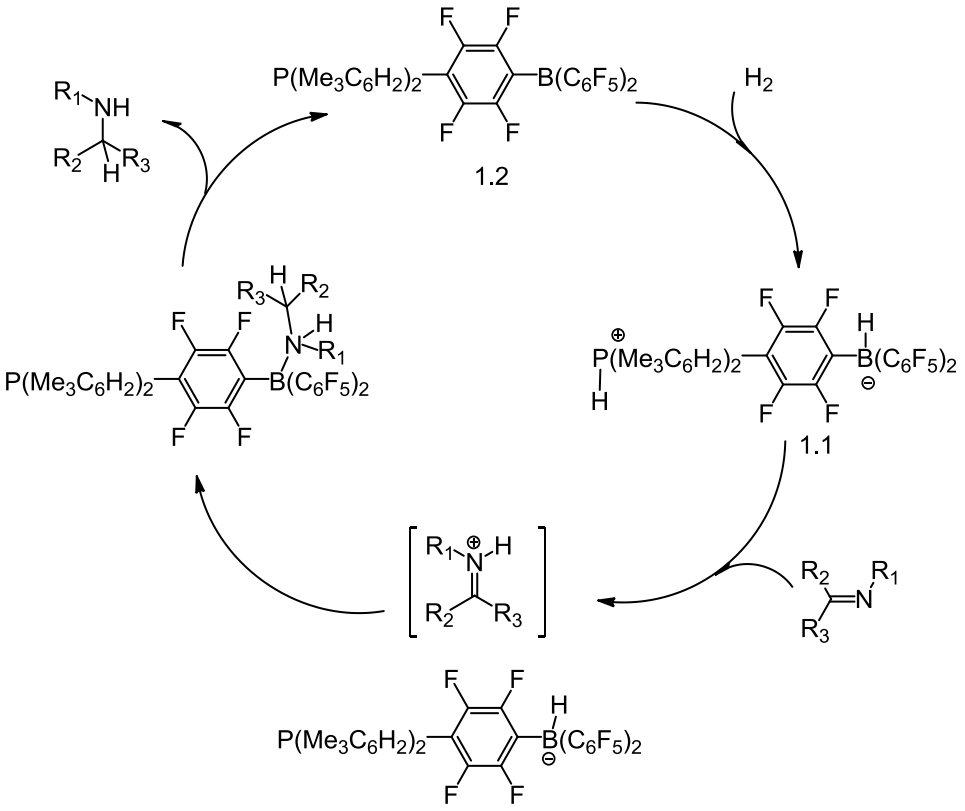

Figure 1.9. The proposed mechanism of a FLP as a catalyst for imine hydrogenation.

Similar experiments performed with the ethylene-linked phosphonium-borane **1.3** reported by Erker and co-workers revealed it to be a far superior catalyst for the hydrogenation of imines (Figure 1.10).[11] Hydrogenation of aldimines and ketamines were found to occur at ambient conditions rather than the elevated temperatures required with the use of **1.1** and **1.2** (80-140 °C). For example, **1.3**/**1.4** can rapidly hydrogenate aldimine at room temperature under 2.5 bar of H_2, albeit with a significant increase in catalyst loading (> 20 mol%).

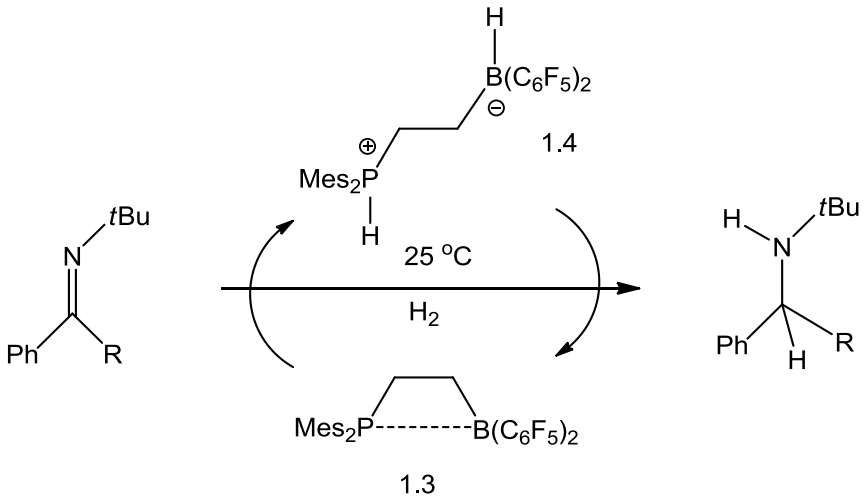

Figure 1.10. Catalytic hydrogenation of imines by **1.3**/**1.4**.

In an effort to develop a new catalyst system, Erker and co-workers designed a bis(diphenylphosphine)naphthalene (**1.5**) - $B(C_6F_5)_3$ FLP system which was shown to reversibly activate H_2.[12] The application of 2 bar H_2 to a toluene solution of **1.5** and $B(C_6F_5)_3$ (1:1) at room temperature resulted in an 80% yield of the desired phosphonium hydridoborate salt (**1.6**). Upon heating a solution of **1.6** to 60 °C, both compound **1.5** and $B(C_6F_5)_3$ were regenerated due to the release of hydrogen (Figure 1.11).

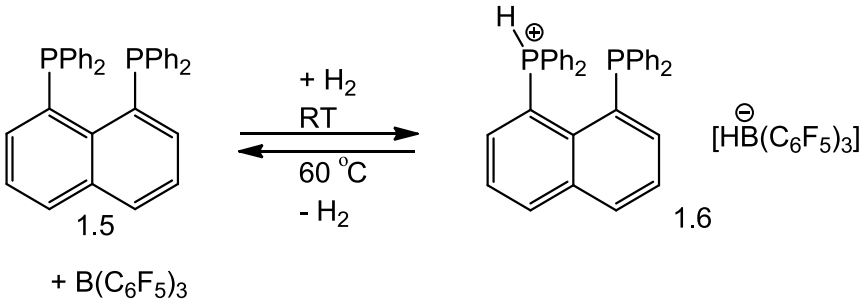

Figure 1.1. Hydrogen activation by diphosphine-borane FLP **1.5**.

Based on these promising results, Erker *et al.* proceeded to investigate the hydrogenation of silyl enol ethers with **1.5** + $B(C_6F_5)_3$/**1.6** as the catalyst (Figure 1.12). Indeed they were able to demonstrate that this

FLP system could be used as an active catalyst for most of the selected silyl enol ether substrates with good conversion efficiencies.

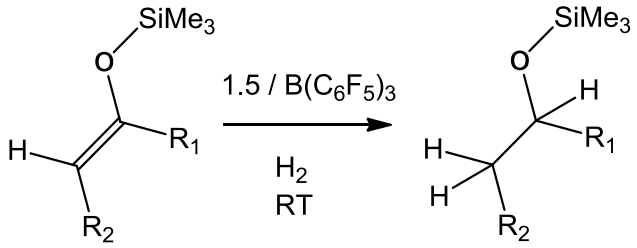

Figure 1.2. Hydrogenation of silyl enol ethers by FLP **1.5**/$B(C_6F_5)_3$.

1.2.3 Phosphine-Borane Based FLPs Reactions with Alkenes and Alkynes

The extraordinary behavior of the FLPs systems grants the possibility to use them in applications such as hydrogenation catalysis or even hydrogen storage materials due to their low cost of production and low environmental impact compared to heavy metal systems. In addition to the activation of H_2, the reactivity of FLPs has been extended to a variety of other substrates such alkenes, alkynes and other small molecules. For example, Stephan and co-workers found that $HB(C_6F_5)_2{\cdot}PR_3$ (R = *t*Bu, or Ph) reacts with 1,4-pentadiene in toluene at room temperature over 2 days yielding a six-membered ring product which has a chair conformation with the PR_3 moiety at the equatorial position. The combination of $HB(C_6F_5)_2$ and tBu_3P can also react with 1,3-butadiene at 60 °C over 18.5 hours to give an analogous five-membered ring product where the tBu_3P substituent adopts a pseudoequatorial position (Figure 1.13).[13]

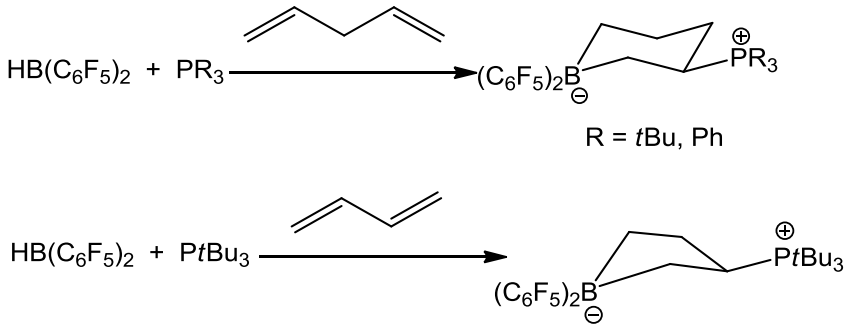

Figure 1.3. Diene addition/cyclization with FLPs.

Stephan group also investigated the reaction of alkynes with FLPs.[14] Depending on the basicity of the chosen phosphine, two competing pathways were established: either deprotonation of the terminal H atom on the alkyne or addition of both the borane and phosphine across the triple bond. Bulkier and more electron rich phosphines such as (tBu)$_3$P in the presence of B(C_6F_5)$_3$/phenyl acetylene yielded [tBu$_3$PH][PhCCB(C_6F_5)$_3$], while the use of (o-tol)$_3$P resulted in the addition product E-(o-tol)$_3$P(Ph)C=C(H)B(C_6F_5)$_3$. This indicates that the addition of FLPs to alkynes is more favoured with less basic phosphines. Mechanistically, the alkyne first attacks the empty orbital of boron to form a transient carbocation. When treated with a strong Lewis base, such as P(tBu)$_3$, a hydrogen atom would be removed, leading to the formation of a alkynyl borate, [tBu$_3$PH][PhCCB(C_6F_5)$_3$]. However, if treated with less basic phosphines such as (o-tol)$_3$P, attack on the carbocation center yields the zwitterionic product with P and B moieties in *trans*-positions (Figure 1.14).

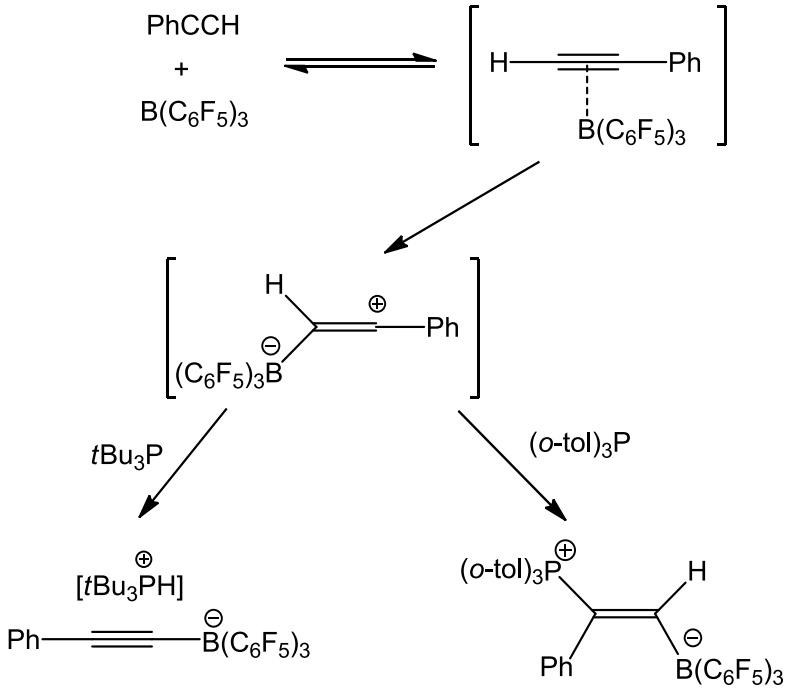

Figure 1.4. Possible activation pathways of alkynes by FLPs.

A similar addition reaction was also discovered in 2008 by Yamaguchi and co-workers.[15] They designed an alkyne-bridged species containing complementary phosphine and borane groups which behave as

electron donating and withdrawing substituents respectively. This system can undergo intramolecular cyclization depending on the nucleophilicity of the phosphine moieties. With increasing electron-donating ability of the dialkylphosphine, the cyclization reaction can even proceed at room temperature. In the case of the less electron rich diphenylphosphine derivative, cyclization is difficult to achieve even at higher temperature (Figure 1.15).

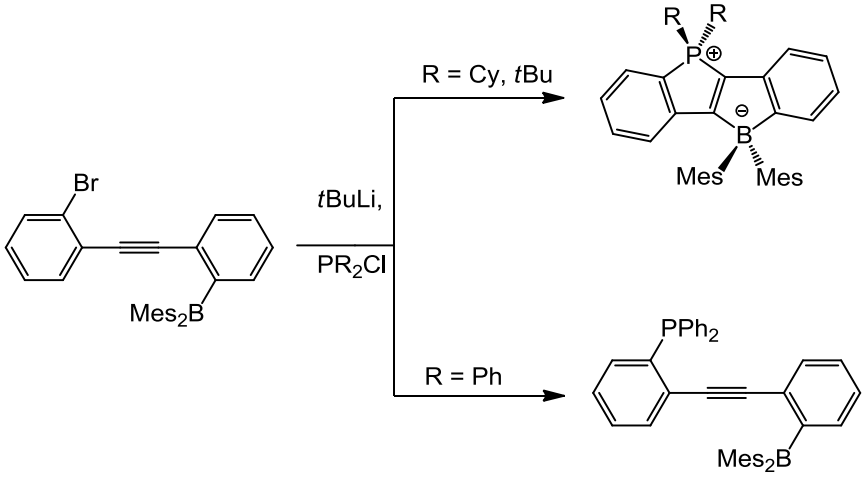

Figure 1.5. Intra-molecular cyclization by phosphine-borane.

1.2.4 Phosphine-Borane Based FLPs Reactions with Other Π-Systems

Aside from the reactivity of FLPs towards alkenes and alkynes, the chemistry of FLPs has also been expanded to other π-systems. For example, Bourissou and co-workers developed ambiphilic phosphine-boranes which can add to the N=N and C=O bonds of diethyl azodicarboxylate and Ph-N=C=O, which stabilizes the zwitterionic species A and B (Figure 1.16),[16] the key intermediates for phosphine-promoted reaction of azodicarboxylates[17] and cyclo-oligomerisation of isocyanates[18] respectively.

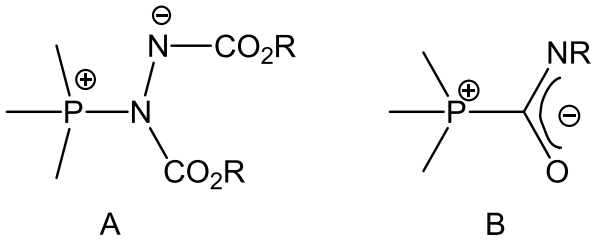

Figure 1.6. Adducts A and B of phosphines with azodicarboxylates and isocyanates.

In the reaction of iPr$_2$P(o-C$_6$H$_4$)BMes$_2$ with diethyl azodicarboxylate, the N=N addition product was formed in toluene at room temperature after 24 hours. In order to investigate the capability of iPr$_2$P(o-C$_6$H$_4$)BMes$_2$ to stabilize the intermediate B, the reaction of same phosphine-borane compound with Ph-N=C=O was studied under the same conditions leading to the analogous product within 1 hour (Figure 1.17). Both products have been fully studied by NMR spectroscopy and X-ray diffraction analysis. The ^{11}B NMR chemical shifts indicate the transformation from a three-coordinated to a four-coordinated environment around the boron center. In the X-ray crystal structures, the short N-B and O-B distances and pyramidalization of boron suggest that the boron groups are stabilized by the electron rich nitrogen and oxygen atoms even though the boron moiety is quite sterically congested due to its two mesityl substituents.

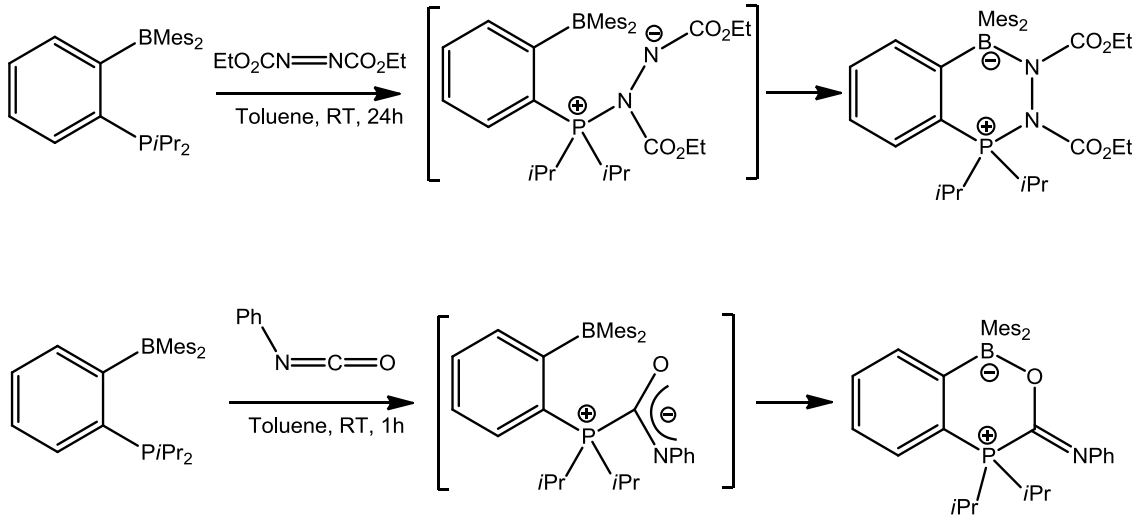

Figure 1.7. N=N and C=O bonds addition by FLPs.

A similar reactivity was also demonstrated for Erker's phosphine-borane bridged compound **1.3**, where the P and B atoms can be added to the C=O and N=O bonds of isocyanate, benzaldehyde, and nitrosobenzene, forming zwitterionic six-membered rings (Figure 1.18).[19]

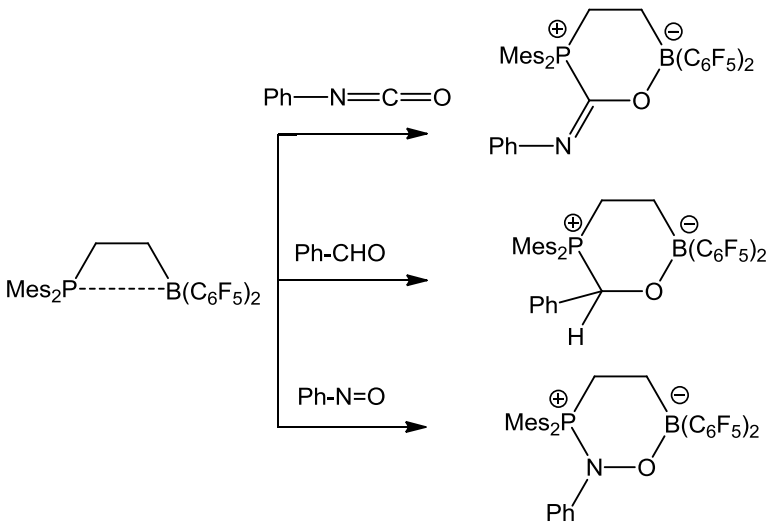

Figure 1.8. Reaction of PhCHO, PhNCO and PhNO and **1.3**.

Furthermore, they found that **1.3** could react with phenyl azide yielding a five-membered ring product at room temperature after 2 days (Figure 1.19). According to NMR spectroscopy and X-ray diffraction experiments, both the phosphorous and boron atoms are attached to the terminal nitrogen of the azide. ^{31}P NMR data also revealed dynamic exchange, indicating the existence of two distinct and interchanging isomers.

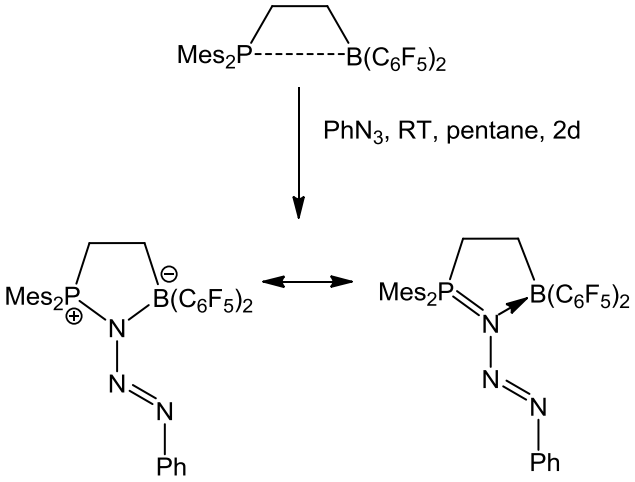

Figure 1.9. Reaction of phenyl azide and **1.3**.

The reaction of **1.3** with pyridine, tert-butyl isocyanide or pivalonitrile only resulted in the simple adduct formation between the boron center and donating atom of the substrate (Figure 1.20).

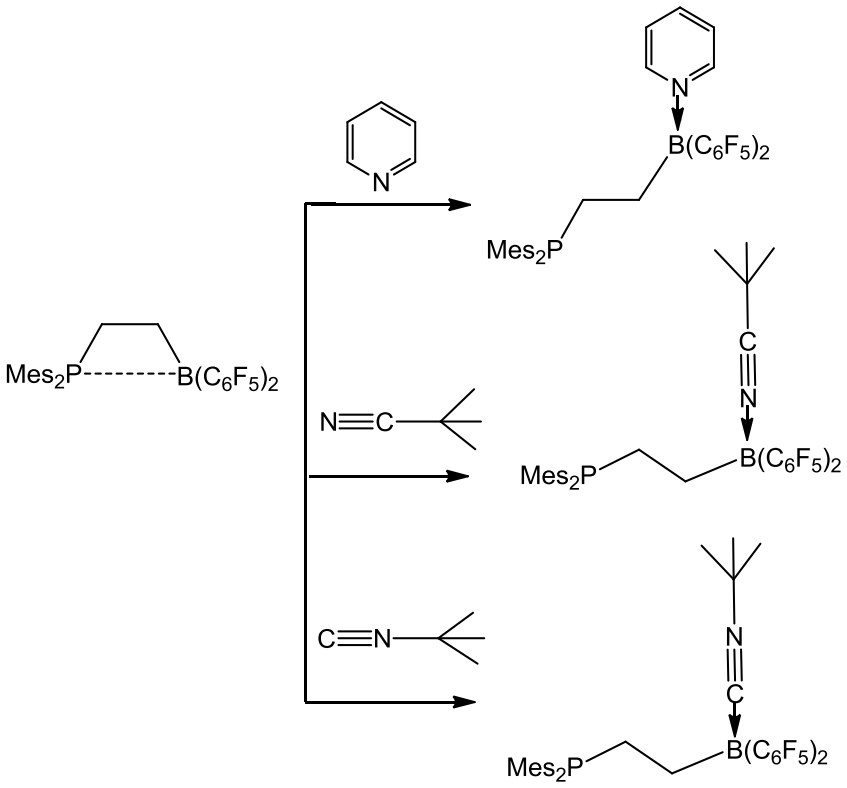

Figure 1.10. Formation of pyridine-, isonitrile- and nitrile adducts of **1.3**.

Further developments by Erker and co-workers yielded another germinal phosphine-borane FLP compound **1.7**, which was found to react with alkenes and alkynes as well as undergo an interesting transformation in the presence of *p*-tolyl isocyanate and mesityl azide.[20] Unlike the simple adduct formation between isocyanate derivative and **1.3**, the germinal FLP **1.7** adds to the C=N bond of *p*-tolyl isocyanate resulting in a newly formed five-membered ring system (Figure 1.21).

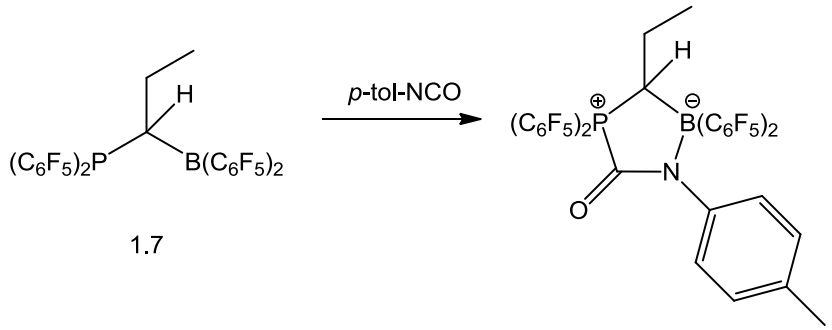

Figure 1.11. Reaction of *p*-tolyl isocyanate and **1.7**.

The reaction of **1.7** and mestiyl azide also proceeds like a 1,3-dipolar cycloaddition, ultimately resulting in the formation of a six-membered ring product containing the FLP with a yield of 50% (Figure 1.22). The X-ray crystal structure shows that the boron center is attached to the nitrogen atom bearing a bulky mesityl substituent while the double bond of the N-N-N moiety appears to be delocalized due to the participation of the phosphorus atom.

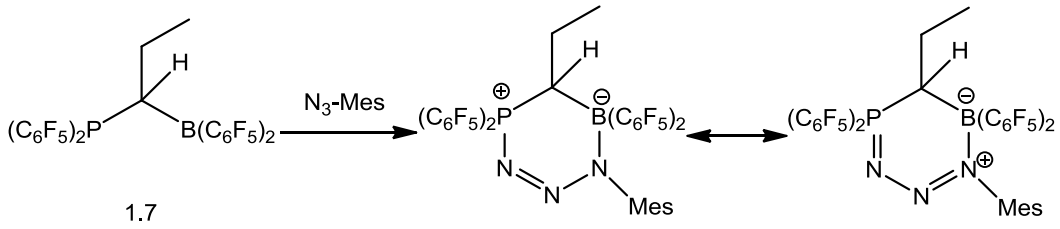

Figure 1.12. Reaction of mesityl azide and **1.7**.

Over the past decade, FLPs chemistry has continued to grow rapidly. The main driving force for this area of research is the increasing variety of reactive un-neutralized Lewis acid/base pairs, many of which have shown great promise towards small-molecule activation. From a fundamental standpoint, this discovery is extremely important as it paves the way for new breakthroughs and ideas. For example, the advance of FLPs chemistry has laid the foundation for applying main-group elements as catalysts in transformations such as hydrogenation; a role typically reserved for transition-metal complexes. The development of metal-free catalysts has become increasingly important due to many concerns over the handling of toxic

metal species as well as the disposal and potential environmental contamination of the catalysts following their use. With the ever expanding library of substrates available to FLPs systems such as alkenes, alkynes, and other π systems, the significance of such acid/base pairs with respect to both their use as catalysts and potential synthetic intermediates in novel activation pathways has been recognized by the chemistry community

Despite all of the examples in the literature of various FLPs systems, there remain several limitations and problems. For instance, most FLPs reported in the literature are quite sensitive to air and moisture due to strong Lewis acidity and basicity. As such, most preparation and storage procedures for FLPs require O_2 and H_2O-free conditions. For applications of H_2 storage materials, gravimetric capacity (H_2 content by mass) has to be considered. However, the requirement of steric congestion to prevent the formation of simple Lewis adducts greatly decreases the hydrogen gravimetric capacity of FLPs-based systems, which remains as a big challenge to this application.

1.3 Triarylborane Compounds as Fluoride Sensors

1.3.1 Introduction

One of the most efficient methods of controlling tooth decay is the fluorination of drinking water. In 1994, the World Health Organization (WHO) declared that the acceptable level of fluoride in drinking water is between 0.5-1.0 mg/L.[21] Fluoride concentrations far in excess to the guidelines set out by the WHO are toxic and can lead to a number of different health concerns including dental/skeletal erosion or even cancer.[22, 23] The US Environmental Protection Agency (EPA) has set 4.0 mg/L or 4 ppm of fluoride as the maximum contaminant level in drinking water, which is the legal threshold limit allowed in public water systems. EPA has also set a secondary standard for fluoride at 2.0 mg/L or 2.0 ppm, which is non-enforceable guidelines regulating contaminants in drinking water.[24] Due to these considerations, an effective fluoride-sensing technique is needed to ensure that the concentration of fluoride in drinking

water does not exceed the recommended limit. Additionally, fluoride sensors could also be used to track UF_6 and phosphorofluoridate nerve agents which release fluoride ions when hydrolyzed.[2a]

As mentioned at the beginning of this chapter, triarylborane compounds with bulky substituents can block nucleophilic attack from Lewis donors, except small anions such as fluoride, cyanide, and hydride which all exhibit relatively strong binding to the boron center even when it is sterically protected. Thus, it is possible to use such boron systems for fluoride sensing. A lone pair of electrons from the fluoride ion can donate into the empty p orbital of the boron center which transforms the three-coordinated boron, stabilized by the surrounding aryl groups due to π-conjugation, to a four-coordinated boron with pyramidal geometry (Figure 1.23). For practical applications based on photophysical properties, the lowest electronic transition in a conjugated triarylborane system is normally dominated by charge transfer processes from an electron-rich aromatic moiety to the electron deficient boron center. This intramolecular charge transfer process is also the origin of the bright fluorescence often exhibited by organoboron compounds. As a result, binding of fluoride ions to such boron centers effectively blocks this intramolecular charge transfer process which leads to the lowest electronic transition being perturbed and a dramatic change in the photophysical properties. This allows triarylborane based π-systems to act as "turn-off" sensors that are highly selective towards the fluoride anion, making them excellent candidates for such applications.

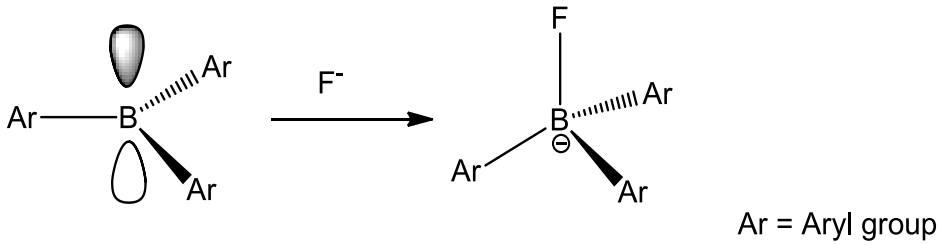

Figure 1.13. Triarylborane compounds as F^- sensors.

In 2001, Shigehiro Yamaguchi and co-workers developed the first organoboron-based systems, (tris(9-anthryl)borane and tris[(10-dimesitylboryl)9-anthryl]borane), capable of acting as fluoride sensors.[25] For example, tris(9-anthryl)borane (Figure 1.24) is both water- and air-stable due to the sterically demanding substituents around boron, and binds fluoride ions in THF with a binding constant of $(2.8 \pm 0.3) \times 10^5\ M^{-1}$. The addition of fluoride to a THF solution of this borane results in a distinct color change from orange to colorless. This compound only weakly binds to AcO^- and OH^-, and does not show any response toward Cl^-, Br^- and ClO_4^-. Nonetheless, this system is not suitable in an aqueous environment, as the resulting anionic complex readily dissociates due to the large hydration enthalpy of fluoride ions ($\Delta H° = -504$ kJ/mol).

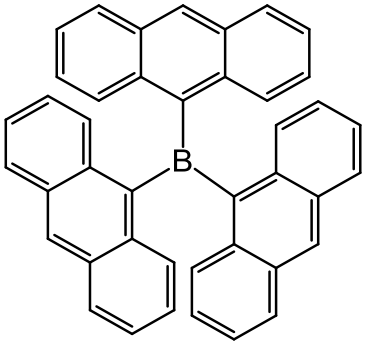

Figure 1.14. Structure of tris(9-anthryl)borane.

1.3.2 Fluoride Sensing by Neutral $BMes_2$ Containing Compounds

In order to improve fluoride affinity and overcome the large hydration enthalpy, many research groups have developed new systems based on triarylborane functionality. One strategy is to develop polydentate triarylborane compounds which can increase the fluoride binding affinity. This is particularly true for compounds which contain a $BMes_2$ moiety, as the boron center is highly protected by the *o*-methyl groups of the two mesityls but still retains comparable Lewis acidity making it far more practical for applications. This was amply demonstrated by Gabbaï and co-workers who synthesized compounds **1.8** (E = O) and **1.9** (E = S) by functionalizing a rigid naphthalene linker with two diarylboryl moieties (Figure 1.25).[26, 27] Both compounds display high selectivity towards fluoride ions over other larger halides, NO_3^- or $H_2PO_4^-$.

The crystal structures of compound **1.8**/**1.9**·F^- showed clearly a B-F-B bridged structure wherein the fluorine atom is trapped between the two boron atoms with a B-F distance of 1.58-1.64 Å. UV-vis absorption spectra were used to monitor the fluoride ions titration experiments of compound **1.8** and **1.9** in THF, where significant quenching was observed. The fluoride binding constant of **1.9** was determined to be about 10^9 M^{-1}, which is a dramatic improvement compared to that measured for $BMes_3$ (~10^5 M^{-1}). Furthermore, a competition binding study performed between **1.9** and $BMes_3$ in THF revealed the quantitative formation of **1.9**·F^- in the presence of a large excess of $BMes_3$ indicating that **1.9**·F^- is formidably stable. This is readily demonstrated upon the addition of water, as the complex does not dissociate. This is quite different compared to its monoboryl counterparts, and was explained in terms of an overall decrease in steric hindrance as a result of the newly distorted tetrahedral geometry which stabilizes the complex.

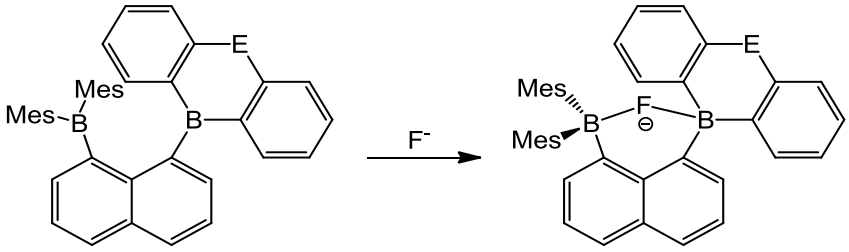

Figure 1.15. Fluoride addition to compound **1.8** (E = O) and **1.9** (E = S).

In an effort to improve upon the triarylborane only systems, many research groups have also developed and explored heteronuclear mutidentate triarylborane molecules. For example, Gabbaï's *et al.* studied the B/Hg containing bidentate Lewis acid compound **1.10** which was synthesized by functionalizing a naphthalene backbone with $BMes_2$ and $Hg(C_6F_5)$ substituents (Figure 1.26).[28] This compound is water-stable with a fluoride binding constant of ~ 10^4 M^{-1} in mixed THF/water (90/10 (v/v)), which is 10,000 times greater than that of $BMes_3$ under the same conditions. The crystal structure further confirmed the chelating structure of the complex. The excellent fluoride binding affinity was attributed to not only bidentate chelation, but also the enhanced Lewis acidity at Hg as a result of the electron-withdrawing C_6F_5 group. Gabbaï's group later described that **1.10** can behave as a phosphorescent chemosensor for

fluoride ions. Compound **1.10** emits red light at 77 K in solid state when the boron center is unsaturated. Upon the binding of fluoride to the boron atom, π conjugation within the molecule is disrupted which results in green phosphorescence emission.

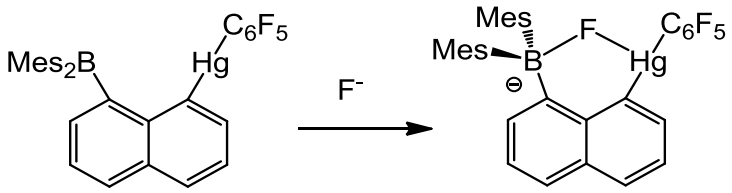

Figure 1.16. Fluoride addition to compound **1.10**.

Gabbaï *et al.* also combined the concepts of heteronuclear chelate with poly-triarylboryl together and created the tridentate Lewis acid **1.11** (Figure 1.27).[29] The crystal structure of **1.11** showed that the two boron centers possess trigonal planar geometry and are ~ 3.5 Å from the mercury atom, which is the appropriate space required to trap two fluoride ions. The second fluoride ion binds much less readily (K_2 = ~ 10^3 M^{-1}) compared to the first one (K_1 = ~ 10^8 M^{-1}) which is due to both increased steric congestion and unfavorable Coulombic repulsion.

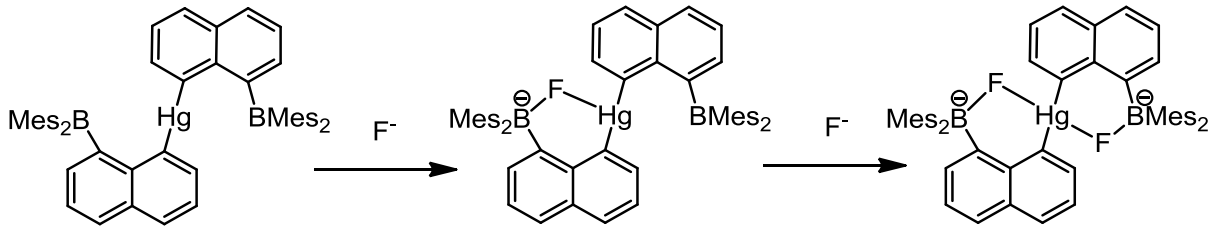

Figure 1.17. Fluoride addition to compound **1.11**.

Another strategy to enhance the Lewis acidity and fluoride affinity of boron is to connect boron moieties within a π-conjugated unit, which was established a number of years ago by Kaim *et al.* using two $BMes_2$ moieties bridged by a phenyl or more expanded π-conjugated linker.[30] In 2007, Wang *et al.* developed a similar but more electron deficient π-conjugated molecule containing two $BMes_2$ moieties bridged by a 2,2'-bipyridyl linker (**1.12**) (Figure 1.28).[31] Compound **1.12** was found to be an excellent chelating ligand for transition-metals such as Pt (**1.13**) and Cu (**1.14**), which further increases the electron deficiency of

boron centers as shown by cyclic voltammetry experiments. Remarkably, **1.13** and **1.14** can be used as colorimetric sensors due to their very distinct color change upon the addition of fluoride. Compound **1.13** and **1.14** have intense colors due to a metal-to-ligand charge transfer (MLCT) band in the visible region. Because the π* orbital of the ligand is mainly localized at the boron center in the MLCT transition, the absorption band of MLCT is blue-shifted due to the increasing energy gap once the energy of the ligand based LUMO increases upon fluoride addition. Compound **1.13** instantly changes from red to orange after one equivalent of fluoride (1:1·F^-:**1.13** adduct) and further changes to light yellow following the second equivalent (2:1·F^-:**1.13** adduct formation). On the other hand, compound **1.14** displayed a color change from orange to yellow with 1 equivalent of fluoride and eventually becomes colorless upon forming the 2:1 (F^- : **1.14**) adduct.

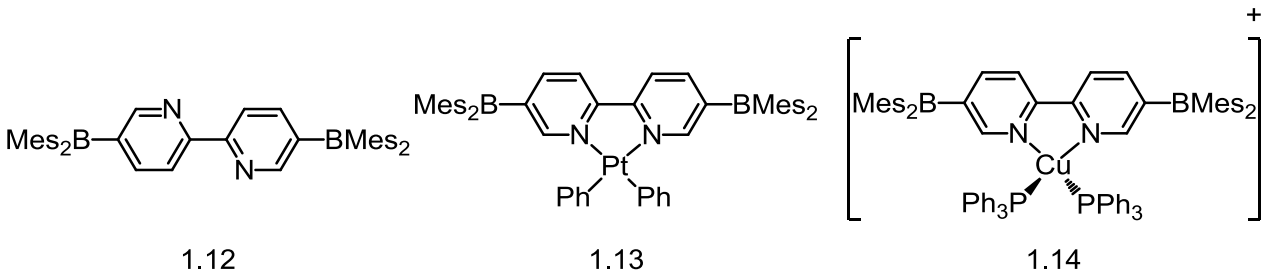

1.12 1.13 1.14

Figure 1.18. π-Conjugate molecule **1.12** and its metal complexes **1.13** and **1.14**.

1.3.3 Fluoride Sensing by Cationic Borane Compounds Containing a $BMes_2$ Moiety

Further developments in fluoride sensing with organoboron systems focused on the use of cation-functionalized triarylborane compounds. Gabbaï *et al.* observed that by functionalizing triarylborane compounds with pnictogen cations such as phosphonium, the boron centers have a greater affinity for fluoride ions due to the Coulombic effects. The fact that the cation-functionalized compounds are salts also increases their solubility in an aqueous solution. For example, the cationic phosphonium-borane compound (**1.15**) shown in Figure 1.29 has a binding constant of (6.5 ± 0.5) $\times 10^6$ M^{-1} with fluoride in $CHCl_3$.[32] The binding constant of **1.15** is higher than that of Yamaguchi's compound (tris(9-

anthryl)borane) even in $CHCl_3$, as it provides a more competitive medium for fluoride binding. As expected, the fluoride binding is unaffected in the presence of chloride and bromide. Remarkably, **1.15** can bind fluoride ions in a solution of H_2O: MeOH (9:1 v/v) with a binding constant of about 10^3 M^{-1} and can be regenerated with the use of an aqueous Al^{3+} solution.

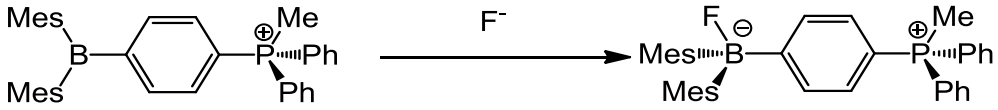

Figure 1.19. The structure of **1.15** and its binding with fluoride.

As mentioned before, the EPA recommends that the fluoride concentration in drinking water should not exceed 2 ppm. It is quite challenging to design a fluoride sensor capable of detecting such low concentrations of fluoride ions as a result of their large hydration enthalpy. In order to reach the EPA standard, Gabbaï *et al.* synthesized a series of phosphonium-triarylborane compounds by functionalizing the phosphorus atom with different substituents such as Me, Et, *n*-Pr and Ph (Figure 1.30).[33] The phosphonium-borane compound with Ph on phosphorus (**1.16**) exhibits the largest F^- binding constant (10500 (±1000) M^{-1} in H_2O: MeOH (9:1 v/v)) among all the analogous compounds. Furthermore, absorbance quenching of **1.16** was successfully detected in the presence of $[F^-]$ = 1.9 ppm in water (pH = 4.9). This pH level is important, as HF formation becomes significant at lower pH, while competitive hydroxide binding to the boron center begins to occur at higher pH. This compound is considered to be one of the most successful molecular sensors based on triarylborane compounds for detection of fluoride in aqueous media, and its water-compatibility, stability, and high sensitivity make it a good candidate for future applications in fluoride sensing.

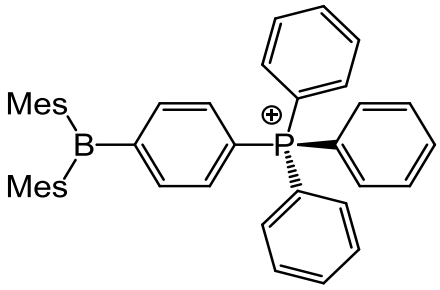

Figure 1.30. Structure of **1.16**.

Gabbaï *et al*. also showed that by combining Coulombic and cooperative effects, a further enhancement of fluoride binding at the boron center can be achieved. This concept was realized by designing a cationic bidentate boron based sensor in which the fluoride ions could be held in place between both the boron and cationic substituents. This new system (**1.17**) showed improvement over the previous bidentate diborane compounds, which displayed high fluoride binding affinity but were incompatible in aqueous media. The cationic chelating system (**1.17**) is shown in Figure 1.31,[34] where it can be seen that the fluoride ion becomes trapped due to the close proximity of the phosphonium and borane. This leads to much stronger binding with F^- compared to the *p*-isomer, as shown by the competition binding experiment in Figure 1.31b. The binding constant of **1.17** in MeOH is about 10^6 M^{-1}, which is much higher than that measured for **1.15** (400 M^{-1}) under the same conditions. NMR data and X-ray crystal structure analysis indicate that the fluoride ion binds to the boron center and has a strong interaction with the phosphonium moiety, which explains the improved fluoride affinity of this system. However, the stability of **1.17** in water is still an issue.

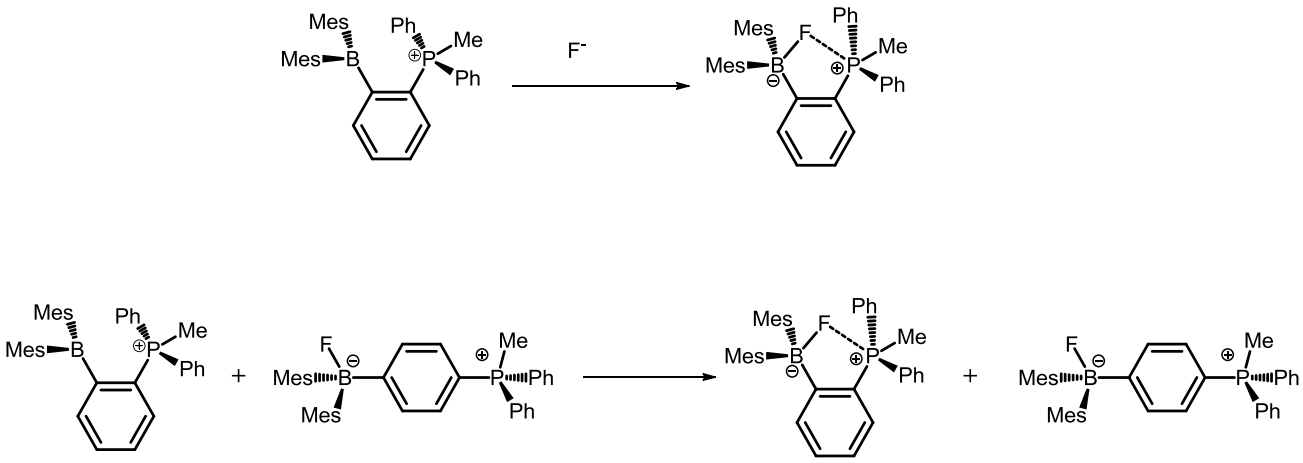

Figure 1.20. a) The structure of **1.17** and its binding with fluoride; b) Competition experiment between **1.17** and **1.15** in $CDCl_3$.

The effect of having multiple cationic substituents has also been investigated. For example, Lee *et al.* synthesized a triphosphonium functionalized triarylborane compound **1.18** (Figure 1.32)[35] and studied its fluoride affinity in the mixed solvent system DMSO/H_2O (7:3 v/v). Due to the enhanced Coulombic effect from three phosphonium groups, the boron center was far more electron deficient compared to the mono- or di-phosphonium substituted compounds with a fluoride binding constant of 10^7 M^{-1}.

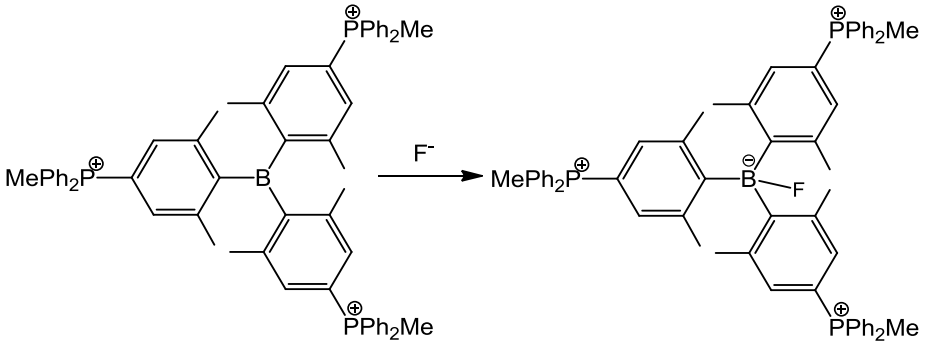

Figure 1.21. Fluoride sensing by compound **1.18**.

1.3.4 "Turn-on" Luminescent Compound for Fluoride Sensing

Most of the fluoride sensing molecules described thus far act as "turn-off" sensors, where the binding of fluoride to the boron center causes quenching of either absorption or emission peaks in the UV-visible or

fluorescence spectra of the molecules. For practical applications, it is far more effective to use "turn-on" sensors, or even better, sensors which display a distinct color change. Besides the previously mentioned colorimetric sensors such as complexes **1.13** and **1.14**, another strategy of detecting fluoride ions by luminescent color changing is developed by manipulating the charge-transfer transitions within molecules. For example, Műllen's group has demonstrated that the ladder type diboron compound **1.19** (Figure 1.33) has an intense intramolecular CT emission originated from the negative boron center to the empty orbital of the other boron center, once the molecule is bound to one fluoride. Furthermore this CT emission will be "turned off" when both boron moieties are charged by fluoride.[36]

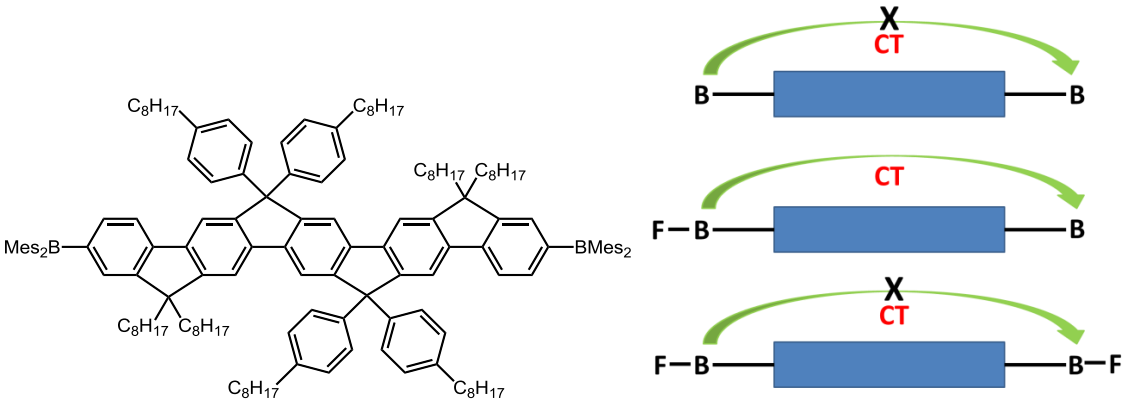

Figure 1.22. Structure of compound **1.19** and its emission processes upon addition of F^-.

Previously, our group has successfully demonstrated that V-shaped (compound **1.20** and **1.21**) and U-shaped (compound **1.22** and **1.23**) donor-acceptor triarylborane compounds not only display highly efficient fluorescence, but also show distinct fluorescent color changes upon the addition of fluoride (Figure 1.34).[37, 38]

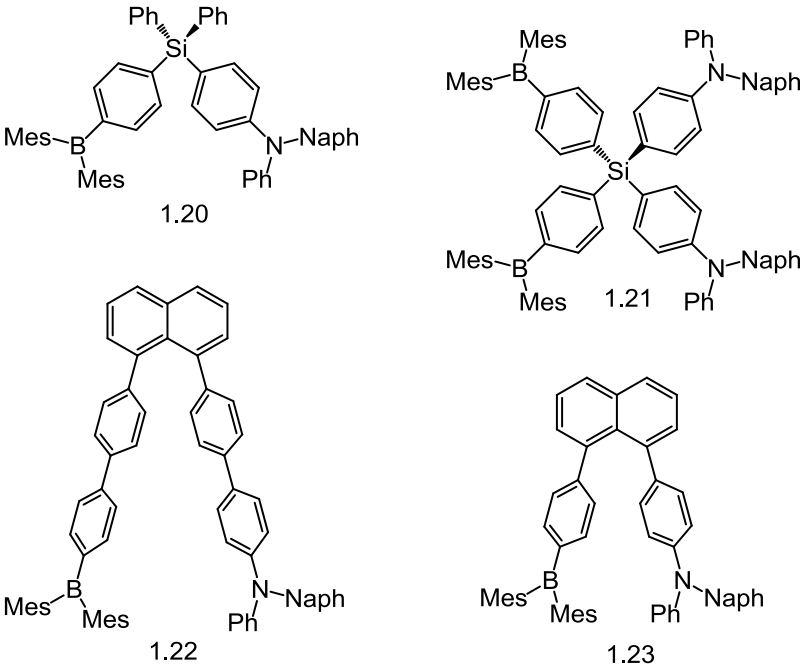

Figure 1.23. V-shaped and U-shaped donor-acceptor systems.

The fluorescence of these compounds is mainly due to through-space charge transfer from the amino group to the boron center. When the boron center binds to a fluoride ion, the charge transfer pathway is blocked, switching the emission to a π-π* transition from the π-backbone. As a result, an obvious change in fluorescent color is observed (Figure 1.35).

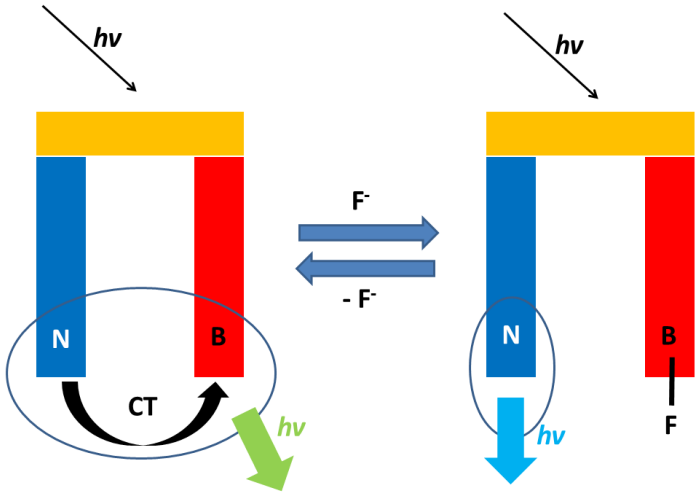

Figure 1.24. Operating principle of "turn-on" sensors for fluoride.

More recently, our group designed a different U-shaped triarylborane compound (**1.24**) which contains a dimethylamino group as the electron donor (Figure 1.36).[39] This molecule exhibited a binding constant of $(1.7\pm 0.5) \times 10^4\ M^{-1}$ in CH_2Cl_2 which is comparable to those of **1.22** and **1.23**. It also shows selectivity for F^- over Cl^- and Br^-. Significantly, this compound shows distinct fluorescent color changes when either a fluoride ion or proton is bound. Under neutral conditions, the compound emits bright green light due to charge transfer from the dimethylamino donor to the electron accepting boron. Upon addition of fluoride ions, the boron center is blocked by F^-, switching the emission from green to sky blue. Under acidic conditions where the amino group picks up a proton, the fluorescent color changes to purple. Most important is that all of these processes are reversible.

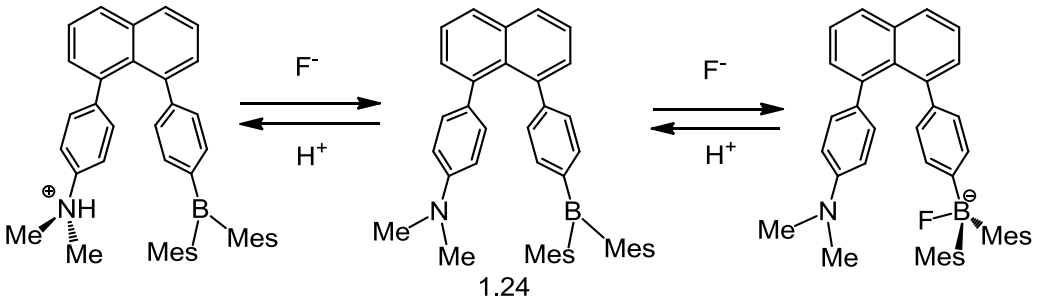

Figure 1.25. Compound **1.24** and its fluoride-, proton-adducts.

Aside from the previously discussed systematic approaches, many other types of triarylborane compounds for use as fluoride sensors have been examined (Figure 1.37). For example, Thilagar *et al.* synthesized a V-shaped boryl-BODIPY substituted compound (**1.25**) which displays a distinct emission color change upon the binding of fluoride.[40] Hu *et al.* developed triarylborane-containing polyacetylene compounds (**1.26**) which show different photophysical responses towards fluoride ions depending on the spacer between $BMes_2$ and the main chain.[41] Finally, Lu *et al.* designed a donor-π-acceptor compound (**1.27**) with a phenothiazine unit as the electron donating group and $BMes_2$ as the electron acceptor group, in which two groups are connected by fluorenevinylene.[42] For this system, the addition of fluoride or cyanide can be observed by the naked eye, where the solution color of **1.27** changes from yellow to yellowish-green and the emission is significantly increased simultaneously.

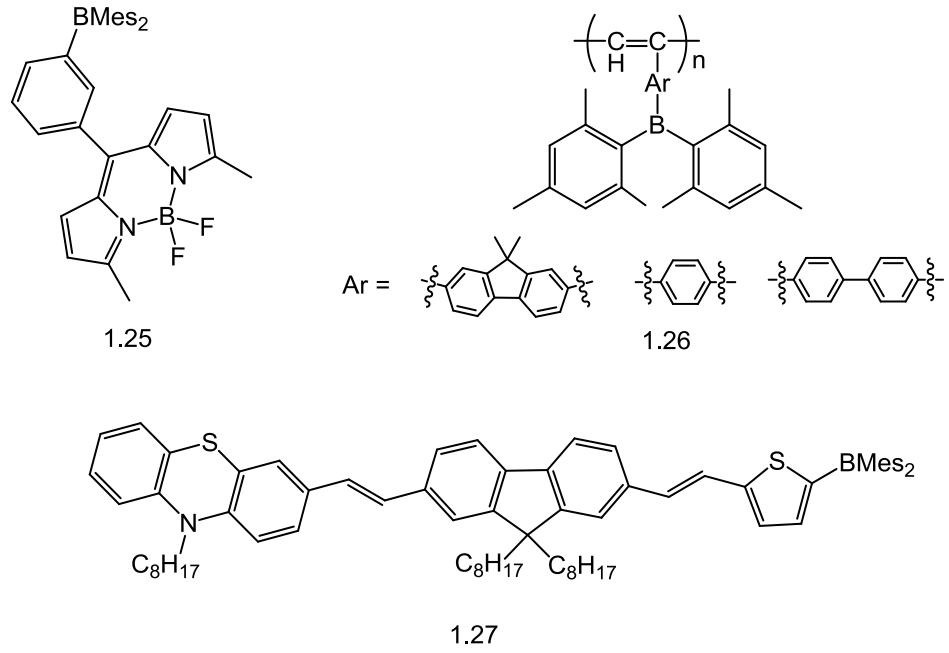

Figure 1.26. Molecular structures of compounds **1.25**, **1.26**, and **1.27**.

1.4 N-Heterocyclic Carbene Reactions by FLPs

1.4.1 Introduction

As mentioned previously, FLPs are not only capable of activating small molecules such as H_2, CO_2, N_2O, olefins, alkynes, but also show promising reactivity towards heterocyclic rings. In 1950, Wittig and Rückert[43] found that the ring of THF could be readily opened in the presence of $Na[Ph_3C]$ and $THF(BPh_3)$ which yields $[Ph_3C(CH_2)_4OBPh_3]^-$ as the product. In 1992, Breen and Stephan[44] demonstrated that a combination of $[ZrCl_4(THF)_2]$ and PCy_3 generates the zwitterionic compound $[ZrCl_4(\mu\text{-}OCH_2CH_2CH_2CH_2PCy_3)]_2$ as a result of THF-ring opening at room temperature (Figure 1.38).

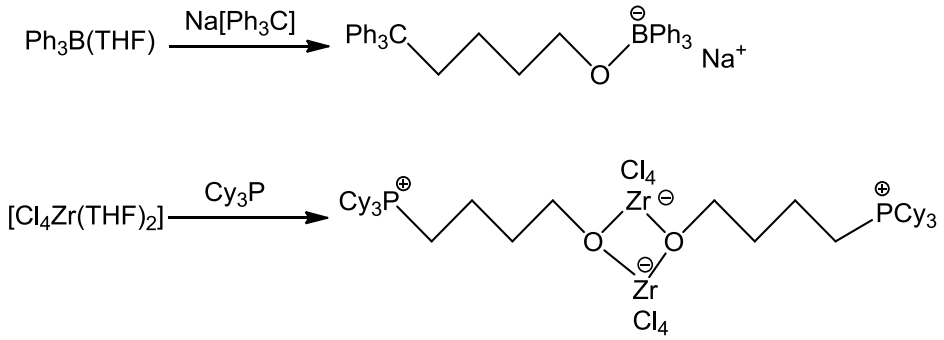

Figure 1.27. Examples of Lewis acid prompted THF ring-opening reactions.

Later on, this type of ring opening reactivity was extended to various types of FLPs and related heterocycles compounds. For example, the THF-$B(C_6F_5)_3$ adduct can be reacted with numerous different kinds of sterically hindered Lewis bases which results in a variety of ring-opened products (Figure 1.39).[45, 46, 47]

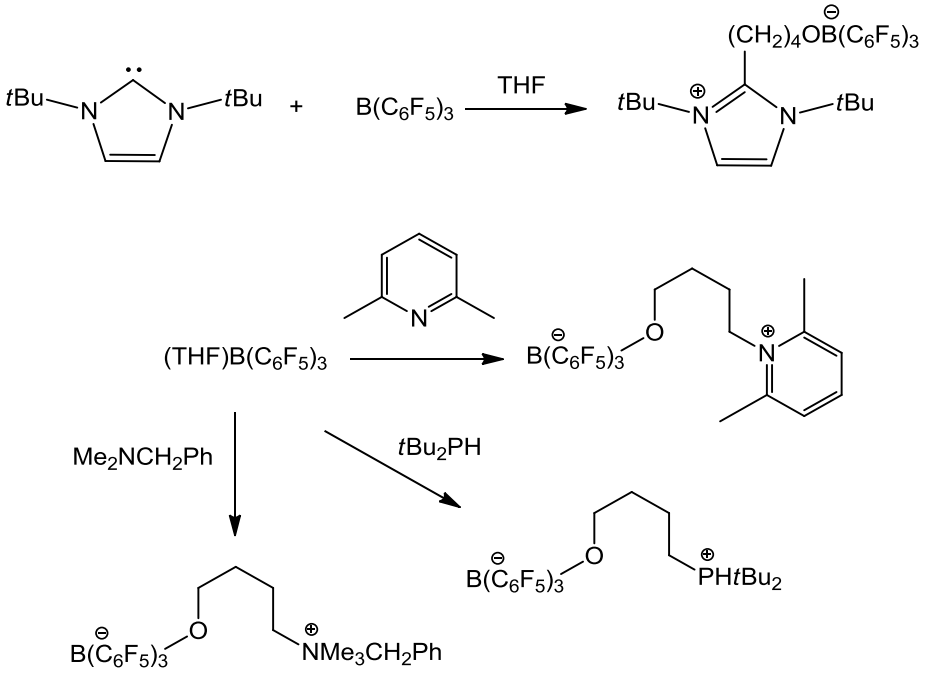

Figure 1.28. Ring opening reactions of THF by FLPs.

Similar reactivity has been observed for related heterocylic compounds such as dioxane, thioxane, lactone, and lactide. In the case of 1,4-dioxane and thioxane, each can be ring opened to yield corresponding products from FLPs of $B(C_6F_5)_3$ and various Lewis bases such as NHCs, phosphines, or even N-bases (Figure 1.40).[47]

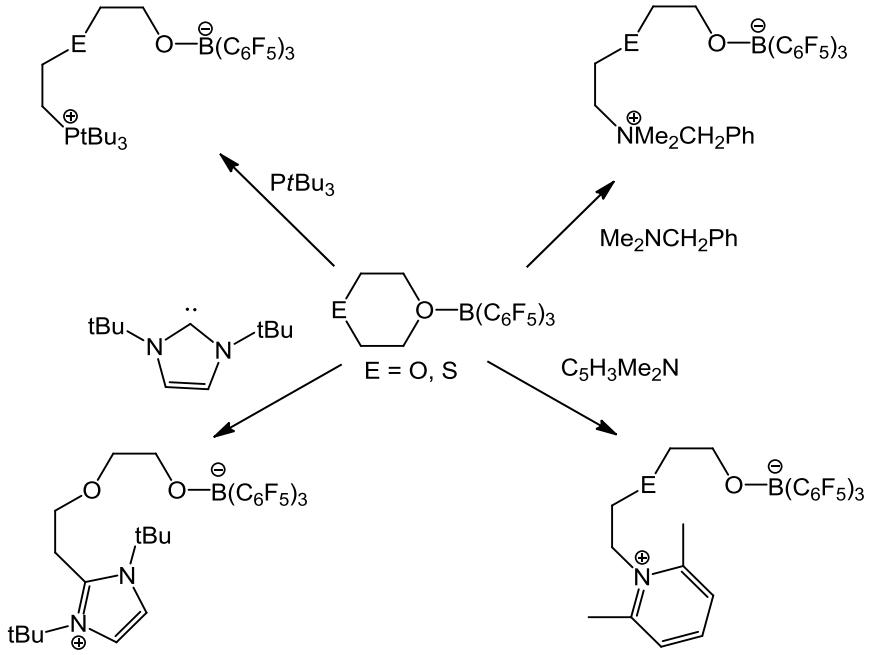

Figure 1.40. Ring opening reactions of 1,4-dioxane and thioxane by FLPs.

1.4.2 Ring Expansion of N-Heterocyclic Carbenes

In all the molecule activation reactions available to FLPs with NHCs, the strong σ-donating Lewis bases NHCs behave as such phosphine or N bases and provide a lone pair of electrons. The chemistry of NHCs and their analogs is an incredibly important and has been widely studied over the last few decades. Due to their broad applicability, NHCs have been used in numerous areas such as transition-metal and main-group chemistry.[48] For the most part, NHCs are considered robust and act as ligands to stabilize low oxidation state transition-metal or main-group elements through the donation of their lone pair of electrons. Applications of such transition metal complexes have been mainly geared towards the activation of various bonds such as C-H, C-N and C-C.[49] Recently however, the integrity of NHCs has been called into question as a result of their ability to undergo C-N bond cleavage and ring expansion

reactions (RER) with either transition metal or main group elements. In 2006, Grubbs and co-workers observed the insertion of nickel into an N-heterocyclic ring while trying to synthesize a new catalyst. In addition to the insertion of a nickel atom, the phenyl group initially bound to nickel migrated during the reaction between the NHC precursor, base, and $NiClPh(PPh_3)_2$ (Figure 1.41).[50]

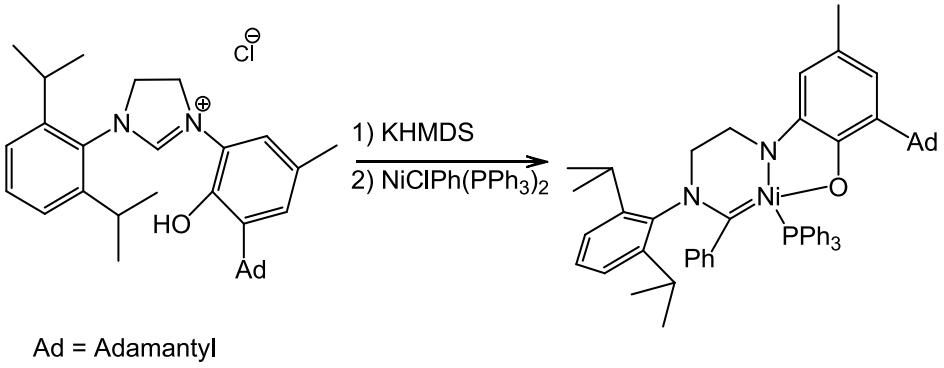

Figure 1.29. Ni-insertion into NHC.

In 2010, Bertrand *et al.* discovered the first room temperature C-N bond cleavage and insertion into an NHC ring involving pinacolborane (HBpin).[51] Later in 2012, Hill and co-workers demonstrated the first reaction between a NHC functionalized organoberyllium hydride dimer and $PhSiH_3$, which ended up forming a six-membered ring product after 6 hours at 80 °C. The crystal structure of the product revealed that the beryllium atom had successfully inserted into the C-N bond of the IPr (IPr = 1,3-bis(2,6-diisopropylphenyl)imidazol-2-ylidene) ligand. Interestingly, the hydrosilanes are not required for the insertion to occur as the same Be-insertion product was observed after combining the NHC/beryllium dimer and heating them to 120 °C for 24 hours (Figure 1.42).[52]

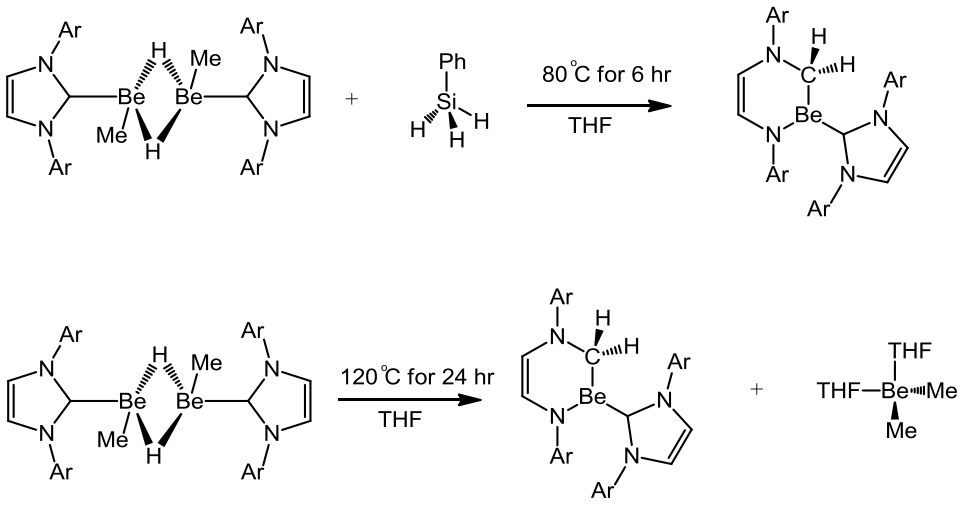

Figure 1.30. Be insertion into NHCs, Ar = 2,6-diisopropylphenyl.

Around the same time, Radius *et al.* found that a similar C-N bond cleavage/insertion could be achieved with silicon by reacting alky-substituted NHCs and phenylsilane $PhSiH_3$ or Ph_2SiH_2 in toluene at 100 °C for three days.[53] Part of this transformation involves the migration of either H atoms or phenyl groups from silicon to the central carbon of the NHC, and insertion of either an SiHPh or $SiPh_2$ unit into the C-N bond yielding a new six membered ring product (Figure 1.43).

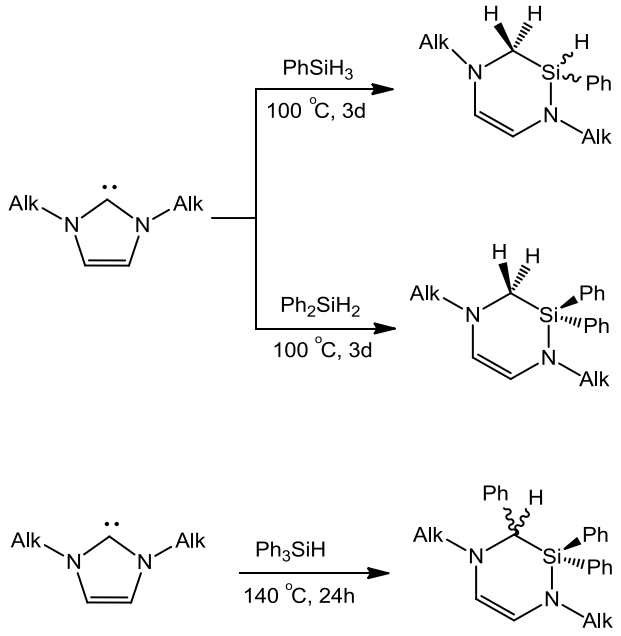

Figure 1.31. Si-insertion of NHCs.

Radius and co-workers proposed a three-step mechanism for their reaction between the NHC and Ph_2SiH_2. Following the initial adduct formation, one hydrogen atom migrates from silicon to the carbonic carbon (T1), which is thought to be the rate limiting step, giving B. Subsequent insertion of the silicon atom into the C-N bond (T2) results in the formation of a new Si-N bond (C) and a pentavalent silicon atom. Finally, the second hydrogen transfers from silicon to the central carbon (T3) which yields the final ring expansion product (D) (Figure 1.44).

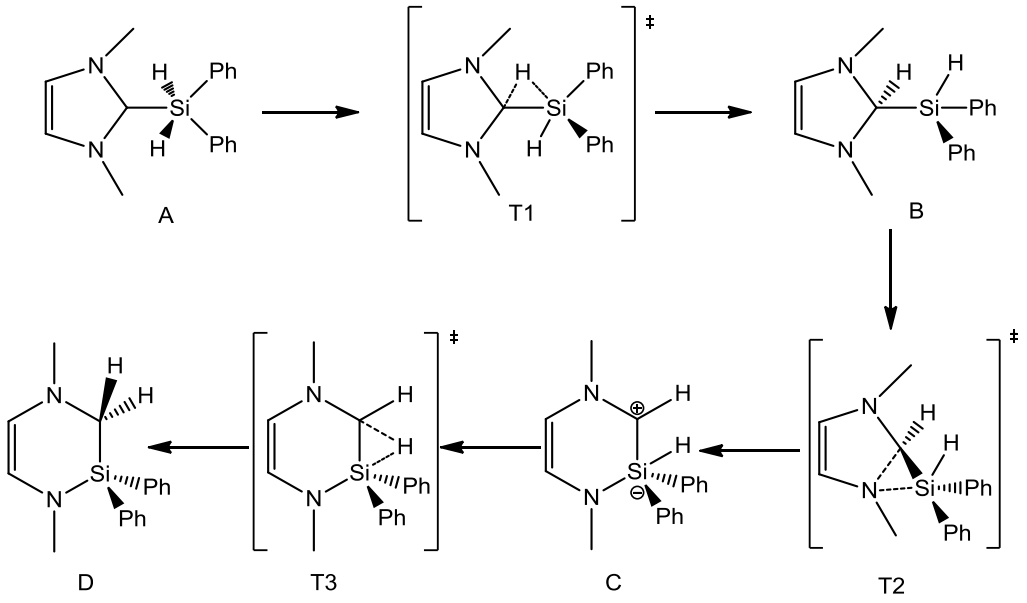

Figure 1.32. Mechanism for ring expansion reaction by silanes.

Similar insertion reactions have also been observed with other elements. For example, Rivard *et al.* established the ring expansion reaction between NHCs and amino-boranes at 100 °C in toluene, where a borane hydride unit was successfully inserted into the NHC ring.[54] Later on, Stephan *et al.* found that phosphine substituted NHCs could be activated by 9-BBN (9-borabicyclo[3.3.1] nonane) and undergo a similar ring expansion reaction at room temperature. The resulting intra-molecular phosphine-borane FLP was further studied for its catalytic activity towards the reduction of CO_2 (Figure 1.45).[55]

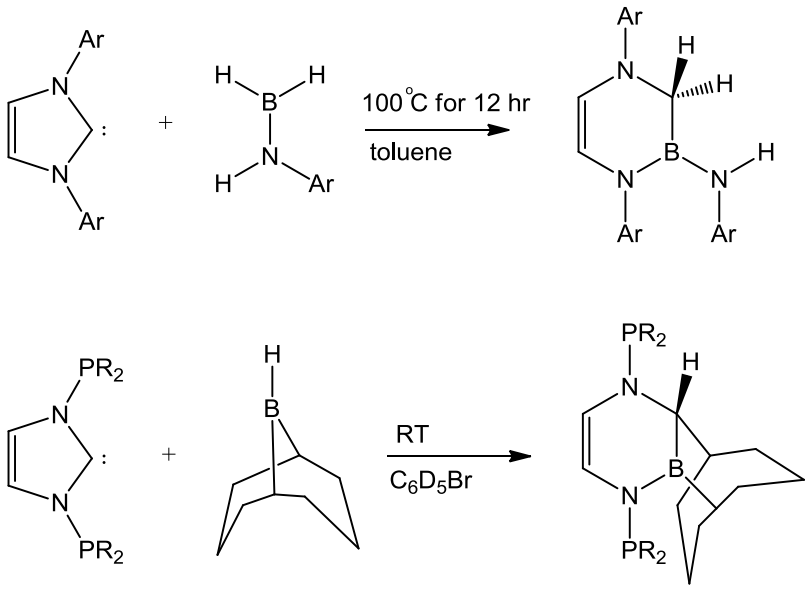

Figure 1.33. Boron insertion of NHCs.

Stephan *et al.* also presented a possible reaction mechanism for their ring expansion reaction which is quite similar to that proposed by Radius and co-workers. After forming the initial NHC-borane adduct with 9-BBN, the hydride of the borane migrates to the electron-deficient central carbon atom of NHC. The N atom then coordinates to the neighboring boron center, which prompts the C-N bond cleavage. Lastly, there is B-C bond cleavage due to electrophilic carbon center which forms a new C-C bond and gives the product (Figure 1.46).

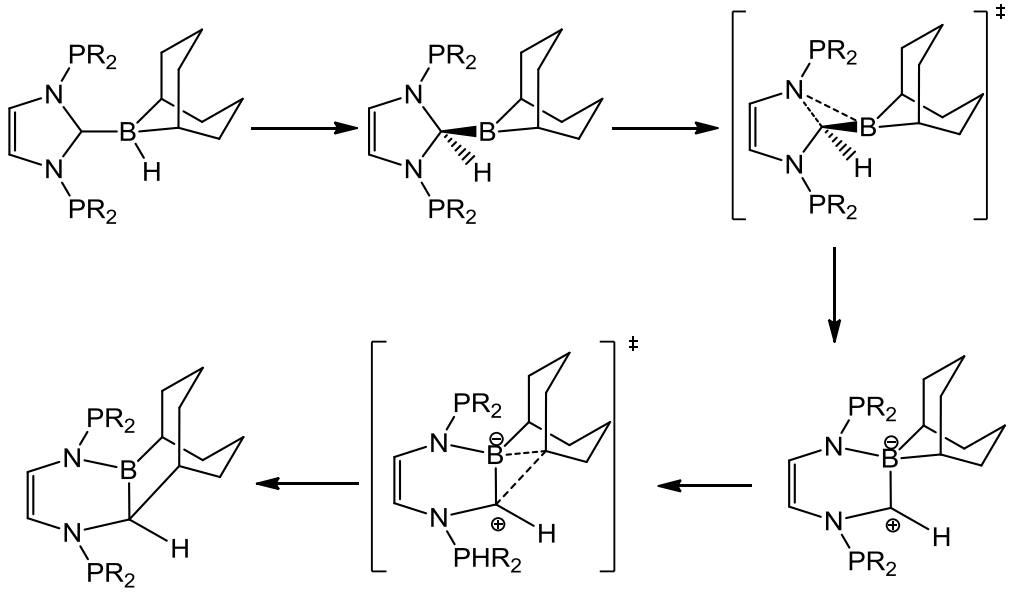

Figure 1.34. Proposed mechanism for NHC reaction with 9-BBN.

Very recently, Marder *et al.* investigated a different ring expansion reaction which involves B-B bond and C-N bond cleavage followed by C-B bond formation.[56] Initially, the diboron reagent B_2cat_2 (cat = 1,2-$O_2C_6H_4$) reacts with one or two equiv. of Me_4Im (Me_4Im=1,3,4,5-tetramethylimidazolin-2-ylidene) which yields the mono- or bis- NHC adducts respectively (Figure 1.47).

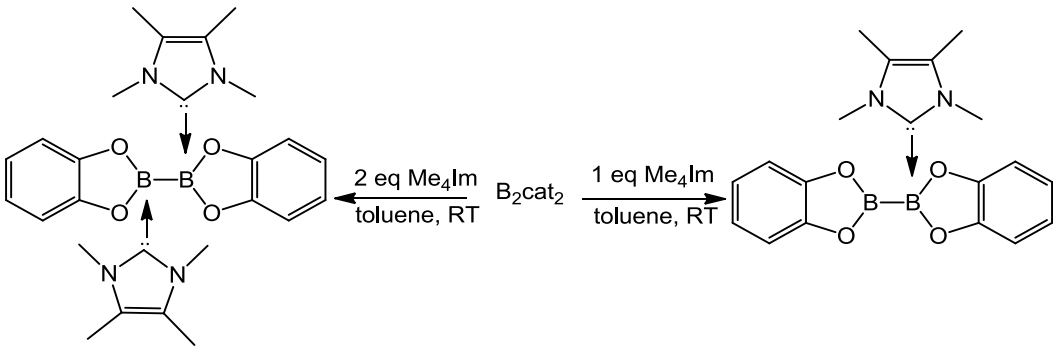

Figure 1.35. Synthesis of B_2cat_2-NHC adducts.

The ring expansion reaction could occur by heating the THF solution of bis-NHC adduct to 70 °C for 16 hours. Compared to B_2cat_2, B_2neops (neop = $OCH_2CMe_2CH_2O$) was found to be much more reactive with both the C-N bond breaking of nPr$_2$Im (nPr = n-propyl) and boron insertion occurring at room

temperature (Figure 1.48). Furthermore, the reaction is quite different from the B_2cat_2 system where the NHC ligand binds to the exocyclic boron atom. In latter reaction, the second NHC is bound to the endocyclic boron which leads to the ring opening of the neopentyl group and formation of the 6- and 8-membered ring structures with oxygen attached to the exocyclic boron. This type of reaction is quite different from the previous elemental insertion reactions which involve an initial H-migration step.

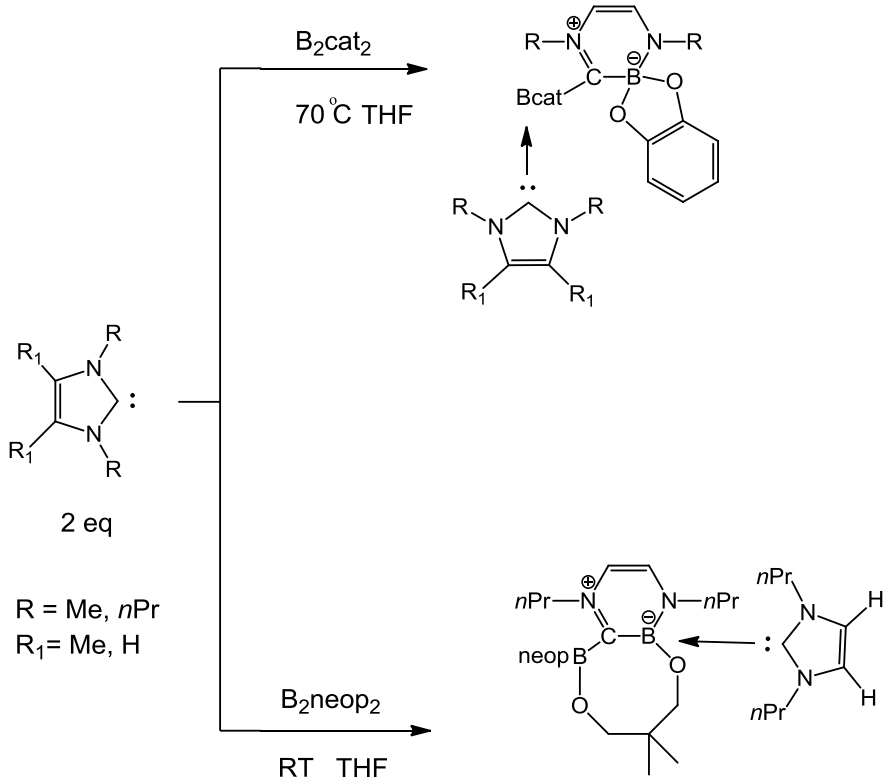

Figure 1.36. Ring expansion reaction by B_2cat_2 and B_2neop_2.

1.5 Scope of This Thesis

The work presented in this thesis focuses mainly on the development of new non-conjugated donor-acceptor systems with sterically demanding triarylphosphine and triarylborane substituents connected by a rigid naphthalene bridge. The aim of this work is to investigate the photophysical properties and reactivity of these systems along with fluoride binding ability for practical application.

Chapter 2 describes the synthesis of a highly congested -$BMes_2$ and -PPh_2 functionalized 1,8-naphthalene species, which was found to be highly stable towards small molecules as a result of the crowding around the donor-acceptor moiety.

Chapter 3 describes a non-conjugated U-shaped donor-acceptor compound functionalized by bulky phosphine and boron substituents. This compound has a very distinct through-space charge transfer transition which facilitates an interesting dual emission pathway and exhibits turn-on luminescent in response to fluoride ions.

Chapter 4 probes the fluoride affinity of the U-shaped system by decreasing the electron density at the phosphorus center by introducing methyl group or metal centers which results in a more electron deficient $BMes_2$. As a result, these compounds display significantly different emission properties following the addition of fluoride ions.

Chapter 5 describes an unusual reactivity available to one U-shaped system discussed in Chapter 4 in the presence of an N-heterocyclic carbene, *N,N'*-dimethylimidazol-2-ylidene (IMe). IMe behaves as a base, generating a phosphorus-ylide, which then tears apart the 2^{nd} equivalent of IMe to afford a vinyl-amine bridged phosphine-borane compound. Chapter 6 provides an overall summary of the research described in this thesis and proposed future work.

References:

(1) a) Jäkle, F. *Chem. Rev.* **2010**, *110*, 3985; b) Noda, T.; Shirota, Y. *J. Am. Chem. Soc.* **1998**, *120*, 9714; c) Hudson, Z. M.; Wang, S. *Acc. Chem. Res*. **2009**, *42*, 1584.

(2) a) Hudnall, T. W.; Chiu, C. W.; Gabbaï, F. P. *Acc. Chem. Res*. **2009**, *42*, 388; b) Wade, .; Broomsgrove, A. E. J.; Aldridge, S.; Gabbaï, F. P. *Chem. Rev.* **2010,** *110*, 3958; c) Zhao, H.; Leamer, L. A; Gabbaï, F, P. *Dalton Trans*., **2013**, *42*, 8164; d) Nishiyabu,R.; Kubo,Y.; James, T. D.; Fossey, J. S. *Chem. Commun.* 2011, 1106; e) Galbraith, E.; James, T. D. *Chem. Soc. Rev.* **2010**, *39*, 3831.

(3) a) Stephan, D. W.; Erker, G. *Angew. Chem., Int. Ed*. **2010**, *49*, 46; b) Stephan, D. W. *Org. Biomol. Chem*. **2012**, *10*, 5740; c) Stephan, D. W. *Dalton Trans*. **2009**, 3129; d) Erker, G.; Stephan, D. W. Frustrated Lewis Pairs I, Uncovering and Understanding, Springer-Verlag Berlin Heidelberg 2013; e) Stephan, D. W.; Erker, G. *Angew. Chem., Int. Ed*. **2015**, *54*, 6400.

(4) Lakowicz, J. R. *Principles of Fluorescence Spectroscopy*, 2nd ed., Kluwer Academic, New York, 1999.

(5) Lewis, G. N. *Valence and the Structure of Atoms and Molecules*, Chemical Catalogue Company, Inc., New York, 1923.

(6) Brown, H. C.; Schlesinger, H. I.; Cardon, S. Z. *J. Am. Chem. Soc.* **1942**, *64*, 325.

(7) Welch, G. C.; San Juan, R. R.; Masuda, J. D.; Stephan, D. W. *Science*. **2006**, *314*, 1124.

(8) Welch, G. C.; Stephan, D. W. *J. Am. Chem. Soc*. **2007**, *129*, 1880.

(9) Spies, P.; Erker, G.; Kehr, G.; Bergander, K.; Frohlich, R.; Grimme, S.; Stephan, D. W. *Chem. Commun*. **2007**, *47*, 5072.

(10) Chase, P. A.; Welch, G. C.; Jurca, T.; Stephan, D. W. *Angew. Chem., Int. Ed*. **2007**, *46*, 8050.

(11) Spies, P.; Schwendemann, S.; Lange, S.; Kehr, G.; Frohlich, R.; Erker, G. *Angew. Chem., Int. Ed.* **2008**, *47*, 7543.

(12) Wang, H.; Fröhlich, R.; Kehr, G.; Erker, G. *Chem. Commun.*, **2008**, 5966.

(13) Zhao, X.; Stephan, D. W. *J. Am. Chem. Soc.*, **2011**, *133*, 12448.

(14) Dureen, M. A.; Stephan, D. W. *J. Am. Chem. Soc.*, **2009**, *131*, 8396.

(15) Fukazawa, A.; Yamada, H.; Yamaguchi, S. *Angew. Chem. Int. Ed*. **2008**, *47*, 5582.

(16) Moebs-Sanchez, S.; Bouhadir, G.; Saffon, N.; Maron, L.; Bourissou, D. *Chem. Commun.*, 2008, 3435.

(17) a) But, T. Y. S.; Toy, P. H. *Chem. Asian J.*, **2007**, *2*, 1340; b) Dembinski, R. *Eur. J. Org. Chem.*, **2004**, 2763; c) Nair, V.; Menon, R. S.; Sreekanth, A. R.; Abhilash, N.; Biju, A. T. *Acc. Chem. Res.*, **2006**, *39*, 520.

(18) a) Tang, J.; Verkade, J. G. *Angew. Chem., Int. Ed.* **1993**, *32*, 896; b) Tang, J.; Mohan, T.; Verkade, J. G. *J. Org. Chem.*, **1994**, *59*, 4938. c) Pusztai, Z.; Vlád, G.; Bodor, A.; Horváth, I. T.; Lass, H. J.; Halpaap, R.; Richter, F. U. *Angew. Chem., Int. Ed.*, **2006**, *45*, 107.

(19) Mömming, C. M.; Kehr, G.; Wibbeling, B.; Fröhlich, R.; Erker, G. *Dalton Trans.*, **2010**, *39*, 7556.

(20) Stute, A.; Kehr, G.; Fröhlichz, R.; Erker, G. *Chem. Commun*., **2011**, 4288.

(21) WHO Expert Committee on Oral Health Status and Fluoride Use. Fluorides and oral health. 1994.

(22) Fluorine and fluorides. Environmental Health Criteria 36. IPCS International Programme on Chemical Safety, World Health Organization. 1984.

(23) Fluorides. Environmental Health Criteria 227, IPCS International Programme on Chemical Safety, World Health Organization, 2002.

(24) http://water.epa.gov/drink/contaminants/basicinformation/fluoride.cfm.

(25) Yamaguchi, S.; Akiyama, S.; Tamao, K. *J. Am. Chem. Soc.* **2001,** *123*, 11372

(26) Melaïmi, M.; Sole, S.; Chiu, C.; Wang, H.; Gabbaï, F. P. *Inorg. Chem*. **2006**, *45*, 8136.

(27) Solé, S.; Gabbaï, F. P. *Chem. Commun.*, **2004**, 1284.

(28) Melaimi, M.; Gabbaï, F. P. *J. Am. Chem. Soc.* **2005,** *127*, 9680.

(29) Lee, M. H.; Gabbaï, F. P. *Inorg. Chem*. **2007**, *46*, 8132.

(30) a) Kaim, W.; Schulz, A. *Angew. Chem., Int. Ed. Engl.* **1984**, *23*, 615; b) Noda, T.; Shirota, Y. *J. Am. Chem. Soc.* **1998**, *120*, 9714; c) Yamaguchi, S.; Akiyama, S.; Tamao, K. *J. Am. Chem. Soc.* **2000**,

122, 6335; d) Zhao, S.; Wucher, P.; Hudson, Z. M.; McCormick, T. M.; Liu, X.; Wang, S.; Feng, X.; Lu, Z. *Organometallics* **2008**, *27*, 6446.

(31) Sun, Y.; Ross, N.; Zhao, S.; Huszarik, K.; Jia, W.; Wang, R.; Macartney, D.; Wang, S. *J. Am. Chem. Soc*. **2007,** *129*, 7510.

(32) Lee, M. H.; Agou, T.; Kobayashi, J.; Kawashima, T.; Gabbai, F. P. *Chem. Commun.* **2007**, 1133.

(33) Kim, Y.; Gabbai, F. P. *J. Am. Chem. Soc.* **2009**, *131*, 3363.

(34) Hudnall, T. W.; Kim, Y.; Bebbington, M. W. P.; Bourissou, D.; Gabbai, F. P. *J. Am. Chem. Soc.* **2008**, *130*, 10890.

(35) Song, K. C.; Lee, K. M.; Nghia, N. V.; Sung, W. Y.; Do, Y.; Lee, M. H. *Organometallics*, **2013**, *32*, 817.

(36) Zhou, G.; Baumgarten, M.; Műllen, K. *J. Am. Chem. Soc.* **2008**, *130*, 12477.

(37) Liu, X.; Bai, D.; Wang, S. *Angew. Chem., Int. Ed.* **2006**, *45*, 5475.

(38) Bai, D.; Liu, X.; Wang, S. *Chem. Eur. J.* **2007**, *13*, 5713.

(39) Hudson, Z. M.; Liu, X.; Wang, S. *Org. Lett*. **2011**, *13*, 300.

(40) Swamy P, C. A.; Mukherjee, S.; Thilagar, P. *Inorg. Chem.*, **2014**, *53*, 4813.

(41) Hu, Y.; Zhao, Z.; Bai, X.; Yuan, X.; Zhang, Z.; Masuda, T. *RSC Adv*., **2014**, *4*, 55179.

(42) Jia, J.; Xue, P.; Zhang, Y.; Xu, Q.; Zhang, G.; Huang, T.; Zhang, H.; Lu, R. *Tetrahedron* 2014, *70*, 5499.

(43) Wittig, Riickert, *Justus Liebigs Ann. Chem.*, **1950**, ***566***, 101

(44) Breen, T. L.; Stephan, D. W. *Inorg. Chem.*, **1992**, *31*, 4019.

(45) Holschumacher, D.; Bannenberg, T.; Hrib, C. G.; Jones, P. G.; Tamm, M. *Angew. Chem. Int. Ed.* **2008**, *47*, 7428.

(46) Welch, G. C.; Masuda, J. D.; Stephan, D. W. *Inorg. Chem*. **2006**, *45*, 478.

(47) Birkmann, B.; Voss, T.; Geier, S. J.; Ullrich, M.; Kehr, G.; Erker, G.; Stephan, D. W. *Organometallics* **2010**, *29*, 5310.

(48) a) Schuster, O.; Yang, L.; Raubenheimer, H. G.; Albrecht, M. *Chem. Rev.* **2009**, *109*, 3445; b) Diez - Gonzalez, S.; Marion, N.; Nolan, S. P. *Chem. Rev*. **2009**, *109*, 3612; c) Poyatos, M.; Mata, J. A.; Peris, E. *Chem. Rev*. **2009**, *109*, 3677; d) Ghadwal, R. S.; Azhakar, R.; Roesky, H. W. *Acc. Chem. Res.* **2013**, *46*, 444; e) Roesky, H. W. *J. Organomet. Chem.* **2013**, *730*, 57; f) Wang, Y.; Robinson, G. H. *Dalton Trans*. **2012**, *41*, 337; g) Inoue, S.; Driess, M. *Angew. Chem. Int. Ed.* **2011**, *50*; h) Wang, Y.; Robinson, G. H. *Inorg. Chem*. **2011**, *50*, 12326; i) Martin, D.; Soleilhavoup, M.; Bertrand, G. *Chem. Sci*. **2011**, *2*, 389; j) Siemeling, U. *Aust. J. Chem.* **2011**, *64*, 1109; k) Fuchter, M. J. *Chem. Eur. J.* **2010**, *16*, 12286; l) Wang, Y.; Robinson, G. H. *Chem. Commun*. **2009**, 5201.

(49) a) Bramananthan, N.; Mas-Marza, E.; Fernandez, F. E.; Ellul, C. E.; Mahon, M. F.; Whittlesey, M. K. *Eur. J. Inorg. Chem*. **2012**, 2213 and references cited therein; b) Wurtemberger, M.; Ott, T.; Doing, C.; Schaub, T.; Radius, U. *Eur. J. Inorg. Chem.* **2011**, 405; c) Wolf, R.; Plois, M.; Hepp, A. *Eur. J. Inorg. Chem*. **2010**, 918; d) Ohki, Y.; Hatanaka, T.; Tatsumi, K. *J. Am. Chem. Soc.* **2008**, *130*, 17174; e) Curran, D. P.; Boussonniere, A.; Geib, S. J.; Lacote, E. *Angew. Chem. Int. Ed*. **2012**, *51*, 1602; f) Xiang, L.; Xiao, J.; Deng, L. *Organometallics*, **2011**, *30*, 2018; g) Hu, Y.-C.; Tsai, C.-C.; Shih, W.-C.; Yap, G. P. A.; Ong, T.-G. *Organometallics*, **2010**, *29*, 516; h) Liu, L.; Wang, F.; Shi, M. *Eur. J. Inorg. Chem*. **2009**, 1723; i) Burling, S.; Mahon, M. F.; Powell, R. E.; Whittlesey, M. K.; Williams, J. M. J. *J. Am. Chem. Soc*. **2006**, *128*, 13702; j) Caddick, S.; Cloke, F. G. N.; Hitchcock, P. B.; Lewis, A. K. de K. *Angew. Chem. Int. Ed*. **2004**, *43*, 5824; k) Galan, B. R.; Gembicky, M.; Dominiak, P. M.; Keister, J. B.; Diver, S. T.; *J. Am. Chem. Soc*. **2005**, *127*, 15702; l) Galan, B. R.; Pitak, M.; Gembicky, M.; Keister, J. B.; Diver, S. T. *J. Am. Chem. Soc.* **2009**, *131*, 6822.

(50) Waltman, A. W.; Ritter, T.; Grubbs, R. H. *Organometallics*, **2006**, *25*, 4238

(51) Frey, G. D.; Masuda, J. D.; Donnadieu, B.; Bertrand, G. *Angew. Chem. Int. Ed*. **2010**, *49*, 9444.

(52) Arrowsmith, M.; Hill, M. S.; Kociok-Kohn, G.; MacDougall, D. J.; Mahon, M. F. *Angew. Chem. Int. Ed*. **2012**, *51*, 2098.

(53) Schmidt, D.; Berthel, J. H. J.; Pietsch, S.; Radius, U. *Angew. Chem. Int. Ed*. **2012**, *51*, 8881.

(54) Al-Rafia, S. M. I.; McDonald, R.; Ferguson, M. J.; Rivard, E. *Chem. Eur. J*. **2012**, *18*, 13810.

(55) Wang, T.; Stephan, D. W. *Chem. Eur. J.* **2014**, *20*, 3036.

(56) Pietsch, S.; Paul, U.; Cade, I. A.; Ingleson, M. J.; Radius, U.; Marder, T. B. *Chem. Eur. J.* **2015**, *21*, 1.

Chapter 2

Highly Congested Donor-Acceptor PB Compound: Synthesis and Properties of a $BMes_2$- and a PPh_2- Functionalized 1,8-Naphthalene

2.1 Introduction

Frustrated Lewis Pairs (FLPs) containing bulky and complementary Lewis acids and bases have generated intense research interest recently as a result of the unusual reactivity displayed by these unique structures lacking a donor-acceptor bond.[1] Triarylborane and phosphine containing Frustrated Lewis Pairs are one typical class of these reactive species and have been studied comprehensively.[1,2] For the most part, these compounds are bridged by a linker which usually reinforces the desired reactivity.[3] 1,8-Naphthalene is a highly rigid linker that can be used to connect donor and acceptor groups at a fixed distance, helping to control the reactivity of such molecules.[4,5] For instance, functionalizing 1,8-naphthalene with electron deficient groups such as triarylboryl or cationic units has been well investigated and introduces a Coulombic effect for fluoride ion sensing.[6] Erker *et al.* have demonstrated that two phosphine groups attached to 1,8-naphthalene in the presence of $B(C_6F_6)_3$ will behave as an effective catalyst in the FLPs-catalyzed hydrogenation of silyl enol ethers.[7] Our group also established that amine-borane donor-acceptor systems connected by a naphthyl linker display distinct through-space charge transfer luminescence and can be applied as "turn-on" fluorescence fluoride sensors.[8] In order to develop a new phosphine-borane containing donor-acceptor system, we designed a molecule with a rigid naphthalene skeleton which can help to fix the electron donating and accepting moieties at a certain distance with the aim to control reactivity. We chose to employ a bulky diphenylphosphine group as the Lewis base and a dimesitylboron group as the Lewis acid to increase steric hindrance and prevent prematurely forming a phosphine-borane adduct. For the purpose of selectively sensing small ions like fluoride, the $BMes_2Ar$ unit is well known to resist nucleophilic attack by bigger donor groups.[6,8,9] This chapter will introduce

synthetic strategy, characterization and reactivity study of compound **2.1** as shown in Figure 2.1. Recently several phosphine-borane functionalized naphthalene compounds[4] also have been investigated. By manipulating the substituents on phosphine and boron centers, the distances of P-B can be considerably varied by attractive and repulsive forces (2.01 ~ 2.89 Å) to enforce or discourage P-B dative interaction.

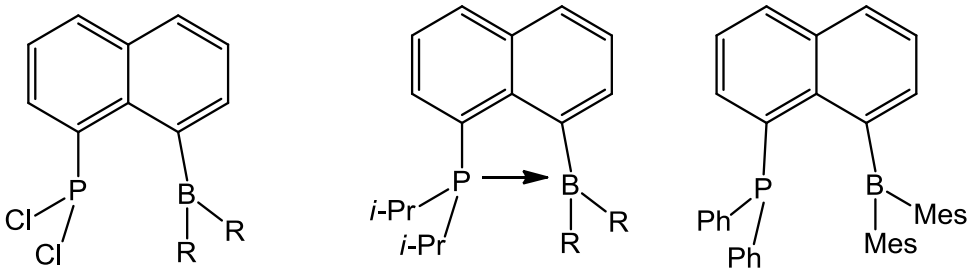

Figure 2.1. Left: the recent examples of P-B compounds reported by Tokitoh and Bourissou *et al*; Right: the target molecule **2.1**.

2.2 Experimental

2.2.1 General Procedures

All reactions were carried out under a nitrogen atmosphere. Reagents were purchased from Aldrich Chemical Company and used without further purification. Thin-layer and flash chromatographies were performed on silica gel. ^{1}H, ^{13}C, ^{11}B, and ^{31}P NMR spectra were recorded on Bruker Avance 300 and 500 MHz spectrometers. Deuterated solvents were purchased from Cambridge Isotopes. UV-vis spectra were recorded on a Varian Cary 50 Bio spectrometer. Melting points were recorded on a Fisher Johns melting point apparatus. High-resolution mass spectra (HRMS) were obtained from an Applied Biosystems Qstar XL spectrometer. Elemental analyses were conducted at Laboratoire d'Analyse Élémentaire de l'Université de Montréal. Photoirradiation experiments were carried out using a Rayonet photochemical

reactor. 1,8-diiodonaphthalene and 1-diphenylphosphino-8-iodonaphthalene were synthesized by a modified literature procedure.[10]

2.2.2 Synthesis of 1,8-Diiodonaphthalene

1,8-Diaminonaphthalene (10.0 g , 63.2 mmol) was dissolved in 120 mL 6.9 M H_2SO_4 solution and then cooled to -20 °C with stirring. 13.1 g (189.6 mmol) $NaNO_2$ dissolved in 50 mL H_2O, were subsequently added dropwise at -15 °C to -20 °C, followed by the addition of 63.0 g (379.5 mmol) KI dissolved in 50 mL H_2O at the same temperature. The reaction mixture was then quickly heated up to 80 °C for a short time. Upon cooling to room temperature, the reaction was neutralized with NaOH, and the resulting solid was filtered off with suction and then extracted with diethyl ether in a Soxhlet apparatus over two days. The extract was washed with 50 mL 10 % HCl solution, saturated $Na_2S_2O_3$ solution and 1 M NaOH solution, respectively. After drying over $MgSO_4$, the solvent was removed by rota-evaporation to afford the crude product as a brown solid. 1,8-Diiodonaphthalene was purified over silica gel with *n*-hexanes as light yellow solid (14.3 g, 60%). ^{1}H NMR (300 MHz, $CDCl_3$, δ): 8.42 (dd, $^3J_{H–H}$ = 7.3 Hz, $^4J_{H–H}$ = 1.2 Hz, 2H), 7.85 (dd, $^3J_{H–H}$ = 8.2 Hz, $^4J_{H–H}$ = 1.2 Hz, 2H), 7.08 (dd, $^3J_{H–H}$ = 8.0 Hz, $^3J_{H–H}$ = 7.5 Hz, 2H) ppm; $^{13}C\{^1H\}$ NMR (75 MHz, $CDCl_3$, δ): 144.0, 135.8, 132.2, 131.0, 126.9, 96.0 ppm.

2.2.3 Synthesis of 1-Diphenylphosphino-8-iodonaphthalene

1,8-Diiodonaphthalene (2.0 g, 5.26 mmol) was dissolved in 30 mL of dry degassed THF in a 100 mL Schlenk flask. The solution was cooled to -78 °C for 15 min; then *n*-BuLi (2.4 mL, 1.60 M in hexanes, 3.84 mmol) was added dropwise by syringe. After the mixture was stirred for 1 h at -78 °C, chlorodiphenylphosphine (0.65 mL, 3.5 mmol) was added dropwise. The mixture was slowly warmed to room temperature and stirred overnight. The solvent was removed by rota-evaporation, and the residue was partitioned between CH_2Cl_2 and water. The water layer was extracted twice with CH_2Cl_2, and the combined organic layers were dried over $MgSO_4$, filtered, and purified on silica gel (10:1 hexanes/CH_2Cl_2 as the eluent) to afford 490 mg of 1-diphenylphosphino-8-iodonaphthalene as a white solid (32% yield).

^{1}H NMR (300 MHz, $CDCl_3$, δ): 8.30 (dd, $^{3}J_{H–H}$ = 7.4 Hz, $^{4}J_{H–H}$ = 1.1 Hz, 1H), 7.86 (m, 1H), 7.80 (dd, $^{3}J_{H–H}$ = 7.6 Hz, $^{4}J_{H–H}$ = 1.9 Hz, 1H), 7.24 - 7.36 (m, 12H), 7.09 (dd, $^{3}J_{H–H}$ = 8.0 Hz, $^{3}J_{H–H}$ = 7.4 Hz, 1H) ppm; $^{13}C\{^{1}H\}$ NMR (75 MHz, $CDCl_3$, δ): 142.9, 138.3, 137.5, 136.1, 134.2, 131.4, 130.3, 128.6, 128.4, 126.7, 125.6, 92.2 ppm; $^{31}P\{^{1}H\}$ NMR (121 MHz, $CDCl_3$, δ): -12.5 ppm.

2.2.4 Synthesis of 2.1

1-Diphenylphosphino-8-iodonaphthalene (300 mg, 0.68 mmol) was dissolved in 20 mL of dry degassed THF in a 50 mL Schlenk flask. The solution was cooled to -78 °C for 15 min; then *n*-BuLi (0.47 mL, 1.60 M in hexanes, 0.75 mmol) was added dropwise by syringe. After the mixture was stirred for 1 h at -78 °C, 10 mL of a THF solution of $BMes_2F$ (183 mg, 0.68 mmol) was added. The mixture was slowly warmed to room temperature and stirred overnight. The solvent was removed in *vacuo*, and the residue was partitioned between CH_2Cl_2 and water. The water layer was extracted twice with CH_2Cl_2, and the combined organic layers were dried over $MgSO_4$, filtered, and purified on silica gel (5:1 hexanes/CH_2Cl_2 as the eluent) to afford 149 mg of **2.1** as a white solid (39% yield). ^{1}H NMR (500 MHz, $CDCl_3$, δ): 8.12 (d, $^{3}J_{H–H}$ = 8.2 Hz, Naph, 1H), 7.80 (d, $^{3}J_{H–H}$ = 6.6 Hz, Naph, 1H), 7.73 (m, Naph, 1H, Ph, 2H), 7.61 (t, $^{3}J_{H–H}$ = 8.2 Hz, Naph, 1H), 7.47 (m, Naph, 2H and Ph, 3H), 7.11 (t, $^{3}J_{H–H}$ = 6.9 Hz, Ph, 1H), 6.86 (t, $^{3}J_{H–H}$ = 6.3 Hz, Ph, 2H), 6.79 (s, Mes, 1H), 6.60 (m, Mes, 1H and Ph, 2H), 6.37 (s, Mes, 1H), 6.04 (s, Mes, 1H), 2.30 (s, Me, 3H), 2.08 (s, Me, 3H), 1.99 (s, Me, 3H), 1.94 (s, Me, 3H), 1.28 (s, Me, 3H), 1.23 (s, Me, 3H) ppm. $^{13}C\{^{1}H\}$ NMR (126 MHz, $CDCl_3$, δ): 143.7, 143.6, 143.5, 142.8, 142.4, 141.5, 135.2, 135.0, 133.2, 133.2, 133.1, 133.0, 132.5, 132.4, 132.4, 132.2, 132.0, 131.8, 131.5, 130.9, 130.6, 130.3, 129.5, 128.9, 128.8, 128.64, 128.6, 128.5, 128.4, 128.2, 126.6, 126.5, 125.3, 124.6, 26.1, 26.0, 25.7, 24.7, 20.9, 20.5 ppm. $^{11}B\{^{1}H\}$ NMR (160 MHz, $CDCl_3$, δ): 13.6 ppm. $^{31}P\{^{1}H\}$ NMR (202 MHz, $CDCl_3$, δ): 11.1 ppm. Melting point: 229 °C. HRMS (EI): calcd for $C_{40}H_{38}BP$ 560.2811, found 560.2829. Anal. Calcd for $C_{40}H_{38}BP$: C 85.70, H, 6.80. Found: C 84.57, H 7.12. This sample was analyzed three times using crystals, and the results consistently showed a low carbon content, which may be caused by incomplete combustion of the boron atom.

2.2.5 Synthesis of 2.2

Compound **2.1** (30 mg, 0.054 mmol) was dissolved in 10 mL of dry degassed THF in a 50 mL Schlenk flask with a stir bar. The solution was cooled to 0 °C for 15 min. Iodobenzenedichloride (15 mg, 0.054 mmol) was added into the solution. The mixture was slowly warmed to room temperature and stirred overnight. The solvent was removed in vacuo, and the residue was dissolved in CH_2Cl_2. The addition of hexanes to the CH_2Cl_2 solution of **2.2** led to the isolation of colorless crystals of **2.2** in ~40% yield. ^{1}H NMR (500 MHz, $CDCl_3$, δ): 8.15 (d, $^3J_{H–H}$ = 8.0 Hz, Naph, 1H), 7.79 (d, $^3J_{H–H}$ = 8.0 Hz, Naph, 1H), 7.67 (br, Ph, 2H), 7.57 (d, $^3J_{H–H}$ = 6.8 Hz, Naph, 1H and Ph, 1H), 7.45 (m, Naph, 2H and Ph, 3H), 7.34 (q, $^3J_{H–H}$ = 6.9 Hz, Naph, 1H), 7.10 (m, Ph, 4H), 6.79 (s, Mes, 1H), 6.71 (s, Mes, 1H), 6.05 (s, Mes, 2H), 2.29 (s, Me, 6H), 1.97 (s, Me, 3H), 1.93 (s, Me, 3H), 1.80 (s, Me, 3H), 0.85 (s, Me, 3H) ppm; ^{13}C{^{1}H} NMR (126 MHz, $CDCl_3$, δ): 144.5, 141.9, 141.2, 140.1, 138.5, 135.1, 134.6, 133.7, 132.7, 131.5, 130.9, 129.5, 128.7, 127.7, 125.7, 122.8, 117.6, 116.7, 30.9, 29.8, 25.9, 25.3, 24.5, 20.5 ppm; ^{11}B{^{1}H} NMR (160 MHz, $CDCl_3$, δ): 7.3 ppm. ^{31}P{^{1}H} NMR (202 MHz, $CDCl_3$, δ): 42.5 ppm. Melting point: 271 °C. HRMS (ESI): calcd for $C_{40}H_{38}BPO$ $(M + H)^+$ 577.2839, found 577.2867. Anal. Calcd for $C_{40}H_{38}BPO$: C 83.30, H 6.60. Found: C 83.17, H 6.74.

2.2.6 Reactivity Studies

2.2.6.1 NMR Experiment of H_2 Activation by 2.1

A sealable J-Young NMR tube was charged with **2.1** (10 mg, 0.018 mmol) dissolved in dry C_6D_6 and sealed forming a clear solution. The sample was processed a freeze-pump-thaw procedure by liquid N_2 in order to degas the solution. The sample was exposed to a positive pressure of H_2 gas for 10 minutes at room temperature. The sample was sealed under 1 atm of H_2 and monitored over one week at room temperature by ^{1}H NMR spectra at different time intervals, which showed that there was no reaction between **2.1** and H_2. The same experiment was then performed at 75 °C. Again no reaction was observed after one week.

2.2.6.2 NMR Experiment of CO_2 Activation by 2.1

Experimental techniques and results are similar as described in **2.2.6.1**.

2.2.6.3 NMR Experiment of O_2 Activation by 2.1

Experimental techniques and results are similar as described in **2.2.6.1**.

2.2.6.4 NMR Experiment of Phenylacetylene Activation by 2.1

Inside of a glove box, a sealable J-Young NMR tube was charged with **2.1** (10 mg, 0.018 mmol) dissolved in dry degassed C_6D_6 with the addition of phenylacetylene (2 μL, 0.018 mmol). The sample was sealed for one week at room temperature followed by recording the ^{1}H NMR spectra at different time intervals without any change. The sample was then heated up to 75 °C for one week and did not show any change.

2.2.6.5 Photoreactivity Study of 2.1

Inside of a glove box, a NMR tube was charged with **2.1** (5 mg, 0.009 mmol) dissolved in dry degassed C_6D_6 and then subjected to UV irradiation at 350 nm inside a Rayonet photochemical reactor followed by recording the ^{1}H NMR spectra at different time intervals. The sample did not show any change.

2.2.7 Computational Studies

The density function theory (DFT) computations for compound **2.1** were performed using the Gaussian09, revision B.01[11a] software package and the High Performance Computing Virtual Laboratory (HPCVL) at Queen's University. The ground-state geometries for **2.1** were fully optimized at the B3PW91[11b–d]/6-31G(d,p)[11e,f] or CAMB3LYP/ SVP[12] level of theory. The initial geometric parameters in the calculations were employed from crystal structure data for geometry optimization. The opened and closed structures of **2.1** were characterized as minima on the potential energy surface through frequency calculations. Further time-dependent density function theory (TD-DFT) calculations were performed to obtain the vertical singlet excitation energies.

2.2.8 X-Ray Diffraction Analysis

Single crystals of **2.1** and **2.2** were mounted on glass fibers and were collected on a Bruker Apex II single-crystal X-ray diffractometer with graphite-monochromated Mo Kα radiation, operating at 50 kV and 30 mA and at 180 K. Data were processed on a PC with the aid of the Bruker SHELXTL software package (version 6.10)[13] and corrected for absorption effects. Compounds **2.1** and **2.2** belong to the monoclinic crystal space group P21/n and P21/c, respectively. All non-hydrogen atoms were refined anisotropically. The crystal data of **2.1** and **2.2** have been deposited at the Cambridge Crystallographic Data Center (CCDC 931932 and 931933).

Table 2.1. Crystal data and structure refinement for compound 2.1

Compound	**2.1**
Formula	C40H38B1P1
Formula weight	560.48
T, K	180(2)
Wavelength, Å	0.71073
Crystal system	Monoclinic
Space group	P2(1)/n
a, Å	10.0715(2)
α, °	90
b, Å	27.7173(4)
β, °	95.0840(10)
c, Å	11.3586(2)
γ, °	90
V, $Å^3$	3158.33(10)
Z	4
Density (calculated), Mg/m^3	1.179
Absorption coefficient, mm^{-1}	0.114
Theta range for data collection, °	2.59 to 27.12
Reflections collected	15267
Independent reflections	6929 [R(int) = 0.0243]
Completeness to theta = 27.04°	99.2 %
Data / restraints / parameters	6929 / 0 / 385
Goodness-of-fit on F^2	1.058
Final R indices [I>2sigma(I)]	
R_1[a]	0.0418
wR_2[b]	0.1040
R indices (all data)	
R_1[a]	0.0556
wR_2[b]	0.1115

[a] $R_1 = \sum [(|F_0| - |F_c|) / \sum |F_0|$

[b] $wR_2 = [\sum w[(F_0^2 - F_c^2)^2] / \sum [w(F_0^2)^2]]^{1/2}$

$w = 1 / [\sigma^2(F_0^2) + (0.075P)^2]$, where $P = [Max (F_0^2, 0) + 2F_c^2] / 3$

Table 2.2. Crystal data and structure refinement for compound 2.2

Compound	**2.2**
Formula	C40H38B1O1P1
Formula weight	576.48
T, K	293(2)
Wavelength, Å	0.71073
Crystal system	Monoclinic
Space group	P2(1)/c
a, Å	12.630(8)
α, °	90
b, Å	12.130(7)
β, °	105.285(7)
c, Å	21.567(13)
γ, °	90
V, $Å^3$	3187(3)
Z	4
Density (calculated), Mg/m^3	1.201
Absorption coefficient, mm^{-1}	0.117
Theta range for data collection, °	1.67 to 26.00
Reflections collected	17007
Independent reflections	6268 [R(int) = 0.1581]
Completeness to theta = 27.04°	99.8 %
Data / restraints / parameters	6268 / 0 / 394
Goodness-of-fit on F^2	0.970
Final R indices [I>2sigma(I)]	
R_1[a]	0.0697
wR_2[b]	0.1341
R indices (all data)	
R_1[a]	0.1954
wR_2[b]	0.1850

[a] $R_1 = \sum [(|F_0| - |F_c|) / \sum |F_0|$

[b] $wR_2 = [\sum w[(F_0^2 - F_c^2)^2] / \sum [w(F_0^2)^2]]^{1/2}$

$w = 1 / [\sigma^2(F_0^2) + (0.075P)^2]$, where $P = [Max (F_0^2, 0) + 2F_c^2] / 3$

Table 2.3. Crystallographic data for compounds 2.1

P(1)-C(7)	1.8098(14)
P(1)-C(17)	1.8200(15)
P(1)-C(11)	1.8274(15)
P(1)-B(1)	2.1612(16)
B(1)-C(1)	1.624(2)
B(1)-C(23)	1.628(2)
B(1)-C(32)	1.648(2)
C(1)-C(6)	1.4218(19)
C(6)-C(7)	1.419(2)
C(7)-P(1)-C(17)	104.53(7)
C(7)-P(1)-C(11)	108.83(6)
C(17)-P(1)-C(11)	103.42(7)
C(7)-P(1)-B(1)	93.92(6)
C(17)-P(1)-B(1)	118.88(6)
C(11)-P(1)-B(1)	124.75(7)
C(1)-B(1)-C(23)	109.58(12)
C(1)-B(1)-C(32)	118.37(12)
C(23)-B(1)-C(32)	118.90(12)
C(1)-B(1)-P(1)	93.82(9)
C(23)-B(1)-P(1)	117.67(10)
C(32)-B(1)-P(1)	95.21(9)
C(2)-C(1)-C(6)	116.78(13)
C(2)-C(1)-B(1)	123.67(13)
C(6)-C(1)-B(1)	119.55(12)
C(7)-C(6)-C(1)	118.62(12)
C(8)-C(7)-P(1)	128.37(12)
C(6)-C(7)-P(1)	110.90(10)
C(18)-C(17)-P(1)	121.36(12)
C(22)-C(17)-P(1)	119.72(12)
C(33)-C(32)-B(1)	124.71(13)
C(37)-C(32)-B(1)	119.34(13)

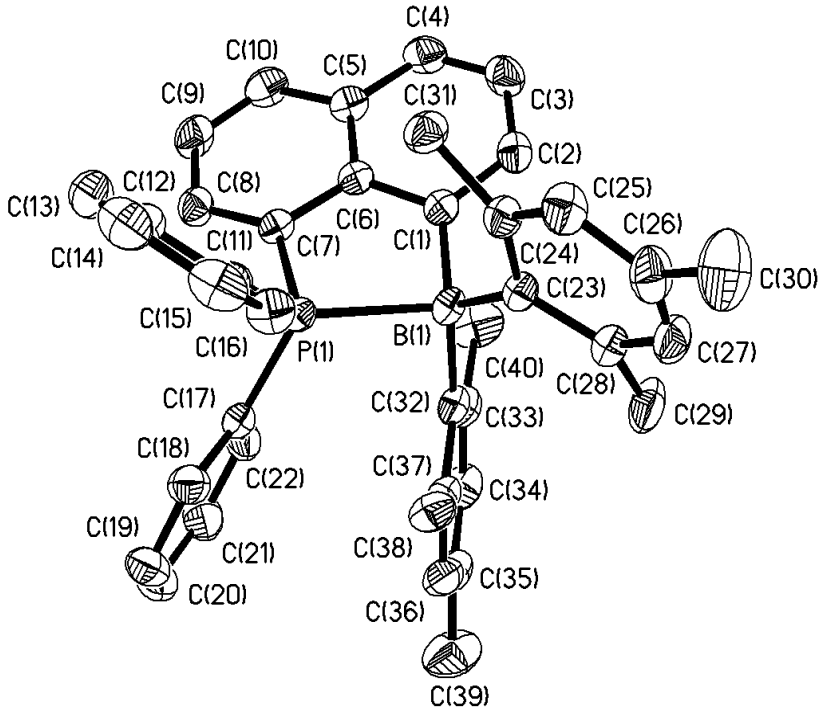

Figure 2.2. The ORETP diagram of compound **2.1** with 50% thermal ellipsoids and labeling schemes. H atoms were omitted for clarity.

Table 2.4. Crystallographic data for compounds 2.2

P(1)-O(1)	1.532(3)
P(1)-C(7)	1.779(4)
P(1)-C(11)	1.789(5)
P(1)-C(17)	1.803(4)
O(1)-B(1)	1.621(6)
B(1)-C(1)	1.623(7)
B(1)-C(32)	1.637(6)
B(1)-C(23)	1.655(6)
O(1)-P(1)-C(7)	108.60(19)
O(1)-P(1)-C(11)	108.64(18)
O(1)-P(1)-C(17)	115.10(18)
C(7)-P(1)-C(17)	110.7(2)
C(11)-P(1)-C(17)	105.4(2)
P(1)-O(1)-B(1)	119.7(2)
O(1)-B(1)-C(1)	103.9(4)
O(1)-B(1)-C(32)	108.2(3)
C(1)-B(1)-C(32)	110.0(4)
O(1)-B(1)-C(23)	101.4(3)
C(1)-B(1)-C(23)	116.8(4)
C(32)-B(1)-C(23)	115.2(4)
C(2)-C(1)-B(1)	121.3(4)
C(6)-C(1)-B(1)	122.1(4)

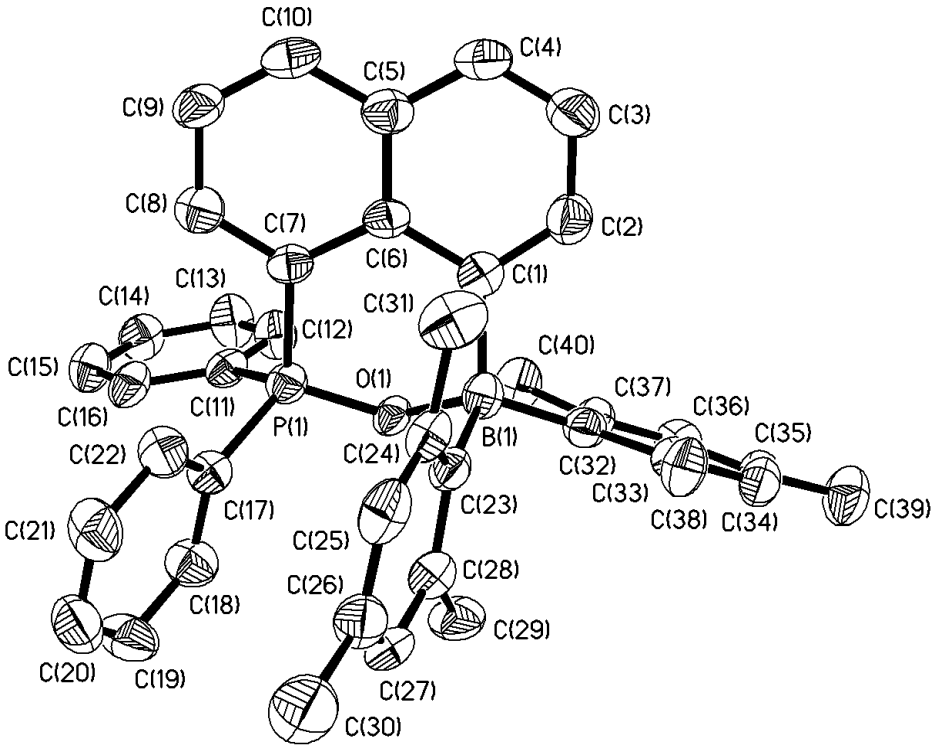

Figure 2.3. The ORETP diagram of compound **2.2** with 50% thermal ellipsoids and labeling schemes. H atoms were omitted for clarity.

2.3 Results and Discussion

2.3.1 Synthesis and Crystal Structure of 2.1

Compound **2.1** was synthesized in two lithiation steps using 1,8-diiodonaphthalene as the starting material. The first lithium-halogen exchange was quenched with PPh_2Cl to afford the intermediate compound 1-diphenylphosphino-8-iodonaphthalene. In the second step, the other iodide atom was replaced by -$BMes_2$ group followed by the conversion to the desired product **2.1** by a similar procedure where the quenching reagent was $BMes_2F$ (39% yield over the last two steps; Figure 2.4).

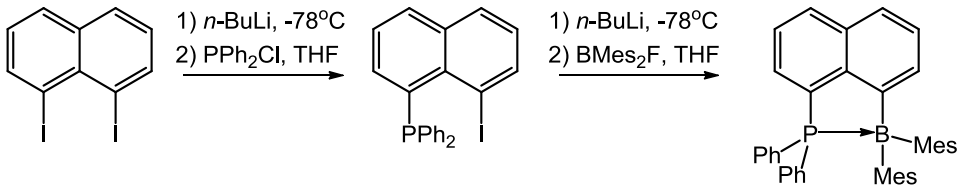

Figure 2.4. Synthetic procedure for compound **2.1**.

Compound **2.1** is a colorless solid and stable under air both in solution and the solid state. It was fully characterized by NMR, single-crystal X-ray diffraction, and elemental analyses. NMR spectroscopic data of compound **2.1** supports the presence of a dative bond between the P and B atoms. The $^{31}P\{^1H\}$ NMR spectrum of **2.1** has a signal at ~11 ppm, which is shifted about 20 ppm downfield compared to that of 1-diphenylphosphino-8-iodonaphthalene (-12.5 ppm). In addition, the ^{11}B NMR spectrum displays a signal at ~14 ppm, which is similar to that[4] of compound **A** shown in Figure 2.1 and is typical of four-coordinated boron in a similar environment.[14] It is noteworthy that the six methyl groups from the two mesityls in **2.1** display their own distinct and well-resolved chemical shifts (Figure 2.5) in the ^1H NMR spectrum at room temperature, indicating a highly congested structure.

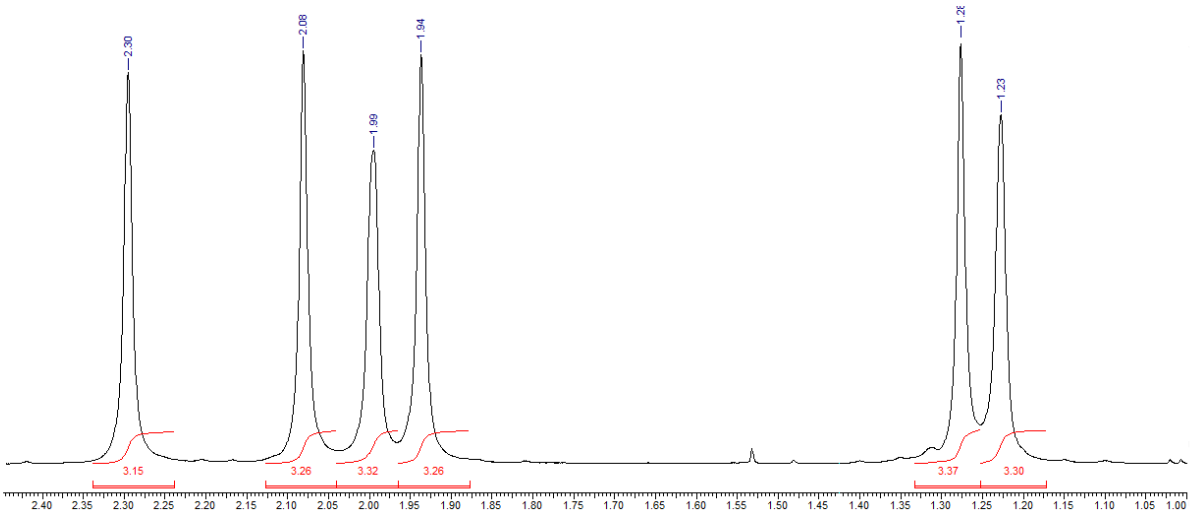

Figure 2.5. ^{1}H NMR (aliphatic region) spectrum of compound **2.1**.

The presence of a P-B bond in **2.1** was confirmed by a single-crystal X-ray diffraction analysis. The crystal structure of **2.1** is shown in Figure 2.6, and the key bond lengths and angles are given in Table 2.3. The P-B bond length is 2.1612(16) Å, which is similar to that[4] of **A** (2.173(4) Å) and some of the previously reported triarylphosphine-triarylborane adducts.[14a,15] The crystal structure confirmed that **2.1** is indeed a highly congested molecule. Each phenyl and mesityl group has a distinct environment and is interlocked because of the extensive intramolecular interactions between the aryl groups. For example, as shown in Figure 2.6, significant π-stacking interactions between a mesityl and phenyl ring with an approximately face-to-face orientation are evident. π-Stacking interactions are also evident in the other pair of mesityl and phenyl rings, albeit to a lesser degree. C-H···π interactions are extensive within this molecule. The boron center is out of the trigonal planar geometry with three aryl groups by ~14°. The average B-C bond length is 1.633(2) Å, typical of four-coordinate $BMes_2$ compounds.[16] The phosphorus atom has a highly distorted tetrahedral geometry with a very small C7-P-B bond angle (93.92(6)°). The side view of the structure shows that **2.1** has an approximately eclipsed conformation with a PC7C1B torsion angle of 13.7°.

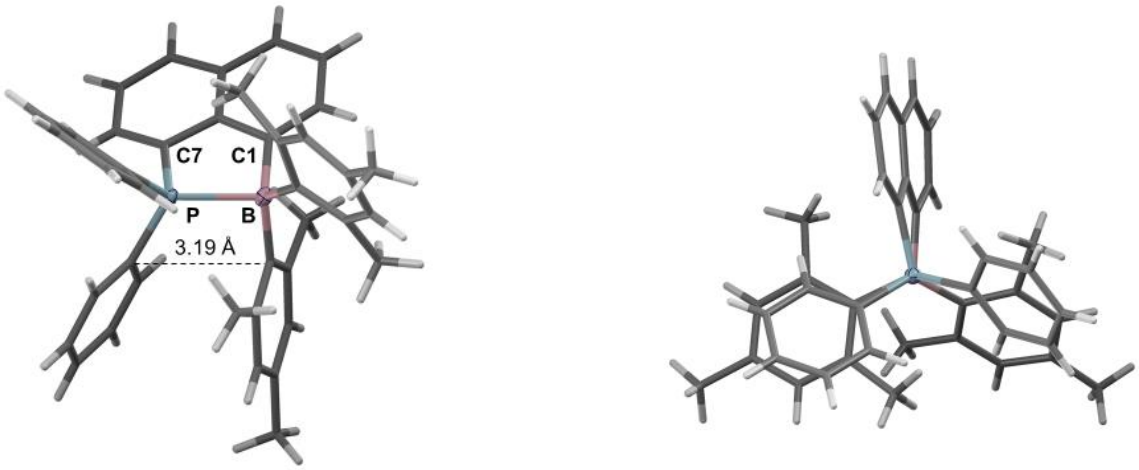

Figure 2.6. The front view (left) and the side-view (right) of the crystal structures of **2.1**.

The formation of the P-B bond in **2.1** in solution and in the crystal lattice is quite surprising, considering the fact that PPh_3 does not bind to $BMes_2Ph$ at all in solution or the solid state and the $BMes_2Ar$ unit is usually not accessible by nucleophiles larger than F^-, OH^-, or CN^-.[8] This phenomenon appears to contradict the commonly accepted consequence of "frustration" imposed by steric congestion.[1] We believe, however, that the formation of the P-B dative bond in **2.1** is mainly facilitated by the rigid 1,8-naphthalene linker, which forces the donor and acceptor to bind together, despite the congestion. Similar congested four-coordinated $BMes_2$ compounds with a five-membered chelate ring are known, which all involve the binding of an internal donor such as a pyridyl, a thiazolyl, or an N-heterocyclic carbene to the boron center.[16] Among all known four-coordinated $BMes_2$ compounds, compound **2.1** is certainly the most congested because of the large and rigid aryl groups on the P and B centers. At ~80 °C in C_6D_6, the ^{11}B signal of **2.1** shifts from ~14 ppm to ~22 ppm (Figure 2.7) and the ^{31}P signal moved from ~11 ppm to ~9 ppm (Figure 2.8), which supports the retention of the P-B bond, albeit a weakened one, compared to that at room temperature.

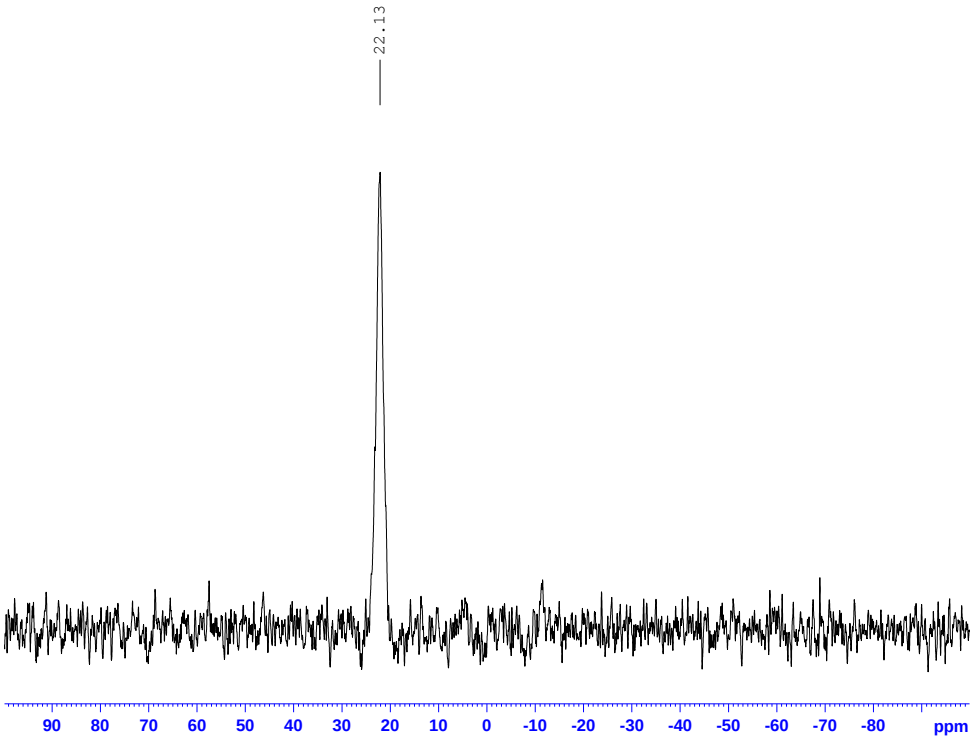

Figure 2.7. $^{11}B\{^{1}H\}$ NMR spectrum of **2.1** at 353 K in C_6D_6.

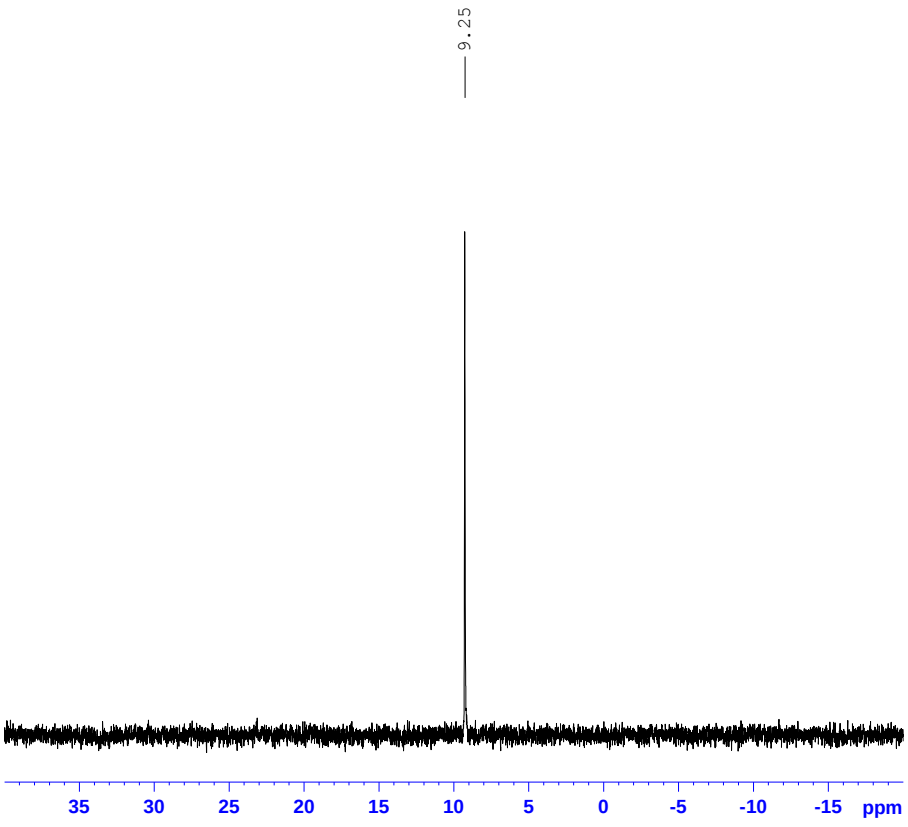

Figure 2.8. $^{31}P\{^{1}H\}$ NMR spectrum of **2.1** at 353 K in C_6D_6.

DFT computational analyses using the Gaussian 09 suite of programs[11a] at either the B3PW91[11b–d]/6-31G(d,p)[11e,f] or the CAM-B3LYP/SVP[12] level of theory were performed. The non-bound (open) and the bound (closed) form of **2.1** were found as two minima on the potential energy surface through frequency calculations. For the open form (Figure 2.9), the calculated P-B separation distance is 3.06 Å (CAM-B3LYP/SVP) or 2.99 Å (B3PW91/6-31G(d,p)), with the lone pair of the phosphine pointing toward the boron center.

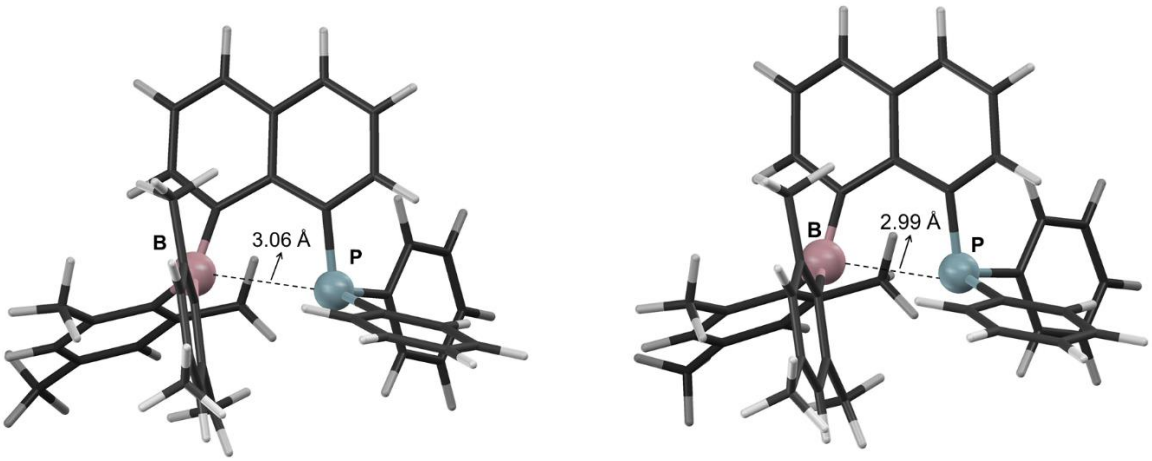

Figure 2.9. DFT-optimized structures of the open form of **2.1** based on CAM-B3LYP/SVP (left) and B3PW91/6-31G(d,p) (right).

For the closed form (Figure 2.10), the calculated P-B bond length is 2.23 Å. Surprisingly, the computational data consistently showed that the open form and the closed form of **2.1** are very similar in energy, as evidenced by the difference of the zero point energy (corrected), 4.43 kJ/ mol, with the open form being the more stable one. The calculated barrier from the open form to the transition state is only 5.28 kJ/mol (B3PW91/6-31G(d,p)). Thus, it is conceivable that compound **2.1** rapidly interconverts between the open and the closed form in solution, with the P-B bond oscillating between 2.23 and 2.99 or 3.06 Å.

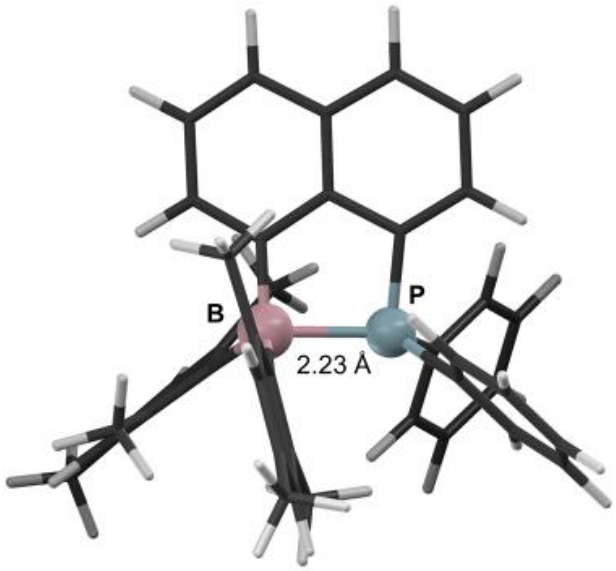

Figure 2.10. DFT-optimized structure of the closed form of **2.1**.

2.3.2 Photophysical Properties and Reactivity of 2.1

Previously we have reported a number of N,C-chelate four-coordinate boron compounds involving the $BMes_2$ unit (e.g., $B(ppy)Mes_2$, ppy = 2-phenylpyridyl) (Figure 2.11).[16d–f,h] The steric congestion in the N,C-chelate $BMes_2$ compounds was found to be one of the key driving forces for their facile and reversible photoisomerization. We were therefore interested in the photoreactivity of the new P,C-chelate compound **2.1**.

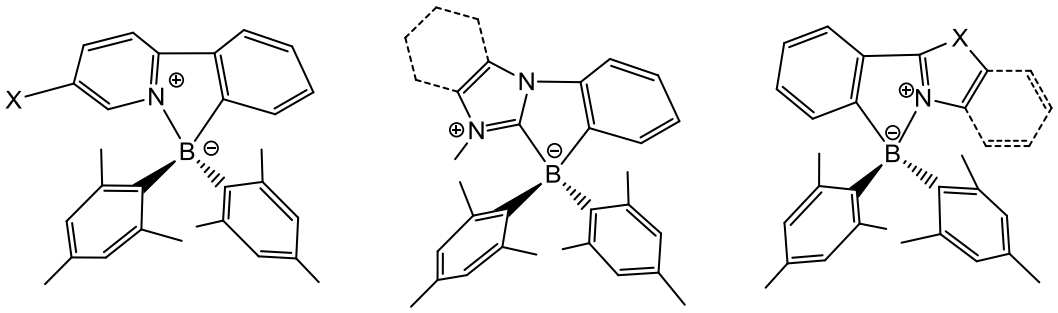

Figure 2.11. Examples of N,C-chelate four-coordinate boron compounds.

As shown in Figure 2.12, the UV-vis spectrum of **2.1** has an intense absorption band in the region of 340 to 390 nm with λ_{max} = ~350 nm. Irradiation at 350 nm, however, did not cause any change of the molecule,

according to NMR and UV-vis spectra. The other interesting observation is that compound **2.1** is not fluorescent at all, unlike B(ppy)Mes_2 and derivatives, which are all fluorescent.

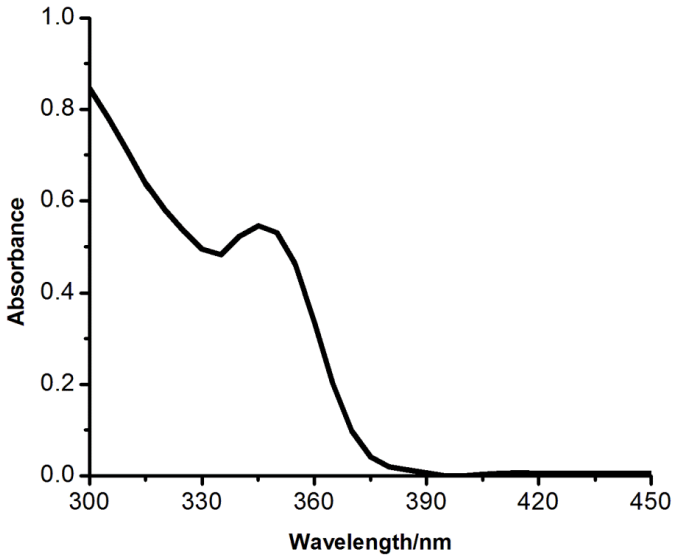

Figure 2.12. Absorption spectrum of **2.1** in CH_2Cl_2 (1.0×10^{-4} M).

DFT calculations indicated that the LUMO level of compound **2.1** is localized on the naphthyl ring with a very large contribution from the P-C7 π orbitals, while the HOMO level is a mixture of π orbitals on the naphthyl and mesityl in addition to a large contribution from the P-B σ bond (Figure 2.13). TD-DFT computational results indicate that the electronic transition involving the first excited state is a HOMO → LUMO transition (97%, f = 0.0452) (mesityl (π) → naph-P (π*) and P-B (σ) → naph-P (π*)). This is quite different from that of B(ppy)Mes_2, in which the HOMO to LUMO transition consists of mainly the mesityl (π)→ ppy (π*) transition, which drives the photo-isomerization process. Because of the rapid oscillation of the P-B bond between the bound and non-bound form in solution, the P-B (σ) → naph-P (π*) transition could effectively quench fluorescence *via* thermal vibrational pathways. The effective competition of the $\sigma_{P-B} \rightarrow \pi_{naph}^*$ transition with the $\pi_{mes} \rightarrow \pi_{naph}^*$ transition could also be responsible for the lack of photoreactivity. Thus, compound **2.1** is a thermally and photochemically stable molecule, despite its highly congested nature.

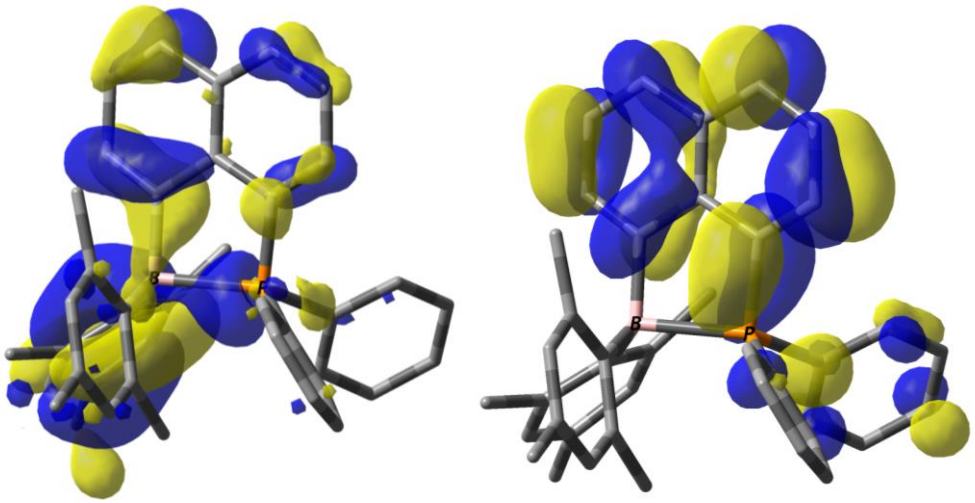

Figure 2.13. HOMO (left) and LUMO (right) orbital diagrams of compound **2.1** (isocontour value = 0.03).

The persistent P-B bond in compound **2.1** is also reflected by its high chemical stability toward small molecules. Compound **2.1** does not react with H_2, O_2, phenylacetylene, or CO_2 upon heating or photoirradiation. The lack of reactivity to activate small molecules like other FLPs is probably due to the steric congestion of the whole compound, which prevents the attack on small reactants. Further, the rigid naphthalene linker fixes the electron donor and acceptor groups to form a relatively stable bond and the boron center is not as electron deficient as $B(C_6F_5)_2Ar$ which is the common Lewis acid component in other reactive FLPs.[1, 2, 3, 7]

The only species that have been found to react with compound **2.1** are halogen molecules such as $PhI{\cdot}Cl_2$ or I_2 (Figure 2.14). However, our attempts to isolate the products from the reaction with halogen oxidants have consistently led to the isolation of an interesting oxo-bridged product, compound **2.2**, presumably due to the hydrolysis of the halide product with adventitious water in the solvent, which is not surprising since PPh_3Cl_2 is well known to hydrolyze, forming $O{=}PPh_3$ as the product.[17]

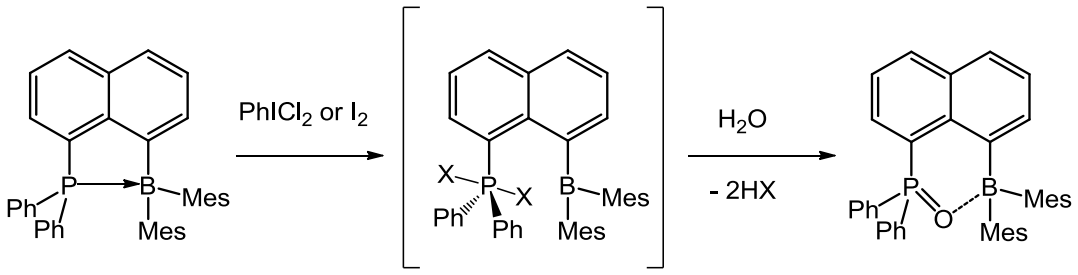

Figure 2.14. Proposed pathway for the formation of compound **2.2**.

^{31}P NMR spectra indeed confirmed the oxidation of **2.1** by PhI·Cl_2 or I_2. However, the reaction with PhI·Cl_2 is very messy, with multiple products (Figure 2.15). The reaction with I_2 is slower but much cleaner. The addition of D_2O to the NMR solutions of the oxidized mixture indeed generated compound **2.2**, along with unidentified species (see Figure 2.16). The precursor compound that led to the formation of compound **2.2** is likely a five-coordinate compound (**2.1**-X_2), as shown in Figure 2.14. The $^{31}P\{^1H\}$ NMR spectrum of **2.2** has a peak at ~43 ppm, which is ~31 ppm downfield from that of compound **2.1**, supporting the change of the phosphorus oxidation state from +3 to +5. Compared to that[18] of O=PPh_3, the ^{31}P chemical shift of **2.2** is about 20 ppm downfield shifted, which can be attributed to the formation of a B-O bond with the same oxygen atom. In fact, it has been demonstrated previously that the formation of a dative bond between the oxygen atom of O=PPh_3 and a Lewis acid can cause a significant downfield shift of the ^{31}P chemical shift.[18] The $^{11}B\{^1H\}$ NMR spectrum of **2.2** exhibits a signal at ~7 ppm, which is about 5 ppm upfield shifted, relative to that of **2.1**, perhaps due to the greater σ donation to the boron atom by the oxygen atom.

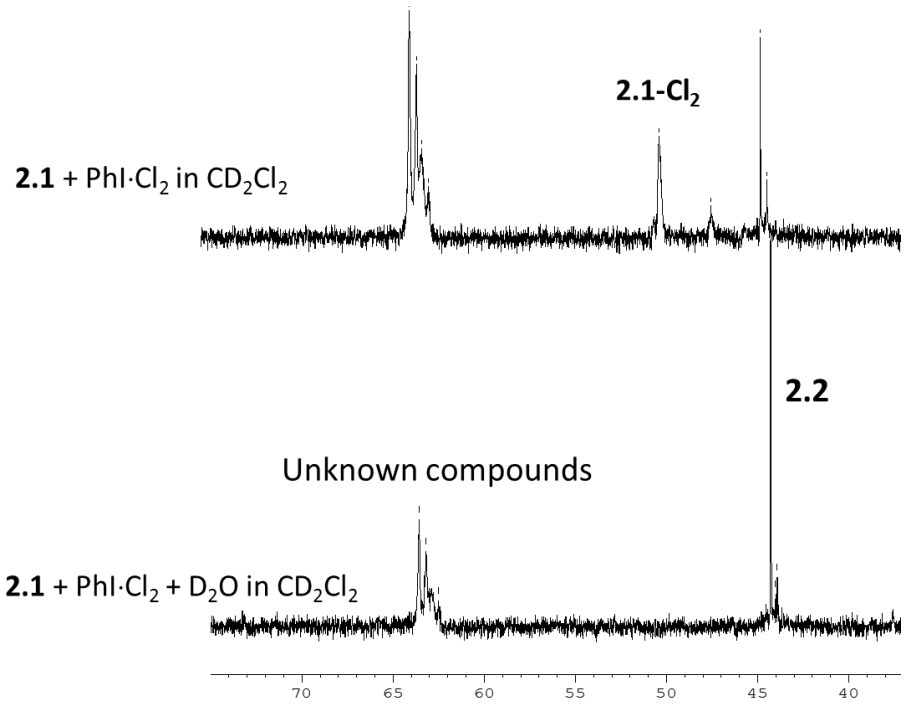

Figure 2.15. Stacked ^{31}P NMR spectra showing the oxidation of **2.1** by $PhI{\cdot}Cl_2$ (1.5 equiv.) and the conversion of the oxidized compounds to **2.2** after the addition of D_2O in CD_2Cl_2.

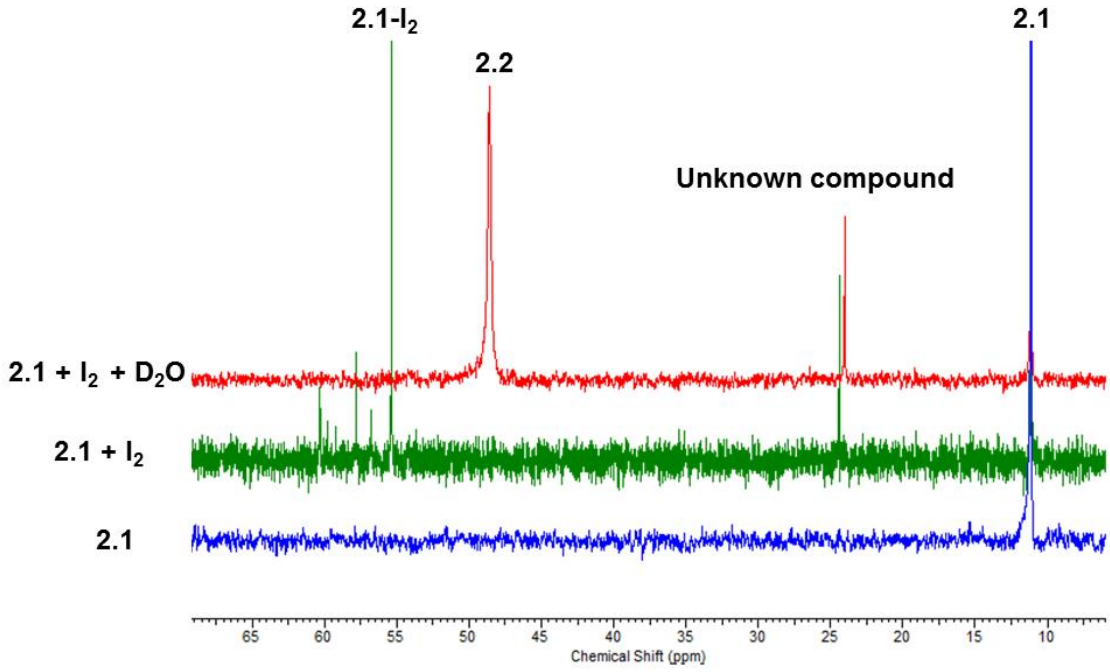

Figure 2.16. Stacked $^{31}P\{^{1}H\}$ NMR spectra showing the oxidation of **2.1** by I_2 (1.5 equiv.) and the conversion of the oxidized compounds to **2.2** after the addition of D_2O in $CDCl_3$.

The crystal structure of **2.2** is shown in Figure 2.17. The P-O bond length (1.532(3) Å) is consistent with a P=O bond, although it is considerably longer than that[19] in $O=PPh_3$ (1.479(2) Å) because of the formation of a dative O-B bond involving the same oxygen atom. The P-O bond in **2.2** is however shorter than that of a 1,2-azaborine adduct with a triphenylphosphine oxide (1.5563(13) Å), in which the boron atom is bound to the oxygen atom with a trigonal planar geometry.[20] The B-O bond length (1.621(6) Å) is somewhat longer than the typical B-O bond lengths reported previously in four-coordinated boron compounds,[21] because of the highly congested environment around the boron center. The P-C bond lengths in **2.2** are all notably shorter than those in **2.1**. The P(1)-C(7)-C(1)-B(1) torsion angle (19.8(4)°) is much greater than that of **2.1**. The POBCCC six-membered ring has a half-chair conformation. The tetrahedral geometry around the phosphorus center is much less distorted compared to that in **2.1** because

of the reduced congestion. Nonetheless, one mesityl ring and one phenyl ring in **2.2** maintain the face-to-face parallel orientation as observed in **2.1** with significant π-stacking interactions.

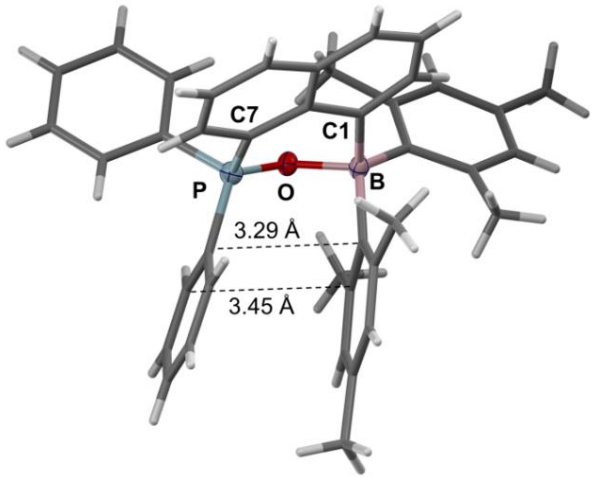

Figure 2.17. The front view of the crystal structures of **2.2**.

The low-energy absorption bands in the UV-vis spectrum of **2.2** is blue-shifted compared to those of **2.1** (Figure 2.18), consistent with the cleavage of the P-B dative bond and the oxidation of the phosphorus center.

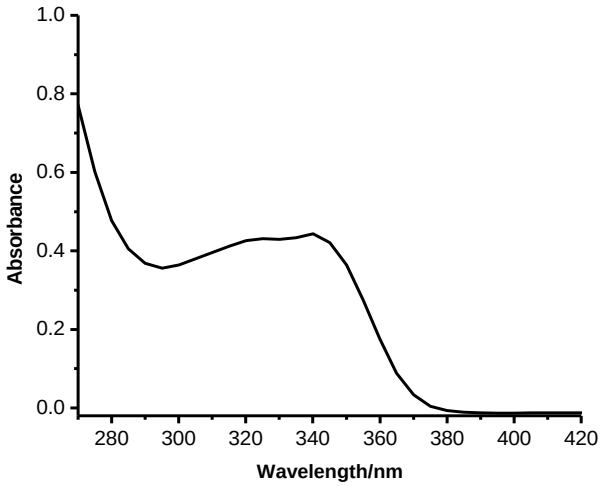

Figure 2.18. Absorption spectrum of **2.2** in CH_2Cl_2 (1.0×10^{-4} M).

2.4 Conclusions

Despite the high degree of steric congestion, compound **2.1** was found to possess a typical P-B dative bond that is persistent in solution, which is surprisingly different from the classical description of "Frustrated Lewis Pairs". Upon exposure of **2.1** to different stimuli such as heat or light, no changes were observed. Based on DFT calculations, **2.1** is believed to exist in equilibrium between two forms, termed as open and closed, which both possess similar ground state energies. Thus, it is conceivable that compound **2.1** rapidly interconverts between these forms in solution, which corresponds to P-B bond oscillation between 2.23 and 3.05 Å. **2.1** displays no reactivity toward common small molecules, with the exception of halogens reagents such as I_2 or $PhICl_2$. The high stability of **2.1** can be attributed to the highly congested nature of the molecule and the highly rigid 1,8-naphthyl linker which prevents the existence of a "non-neutralized" donor-acceptor species. The reaction of **2.1** with halogens in the presence of water leads to the formation and isolation of a P-O-B compound **2.2**, which is also very sterically congested.

References:

(1) For recent reviews, see: (a) Stephan, D. W.; Erker, G. *Angew. Chem., Int. Ed.* **2010**, *49*, 46. (b) Voss, T.; Chen, C.; Kehr, G.; Nauha, E.; Erker, G.; Stephan, D. W. *Chem. Eur. J*. **2010**, *16*, 3005.(c) Stephan, D. W. *Dalton Trans*. **2009**, 31229. (d) Stephan, D. W.; Greenberg, S.; Graham, T. W.; Chase, P.; Hastie, J. J.; Geier, S. J.; Farrell, J. M.; Brown, C. C.; Heiden, Z. M.; Welch, G. C.; Ullrich, M. *Inorg. Chem*. **2011**, *50*, 12338.

(2) (a) Stephan, D. W. *Org. Biomol. Chem*. **2012**, *10*, 5740 and references therein. (b) Stephan, D. W.; Erker, G. *Angew. Chem. Int. Ed*. **2015**, *54*, 6400 and references therein.

(3) (a) Welch, G. C.; San Juan, R. R.; Masuda, J. D.; Stephan, D. W. *Science* **2006**, *314*, 1124. (b) Chase, P. A.; Welch, G. C.; Jurca, T.; Stephan, D. W. *Angew. Chem., Int. Ed*. **2007**, *46*, 8050. (c) Spies, P.; Erker, G.; Kehr, G.; Bergander, K.; Frohlich, R.; Grimme, S.; Stephan, D. W. *Chem. Commun*. **2007**, *47*, 5072. (d) Spies, P.; Schwendemann, S.; Lange, S.; Kehr, G.; Frohlich, R.; Erker, G. *Angew. Chem., Int. Ed*. **2008**, *47*, 7543.

(4) (a) Tsurusaki, A.; Sasamori, T.; Wakamiya, A.; Yamaguchi, S.; Nagura, K.; Irle, S.; Tokitoh, N. *Angew. Chem., Int. Ed*. **2011**, *50*, 10940. (b) Bontemps, S.; Devillard, M.; Mallet-Ladeira, S.; Bouhadir, G.; Miqueu, K.; Bourissou, D. *Inorg. Chem*. **2013**, *52*, 4714.

(5) For general review articles, see: (a) Hoefelmeyer, J. D.; Schulte, M.; Tshinkl, M.; Gabbaï. *Coord. Chem. Rev*. **2002**, *235*, 93 and references therein. (b) Killian, P.; Knight, F. R.; Woollins, J. D. *Chem. Eur. J*. **2011**, *17*, 2302 and references therein.

(6) (a) Zhao, H.; Gabbaï, F. P. *Organometallics* **2012**, *31*, 2327. (b) Zhao, H.; Gabbaï, F. P. *Nat. Chem*. **2010**, *2*, 984. (c) Chiu, C.-W.; Gabbaï, F. P. *Dalton Trans*. **2008**, *6*, 814. (d) Chiu, C.-W.; Gabbaï, F. P. *J. Am. Chem. Soc.* **2006**, *128*, 14248. (e) Melaimi, M.; Sole, S.; Chiu, C.-W.; Wang, H.; Gabbaï, F. P. *Inorg. Chem*. **2006**, *45*, 8136.

(7) Wang, H.; Frohlich, R.; Kehr, G.; Erker, G. *Chem. Commun*. **2008**, *45*, 5966.

(8) (a) Liu, X.; Bai, D.; Wang, S. *Angew. Chem., Int. Ed.* **2006**, *45*, 5475. (b) Bai, D.; Liu, X.; Wang, S. *Chem. Eur. J.* **2007**, *13*, 5713. (c) Hudson, Z. M.; Liu, X.; Wang, S. *Org. Lett.* **2011**, *13*, 300. (d) Li, Y.; Kang, Y.; Lu, J.; Wyman, I.; Ko, S.; Wang, S. *Organometallics*, **2014**, *33*, 964 -973.

(9) Wade, C. R.; Broomsgrove, A. E. J.; Aldridge, S.; Gabbaï, F. P. *Chem. Rev.* **2010**, *110*, 3958.

(10) (a) House, H. O.; Koepsell, D. G.; Campbell, W. J. *J. Org. Chem.* **1972**, *37*, 1003. (b) Schiemenz, G. P. *Phosphorus, Sulfur Silicon* **2000**, *163*, 185.

(11) (a) Frisch, M. J.; Trucks, G. W.; Schlegel, H. B.; Scuseria, G. E.; Robb, M. A.; Cheeseman, J. R.; Scalmani, G.; Barone, V.; Mennucci, B.; Petersson, G. A.; Nakatsuji, H.; Caricato, M.; Li, X.; Hratchian, H. P.; Izmaylov, A. F.; Bloino, J.; Zheng, G.; Sonnenberg, J. L.; Hada, M.; Ehara, M.; Toyota, K.; Fukuda, R.; Hasegawa, J.; Ishida, M.; Nakajima, T.; Honda, Y.; Kitao, O.; Nakai, H.; Vreven, T.; Montgomery, J. A., Jr.; Peralta, J. E.; Ogliaro, F.; Bearpark, M.; Heyd, J. J.; Brothers, E.; Kudin, K. N.; Staroverov, V. N.; Keith, T.; Kobayashi, R.; Normand, J.; Raghavachari, K.; Rendell, A.; Burant, J. C.; Iyengar, S. S.; Tomasi, J.; Cossi, M.; Rega, N.; N.; Millam, J. M.; Klene, M.; Knox, J. E.; Cross, J. B.; Bakken, V.; Adamo, C.; Jaramillo, J.; Gomperts, R.; Stratmann, R. E.; Yazyev, O.; Austin, A. J.; Cammi, R.; Pomelli, C.; Ochterski, J. W.; Martin, R. L.; Morokuma, K.; Zakrzewski, V. G.; Voth, G. A.; Salvador, P.; Dannenberg, J. J.; Dapprich, S.; Daniels, A. D.; Farkas, O.; Foresman, J. B.; Ortiz, J. V.; Cioslowski, J.; Fox, D. J. Gaussian09; Gaussian, Inc.: Wallingford, CT, 2010. (b) Perdew, J. P.; Chevary, J. A.; Vosko, S. H.; Jackson, K. A.; Pederson, M. R.; Singh, D. J.; Fiolhais, C. *Phys. Rev. B* **1992**, *46*, 6671. (c) Perdew, J. P.; Chevary, J. A.; Vosko, S. H.; Jackson, K. A.; Pederson, M. R.; Singh, D. J.; Fiolhais, C. *Phys. Rev. B.* **1993**, *48*, 4978. (d) Perdew, J. P.; Burke, K.; Wang, Y. *Phys. Rev. B* **1996**, *54*, 16533. (e) Becke, A. D. *J. Chem. Phys.* **1993**, *98*, 5648. (f) Lee, C.; Yang, W.; Parr, R. G. *Phys. Rev. B.* **1988**, *37*, 785.

(12) (a) Yanai, T.; Tew, D.; Handy, N. *Chem. Phys. Lett.* **2004**, *393*, 51. (b) Schaefer, A.; Horn, H.; Ahlrichs, R. *J. Chem. Phys.* **1992**, *97*, 2571.

(13) *SHELXTL* Version 6.14; Bruker AXS: Madison, WI, 2000-2003.

(14) (a) Guillemot, G.; Castellano, B.; Prangé, T.; Solari, E.; Floriani, C. *Inorg. Chem*. **2007**, *46*, 5149. (b) Sircoglous, M.; Bontemps, S.; Mercy, M.; Miques, K.; Ladeira, S.; Saffon, N.; Maron, L.; Bouhadir, G.; Bourissou, D. *Inorg. Chem*. **2010**, *49*, 3983.

(15) (a) Jacobsen, H.; Berke, H.; Döring, S.; Kehr, G.; Erker, G.; Fröhlich, R.; Meyer, O. *Organometallics* **1999**, *18*, 1724. (b) Bradley, D. C.; Harding, I. S.; Keefe, A. D.; Motevalli, M.; Zheng, D. H. J. *Chem. Soc., Dalton Trans*. **1996**, 3931.

(16) (a) Wakamiya, A.; Taniguchi, R.; Yamaguchi, S. *Angew. Chem., Int. Ed*. **2006**, *45*, 3170. (b) Bebbington, M. W. P.; Bontemps, S.; Bouhadir, G.; Bourissou, D. *Angew. Chem., Int. Ed*. **2007**, *46*, 3333. (c) Fukazawa, A.; Yamada, H.; Yamaguchi, S. *Angew. Chem., Int. Ed*. **2008**, *47*, 5582. (d) Rao, Y. L.; Amarne, H.; Zhao, S. B.; McCormick, T. M.; Martic, S.; Sun, Y.; Wang, R. Y.; Wang, S. *J. Am. Chem. Soc*. **2008**, *130*, 12898. (e) Amarne, H.; Baik, C.; Murphy, S. K.; Wang, S. *Chem. Eur. J*. **2010**, *16*, 4750. (f) Rao, Y. L.; Chen, L. D.; Brown, M. L.; Mosey, N. J.; Wang, S. *J. Am. Chem. Soc*. **2012**, *134*, 11026. (g) Nagura, K.; Saito, S.; Fröhlich, R.; Glorius, F.; Yamaguchi, S. *Angew. Chem., Int. Ed*. **2012**, *51*, 7762. (h) Rao, Y. L.; Amarne, H.; Chen, L. D.; Brown, M. L.; Mosey, N. J.; Wang, S. *J. Am. Chem. Soc*. **2013**, *135*, 3407.

(17) Yano, T.; Kuroboshi, M.; Tanaka, H. *Tetrahedron Lett*. **2010**, *51*, 698.

(18) Zeldin, M.; Mehta, P.; Vernon, W. D. *Inorg. Chem*. **1979**, *18*, 463.

(19) Al-Farhan, K. A. *J. Crystallogr. Spectrosc. Res*. **1992**, *22*, 687.

(20) Marwitz, A. J. V.; Jenkins, J. T.; Zakharov, L. N.; Liu, S.-Y. *Organometallics* **2011**, *30*, 52.

(21) (a) Cui, Y.; Liu, Q. D.; Bai, D. R.; Jia, W. L.; Tao, Y.; Wang, S. *Inorg. Chem*. **2005**, *44*, 601. (b) Wu, Q.; Esteghamatian, M.; Hu, N.-X.; Popovic, Z.; Enright, G.; Wang, S.; Tao, Y.; D'Iorio, M. *Chem. Mater*. **2000**, *12*, 79.

Chapter 3

A Dual-Emissive Phosphine-Borane Lewis Pair with a U-Shaped Linker and Its Fluoride Binding Study

3.1 Introduction

Triarylboryl functionalized donor-acceptor compounds can display charge transfer (CT) transitions from electron donating groups to empty p orbitals of electron accepting groups. The fluorescence intensity of these systems usually depends on the linker used to connect the donor and acceptor components,[1,2a-c] and have been extensively studied for applications in optoelectronic and sensing materials.[1,2] Nonconjugated donor-acceptor compounds containing triarylboryl groups are particularly interesting because they facilitate turn-on fluorescent sensing for small anions[2a-c] and may possess unusual reactivity such as those observed for Frustrated Lewis Pairs.[3] Previously our group has fully investigated V- and U-shaped nonconjugated donor-acceptor amino-borane systems which display through-space CT fluorescence and affinity for fluoride and other small nucleophiles.[2a-c] Recently a number of nonconjugated phosphine-borane compounds, which contain triarylphosphines as electron donating groups, have been reported where each moiety is directly attached to a 1,8-naphthyl backbone.[4] However, because the donor and acceptor groups in these systems can form dative bonds with each other or are in very close proximity (P-B distance 2.08 - 3.05 Å) due to the rigid naphthalene skeleton, they show few interesting photophysical or chemical properties.[4] To obtain a greater distance between the phosphine/borane moieties and facilitate through-space CT fluorescence, one effective approach is to insert a linker between the naphthyl and the P and B atoms to force the donor and acceptor groups apart. Such systems would allow us to access not only new through-space CT systems for sensing applications but also unusual reactivity introduced by the bulky phosphine group, which is much more reactive than the conjugated amino group.[3] On the basis of these considerations, we have synthesized and investigated the first example of a U-shaped nonbound

donor-acceptor compound containing triarylphosphine as the Lewis base and triarylborane as the Lewis acid **3.1** (Figure 3.1), which displays intense dual emission and can be used as a turn-on fluoride senor.

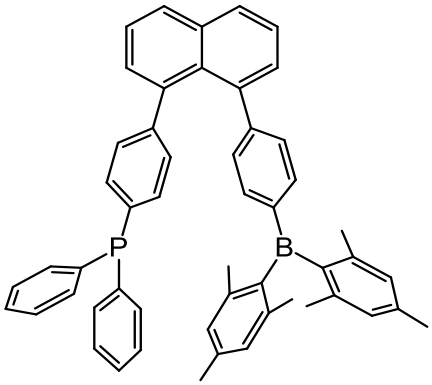

Figure 3.1. Target molecule **3.1**.

3.2 Experimental

3.2.1 General Procedures

All reactions were carried out under a nitrogen atmosphere. Reagents were purchased from Aldrich Chemical Company and used without further purification. Thin-layer and flash chromatography were performed on silica gel. ^{1}H, ^{13}C and ^{31}P NMR spectra were recorded on Bruker Avance 400 or 500 MHz spectrometers. Deuterated solvents were purchased from Cambridge Isotopes. UV-vis spectra were recorded on a Varian Cary 50 Bio spectrometer. Emission spectra were recorded using a Photon Technologies International QuantaMaster Model 2 spectrometer. Solution quantum yields were calculated using optically dilute solutions ($A \approx 0.1$) relative to 9,10-diphenylanthracene ($\Phi = 0.90$). Elemental analyses were conducted at Laboratoire d'Analyse Élémentaire de l'Université de Montréal.

3.2.2 Synthesis of 1,8-Diiodonaphthalene

Experimental techniques and synthetic procedure are as same as described in **2.2.2**.

3.2.3 Synthesis of 1-Diphenylphosphino-4-bromobenzene

1,4-Dibromobenzene (3 g, 12.7 mmol) was dissolved in 30 mL dry degassed THF in a 50 mL Schlenk flask with a stir bar. The solution was cooled to -78 °C for 15 min, then *n*-BuLi (5.6 mL, 2.5 M in hexanes, 14.0 mmol) was added dropwise by syringe. The mixture was stirred 1 hour at -78 °C and 2.35 mL of $ClPPh_2$ (12.7 mmol) is added in a dropwise manner. After warming the mixture to ambient temperature and stirring overnight. The solvent is removed by rota-evaporation and the residue was partitioned between CH_2Cl_2 and water. The mixture was extracted twice with CH_2Cl_2, and the combined organic layers were dried using $MgSO_4$ and filtered. The mixture was purified on silica gel (hexanes as eluent) to afford 4.1 g of 1-diphenylphosphino-4-bromo-benzene as white solid (95% yield). ^{1}H NMR (300 MHz, d_6-acetone, δ): 7.52 (2H), 7.37 - 7.33 (6H), 7.26 (4H), 7.16 (2H) ppm; ^{13}C NMR (75.4 MHz, d_6-acetone, δ): 137.28, 137.04, 135.38, 133.72, 131.67, 128.66, 128.94, 123.26 ppm; ^{31}P NMR (121 MHz, d_6-acetone, δ): -5.7 ppm.

3.2.4 Synthesis of 1-Dimesitylboryl-4-bromobenzene

1,4-Dibromobenzene (1 g, 4.2 mmol) was dissolved in 20 mL dry degassed THF in a 50 mL Schlenk flask with a stir bar. The solution was cooled to -78 °C for 15 min, then *n*-BuLi (2.9 mL, 1.6 M in hexanes, 4.6 mmol) was added dropwise by syringe. The mixture was stirred 1 hour at -78 °C and 1.14 g of $BMes_2F$ (4.2 mmol) is added. After warming the mixture to ambient temperature and stirring overnight. The solvent is removed by rota-evaporation and the residue was partitioned between CH_2Cl_2 and water. The mixture was extracted twice with CH_2Cl_2, and the combined organic layers were dried using $MgSO_4$ and filtered. The mixture was purified on silica gel (hexanes as eluent) to afford 1.03 g product as a white solid (60% yield). ^{1}H NMR (400 MHz, $CDCl_3$, δ): 7.48 (2H), 7.36 (2H), 6.83 (4H), 2.31 (6H), 2.00 (12H) ppm; ^{13}C NMR (100 MHz, $CDCl_3$, δ): 140.92, 139.08, 137.94, 131.45, 128.41, 127.51, 23.57, 21.36 ppm.

3.2.5 Synthesis of 1-Iodo-8-(*p*-dimesitylborylphenyl)naphthalene 3.1a

1-Dimesitylboryl-4-bromobenzene (405 mg, 1.0 mmol) was dissolved in 20 mL dry degassed THF in a 50 mL Schlenk flask with a stir bar. The solution was cooled to -78 °C for 15 min, then *n*-BuLi (0.75 mL, 1.6 M in hexanes, 1.2 mmol) was added dropwise by syringe. The mixture was stirred 1 hour at -78 °C, then $ZnCl_2$(TMEDA) (303 mg, 1.2 mmol) was added into the solution. The mixture was warmed up to room temperature slowly and kept stirring for 1 hour. Then 1,8-diiodonaphthalene (380 mg, 0.5 mmol) and $Pd(PPh_3)_4$ (30 mg, 0.05 mmol) were added. The mixture was stirred and refluxed for 24 hrs. The solvent was removed *in vacuo* and the residue was partitioned between CH_2Cl_2 and water. The mixture was extracted twice with CH_2Cl_2, and the combined organic layers were dried using $MgSO_4$ and filtered. The mixture was purified on silica gel (10:1 hexanes: CH_2Cl_2 as eluent) to afford 225 mg **3.1a** as white solid (40% yield). ^{1}H NMR (300 MHz, CD_2Cl_2, δ): 7.88 (1H), 7.79 (1H), 7.56 (2H), 7.42 (6H), 6.89 (4H), 2.35 (6H), 2.12 (12H) ppm; ^{13}C NMR (126 MHz, $CDCl_3$, δ): 144.4, 141.3, 140.7, 138.9, 137.8, 131.3, 128.3, 23.4, 21.2 ppm.

3.2.6 Synthesis of 1-(*p*-diphenylphosphinophenyl)-8-(*p*-dimesitylborylphenyl)naphthalene (3.1)

1-Diphenylphosphino-4-bromobenzene (316 mg, 0.926 mmol) was dissolved in 20 mL dry degassed THF in a 50 mL Schlenk flask with a stir bar. The solution was cooled to -78 °C for 15 min, then *n*-BuLi (0.64 mL, 1.6 M in hexanes, 1.020 mmol) was added dropwise by syringe. The mixture was stirred 1 hour at -78 °C, then $ZnCl_2$(TMEDA) (292 mg, 1.158 mmol) was added into the solution. The mixture was warmed up to room temperature slowly and kept stirring for 1 hour. Then **3.1a** (359 mg, 0.620 mmol) and $Pd(PPh_3)_4$ (80 mg, 0.069 mmol) were added. The mixture was stirred and refluxed for 24 hrs. The solvent was removed *in vacuo* and the residue was partitioned between CH_2Cl_2 and water. The mixture was extracted twice with CH_2Cl_2, and the combined organic layers were dried using $MgSO_4$ and filtered. The mixture was purified on silica gel (5:1 hexanes: CH_2Cl_2 as eluent) to afford 257 mg **3.1** as a white solid (39% yield). ^{1}H NMR (500 MHz, CD_2Cl_2, δ) 7.98 (d, $^3J_{H-H}$ = 7.88 Hz, Naph, 2H), 7.61 (m, Naph, 2H), 7.43 (t, $^3J_{H-H}$ = 5.6 Hz, Naph, 2H), 7.26 (m, Ph, 12H), 7.10 (t, $^3J_{H-H}$ = 7.0 Hz, Ph, 4H), 7.01 (t, $^3J_{H-H}$ = 6.94 Hz, Ph, 2H), 6.88 (s, Mes, 4H), 2.36 (s, Me, 6H), 2.03 (s, Me, 12H) ppm; ^{31}P{^{1}H} NMR (202 MHz,

CD_2Cl_2, δ) -6.0 ppm; ^{13}C NMR (126 MHz, CD_2Cl_2, δ) 148.4, 144.6, 142.1, 141.4, 140.9, 140.6, 138.9, 138.4, 138.3, 137.3, 136.2, 135.0, 134.9, 134.3, 134.2, 134.0, 133.7, 133.5, 132.0, 131.7, 130.2, 130.1, 129.7, 129.6, 129.1, 129.0, 128.9, 128.7, 125.9, 125.8, 24.4, 21.5 ppm. Anal. Found: C 87.72, H 6.56. Calcd for $C_{52}H_{46}BP$: C 87.6, H 6.4.

3.2.7 Computational Study

The DFT calculations were performed using the Gaussian 09, revision B.01,[5] software package and the High Performance Computing Virtual Laboratory (HPCVL) at Queen's University. The ground-state geometries were fully optimized at the B3LYP[6] level using the 6-31G(d) basis set for all other atoms.[7] The initial geometric parameters in the calculations were employed from crystal structure data for geometry optimization except for the fluoride adducts of **3.1**, for which the initial geometry parameters were established by Gauss View (version 3.08). TD-DFT calculations were performed to obtain the vertical singlet and triplet excitation energies.

3.2.8 X-Ray Diffraction Analysis

Single crystal of **3.1** was recrystallized by slow evaporation from the solution of hexanes. The crystal was mounted on glass fibers and was collected on a Bruker Apex II single-crystal X-ray diffractometer with graphite-monochromated Mo Kα radiation, operating at 50 kV and 30 mA and at 180 K. Data were processed on a PC with the aid of the Bruker SHELXTL software package (version 6.10) and corrected for absorption effects. The crystal structure data of **3.1** have been deposited at the Cambridge Crystallographic Data Center (CCDC Nos. 967364) and are shown in Table 3.1. The selected bond lengths and angles are given in Table 3.2.

3.2.9 UV-Visible and Fluorescence Titration of 3.1 with Tetrabutylammonium Fluoride (TBAF) and Fluoride Binding Constant Calculation

3.2.9.1 Fluoride Titration

Fluoride titrations were monitored via UV-visible and Fluorescence spectroscopy. A titration was performed between **3.1** (1.0×10^{-5} M in 3 mL of CH_2Cl_2) and TBAF, in which case the concentration of TBAF was increased incrementally from 0 M up to 7.8×10^{-5} M. The titrations of the UV-visible and Fluorescence spectra were recorded after each addition, and a spectrum of **3.1** was also recorded in the absence of TBAF prior to the titration.

3.2.9.2 Fluoride Binding Constant Calculation

Once the titrations were complete, plots of the change in the Absorption versus the fluoride concentration were subsequently prepared. Wavelengths were carefully chosen to ensure that the strength of the absorbance signal was sensitive to complex formation between the ligand and the fluoride ions, and that the changes in the absorbance signal were not due to other phenomena. The changes in the observed absorbance intensity ($\Delta A_{obs} = A\text{-}A_0$) observed at complexation-sensitive wavelengths were reported relative to the absorbance intensity that was exhibited by **3.1** in the absence of the fluoride ions. Whenever possible, the binding constants were determined using a least squares fitting method based on a 1:1 binding isotherm utilized previously by Macartney and co-workers,[8] in which the binding constant (K) and the limiting change in the absorbance intensity ($\Delta A_{limiting}$) were taken as floating parameters. In particular, a plot of the predicted change in absorbance versus the fluoride ion concentration ($\Delta A_{predicted}$ vs. $[F^-]$) was compared with a plot of the observed change in absorbance versus the fluoride ion concentration (ΔA_{obs} vs. $[F^-]$). The values of $\Delta A_{predicted}$ were calculated based on the 1:1 binding isotherm expressed by equation according to equations 1-3:

$$[H{\cdot}G] = (b - (b^2 - 4[G]_{total}[H]_{total})^{1/2})/2 \quad (1)$$

$$\text{where } b = [G]_{total} + [H]_{total} + K^{-1} \quad (2)$$

$$\Delta A_{predicted} = \Delta A_{limiting} \times ([H{\cdot}G]/[G]_{total}) \quad (3)$$

Table 3.1. Crystal data and structure refinement for compound 3.1

Compound	**3.1**
Formula	C52H46B1P1
Formula weight	712.67
T, K	180(2)
Wavelength, Å	0.71073
Crystal system	Monoclinic
Space group	P2(1)/c
a, Å	27.139(4)
α, °	90
b, Å	11.1890(19)
β, °	104.292(3)
c, Å	13.706(2)
γ, °	90
V, $Å^3$	4033.0(11)
Z	4
Density (calculated), Mg/m^3	1.174
Absorption coefficient, mm^{-1}	0.103
Theta range for data collection, °	1.98 to 27.04
Reflections collected	15900
Independent reflections	8593 [R(int) = 0.0487]
Completeness to theta = 27.04°	97.1 %
Data / restraints / parameters	8593 / 0 / 493
Goodness-of-fit on F^2	1.037
Final R indices [I>2sigma(I)]	
R_1[a]	0.0585
wR_2[b]	0.1402
R indices (all data)	
R_1[a]	0.1026
wR_2[b]	0.1648

[a] $R_1 = \sum [(|F_0| - |F_c|) / \sum|F_0|$

[b] $wR_2 = [\sum w[(F_0^2-F_c^2)^2] / \sum [w(F_0^2)^2]]^{1/2}$

$w = 1 / [\sigma^2(F_0^2) + (0.075P)^2]$, where $P = [Max (F_0^2, 0) + 2F_c^2] / 3$

Table 3.2. Selected bond lengths (Å) and angles (°) for compound 3.1

P(1)-C(1)	1.831(2)
P(1)-C(29)	1.832(3)
P(1)-C(23)	1.833(3)
B(1)-C(7)	1.561(3)
B(1)-C(35)	1.575(4)
B(1)-C(44)	1.576(3)
C(4)-C(13)	1.489(3)
C(7)-C(12)	1.393(3)
C(10)-C(21)	1.488(3)
C(13)-C(22)	1.431(3)
C(17)-C(22)	1.433(3)
C(23)-C(28)	1.382(3)
C(1)-P(1)-C(29)	103.43(11)
C(1)-P(1)-C(23)	100.64(10)
C(29)-P(1)-C(23)	102.85(11)
C(7)-B(1)-C(35)	121.4(2)
C(7)-B(1)-C(44)	119.7(2)
C(35)-B(1)-C(44)	118.9(2)
C(9)-C(10)-C(21)	119.6(2)
C(11)-C(10)-C(21)	121.7(2)
C(11)-C(12)-C(7)	122.8(2)
C(14)-C(13)-C(22)	119.5(2)
C(14)-C(13)-C(4)	117.2(2)
C(22)-C(13)-C(4)	122.8(2)
C(18)-C(17)-C(22)	119.6(3)
C(16)-C(17)-C(22)	119.4(3)
C(19)-C(18)-C(17)	121.3(3)
C(18)-C(19)-C(20)	119.8(3)

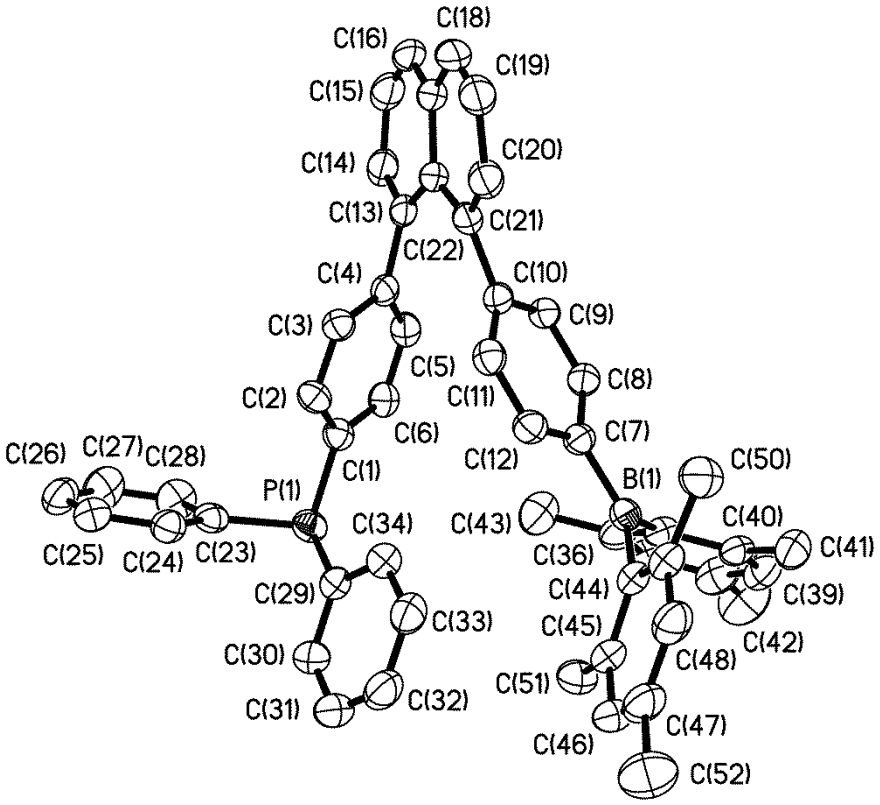

Figure 3.2. Crystal structure of **3.1** with 35% thermal ellipsoids. H atoms are omitted for clarity.

3.3 Results and Discussion

3.3.1 Synthesis and Crystal Structure of 3.1

The synthesis of the desired P-B compound **3.1** was readily achieved in a stepwise fashion using 1-dimesitylboryl-4-bromobenzene, 1-diphenylphosphino-4-bromobenzene and 1,8-diiodonaphthalene as precursors (Figure 3.3). Both the phosphorus and boron fragments were prepared *via* the lithiation of 1,4-dibromobenzene which was quenched with either $BMes_2F$ or PPh_2Cl to afford the triarylborane and phosphine precursors in 60% and 95% yield respectively. Following two subsequent Negishi couplings, both P(*p*-Br-Ph)Ph_2 and B(*p*-Br-Ph)Mes_2 moieties were attached to the 1,8-diiodonaphthalene linker in decent yield of ~40% for each reaction, and the final product **3.1** was isolated as a white solid *via* column chromatography. Unlike the previously reported N-B system,[4] the Negishi couplings were held at reflux in order to accelerate the reaction and $ZnCl_2$(TMEDA) was used as a relatively moisture stable alternative to $ZnCl_2$.

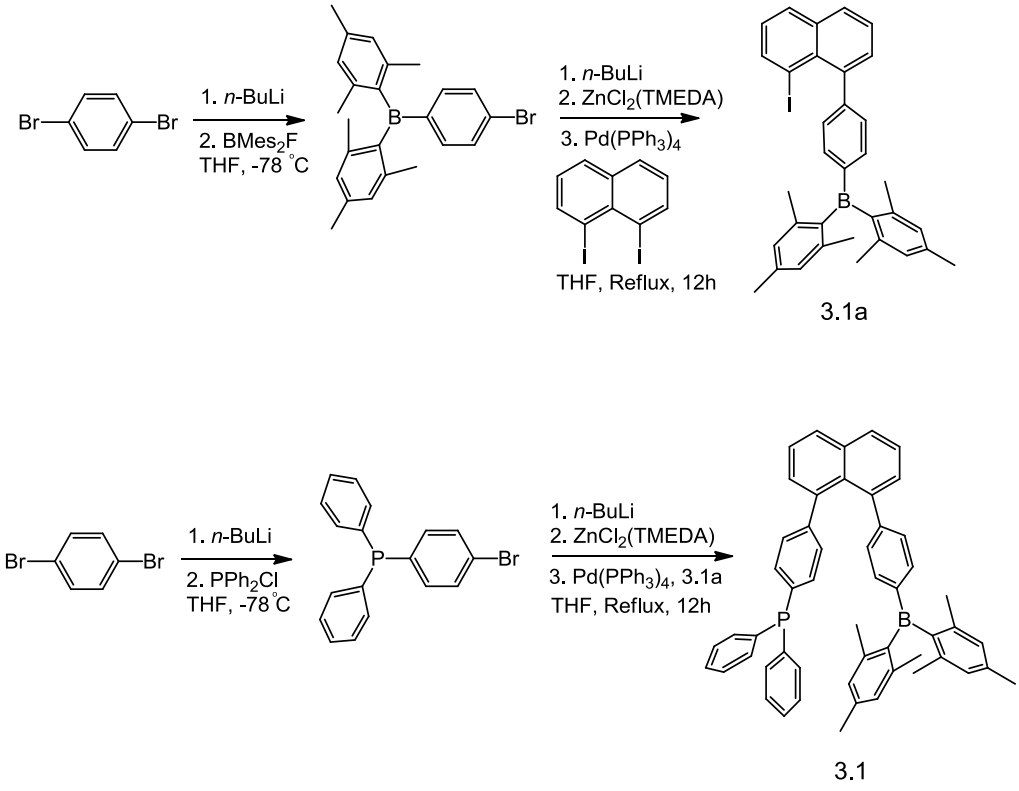

Figure 3.3. Synthetic procedure for compound **3.1**.

Compound **3.1** was fully characterized by NMR and elemental analyses. In the ^{31}P NMR spectra, **3.1** displays a characteristic phosphine signal at -6.0 ppm. Compound **3.1** was recrystallized from hexanes to afford as colorless crystals which were suitable for single-crystal X-ray diffraction experiments. As shown in Figure 3.4, the phosphine center in **3.1** has a typical pyramidal geometry while the boron atom has a typical trigonal planar geometry. Because of steric interactions, the two phenyl linkers are forced to be away from each other and the dihedral angles between the phenyl and the naphthyl aromatic rings are significantly distorted from 90° (~127°). The C-C bond lengths between the phenyl linkers and the naphthyl carbon atoms are 1.488(3) Å and 1.489(3) Å, respectively, typical of a C-C single bond. The naphthyl ring is also considerably distorted from planarity as indicated by the 16.2° dihedral angle between the two fused benzene rings and the side view of the structure in Figure 3.4. The separation distance between the B and the P atom is 6.24(1) Å, ruling out the presence of any bonding interactions. The P-B distance is much longer than those of the closely related N-B systems (~5.5 Å),[2c] and can be attributed to the sterically demanding pyramidal geometry of P unit and trigonal planar geometry of the boron moiety.

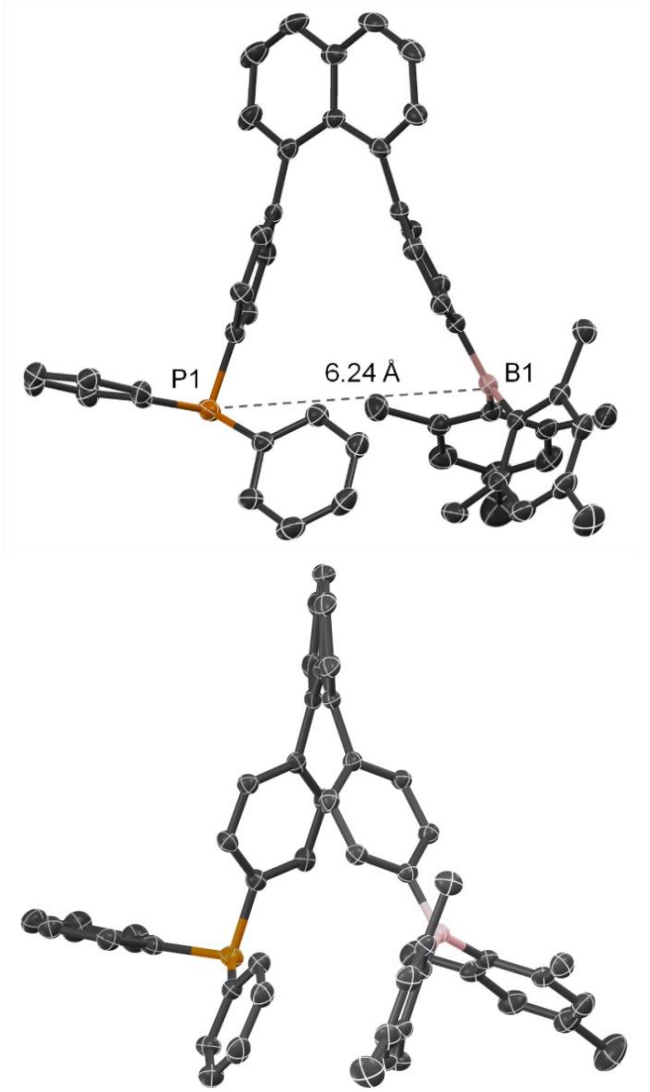

Figure 3.4. Crystal structures of **3.1** with 35% thermal ellipsoids (top: front view, bottom: side view). H atoms are omitted for clarity.

3.3.2 Photophysical Properties

Compound **3.1** has an intense absorption band at λ_{max} = 330 nm that does not change significantly with solvent polarity (see Table 3.3 and Figure 3.5).

Table 3.3. Photophysical properties of **3.1**

Solvent	Absorption		Fluorescence	
	λ_{max} (nm)	Logε	λ_{em}	Φ_{FL}
Hexanes	330	4.53	400 (shoulder), 460	0.3
Toluene	335	4.45	404 (shoulder), 493	0.31
CH_2Cl_2	330	4.5	407, 532	0.13
THF	335	4.41	404, 530	0.04
Acetone	335	4.43	415, 554	0.07
DMSO	335	4.40	422	0.25

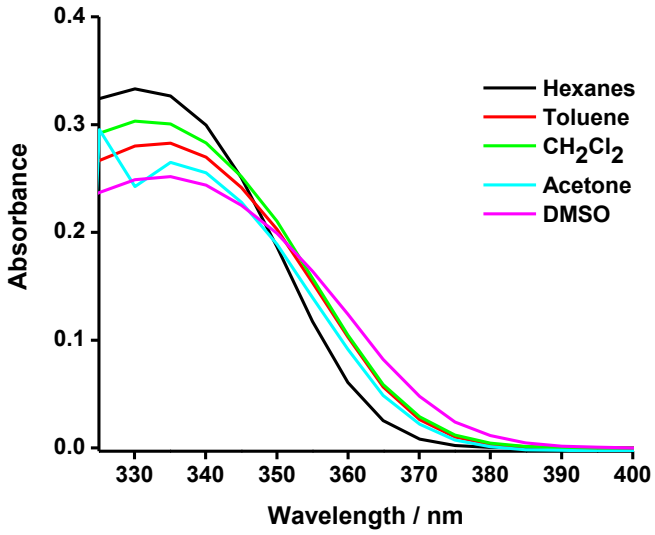

Figure 3.5. Absorption spectra of **3.1** in different solvents.

In the fluorescence spectrum, **3.1** shows dual emission in most solvents except coordinating solvents such as DMSO, DMF, and CH_3CN, in which the fluorescence spectrum of **3.1** displays either one emission peak at ~410 nm (DMSO, DMF) or is dominated by the 410 nm emission peak (CH_3CN) (see Figure 3.6 and Figure 3.7). The high energy emission peak of **3.1** exhibits a small red shift (e.g., λ_{max} 400 nm in

hexanes and 415 nm in acetone) with increasing solvent polarity, while the low-energy signal shows a pronounced red shift (λ_{max} 460 nm in hexanes and 554 nm in acetone). Because of the dual emission, **3.1** has a white fluorescence color in THF and CH_2Cl_2 (see Figure 3.8)

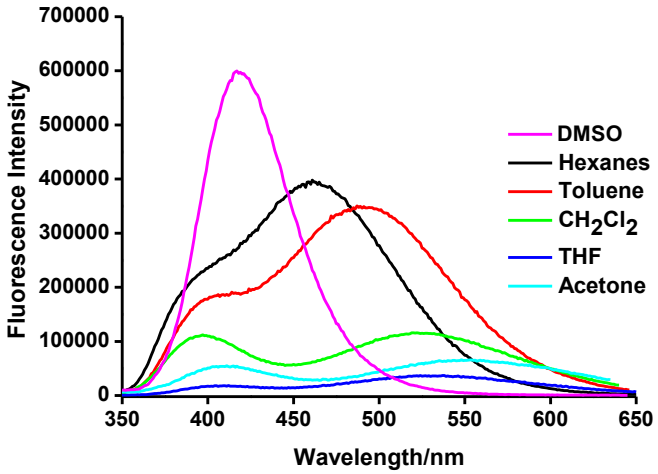

Figure 3.6. Fluorescence spectra of **3.1** in various solvents (1.0×10^{-5} M) with relative intensities.

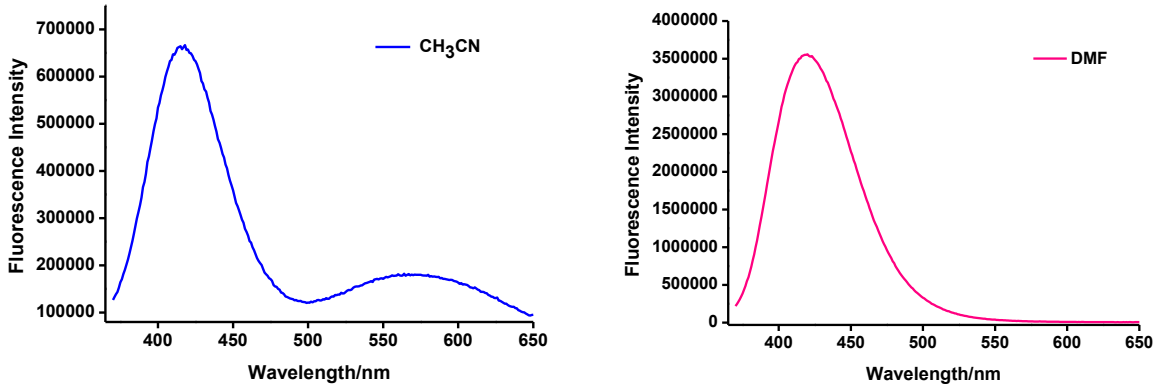

Figure 3.7. Fluorescence spectra of **3.1** in CH_3CN (left) and in DMF (right) (1.0×10^{-5} M).

Figure 3.8. Photographs showing the emission color of **3.1** in various solvents.

The dual emissive behavior of **3.1** is in sharp contrast to the previously reported U-shaped amino-$BMes_2$ molecules with a similar 1,8-diphenylnaphthyl linker between an NMe_2 or NAr_2 donor and $BMes_2$ acceptor, which display the N → B CT emission peak exclusively.[2c] This difference can be explained by the stabilization of the amino radical cation through π conjugation with the aryl group that stabilizes the charge-separated excited state in the N-B compounds, making the CT emission an efficient and competitive relaxation pathway in the N-B compounds.

On the basis of the solvent dependence of the dual emission and the previous study on the related N-B systems, the low energy peak of **3.1** was assigned to a P → B through-space CT transition while the high-energy peak corresponds to a Mes (π) → B-Ph (π*) transition. This assignment was further supported by the fact that a similar diboron compound displays the high-energy emission peak only.[2d] The abnormal behavior of **3.1** in DMSO, DMF, and CH_3CN was most likely caused by the weak coordination of these solvent molecules to the B center which blocks the P → B CT, since a similar phenomenon was observed in the previously reported U-shaped N-B molecules.[2] Thermal quenching of the CT emission may also be a factor due to the low energy of the CT state in the high-polarity solvents. The fluorescent quantum efficiency (Φ_{FL} = 0.07 in acetone, 0.13 in CH_2Cl_2, and 0.30 in hexane) of **3.1** increased with decreasing solvent polarity, as the P → B CT peak shifts toward higher energy.

3.3.3 TD-DFT Calculations

The assignment of the dual emission in **3.1** was also supported by TD-DFT calculation data of the vertical excitation from the ground state (Table 3.4 and Figure 3.9). The S_1 transition of **3.1** is mainly the P lone pair (HOMO) → B-Ph (π*, LUMO) CT transition with significant contributions from naphthyl to the HOMO and a large oscillator strength (f = 0.2522). The S_2 transition (HOMO -2 → LUMO, 80%) is mainly from the Mes (π) → B-Ph (π*) transition with a smaller oscillator strength (0.0806). The calculated vertical excitation energies of these two states are close. In solution, the S_1 state could be greatly stabilized by polar solvent molecules due to the highly polarized nature of this state, leading to the distinct solvent polarity dependent CT emission. Thus, the high-energy and low-energy emission peaks of **3.1** are most likely from the S_2 and S_1 states, respectively.

Table 3.4. TD-DFT calculated vertical excitation energy and oscillator strengths for **3.1**

Compound	State	Transition	Energy (nm)	Oscillator Strength (f)
3.1	S_1	HOMO → LUMO (80%)	362	0.2522
	S_2	HOMO -2 → LUMO (80%)	359	0.0806

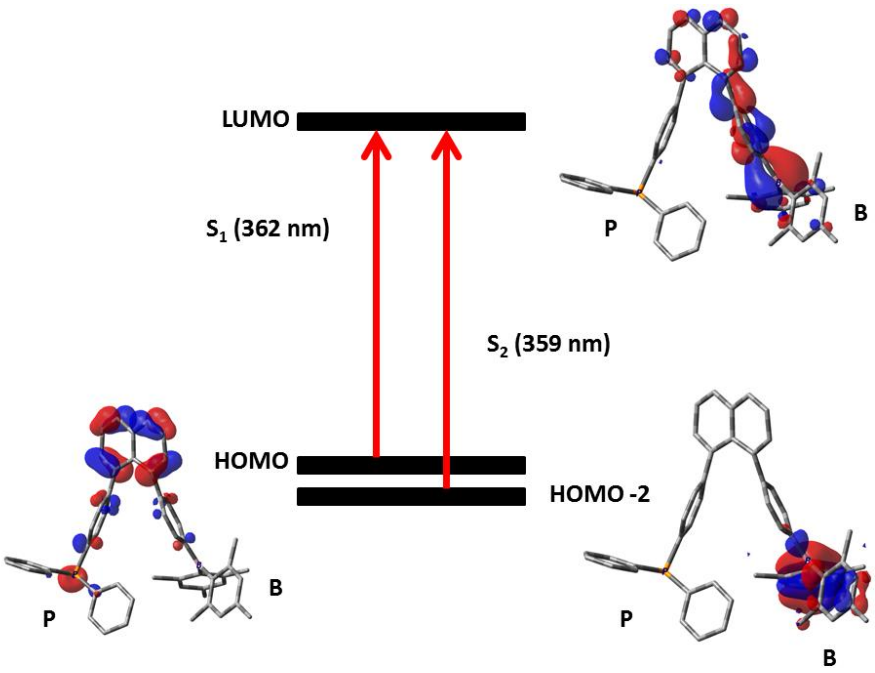

Figure 3.9. Electronic transitions and the associated MO diagrams which are responsible for the low-energy absorption bands of **3.1**. The MO diagrams are plotted with an isocontour value of 0.03.

3.3.4. UV-Visible and Fluorescence Titration of 3.1 with TBAF

Fluoride titrations were monitored by UV-vis and Fluorescence spectra, which were performed with **3.1** (1.0×10^{-5} M in 3 mL of CH_2Cl_2) and TBAF, in which case the concentration of TBAF was increased incrementally from 0 M up to 7.8×10^{-5} M. From the UV-vis titration, least squares fitting using the method described above yielded a binding constant of $(4.3 \pm 0.5) \times 10^4$ M^{-1}. In the absorption spectra, the addition of fluoride ions caused a substantial intensity increase of the 330 nm peak for **3.1** (Figure 3.10).

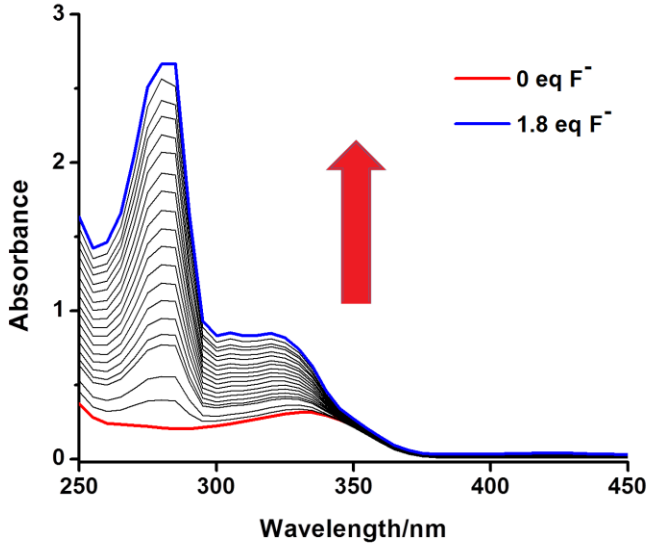

Figure 3.10. Absorption spectral changes of **3.1** in CH_2Cl_2 upon the addition of TBAF.

In the fluorescence spectrum, the addition of fluoride ions led to quenching of the low-energy CT peak and enhancement of the high-energy emission peak of **3.1**, with Φ_{FL} increasing from 0.13 to 0.29 and an emission color change from whitish yellow to deep blue, as shown in Figure 3.11 and Figure 3.12. This response could be described as "turn-on" or "switchable" fluorescence sensing, a phenomenon similar to that observed in the related N-B compounds, although the high-energy emission peak only appears after the addition of fluoride ions in the N-B compounds.[2b,c] The fluorescence quantum efficiency more than doubled compared to **3.1** after the addition of fluoride ions which is in sharp contrast to the case for the related N-B compounds,[2b,c] making **3.1** a more sensitive ratiometric probe for fluoride ions.

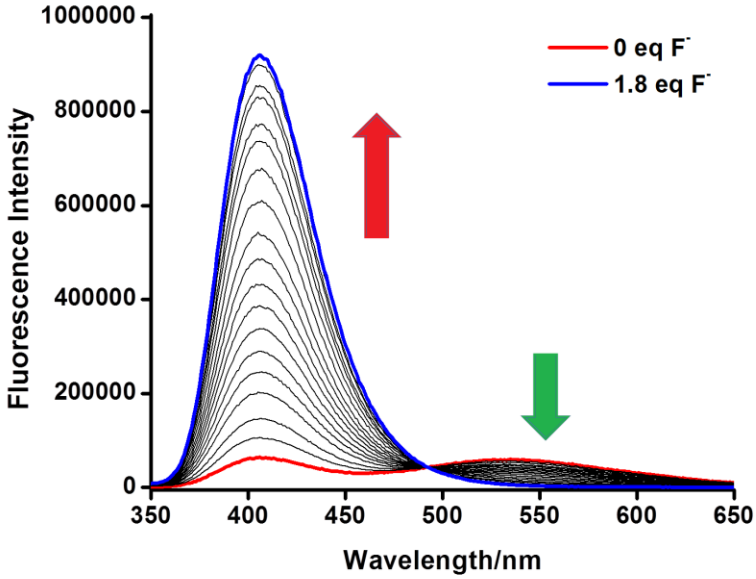

Figure 3.11. Fluorescence spectral changes of **3.1** in CH_2Cl_2 upon the addition of TBAF. The fluorescence spectra were recorded using 330 nm excitation.

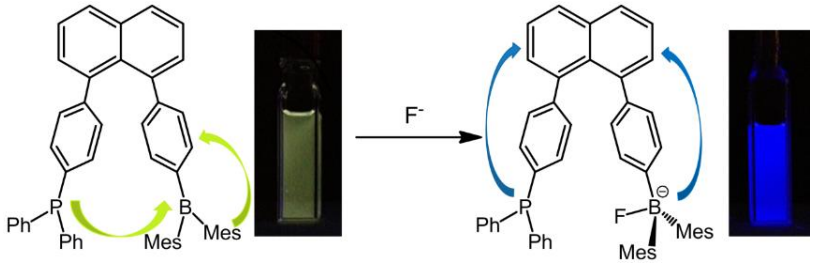

Figure 3.12. Emission color changes of **3.1** and its fluoride-adducts in CH_2Cl_2. Proposed fluorescence change mechanism of **3.1** upon the addition of fluoride ions. The arrows indicate the charge transfer states that are likely responsible for the fluorescence of these molecules.

Indeed, ~1.8 equiv of F^- was needed to reach the saturation point for **3.1**, while more than 20 equiv of F^- was needed to achieve the same effect for the related N-B compounds.[2b,c] The large emission energy difference between the P → B CT peak in **3.1** and the fluorescent peak in [**3.1**·F]$^-$ in comparison to that for the related N-B compounds may be partially responsible for the great quantum efficiency increase. The increase of the absorbance of the excitation band at 330 nm with fluoride addition, as shown in

Figure 3.10, was clearly a key factor for the enhancement of the high-energy emission peak in **3.1**. The quenching of the CT band was caused by the blocking of the empty p orbital of the B center by the fluoride ion. The binding of fluoride to the B center in **3.1** was confirmed by the characteristic four-coordinated ^{11}B chemical shift (3.8 ppm) observed for [**3.1**·F]$^-$ and the ^{19}F chemical shift (-175.7 ppm) (see Figure 3.13 and Figure 3.14), typical for fluoride ions bound to a $BMes_2Ar$ unit.[2]

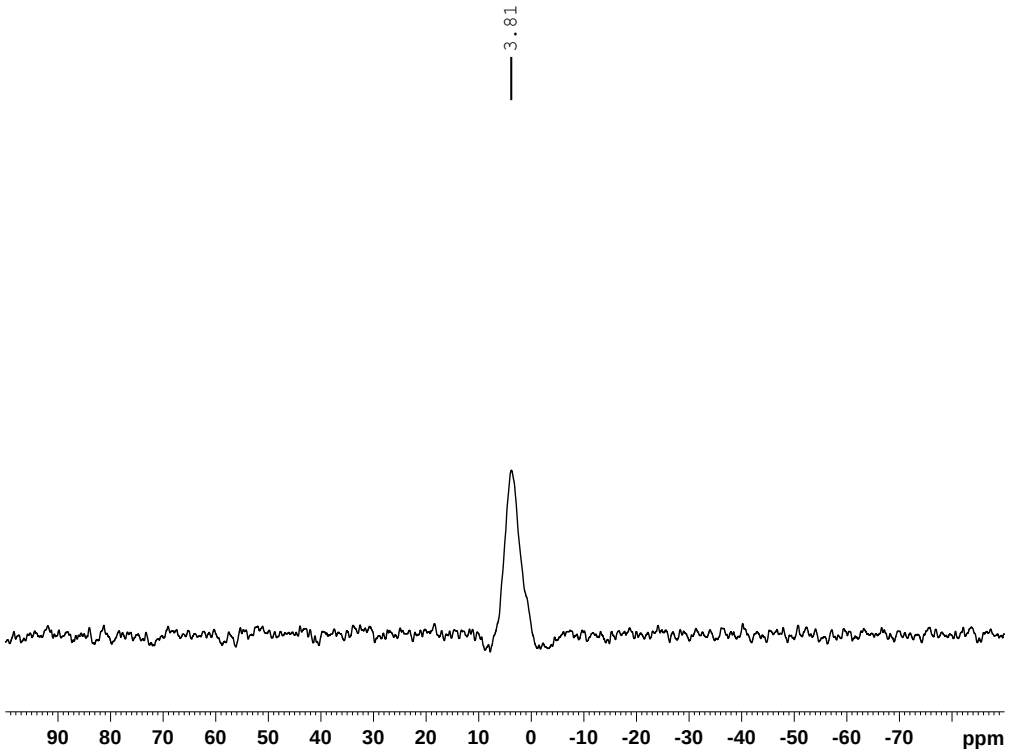

Figure 3.13. ^{11}B NMR spectrum of compound **3.1** with ~2.0 equiv. of TBAF (CD_2Cl_2).

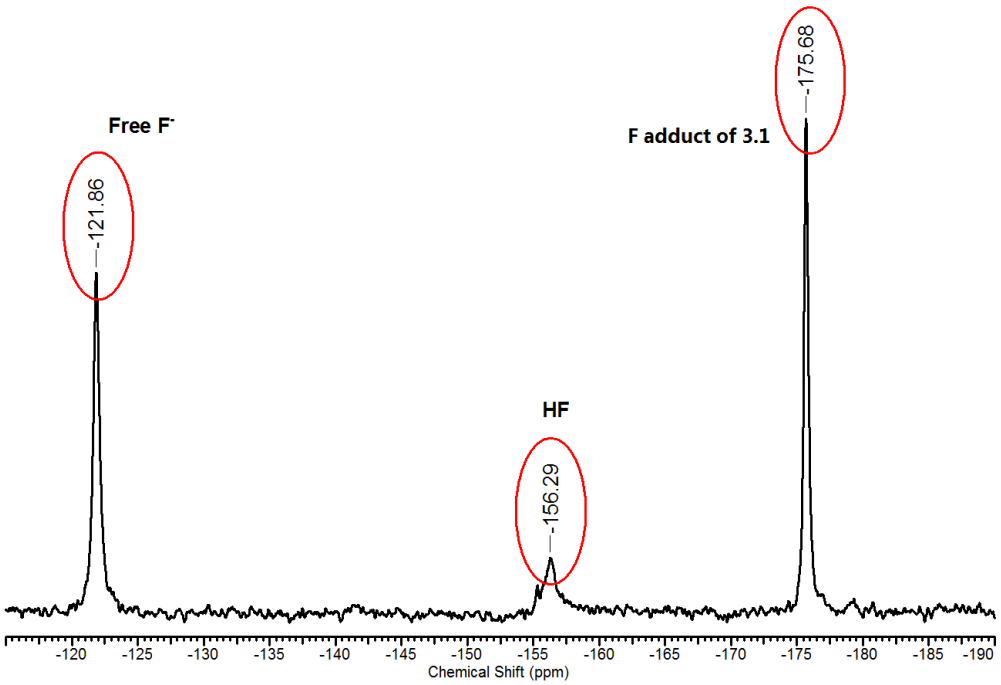

Figure 3.14. ^{19}F NMR spectrum of compound **3.1** with ~2.0 equiv. of TBAF (CD_2Cl_2).

As shown by the TD-DFT data in Table 3.5 and Figure 3.15, the S_1 state of the fluoride adduct [**3.1**·F]$^-$ is lower in energy than that of **3.1** and involves the transition from the $BFMes_2$ unit (HOMO) to the naphthyl π* (LUMO) with a very weak oscillator strength (0.0026). This is in agreement with the appearance of a very weak absorption band at about 430 nm in the absorption spectrum of NBu_4[**3.1**·F] (Figure 3.10). The fact that [**3.1**·F]$^-$ is non-emissive on excitation at 430 nm supports that the fluorescence of [**3.1**·F]$^-$ is not from the S_1 state. Therefore, we suggest that the fluorescence of [**3.1**·F]$^-$ is likely from the S_3 or the S_4 state that involves a transition from either the $BFMes_2$-Ph (π, HOMO -2) or the PPh_2-Ph (π, HOMO -3) to the naphthyl (π*, LUMO), which happens to have an energy similar to that of the S_2 state of **3.1**.

Table 3.5. TD-DFT calculated vertical excitation energy and oscillator strengths for the fluoride adduct of **3.1**

Compound	State	Transition	Energy (nm)	Oscillator strength (f)
NMe_4[**3.1**·F]	S_1	HOMO → LUMO (99%)	417	0.0026
	S_2	HOMO -1 → LUMO (100%)	391	0.0001
	S_3	HOMO -2 → LUMO (77%)	369	0.0490
		HOMO -3 → LUMO (19%)		
	S_4	HOMO -2 → LUMO (21%)	358	0.1818
		HOMO -3 → LUMO (76%)		

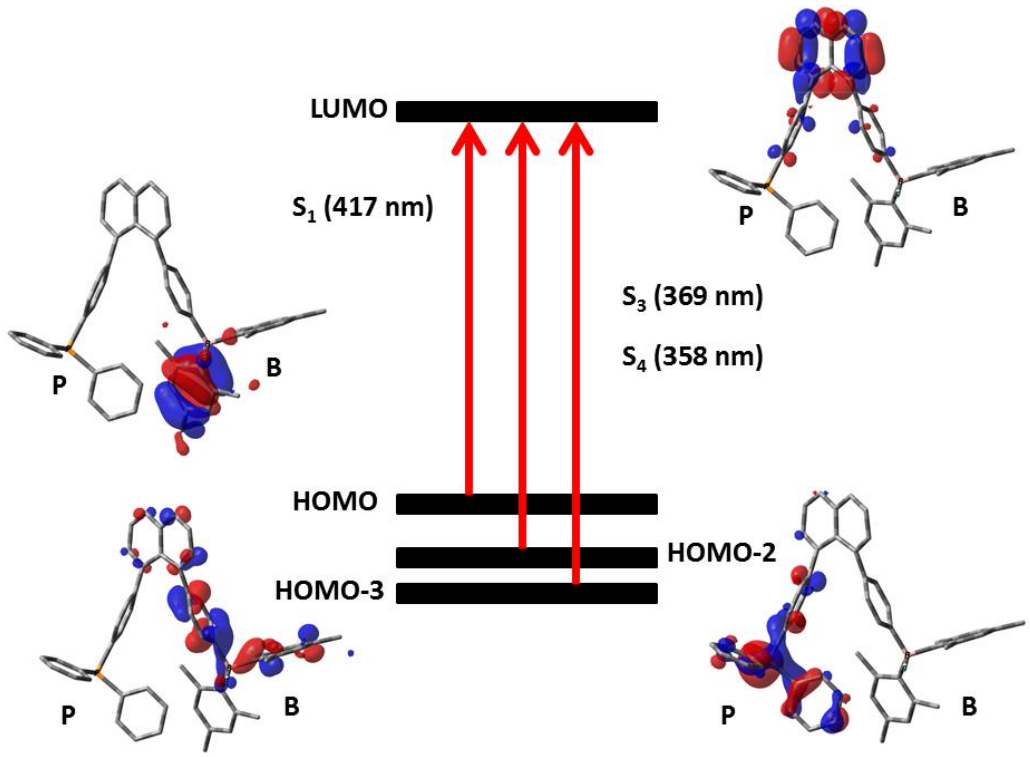

Figure 3.15. Electronic transitions and the associated MO diagrams which are responsible for the low-energy absorption bands of NMe_4[**3.1**·F]. The MO diagrams are plotted with an isocontour value of 0.03. The NMe_4^+ cation was omitted for clarity.

3.4 Conclusions

An unbound phosphine-borane compound **3.1**, a derivative of **2.1** where a phenyl linker has been placed between the P/B-naphthyl bonds, was prepared. This strategy effectively separates the phosphorus and boron centers with a new P-B distance of 6.24 Å, likely due to the π-π repulsions experienced by the phenyl "legs" and steric hindrance from the bulky substituents on the P and B centers. Due to its unbound structure, **3.1** displays a distinct through-space CT transition from the electron-rich phosphine group to the empty p orbital of the boron center, which was confirmed by the solvatochromic behavior of the compound. As might be expected, the boron atom of **3.1** does coordinate weakly to some donor solvent molecules such as DMF, DMSO and CH_3CN. In addition to the CT emission, π-π* transitions were confirmed for **3.1** in the polar coordinating solvents while this dual emission phenomenon was supported by TD-DFT calculations. Due to the multiple emitting states, **3.1** can be used in turn-on/switchable fluorescence for the sensing of fluoride which has been demonstrated. Upon the binding of fluoride to the boron center, the CT emission is quenched while the π-π* transition is enhanced which results in a change of both emission color and intensity. The P-B compound **3.1** was found to have a ratiometric response toward fluoride ions greater than that of the related N-B analogue with a fluoride binding constant of $(4.3 \pm 0.5) \times 10^4\ M^{-1}$ in the solvent of CH_2Cl_2.

References:

(1) a) Entwistle, C. D.; Marder, T. B. *Chem. Mater*. **2004**, *16*, 4574 and references therein; b) Jia, W.; Feng, X.; Bai, D.; Lu, Z.; Wang, S.; Vamvounis, G. *Chem. Mater*. **2005**, *17*, 164; c) Jia, W.; Moran, M. J.; Yuan, Y.; Lu, Z.; Wang, S. *J. Mater. Chem*. **2005**, *15*, 3326; d) Yamaguchi, S.; Wakamiya, A. *Pure Appl. Chem*. **2006**, *78*, 1413; e) Hudson, Z. M.; Wang, S. *Acc. Chem. Res*. **2009**, *42*, 1584; f) Jäkle, F. *Chem. Rev*. **2010**, *110*, 3985; g) Chen, P.; Lalancette, R. A.; Jäkle, F. *Angew. Chem. Int. Ed*. **2012**, *51*, 7994; h) Wade, C. R.; Broomsgrove, A. E. J.; Aldridge, S.; Gabbaï, F. P. *Chem. Rev*. **2010**, *110*, 3958 and references therein; i) Agou, T.; Sekine, M.; Kobayashi, J.; Kawashima, T. *Chem. Eur. J*. **2009**, *15*, 5056; j) Song, K. C.; Lee, K. M.; Nghia, N. V.; Sung, W. Y.; Do, Y.; Lee, M. H. *Organometallics*, **2013**, *32*, 817.

(2) a) Liu, X.; Bai, D.; Wang, S. *Angew. Chem. Int. Ed*. **2006**, *45*, 5475; b) Bai, D.; Liu, X.; Wang, S. *Chem. Eur. J*. **2007**, *13*, 5713; c) Hudson, Z. M.; Liu, X.; Wang, S. *Org. Lett*. **2011**, *13*, 300; d) Zhao, S.-B.; Wucher, P.; Hudson, Z. M.; McCormick, T. M.; Liu, X.-Y.; Wang, S. *Organometallics*. **2008**, *27*, 6446.

(3) a) Stephan, D. W. *Org. Biomol. Chem*. **2012**, *10*, 5740 and references therein; b) Stephan, D. W.; Erker, G. *Angew. Chem., Int. Ed*. **2010**, *49*, 46; c) Stephan, D. W. *Dalton Trans*. **2009**, 3129; d) Voss, T.; Chen, C.; Kehr, G.; Nauha, E.; Erker, G.; Stephan, D. W. *Chem. Eur. J*. **2010**, *16*, 3005; e) Stephan, D. W.; Greenberg, S.; Graham, T. W.; Chase, P.; Hastie, J. J.; Geier, S. J.; Farrell, J. M.; Brown, C. C.; Heiden, Z. M.; Welch, G. C.; Ullrich, M. *Inorg. Chem*. **2011**, *50*, 12338 and references therein; f) Moret, M.-E.; Peters, J. C. *Angew. Chem., Int. Ed*. **2011**, *90*, 2063.

(4) a) Tsurusaki, A.; Sasamori, T.; Wakamiya, A.; Yamaguchi, S.; Nagura, K.; Irle, S.; Tokitoh, N. *Angew. Chem., Int. Ed*. **2011**, *50*, 10940; b) Li, Y.; Kang, Y.; Ko, S.; Rao, Y.; Sauriol, F.; Wang, S. *Organometallics*, **2013**, *32*, 3063; c) Beckmann, J.; Hupf, E.; Lork, E.; Mebs, S. *Inorg. Chem*. **2013**, *52*, 11881; d) Bontemps, S.; Devillard, M.; Mallet-Ladeira, S.; Bouhadir, G.; Miqueu, K.; Bourissou, D. *Inorg. Chem*. **2013**, *52*, 4714.

(5) Frisch, M. J.; Trucks, G. W.; Schlegel, H. B.; Scuseria, G. E.; Robb, M. A.; Cheeseman, J. R.; Scalmani, G.; Barone, V.; Mennucci, B.; Petersson, G. A.; Nakatsuji, H.; Caricato, M.; Li, X.; Hratchian, H. P.; Izmaylov, A. F.; Bloino, J.; Zheng, G.; Sonnenberg, J. L.; Hada, M.; Ehara, M.; Toyota, K.; Fukuda, R.; Hasegawa, J.; Ishida, M.; Nakajima, T.; Honda, Y.; Kitao, O.; Nakai, H.; Vreven, T.; Montgomery, J. A., Jr.; Peralta, J. E.; Ogliaro, F.; Bearpark, M.; Heyd, J. J.; Brothers, E.; Kudin, K. N.; Staroverov, V. N.; Keith, T.; Kobayashi, R.; Normand, J.; Raghavachari, K.; Rendell, A.; Burant, J. C.; Iyengar, S. S.; Tomasi, J.; Cossi, M.; N. Rega, N.; Millam, J. M.; Klene, M.; Knox, J. E.; Cross, J. B.; Bakken, V.; Adamo, C.; Jaramillo, J.; Gomperts, R.; Stratmann, R. E.; Yazyev, O.; Austin, A. J.; Cammi, R.; Pomelli, C.; Ochterski, J. W.; Martin, R. L.; Morokuma, K.; Zakrzewski, V. G.; Voth, G. A.; Salvador, P.; Dannenberg, J. J.; Dapprich, S.; Daniels, A. D.; Farkas, O.; Foresman, J. B.; Ortiz, J. V.; Cioslowski, J.; Fox, D. J. *Gaussian09*, revision B.01; Gaussian, Inc., Wallingford, CT, 2010.

(6) a) Lee, C.; Yang, W.; Parr, R. G. *Phys. Rev. B*, **1988**, *37*, 785; b) Becke, A. D. *J. Chem. Phys*. **1993**, *98*, 5648.

(7) Hay, P. J. *J. Phys. Chem. A*. **2002**, *106*, 1634.

(8) Wylie, R. S.; Macartney, D. H. *Inorg. Chem.* **1993**, *32*, 1830.

Chapter 4

Impact of Methylation and Complexation of Phosphine-Borane System on Fluoride Binding Ability

4.1 Introduction

As mentioned in Chapter 1.3, one of the main challenges associated with fluoride sensing in water is to overcome the substantial hydration enthalpy of the fluoride ion (-504 kJ/mol) and poor water solubility of neutral triarylborane compounds. In order to enhance the Lewis acidity and solubility of boron-based fluoride sensors, introducing polarity into the triarylborane framework in the form of electron-withdrawing groups or cationic substituents is a well-established research direction.[1] In the case of the latter, the positively charged portion of the molecule can enhance the affinity for fluoride ions due to the Coulombic attraction[2] and stabilize the resulting fluorinated organoboron adducts, particularly when the positive charge resides in spatial proximity to the boron center.[3] This is especially relevant in the case of onium ions, as they can generally form chelating structures with the boron-fluoride adduct. Another method of enhancing the Lewis acidity of triarylboron sensors bearing pnictogen substituents is to introduce transition metals. Coordination of the nucleophilic heteroatoms has been shown by cyclic voltammetry measurements to significantly increase the electron-accepting ability of the boron centers compared to their non-coordinated counterparts.[4] Further, the addition of a heavy metal atom can induce phosphorescence *via* spin-orbital coupling, meaning the achievement of phosphorescent sensors is possible with this strategy.[5] To these ends, a phosphonium salt **4.1** and metal complexes **4.2-4.3** have been synthesized based on **3.1** which was previously described in Chapter 3 (Figure 4.1). These compounds display distinctively different responses towards fluoride ions compared to **3.1**, and the details are presented herein.

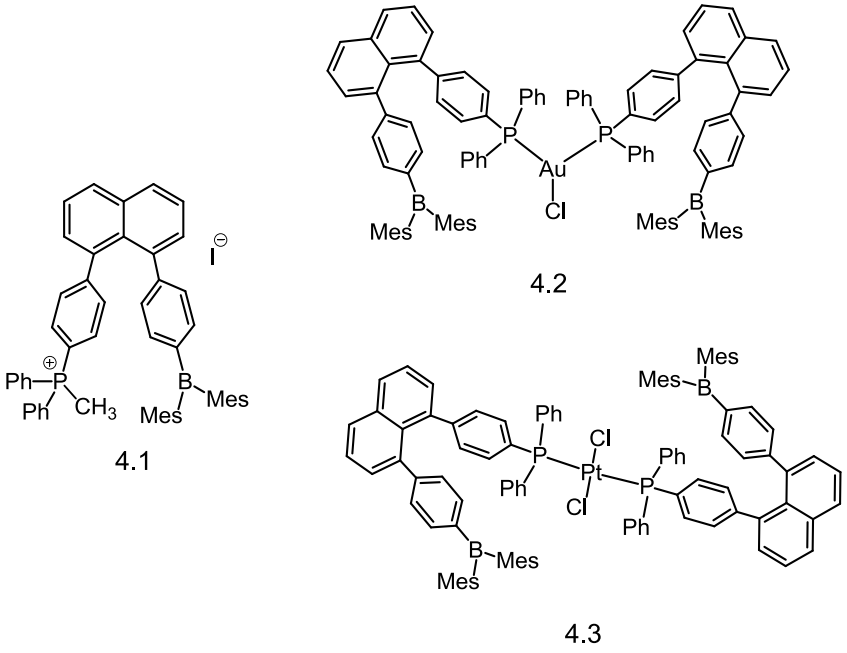

Figure 4.1. Phosphonium salt and metal complexes.

4.2 Experimental

4.2.1 General Procedures

All reactions were carried out under a nitrogen atmosphere. Reagents were purchased from Aldrich Chemical Company and used without further purification. Thin-layer and flash chromatography were performed on silica gel. ^{1}H, ^{13}C and ^{31}P NMR spectrum were recorded on Bruker Avance 400 or 500 MHz spectrometers. Deuterated solvents were purchased from Cambridge Isotopes. UV-vis spectra were recorded on a Varian Cary 50 Bio spectrometer. Emission spectra were recorded using a Photon Technologies International QuantaMaster Model 2 spectrometer. Solution quantum yields were calculated using optically dilute solutions ($A \approx 0.1$) relative to 9,10-diphenylanthracene ($\Phi = 0.90$). High-resolution mass spectra (HRMS) were obtained from an Applied Biosystems Qstar XL spectrometer. Elemental analyses were conducted at Laboratoire d'Analyse Élémentaire de l'Université de Montréal.

4.2.2 Synthesis of 4.1

Compound **3.1** (50 mg, 0.07 mmol) was dissolved in 10 mL of dry and degassed THF. Iodomethane (4.4 μL, 0.07 mmol) was added to the solution dropwise. The mixture was stirred and refluxed overnight. After the solvent was removed in *vacuo* and 5 mL of hexanes was added, a precipitate was obtained and washed with diethyl ether to afford 53 mg of **4.1** as a colorless solid (89% yield). ^{1}H NMR (400 MHz, CD_2Cl_2, δ): 8.06 (d, $^{3}J_{H–H}$ = 8.06 Hz, Naph, 1H), 8.03 (d, $^{3}J_{H–H}$ = 8.31 Hz, Naph, 1H), 7.84 (t, $^{3}J_{H–H}$ = 7.55 Hz, Naph, 2H), 7.63 (m, Naph and Ph, 6H), 7.51 (m, Ph, 6H), 7.39 (m, Ph, 6H), 7.14 (d, Ph, $^{3}J_{H–H}$ = 7.81 Hz, 2H), 6.85 (s, Mes, 4H), 2.81 (d, Me, $^{2}J_{H–P}$ = 13.09 Hz, 3H), 2.35 (s, Me, 6H), 1.85 (s, Me, 12H) ppm. ^{31}P{^{1}H} NMR (162 MHz, CD_2Cl_2, δ): 22.4 ppm. ^{13}C NMR (100 MHz, CD_2Cl_2, δ): 150.9 (Ph), 148.0 (Naph), 147.0 (Ph), 141.5 (Mes), 141.3 (Ph), 140.0 (Mes), 139.6 (Naph), 138.9 (Mes), 137.6 (Naph), 137.0 (Ph), 134.9 (d, Ph, J_{C-P} = 10.6 Hz), 132.9 (d, Ph, J_{C-P} = 10.9 Hz), 132.4 (d, Ph, J_{C-P} = 14.6 Hz), 131.1 (naph), 130.9 (d, Ph, J_{C-P} = 12.8 Hz), 130.1 (Ph), 129.0 (Ph), 128.3 (Mes), 128.2 (Naph), 125.4 (Naph), 125.2 (Naph), 118.0 (d, Ph, J_{C-P} = 88.9 Hz), 114.0 (d, Ph, J_{C-P} = 90.3 Hz), 24.3 (Me), 21.5 (Me), 11.7 (d, J_{C-P} = 57.9 Hz, P-CH_3) ppm. The ^{11}B NMR chemical shift for **4.1** was not observed, perhaps because of the congested nature and the low symmetry of the molecule. Elemental analysis, calcd for $C_{53}H_{49}BPI{\cdot}1H_2O$: C 72.95, H 5.89; found: C 73.19, H 6.04.

4.2.3 Synthesis of 4.2

3.1 (50 mg, 0.07 mmol) and $Au(SMe_2)Cl$ (10 mg, 0.035 mmol) were dissolved in 15 mL of dry and degassed THF. The mixture was stirred overnight at ambient temperature. After the removal of the solvent in vacuo the residue was recrystallized from $CHCl_3$ and hexane, affording a colorless crystalline solid of **4.2** (49 mg, 84%). ^{1}H NMR (400 MHz, $CDCl_3$, δ): 7.96 (d, $^{3}J_{H-H}$ = 7.05 Hz, Naph, 4H), 7.59 (td, $^{3}J_{H-H}$ = 7.3 Hz, $^{4}J_{H-H}$ = 3.27 Hz, Naph, 4H), 7.46 (m, Naph and Ph, 4H), 7.35 (m, Naph and Ph, 28H), 7.25 (d, $^{3}J_{H-H}$ = 6.29 Hz, Ph, 4H), 7.08 (d, $^{3}J_{H-H}$ = 7.81 Hz, Ph, 4H), 6.84 (s, Mes, 8H), 2.34 (s, Me, 12H), 1.91 (s, Me, 24H) ppm. ^{31}P{^{1}H} NMR (162 MHz, $CDCl_3$, δ): 33.5 ppm. ^{13}C NMR (100 MHz, $CDCl_3$, δ): 147.9, 147.5, 140.8, 140.2, 138.9, 138.6, 137.0, 135.5, 133.8, 133.6, 131.7, 131.5, 131.2, 129.2, 129.1,

129.0, 128.9, 128.5, 128.3, 125.6, 125.4, 24.0 (Me), 21.2 (Me) ppm. Some of the carbon chemical shifts were not observed, and the full assignment of the ^{13}C NMR spectrum could not be completed because of the low intensity and poor resolution of the ^{13}C chemical shifts caused by the poor solubility of this molecule. The ^{11}B NMR chemical shift for **4.2** was not observed, perhaps because of the congested nature and the low symmetry of the molecule. HRMS (ESI): calcd for $C_{104}H_{92}B_2P_2AuCl$ $[M\text{-}Cl]^+$ 1622.6577, found 1621.6555.

4.2.4 Synthesis of 4.3

3.1 (50 mg, 0.07 mmol) and $Pt(SMe_2)_2Cl_2$ (14 mg, 0.035 mmol) were dissolved in 15 mL of dry and degassed THF. The mixture was stirred and refluxed for 5 hrs. After the removal of the solvent in vacuo the residue was purified on a silica gel column (CH_2Cl_2 as the eluent), producing 49 mg of **4.3** as a pale yellow solid (83% yield). ^1H NMR (400 MHz, $CDCl_3$, δ): 7.81 (dd, $^3J_{H\text{-}H}$ = 8.08 Hz, $^4J_{H\text{-}H}$ = 3.28 Hz, naph, 4H), 7.41 (m, Naph and Ph, 16H), 7.24 (m, Naph and Ph, 12H), 7.12 (t, $^3J_{H\text{-}H}$ = 7.58 Hz, Ph, 8H), 7.02 (d, $^3J_{H\text{-}H}$ = 6.31 Hz, Ph, 4H), 7.93 (d, $^3J_{H\text{-}H}$ = 6.06 Hz, Ph, 4H), 6.63 (s, Mes, 8H), 2.18 (s, Me, 12H), 1.76 (s, Me, 24H) ppm. $^{31}P\{^1H\}$ NMR (162 MHz, $CDCl_3$, δ): 19.5 ppm ($J_{P\text{-}Pt}$ = 2646 Hz). ^{13}C NMR (100 MHz, $CDCl_3$, δ): 147.9, 145.8, 141.4, 141.0, 140.6, 139.9, 138.2, 137.2, 135.5, 134.9, 131.0, 130.6, 130.3, 129.7, 129.2, 128.1, 127.7, 125.5, 125.3, 26.7 (Me), 21.2 (Me) ppm. Some of the carbon chemical shifts were not observed, and the full assignment of the ^{13}C NMR spectrum could not be completed because of the low intensity and poor resolution of the ^{13}C chemical shifts caused by the poor solubility of this molecule. The ^{11}B NMR chemical shift for **4.3** was not observed, perhaps because of the congested nature and the low symmetry of the molecule. Anal. Calcd for $C_{104}H_{92}B_2P_2PtCl_2 \cdot 0.5CH_2Cl_2$: C, 72.39; H, 5.41. Found: C, 71.97; H, 5.66.

4.2.4 Computational Study

The DFT calculations were performed using the Gaussian 09, revision B.01,[6] software package and the High Performance Computing Virtual Laboratory (HPCVL) at Queen's University. The ground-state

geometries were fully optimized at the B3LYP[7] level using the LANL2DZ basis set for platinum and gold metal atoms and the 6-31G(d) basis set for all other atoms.[8] The initial geometric parameters in the calculations were employed from crystal structure data for geometry optimization except for compound **4.1** and the fluoride adducts of **4.1**, for which the initial geometry parameters were established by Gauss View (version 3.08). TD-DFT calculations were performed to obtain the vertical singlet and triplet excitation energies.

4.2.5 UV-Visible and Fluorescence Titration of 4.1 and 4.3 with TBAF and Fluoride Binding Constant Calculation

4.2.5.1 Fluoride Titration of 4.1 by TBAF

Fluoride titrations were monitored *via* UV-visible and Fluorescence spectroscopy. In a typical UV-visible titration, TBAF was incrementally added to a CH_2Cl_2 solution of **4.1**, which was at a concentration of 1.0×10^{-5} M. The titrations of the UV-visible and Fluorescence spectra were recorded after each addition, and spectra of **4.1** were also recorded in the absence of TBAF prior to the titration.

4.2.5.2 Fluoride titration of 4.3 by TBAF

Experimental techniques are similar as described in **4.2.5.1**.

4.2.5.3 Fluoride Binding Constant Calculation of 4.2

Calculation methods[9] are the same as described in **3.2.9.2**.

4.2.5.4 Fluoride Binding Constant Calculation of 4.3

The binding constants were determined via Benesi-Hildebrand double reciprocal plots.[10,11] In these cases the inverse of the change in absorbance (ΔA) at a wavelength at which the absorbance signal was responsive to complexation was plotted against the inverse of the fluoride ion concentration. The slope was then determined from the ratio between the intercept on the *y* axis (where $1/[F^-] = 0$), by dividing the intercept value by the slope. This calculation can be expressed as Equation 1:

$$K = \Delta A_0^{-1}/[(\Delta A_2 - \Delta A_1)^{-1}([F^-]_2 - [F^-]_1) \qquad (1)$$

where ΔA_0^{-1} is the *y*-intercept, and ΔA_2 and ΔA_1 are the observed ΔA values at points 2 and 1, respectively in the double reciprocal plot. Likewise, $[F^-]_2$ and $[F^-]_1$ correspond to the fluoride concentrations at points 2 and 1, respectively.

4.2.6 X-Ray Diffraction Analysis

Single crystals of **4.2** and **4.3** were mounted on glass fibers and were collected on a Bruker Apex II single-crystal X-ray diffractometer with graphite-monochromated Mo Kαradiation, operating at 50 kV and 30 mA and at 180 K. Data were processed on a PC with the aid of the Bruker SHELXTL software package (version 6.10)[12] and corrected for absorption effects. Compounds **4.2** belong to the monoclinic crystal space group C2/c. The crystals of **4.3** belong to the triclinic crystal space group P-1. All non-hydrogen atoms were refined anisotropically. In the crystal lattice of **4.2**, $CHCl_3$ solvent molecules (4 $CHCl_3$/per **4.2**) were located and refined successfully. Two of the $CHCl_3$ solvent molecules form H bonds with the Cl ligand bound to the Au(I) atom. The crystal structure data of **4.2 and 4.3** have been deposited at the Cambridge Crystallographic Data Center (CCDC No. 967365 and 967366). The crystal data of **4.2** and **4.3** are reported in Table 4.1 and Table 4.2. The selected bond lengths and angles are given in Table 4.3 for **4.2** and Table 4.4 for **4.3**.

Table 4.1. Crystal data and structure refinement for compound 4.2

Compound	**4.2**
Formula	C108H96Au1B2Cl1P2
Formula weight	2135.22
T, K	293(2)
Wavelength, Å	0.71073
Crystal system	Monoclinic
Space group	C2/c
a, Å	21.703(3)
α, °	90
b, Å	14.949(2)
β, °	107.259(2)
c, Å	32.914(5)
γ, °	90
V, $Å^3$	10198(2)
Z	4
Density (calculated), Mg/m^3	1.391
Absorption coefficient, mm^{-1}	1.861
Theta range for data collection, °	2.80 to 26.00
Reflections collected	21352
Independent reflections	9946 [R(int) = 0.0851]
Completeness to theta = 27.04°	99.1 %
Data / restraints / parameters	9946 / 0 / 575
Goodness-of-fit on F^2	1.041
Final R indices [I>2sigma(I)]	
R_1[a]	0.0696
wR_2[b]	0.1463
R indices (all data)	
R_1[a]	0.1156
wR_2[b]	0.1706

[a] $R_1 = \sum [(|F_0| - |F_c|) / \sum |F_0|$

[b] $wR_2 = [\sum w[(F_0^2 - F_c^2)^2] / \sum [w(F_0^2)^2]]^{1/2}$

$w = 1 / [\sigma^2(F_0^2) + (0.075P)^2]$, where $P = [Max (F_0^2, 0) + 2F_c^2] / 3$

Table 4.2. Crystal data and structure refinement for compound 4.3

Compound	**4.3**
Formula	C52H46B1Cl1P1Pt0.50
Formula weight	845.66
T, K	180(2)
Wavelength, Å	0.71073
Crystal system	Triclinic
Space group	P-1
a, Å	8.5880(14)
α, °	75.467(2)
b, Å	12.0714(19)
β, °	83.659(2)
c, Å	20.917(3)
γ, °	84.927(2)
V, $Å^3$	2082.1(6)
Z	2
Density (calculated), Mg/m^3	1.349
Absorption coefficient, mm^{-1}	1.837
Theta range for data collection, °	1.75 to 27.16
Reflections collected	23446
Independent reflections	9075 [R(int) = 0.1602]
Completeness to theta = 27.04°	98.3 %
Data / restraints / parameters	9075 / 0 / 508
Goodness-of-fit on F^2	0.954
Final R indices [I>2sigma(I)]	
R_1[a]	0.0731
wR_2[b]	0.0946
R indices (all data)	
R_1[a]	0.1814
wR_2[b]	0.1207

[a] $R_1 = \sum [(|F_0| - |F_c|) / \sum |F_0|$

[b] $wR_2 = [\sum w[(F_0^2 - F_c^2)^2] / \sum [w(F_0^2)^2]]^{1/2}$

$w = 1 / [\sigma^2(F_0^2) + (0.075P)^2]$, where $P = [Max (F_0^2, 0) + 2F_c^2] / 3$

Table 4.3. Crystallographic data for compounds 4.2

Au(1)-P(1)#1	2.3188(18)
Au(1)-P(1)	2.3188(18)
Au(1)-Cl(1)	2.787(3)
P(1)-C(47)	1.819(7)
P(1)-C(20)	1.822(7)
P(1)-C(41)	1.826(7)
B(1)-C(1)	1.564(11)
B(1)-C(32)	1.585(11)
B(1)-C(23)	1.590(11)
P(1)#1-Au(1)-P(1)	158.31(9)
P(1)#1-Au(1)-Cl(1)	100.84(5)
P(1)-Au(1)-Cl(1)	100.84(5)
C(47)-P(1)-C(20)	101.6(3)
C(47)-P(1)-C(41)	104.3(3)
C(20)-P(1)-C(41)	105.2(3)
C(47)-P(1)-Au(1)	115.8(2)
C(20)-P(1)-Au(1)	115.6(2)
C(41)-P(1)-Au(1)	112.8(2)
C(1)-B(1)-C(32)	118.0(6)
C(1)-B(1)-C(23)	117.9(7)
C(21)-C(20)-P(1)	119.2(5)
C(19)-C(20)-P(1)	121.1(5)
C(33)-C(32)-B(1)	121.6(6)
C(37)-C(32)-B(1)	119.9(6)
C(46)-C(41)-P(1)	118.1(6)
C(42)-C(41)-P(1)	122.1(6)
C(48)-C(47)-P(1)	122.0(6)
C(52)-C(47)-P(1)	118.2(6)

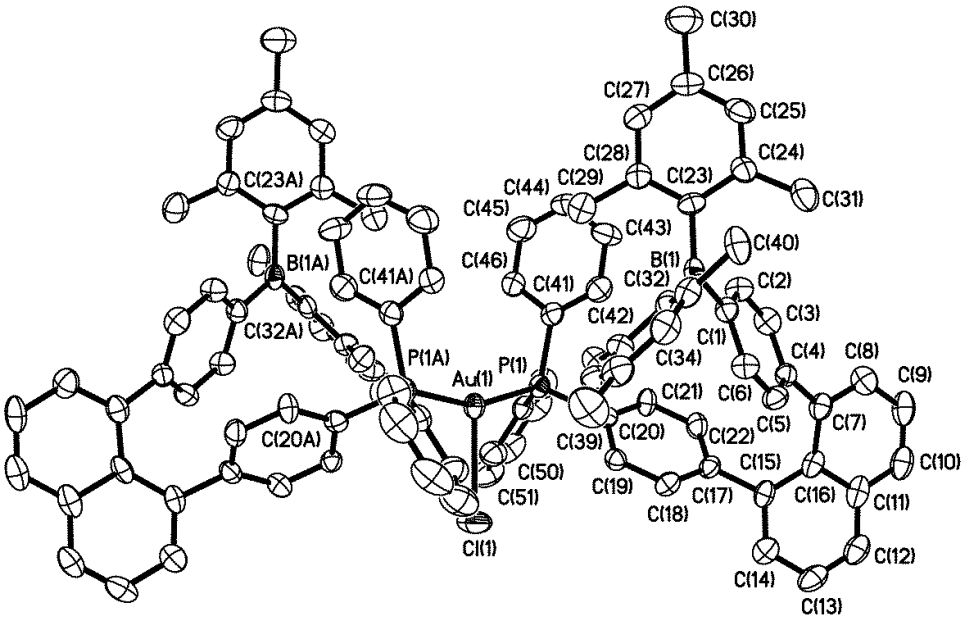

Figure 4.2. Crystal structure of compound **4.2** with 35% thermal ellipsoids. H atoms are omitted for clarity.

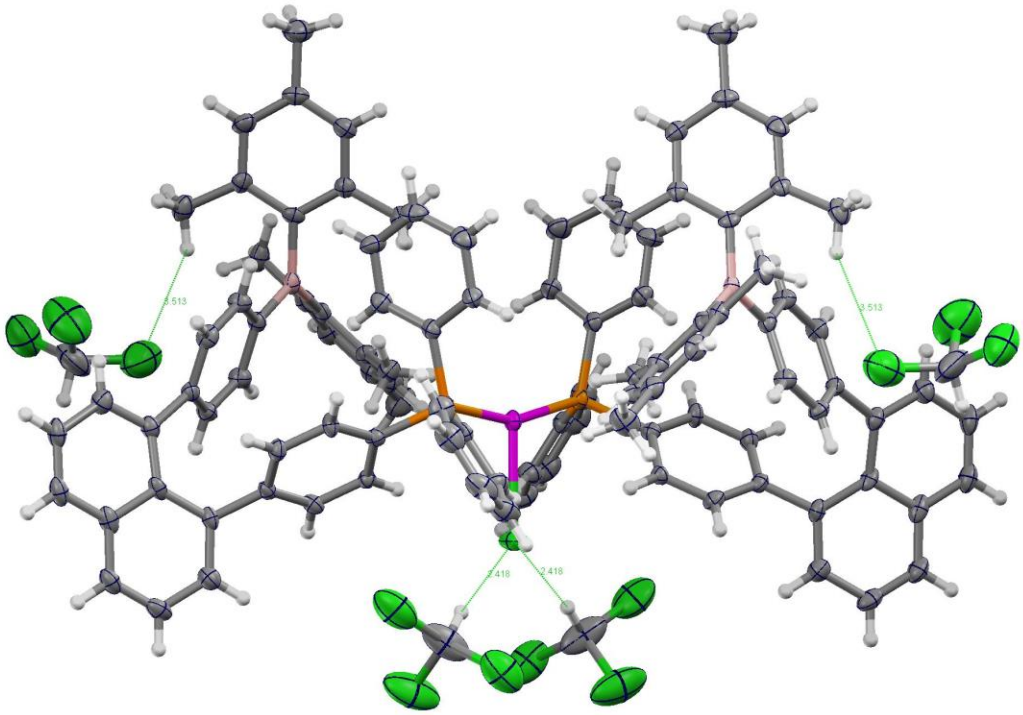

Figure 4.3. A diagram showing the $CHCl_3$ solvent molecules and the locations of H bonds.

Table 4.4. Crystallographic data for compounds 4.3

Pt(1)-Cl(1)	2.3011(18)
Pt(1)-Cl(1)#1	2.3011(18)
Pt(1)-P(1)	2.3163(19)
Pt(1)-P(1)#1	2.3163(19)
P(1)-C(20)	1.811(6)
P(1)-C(29)	1.830(7)
P(1)-C(23)	1.851(8)
B(1)-C(35)	1.551(9)
B(1)-C(44)	1.569(10)
B(1)-C(1)	1.577(10)
Cl(1)-Pt(1)-Cl(1)#1	180.00(9)
Cl(1)-Pt(1)-P(1)	94.34(7)
Cl(1)#1-Pt(1)-P(1)	85.66(7)
Cl(1)-Pt(1)-P(1)#1	85.66(7)
Cl(1)#1-Pt(1)-P(1)#1	94.34(7)
P(1)-Pt(1)-P(1)#1	180.0
C(20)-P(1)-C(29)	106.4(3)
C(20)-P(1)-C(23)	104.2(3)
C(29)-P(1)-C(23)	105.7(3)
C(20)-P(1)-Pt(1)	109.4(2)
C(29)-P(1)-Pt(1)	116.1(2)
C(23)-P(1)-Pt(1)	114.1(2)
C(35)-B(1)-C(44)	124.0(6)
C(35)-B(1)-C(1)	117.5(6)
C(44)-B(1)-C(1)	118.5(6)
C(6)-C(1)-B(1)	122.1(6)
C(2)-C(1)-B(1)	121.8(6)
C(19)-C(20)-P(1)	121.8(5)
C(21)-C(20)-P(1)	119.8(5)
C(28)-C(23)-P(1)	121.8(6)
C(24)-C(23)-P(1)	118.8(6)
C(36)-C(35)-B(1)	122.4(6)

C(40)-C(35)-B(1)	120.5(7)
C(49)-C(44)-B(1)	121.1(6)
C(45)-C(44)-B(1)	122.3(7)

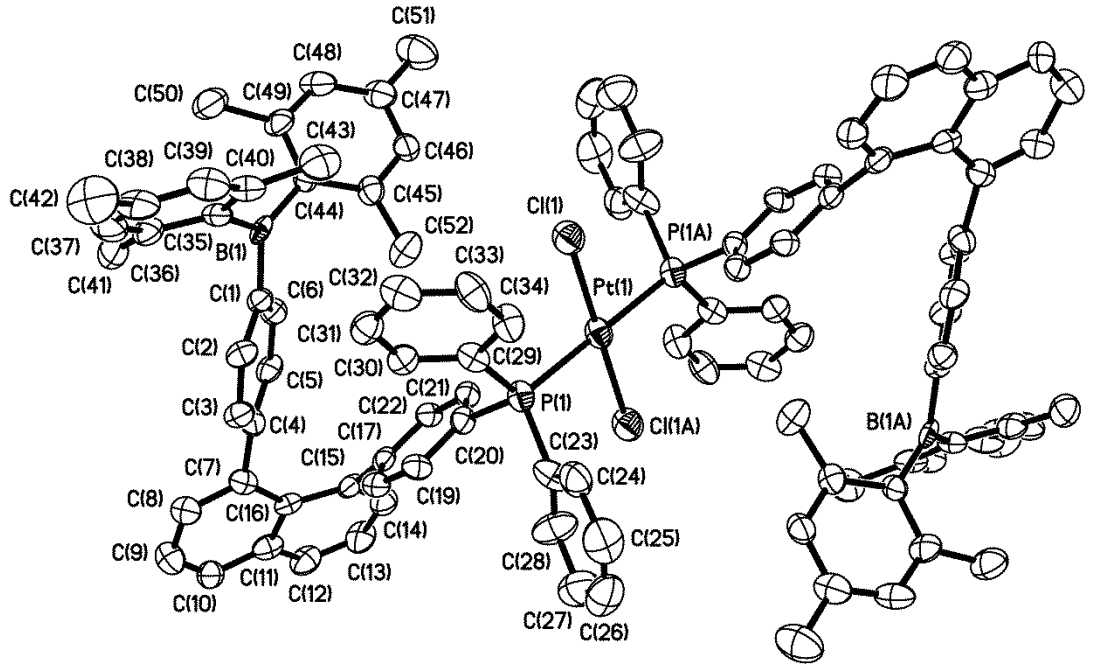

Figure 4.4. Crystal structure of compound **4.3** with 35% thermal ellipsoids. H atoms are omitted for clarity.

4.3 Results and Discussion

4.3.1 Synthesis and Crystal Structures of 4.2, 4.3

Compound **3.1** was readily methylated by reacting with CH_3I in a 1:1 ratio in refluxing THF, producing the phosphonium compound **4.1** in high yield (Figure 4.5). In the ^{31}P NMR spectrum, compared to compound **3.1** which displays a characteristic phosphine signal at -6.0 ppm, **4.1** appears at 22.4 ppm, as is typical of phosphonium.[3a, 13]

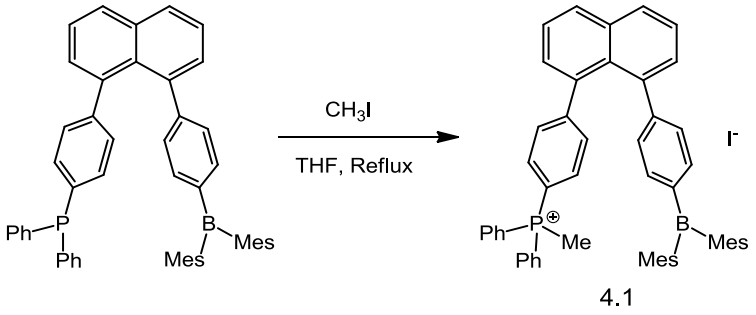

4.1

Figure 4.5. Synthetic method of compound **4.1**.

Furthermore, despite the highly congested nature of molecule **3.1**, it could also bind readily to transition-metal ions, generating the metal complexes in high yields. The Au(I) complex **4.2** and Pt(II) complex **4.3** were obtained by the reaction of **3.1** with $Au(SMe_2)Cl$ and $Pt(SMe_2)_2Cl_2$, respectively, according to Figure 4.6. Both complexes have a metal to ligand **3.1** ratio of 1:2. The 1:1 complex for the Au(I) metal ion was not observed when a 1:1 ratio of **3.1** and $Au(SMe_2)Cl$ was used in the reaction. The metal complexes were fully characterized by NMR and elemental analyses. For the metal complexes, the ^{31}P chemical shift appears at 33.5 ppm for **4.2** and 19.5 ppm for **4.3**, indicating that the phosphine center donates electrons to the AuCl unit more effectively than to the $PtCl_2$ unit.[14]

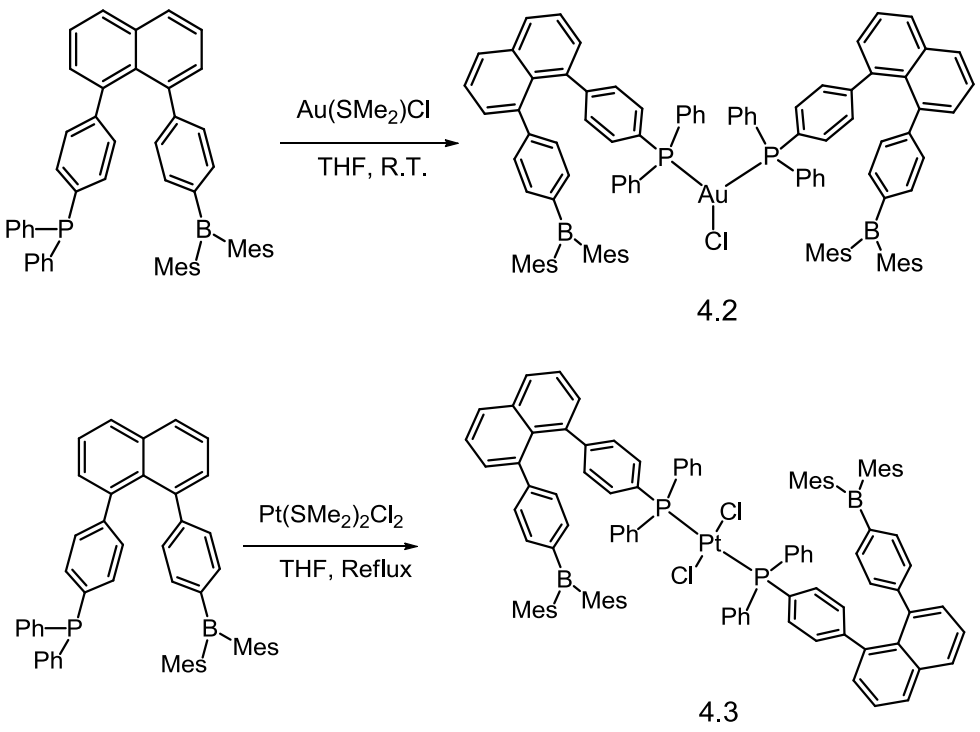

Figure 4.6. Synthetic pathways of complexes **4.2** and **4.3**.

To fully understand the properties of these new compounds, the crystal structures of **4.2** and **4.3** were determined by X-ray diffraction analysis. Efforts to grow single crystals of compound **4.1** were unsuccessful. The crystal structures of **4.2** and **4.3** are shown in Figures 4.7 and Figure 4.8, respectively. The molecule of **4.2** has a crystallographically imposed C_2 symmetry with a helical arrangement of the two **3.1** ligands. The Au(1) atom has a triangular arrangement with the two B atoms (Au(1)···B(1) = 6.53 Å, B(1)···Au(1)···B(1A) = 122.0°). The Au(I) center is bound by two P atoms and one Cl anion with an approximate T shape, as evidenced by the P(1)−Au(1)−P(1A) angle (158.31(9)°) and the P(1)−Au(1)−Cl(1) angle (100.84(5)°). Although many examples of three-coordinated Au(I) compounds with a T-shaped geometry have been known previously,[15] the structure of **4.2** is unusual. In comparison to the closely related compound $Au(PPh_3)_2Cl$, which has an approximate trigonal-planar geometry with a P-Au-P angle of 132.1(1)° and P-Au-Cl angles of 109.2(1) and 112.8(1)°,[15b] **4.2** is much more distorted from a trigonal-planar geometry. Furthermore, the Au(1)−P(1) bond length (2.319(2) Å) in **4.2** is similar

to those in $Au(PPh_3)_2Cl$ (2.323(4), 2.339(4) Å), but the Au(1)-Cl(1) bond (2.787(3) Å) is much longer than that in $Au(PPh_3)_2Cl$ (2.500(4) Å) and the sum of the covalent radii[16] of Au(I) and Cl^- (2.33 Å). Thus, the Au(I) center in **4.2** may be best described as a distorted-linear geometry with a weakly bound Cl^-. The significant departure of **4.2** from the trigonal-planar geometry displayed by $Au(PPh_3)_2Cl$ may be attributed to the steric bulkiness of ligand **3.1**. In the crystal lattice, there are $CHCl_3$ solvent molecules (4 $CHCl_3$/per **4.2**), two of which form H bonds with the Cl ion in **4.2**. Because of the steric congestion, no short Au···Au interactions are present in the lattice.

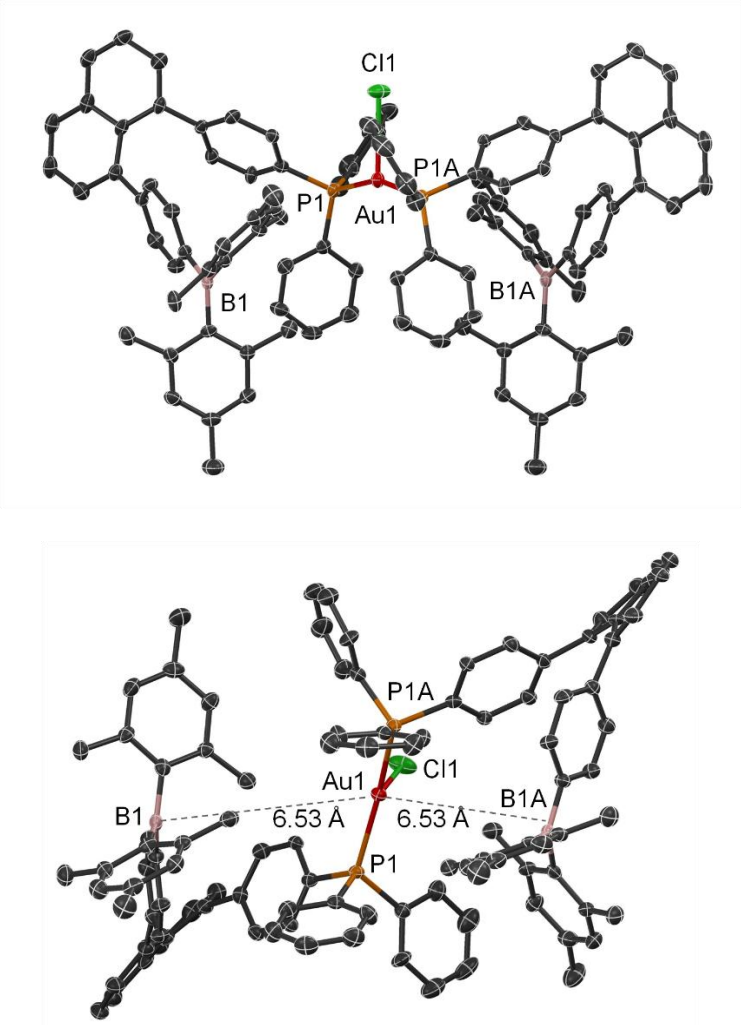

Figure 4.7. Diagrams showing the structure of **4.2** with 35% thermal ellipsoids: (top) side view; (bottom) front view. H atoms are omitted for clarity.

The structure of **4.3** is shown in Figure 4.8. Like the **4.2** molecule, the Pt(II) center is also bound by two **3.1** ligands. The molecule of **4.3** has a crystallographically imposed inversion center with a trans square-planar geometry. Unlike Au complex **4.2**, which has a very long Au-Cl bond, the Pt-P and Pt-Cl bond lengths are typical. The higher coordination number and the much shorter Pt-Cl bonds in **4.3**, in comparison to those of **4.2**, are consistent with the greater donation of the P atoms to the Au(I) metal center in **4.2**. The Pt···B distance is very long at 7.31 Å. The chloride ions are oriented to the B atoms with a separation distance of 6.38 Å. In solution, the *trans*-isomer was observed exclusively, which is clearly favored by the bulky ligand **3.1**. In the crystal lattice, the Pt(II) units of **4.3** are stacked along the a axis with a very long Pt···Pt separation distance (8.59 Å).

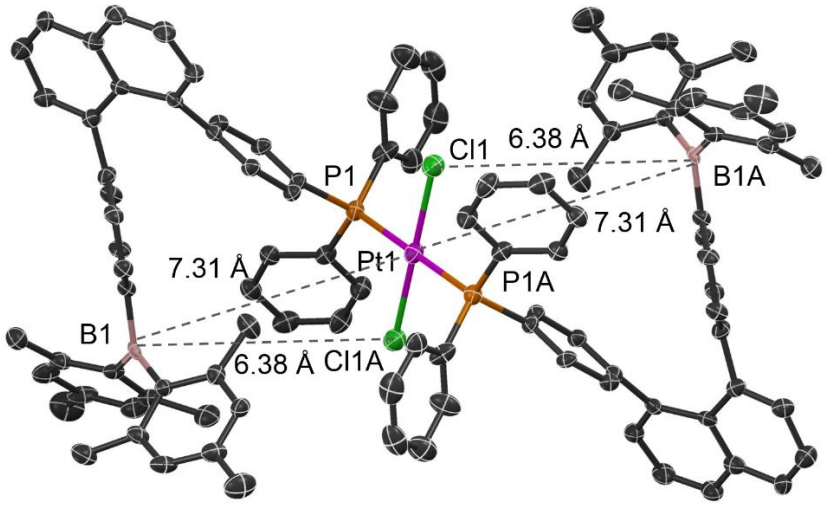

Figure 4.8. Diagram showing the structure of **4.3** with 35% thermal ellipsoids. H atoms are omitted for clarity.

4.3.2 Absorption and Fluorescence Spectra

The absorption spectrum of **4.1** is red-shifted (340 nm) (Figure 4.9) in comparison to that of **3.1** (330 nm). The fluorescence spectrum of **4.1** has only one emission peak at 410 nm in CH_2Cl_2 (Figure 4.10) that is red-shifted by a few nanometers, in comparison to that of **3.1** (407 nm, 532 nm). The absence of the low-energy emission peak in the spectrum of **4.1** further confirmed that the low-energy peak of **3.1** is indeed from a P → B CT transition, since such a transition is not possible in **4.1**.

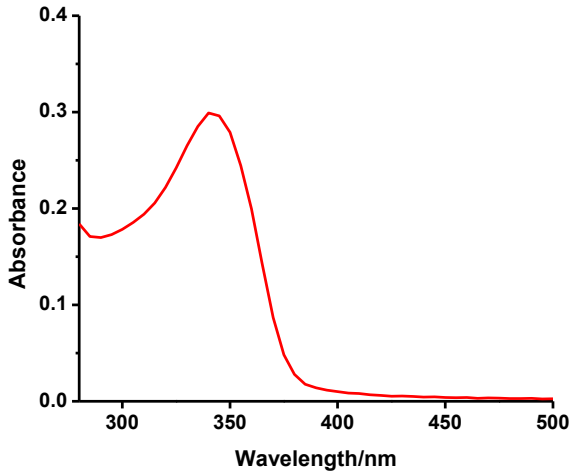

Figure 4.9. Absorption spectrum of **4.1** in CH_2Cl_2 (1.0×10^{-5} M).

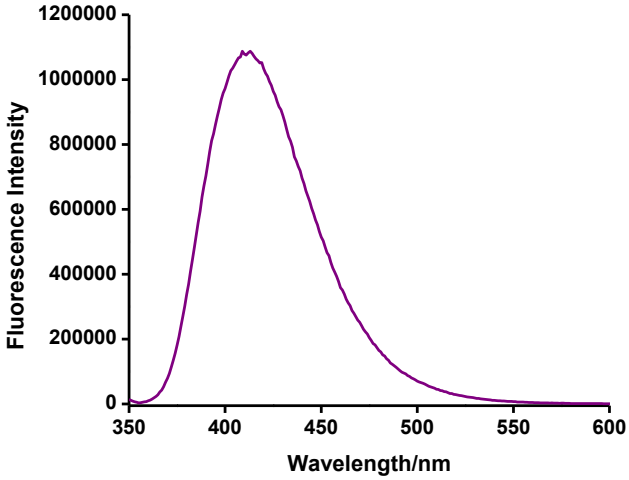

Figure 4.10. Fluorescence spectrum of **4.1** in CH_2Cl_2 (λ_{ex} = 340 nm, 1.0×10^{-5} M).

The fluorescence quantum efficiency (0.55 in CH_2Cl_2) of **4.1** is much higher than that of **3.1** (0.13). TD-DFT computational results of **4.1** indicate that the S_1 transition is mainly from a HOMO → LUMO transition (91%, oscillator strength 0.0113) and is 7 nm lower in energy than that of **3.1**, while the S_2 transition that is close in energy is dominated by a HOMO → LUMO +1 transition (70%, oscillator strength 0.0878) (Table 4.5). As shown in Figure 4.11, the HOMO and LUMO levels of **4.1** are localized

on the mesityl ring and the phosphonium unit, respectively, while LUMO +1 is mainly on the phenyl linker between the phosphonium and the naphthyl with a significant contribution from the empty p orbital of the boron atom. The fluorescence of **4.1** may be therefore attributed to a mixed transition of Mes (π) → phosphonium (π*) and Mes (π) → Ph (π*).

Table 4.5. TD-DFT calculated vertical excitation energy and oscillator strengths for **4.1**

Compound	State	Transition	Energy (nm)	Oscillator Strength (f)
4.1[a]	S_1	HOMO → LUMO (91%)	369	0.0113
	S_2	HOMO → LUMO +1 (70%)	361	0.0878

[a]The anion used in the computation for **4.1** is PF_6^-.

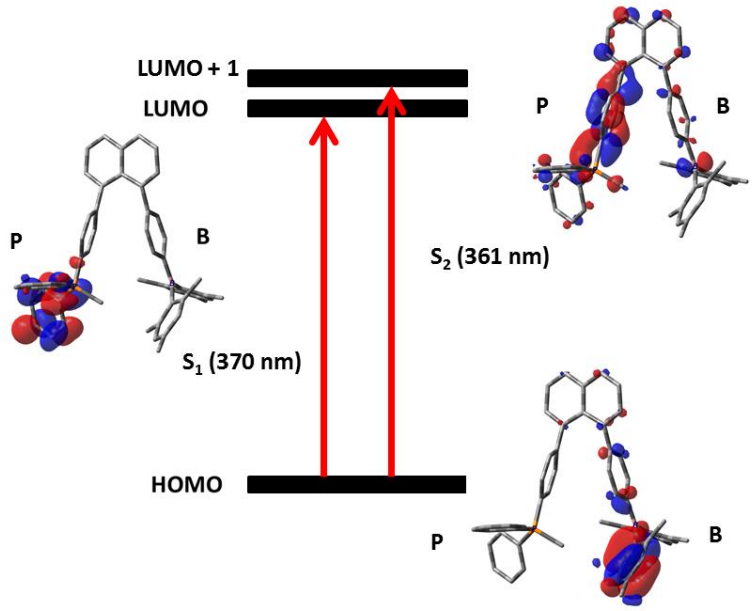

Figure 4.11. Electronic transitions and the associated MO diagrams which are likely responsible for the low-energy absorption bands of **4.1**. The MOs are plotted with an isocontour value of 0.03. The PF_6^- anion in **4.1** is omitted for clarity.

The absorption spectra of the metal complexes are similar to that of **3.1** (Figure 4.12). No phosphorescence was observed for **4.2** and **4.3** even at 77 K. The fluorescence spectra of **4.2** and **4.3** resemble that of **4.1** with λ_{max} at 402 and 408 nm, respectively (Figure 4.13), consistent with the blocking of the P → B CT transition by metal ion coordination. Surprisingly, the Φ_{FL} value (0.44 in CH_2Cl_2) of **4.2** is much higher than that of **3.1**, but that of **4.3** is much lower (0.02 in CH_2Cl_2).

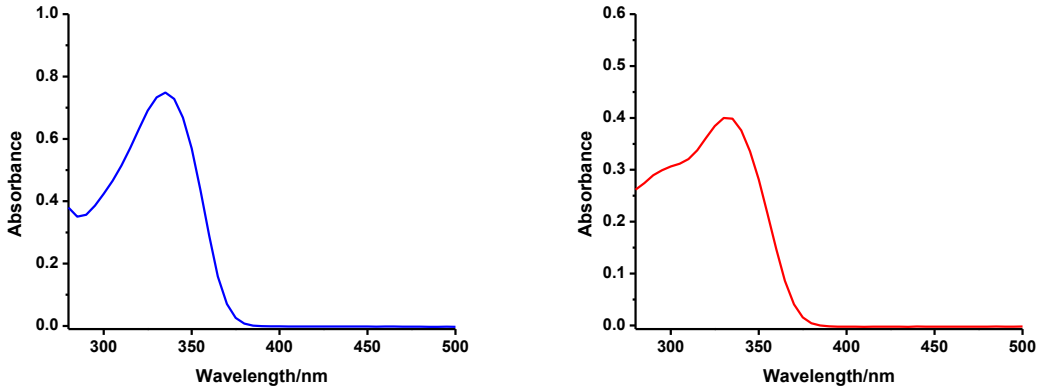

Figure 4.12. Absorption spectra of **4.2** (left) and **4.3** (right) in CH_2Cl_2 (1.0×10^{-5} M).

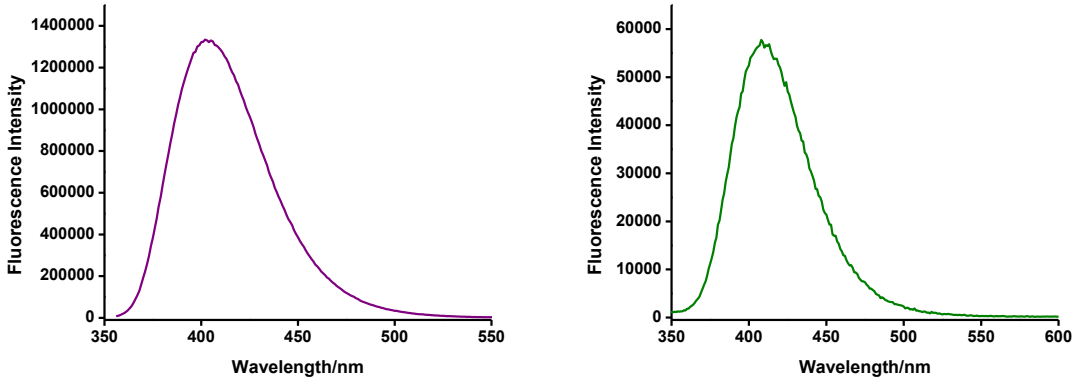

Figure 4.13. Fluorescence spectra of **4.2** (left) and **4.3** (right) in CH_2Cl_2 (λ_{ex} = 330 nm, 1.0×10^{-5} M).

TD-DFT data show that for **4.3** the S_1-S_3 states all have an oscillator strength of 0.000 involving mostly the transition of the Cl^- lone pair electrons and the Pt(II) d electrons to a Pt-ligand σ* orbital (n → σ*); thus, they are unlikely to be responsible for the observed fluorescence. The S_4 and S_5 states of **4.3** are degenerate with an appreciable oscillator strength, involving transitions of HOMO -3/HOMO -4 to

LUMO/LUMO +1 that may be described as Mes (π) → B-Ph (π*) transitions, similar to the S_2 state of **3.1** and **4.1**, as shown in Figure 4.14 and Table 4.6. The fluorescence of **4.3** is therefore most likely from these transitions.

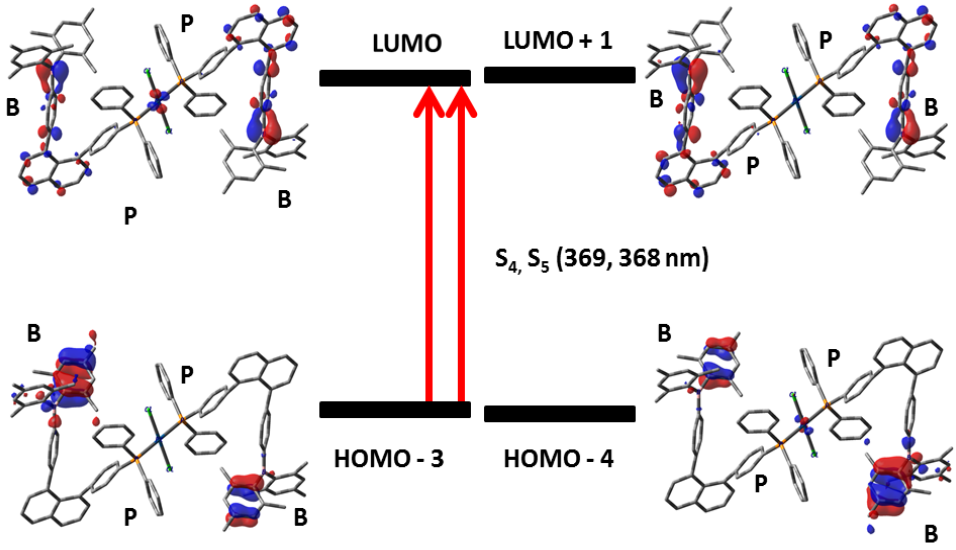

Figure 4.14. Electronic transitions and the associated MO diagrams which are likely responsible for the low-energy absorption bands of **4.3**. The MOs are plotted with an isocontour value of 0.03.

For the complex **4.2**, TD-DFT data indicate that the S_1–S_8 states all have either a 0 or a very small oscillator strength (<0.004) involving transitions mostly from the lone pairs of the chloride ion to the B-Ph π* orbitals (Cl^- → π*). They are therefore not likely to be responsible for the bright fluorescence of **4.2**. Similar to those observed in **4.3**, the S_9 and S_{10} transitions in **4.2** are degenerate, involving HOMO -5/ HOMO -6 to LUMO/LUMO +1 transitions, and may be described as Mes (π) → B-Ph (π*) transitions, as shown in Figure 4.15 and Table 4.6.

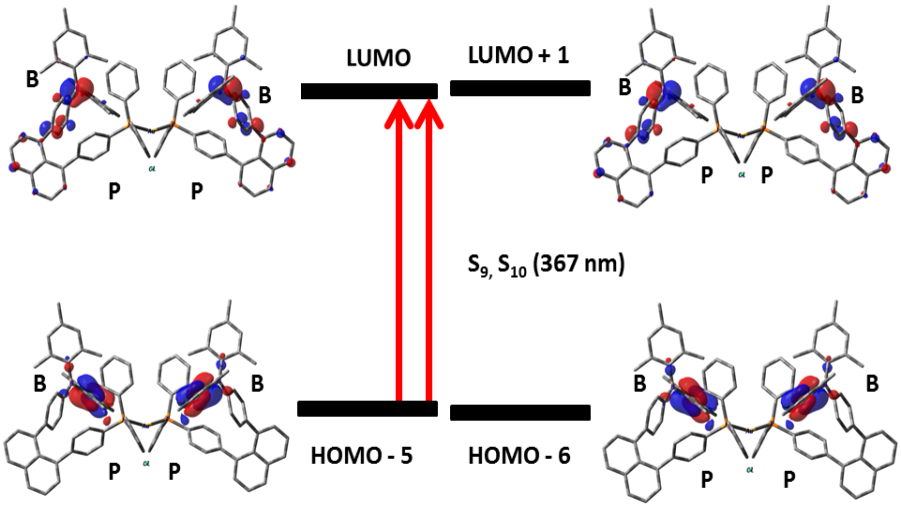

Figure 4.15. Electronic transitions and the associated MO diagrams which are likely responsible for the low-energy absorption bands of **4.2**. The MOs are plotted with an isocontour value of 0.03.

Furthermore, the vertical excitation energies of S_9 and S_{10} in **4.2** are similar to those of S_4 and S_5 in **4.3**. We therefore suggest that the fluorescence of **4.2** likely has the same origin as that of **4.3**: namely, the Mes (π) → B-Ph (π^*) transition. The low fluorescent Φ_{FL} value of **4.3** is likely caused by partial quenching of the Mes (π) → B-Ph (π^*) transition by the low-lying n → σ^* states. Similar quenching in **4.2** by the low-lying Cl^- → π^* states is likely to a much lesser degree due to the weak association of the chloride ion with the complex, as indicated by the very long Au-Cl bond in the crystal structure, which is very likely fully dissociated in solution, giving the propensity of the Au(I) ion to adapt a linear two-coordinate structure.

Table 4.6. TD-DFT calculated vertical excitation energy and oscillator strengths for **4.2** and **4.3**

Compound	State	Transition	Energy (nm)	Oscillator Strength (f)[a]
4.2	S_1	HOMO → LUMO (93%)	436	0.0030
	S_3	HOMO -1 → LUMO +1 (93%)	399	0.0030
	S_7	HOMO → LUMO +3 (95%)	379	0.0040
	S_8	HOMO → LUMO +2 (92%)	378	0.0030
		HOMO -6 → LUMO +1 (32%)		
	S_9	HOMO -5 → LUMO (33%)	367	0.0112
		HOMO -6 → LUMO +1 (32%)		
	S_{10}	HOMO -6 → LUMO (32%)	367	0.2075
		HOMO -5 → LUMO +1 (32%)		
4.3	S_4	HOMO -4 → LUMO (22%)	369	0.0159
		HOMO -3 → LUMO +1 (39%)		
	S_5	HOMO -4 → LUMO +1 (33%)	368	0.1019
		HOMO -3 → LUMO (25%)		

[a]Vertical excitation states with f < 0.001 are not given.

4.3.4 UV-Visible and Fluorescence Titrations of 4.1 and 4.3 with TBAF

The addition of fluoride ions to **4.1** caused partial quenching of the 340 nm peak in the absorption spectra and the emission peak at 410 nm in the fluorescence spectra of **4.1** with a Φ_{FL} change from 0.55 to 0.06 resulting in the disappearance of the deep blue emission color (Figure 4.16 and Figure 4.17).

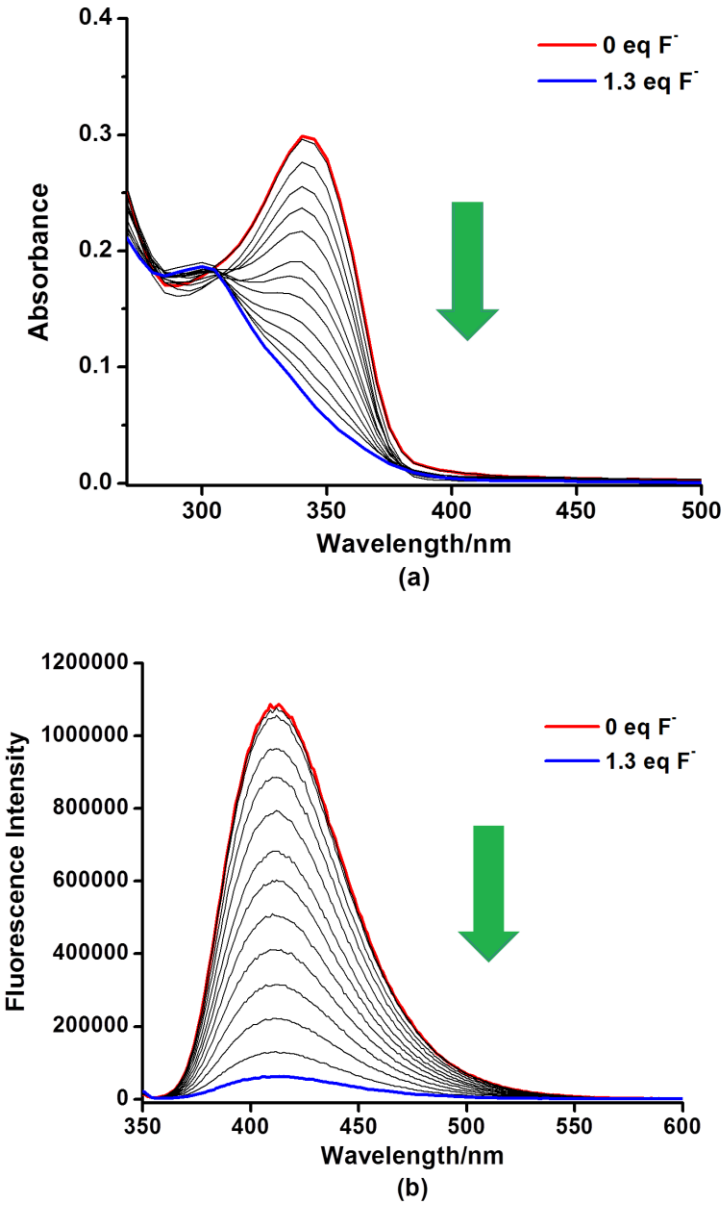

Figure 4.16. (a) Absorption spectral changes of **4.1** in CH_2Cl_2 upon the addition of NBu_4F; (b) Fluorescence spectral changes of **4.1** in CH_2Cl_2 upon the addition of NBu_4F. The fluorescence spectra were recorded using 340 nm excitation.

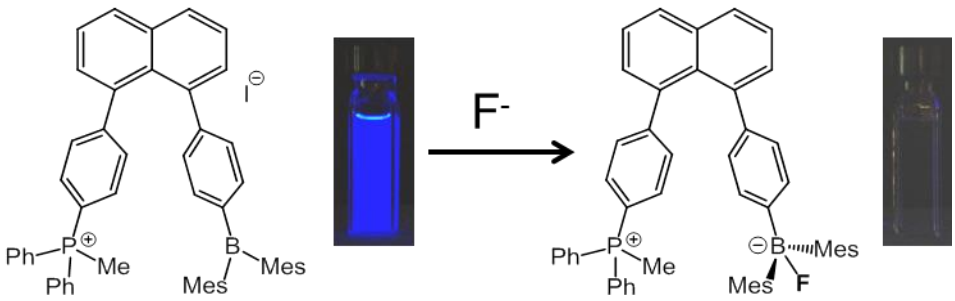

Figure 4.17. Fluorescent color change of **4.1** before and after addition of fluoride ions.

Clearly the decrease of absorbance at 340 nm, the excitation energy used, was responsible for the decrease of the emission peak and the emission quantum efficiency. The binding of fluoride to the B center in **4.1** was also confirmed by the ^{11}B chemical shift (3.5 ppm) observed for [**4.1**·F] and the ^{19}F chemical shift (-167.7 ppm) which are similar to those observed for [**3.1**·F]$^-$ (Figure 4.18 and Figure 4.19).

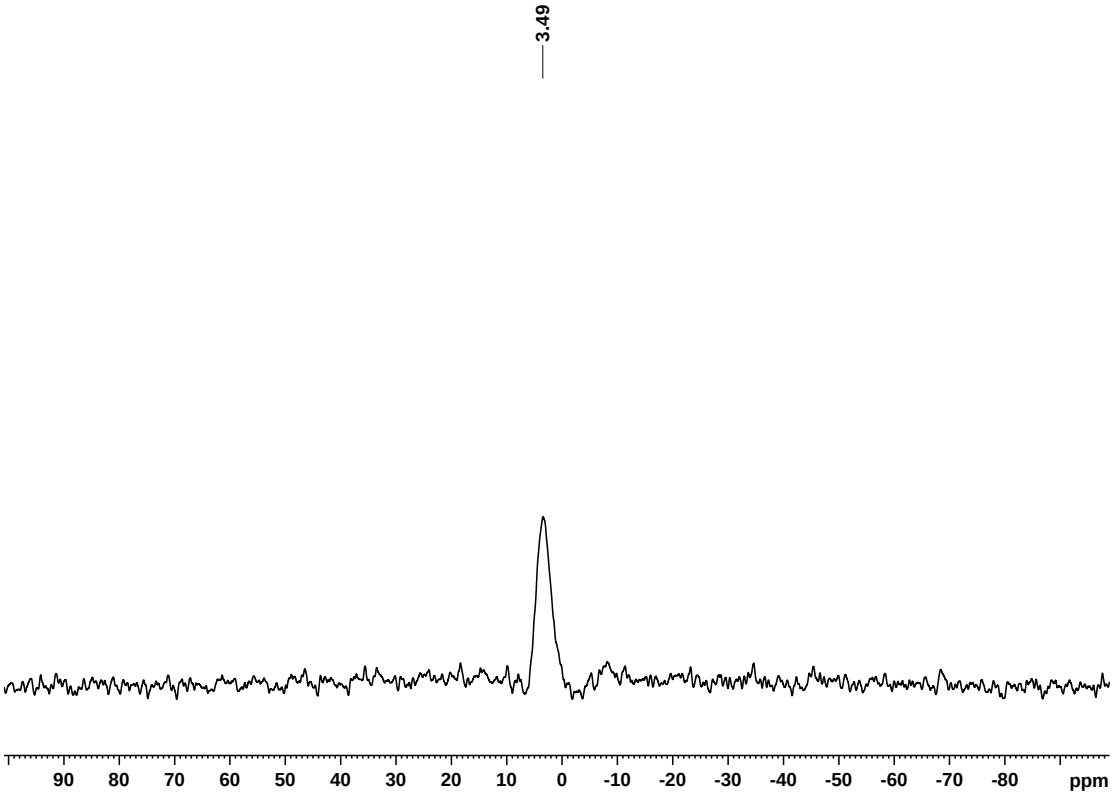

Figure 4.18. ^{11}B NMR spectrum of compound **4.1** with ~2.5 equiv. TBAF (CD_2Cl_2).

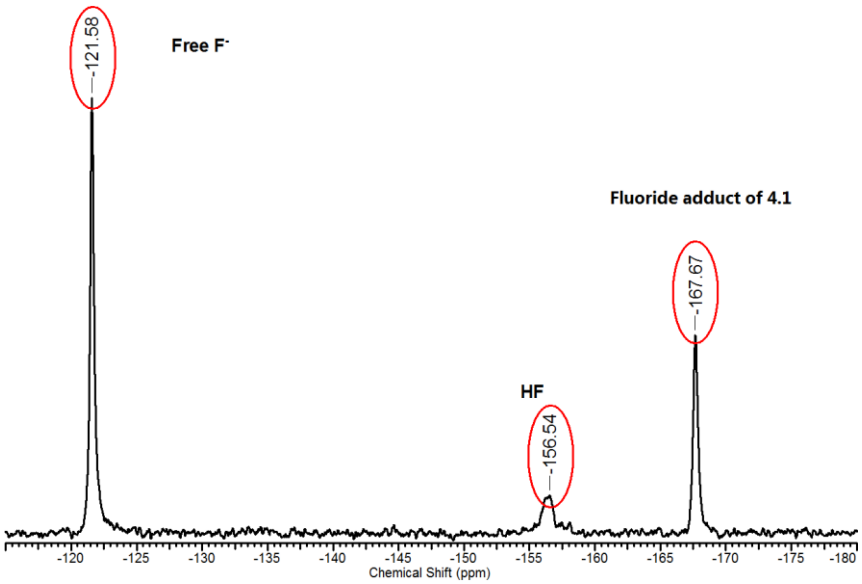

Figure 4.19. ^{19}F NMR spectrum of compound **4.1** with ~2.5 equiv. TBAF (CD_2Cl_2).

TD-DFT data show that the S_1-S_{15} states in [**4.1**·F] all have either 0.000 or very weak oscillator strength, which is in agreement with the observed quenching in absorption and fluorescence spectra of **4.1** upon the addition of fluoride ions. The first two excited states S_2 and S_4 in [**4.1**·F] which have appreciable oscillator strength are shown in Figure 4.20 and Table 4.7.

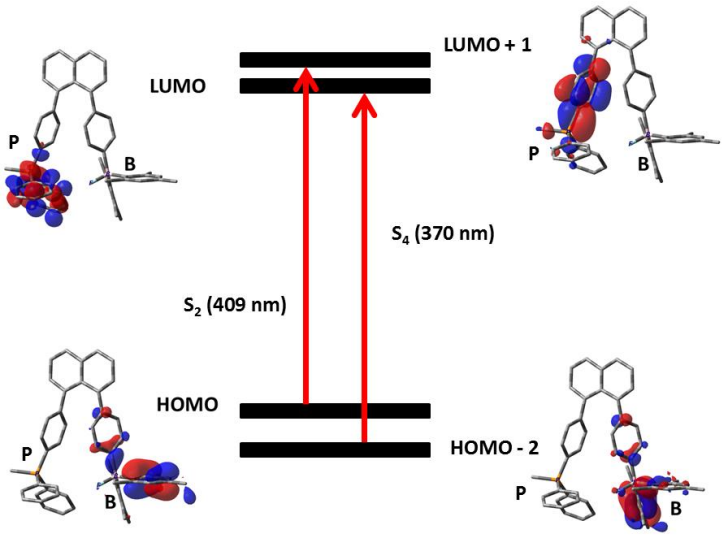

Figure 4.20. Electronic transitions and the associated MO diagrams which are likely responsible for the low-energy absorption bands of [**4.1**·F]. The MOs are plotted with an isocontour value of 0.03.

Table 4.7. TD-DFT calculated vertical excitation energy and oscillator strengths for [**4.1**·F]

Compound	State	Transition	Energy (nm)	Oscillator Strength (f)
[**4.1**·F]	S_1	HOMO → LUMO (91%)	465	0.0000
	S_2	HOMO → LUMO +1 (98%)	409	0.0083
	S_3	HOMO -1 → LUMO (97%)	376	0.0002
		HOMO -2 → LUMO (3%)		
	S_4	HOMO -2 → LUMO (93%)	371	0.0024

For Pt complex **4.3**, the addition of fluoride ions enhanced the absorption band at 330 nm and the emission peak at 408 nm with a Φ_{FL} increasing from 0.02 to 0.10, in a manner similar to that observed for **3.1** (Figure 4.21). The increase of the fluorescence intensity in the fluoride adduct of **4.3** was attributed to the increase of absorbance of the excitation band.

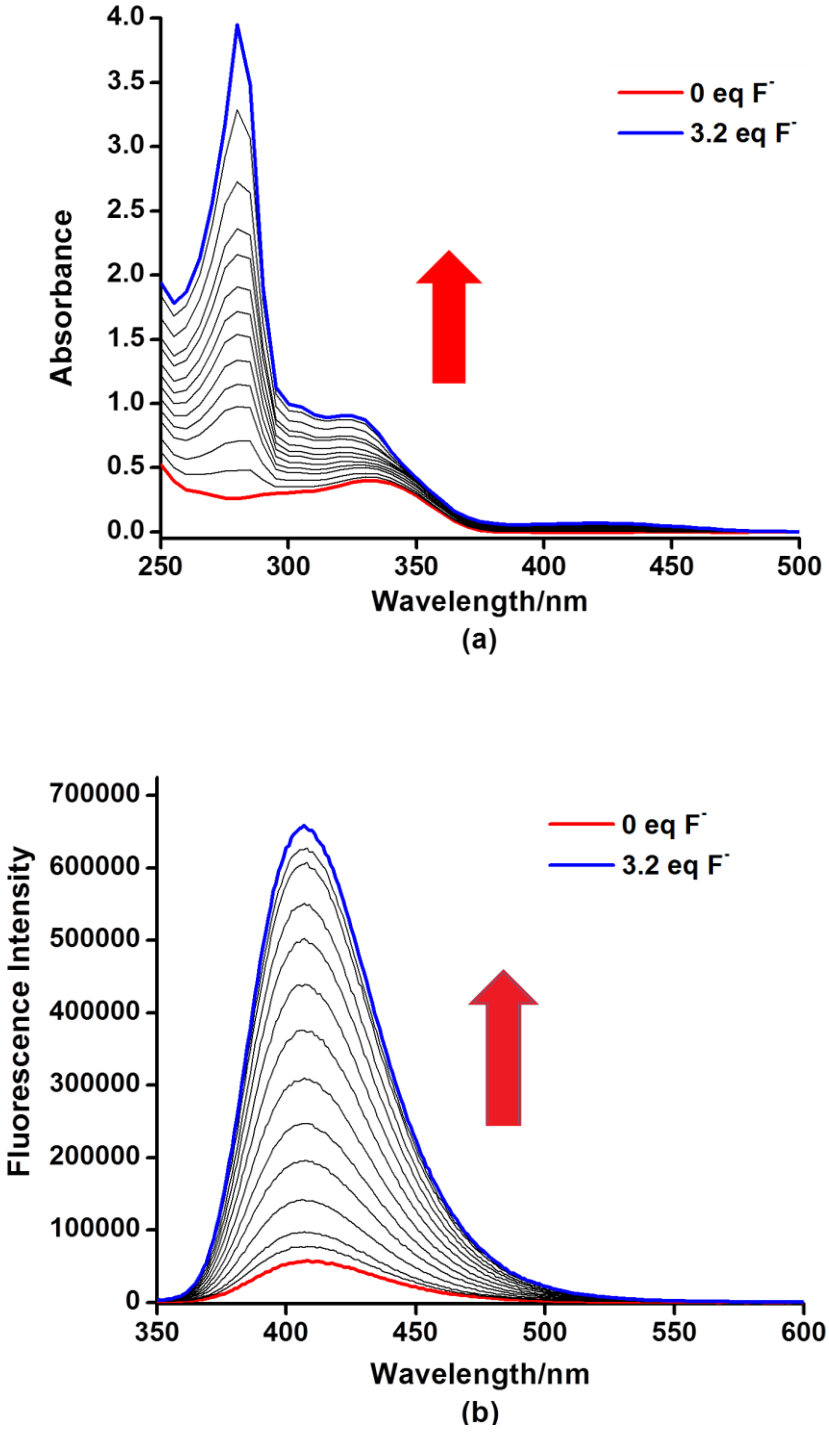

Figure 4.21. (a) Absorption spectral changes of **4.3** in CH_2Cl_2 upon the addition of NBu_4F; (b) Fluorescence spectral changes of **4.3** in CH_2Cl_2 upon the addition of NBu_4F. The fluorescence spectrum was recorded using 330 nm excitation.

A low-energy absorption band at ~425 nm was observed for the fluoride adduct of **4.3**, which likely shares the same origin as that of [**3.1**·F]$^-$ ($BFMes_2$ → naphthyl). Although TD-DFT calculations were not performed for the fluoride adduct of **4.3** due to the large size of the molecule, on the basis of the similarity of the absorption and fluorescence profiles and energies, we suggest that the fluorescence of the fluoride adduct of **4.3** is likely from the state of $BFMes_2$-Ph → naphthyl, similar to that observed in [**3.1**·F]$^-$. The impact of fluoride on fluorescence and the possible origin of fluorescence for **4.3** and its fluoride adduct are illustrated in Figure 4.22.

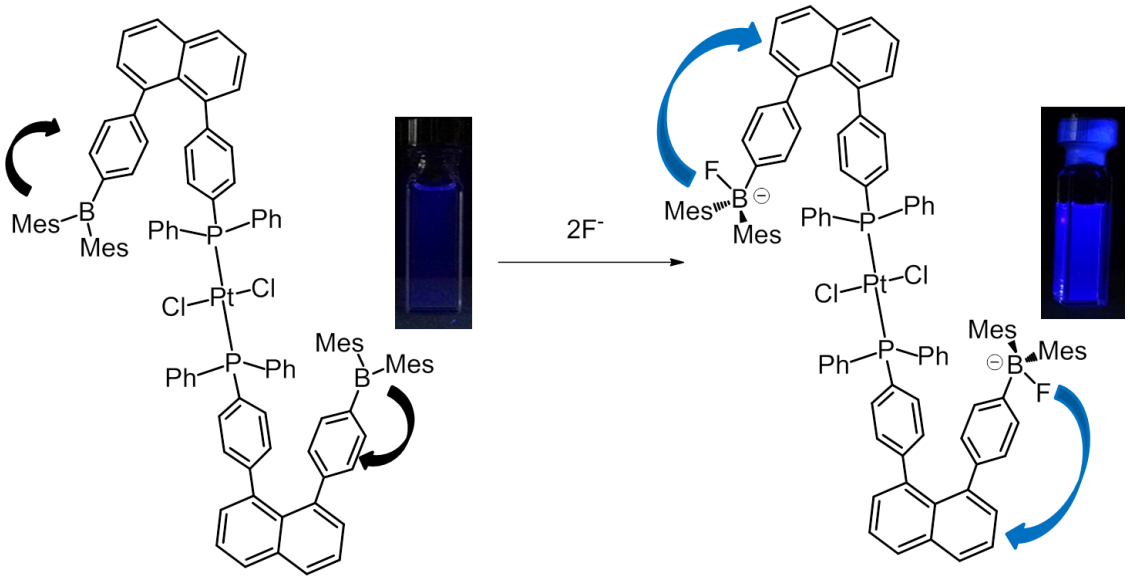

Figure 4.22. Emission color changes of **4.3** and its fluoride-adducts in CH_2Cl_2. Proposed fluorescence change mechanism of **4.3** upon the addition of fluoride ions. The arrows indicate the charge transfer states that are likely responsible for the fluorescence of these molecules.

To examine the effect of the Coulombic force on the fluoride binding strength of the boron center in **4.1**, the binding constants of **3.1** and **4.1** with F^- were compared. The binding constant of **3.1** is (4.3 ± 0.5) × 10^4 M^{-1}, while the binding constant of **4.1** with F^- ((3.2 ± 1.0) × 10^6 M^{-1}) was found to be about 100 times greater than that of **3.1**. The large binding constant increased from **3.1** to **4.1** can be attributed to the Coulombic attraction exerted by the phosphonium ion, despite its long distance from the boron group. Combining Coulombic interactions with a boron center by attaching a peripheral cationic group such as a phosphonium has been demonstrated previously to be highly effective in enhancing the binding strength

of F^- to the sensor by Gabbaï and others.[2,13] However, in our case, the evidence of chelating the fluoride ion by P-CH_3 and B has not been found. The K_1 and K_2 binding constants of **4.3** with F^- were found to be $(5.2 \pm 1.0) \times 10^4$ and $(7.9 \pm 2.0) \times 10^3$ M^{-1}, respectively, indicating that the attachment of a neutral metal unit to the phosphine center in the U-shaped molecule **3.1** has little influence on the sensitivity of the boron center towards fluoride ions, perhaps due to the greatly increased steric congestion and the long separation distance between the metal and the boron atom.

4.4 Conclusions

Converting the donor-acceptor phosphine-borane compound **3.1** to its phosphonium salt **4.1** by methylation greatly enhanced the fluoride binding affinity of the boron center (10^2) due to the Coulombic effect. The emission color of **4.1** is intense deep blue and originates from a π-π* transition which is supported by TD-DFT data. Compared to the emission of **3.1**, the through-space CT pathway is not possible due to the methyl group on the phosphorus atom. Upon the addition of fluoride, **4.1** acts as a "turn-off" sensor due to both the absorption and emission being severely quenched. Based on the large distance between the P and B atoms, we suspect that the fluoride ion is not bridging between P-CH_3 and B. This is quite different from Gabbaï's bifunctionalized chelating triarylborane compound **1.17** previously mentioned, which possesses a relatively short distance between P-CH_3 and B moieties.

Despite its steric congestion, **3.1** was found to be an effective ligand for metal ions such as Au(I) and Pt(II) coordination yielding complexes **4.2** and **4.3** with the ratio of metal to ligand = 1:2. Single crystal structures of both complexes were obtained. The structure of **4.2** shows that the Au center is bound to two P atoms and one Cl anion with an approximate T shape, which is quite different from the trigonal-planar geometry displayed by $Au(PPh_3)_2Cl$. The molecule **4.3** has a *trans* square-planar geometry, which is clearly favored by the bulky ligand **3.1**. The fluorescence spectra of **4.2** and **4.3** resemble that of **4.1**, consistent with blocking of the P → B CT transition by metal ion coordination. Fluoride titration

experiment was only performed on complex **4.3**, which showed a significantly different response towards fluoride compared with that of **4.1**. Complex **4.3** displays interesting "turn-on" fluorescence in response to fluoride ions. However, the attachment of a neutral metal unit to the phosphine center has little effect on the binding ability of the boron center towards fluoride ions.

References

(1) a) Hudnall, T. W.; Chiu, C. W.; Gabbaï, F. P. *Acc. Chem. Res*. **2009**, *42*, 388 and references therein; b) Wade, C. R.; Broomsgrove, A. E. J.; Aldridge, S.; Gabbaï, F. P. *Chem. Rev.* **2010**, *110*, 3958-3984 and references therein.

(2) a) Kim, Y.; Gabbaï, F. P. *J. Am. Chem. Soc*. **2009**, *131*, 3363; b) Broomsgrove, A. E. J.; A. Addy, D.; Di Paolo, A.; Morgan, I. R.; Bresner, C.; Chislett, V.; Fallis, I. A.; Thompson, A. L.; Vidovic, D.; Aldridge, S. *Inorg. Chem.* **2010**, *49*, 157; c) Kim, Y.; Huh, H.-S.; Lee, M. H.; Lenov, I. L.; Zhao, H.; Gabbaï, F. P. *Chem. Eur. J.* **2011**, *17*, 2057; d) Zhao, H.; Leamer, L. A.; Gabbaï, F. P. *Dalton Trans*. **2013**, *42*, 8164 and references therein.

(3) a) Hudnall, T. W.; Kim, Y.; Bebbington, M. W. P.; Bourissou, D.; Gabbaï, F. P. *J. Am. Chem. Soc*. **2008**, *130*, 10890; b) Zhao, H.; Gabbaï, F. P. *Organometallics* **2012**, *31*, 2327; c) Wade, C. R.; Gabbaï. F. P. *Organometallics* **2011**, *30*, 4479; d) Zhao, H.; Gabbaï, F. P. *Nature Chem.* **2010**,*2*, 984.

(4) a) Sun, Y.; Ross, N.; Zhao, S.; Huszarik, K.; Jia, W.; Wang, R.; Macartney, D.; Wang, S. *J. Am. Chem. Soc*. **2007**, *129*, 7510; b) Dorsey, C. L.; Jewula, P.; Hudnall, T. W.; Hoefelmeyer, J. D.; Taylor, T. J.; Honesty, N. R.; Chiu, C.-W.; Schulte, M.; Gabbaï, F. P. *Dalton Trans.* **2008**, 4442.

(5) Melaimi, M.; Gabbaï, F. P. *J. Am. Chem. Soc.* **2005**, *127*, 9680.

(6) Frisch, M. J.; Trucks, G. W.; Schlegel, H. B.; Scuseria, G. E.; Robb, M. A.; Cheeseman, J. R.; Scalmani, G.; Barone, V.; Mennucci, B.; Petersson, G. A.; Nakatsuji, H.; Caricato, M.; Li, X.; Hratchian, H. P.; Izmaylov, A. F.; Bloino, J.; Zheng, G.; Sonnenberg, J. L.; Hada, M.; Ehara, M.; Toyota, K.; Fukuda, R.; Hasegawa, J.; Ishida, M.; Nakajima, T.; Honda, Y.; Kitao, O.; Nakai, H.; Vreven, T.; Montgomery, J. A., Jr.; Peralta, J. E.; Ogliaro, F.; Bearpark, M.; Heyd, J. J.; Brothers, E.; Kudin, K. N.; Staroverov, V. N.; Keith, T.; Kobayashi, R.; Normand, J.; Raghavachari, K.; Rendell, A.; Burant, J. C.; Iyengar, S. S.; Tomasi, J.; Cossi, M.; N. Rega, N.; Millam, J. M.; Klene, M.; Knox, J. E.; Cross, J. B.; Bakken, V.; Adamo, C.; Jaramillo, J.; Gomperts, R.; Stratmann, R. E.; Yazyev, O.; Austin, A. J.; Cammi, R.; Pomelli, C.; Ochterski, J. W.; Martin, R. L.; Morokuma, K.; Zakrzewski, V.

G.; Voth, G. A.; Salvador, P.; Dannenberg, J. J.; Dapprich, S.; Daniels, A. D.; Farkas, O.; Foresman, J. B.; Ortiz, J. V.; Cioslowski, J.; Fox, D. J. *Gaussian09*, revision B.01; Gaussian, Inc., Wallingford, CT, 2010.

(7) a) Lee, C.; Yang, W.; Parr, R. G. *Phys. Rev. B.* **1988**, *37*, 785; b) Becke, A. D. *J. Chem. Phys.* **1993**, *98*, 5648.

(8) Hay, P. J. *J. Phys. Chem. A.* **2002**, *106*, 1634.

(9) Wylie, R. S.; Macartney, D. H. *Inorg. Chem.* **1993**, *32*, 1830.

(10) Benesi, H. A.; Hildebrand, J. H. *J. Am. Chem. Soc.* **1949**, *71*, 2703.

(11) Connors, K. A. *Binding Constants. New York: John Wiley & Sons*, **1987**, 52.

(12) *SHELXTL Version 6.14*; Bruker AXS, Madison, WI, 2000-2003.

(13) Lee, M. H.; Agou, T.; Kobayashi, J.; Kawashima, T.; Gabbaï. F. P. *Chem. Commun.* **2007**, 1133.

(14) a) Gimeno, M. C.; Laguna, A. *Chem. Rev.* **1997**, *97*, 511; b) Rigamonti, L.; Manassero, C.; Rusconi, M.; Manassero, M.; Pasini, A. *Dalton Trans*. **2009**, 1206.

(15) a) Bowmaker, G. A.; Dyason, J. C.; Healy, P. C.; Engelhardt, L. M.; Pakawatchai, C.; White, A. H. J. *Dalton Trans*. **1987**, 1089; b) Baenziger, N. C.; Dittemore, K. M.; Doyle, J. R. *Inorg. Chem*. **1974**, *13*, 805; c) Khan, M. N. I.; Staples, R. J.; King, C.; Fackler, J. P., Jr.; Winpenny, R. E. P. *Inorg. Chem*. **1993**, *32*, 5800; d) Wade, C. R.; Lin, T.-P.; Nelson, R. C.; Mader, E. A.; Miller, J. T.; Gabbaï. *J. Am. Chem. Soc.* **2011**, *133*, 8948.

(16) Marsh, W. C.; Trotter, J. *J. Chem. Soc. A.* **1971**, 1482

Chapter 5

Reactivity Study of Phosphine-Borane Functionalized Naphthalene and Related Compounds towards Small Molecules

5.1 Introduction

Frustrated Lewis Pairs (FLPs)[1] are a relatively new class of compounds which combine bulky electron-rich Lewis bases with bulky electron-poor Lewis acids that cannot form strong adducts in solution due to steric and/or electronic constraints. As a result, these types of systems tend to display unique and unprecedented reactivity such as room temperature heterolytic H_2 activation demonstrated in the pioneering work of Stephan[2] and Erker[3] less than one decade ago. In the following eight years, the field of FLPs chemistry has seen immense growth with respect to both the ever-expanding library of donor-acceptor species[4] and the number of small molecules which they can activate (*e.g.* CO_2,[5] SO_2,[6] N_2O,[7] *etc*). In addition to the activation of small molecules, FLPs systems have also been shown to activate certain heterocycles such as tetrahydrofuran (THF), dioxane, and thioxane.[8] Much less common than the quintessential phosphino-borane FLPs are those where the donor has been replaced by an N-heterocyclic carbene (NHC),[9] despite them possessing similar reactivity towards the activation of several small molecules. NHCs themselves have become incredibly important organic species over the last several decades and are widely studied for applications in transition-metal chemistry[10] and main-group chemistry.[11] NHCs on their own have also been shown to activate all types of different chemical connectivity's such as C-H, C-N and C-C bonds,[12] as well as undergo intramolecular C-N bond cleavage and ring expansion reactions (RER) *via* either transition metal[13] or main group element[14] insertions. In chapter 3 and 4, the non-conjugated naphthalene-linked phosphine-borane compound **3.1** and its methylated phosphonium salt **4.1** (Figure 5.1) were described and their interesting photophysical properties were investigated.[15] Due to the rigid backbone and highly congested environment around both

the phosphorous and boron atoms, we suspected that these systems could potentially behave as FLPs either on their own or in cooperation with a second stronger donor species such as *N,N'*-dimethylimidazol-2-ylidene (IMe). Based on these considerations, a series of reactivity studies towards selected small molecules based on compounds **3.1**, **4.1** and related ylide compound **5.3** have been investigated. Surprisingly, compounds **3.1**, **5.3**, and **4.1** show distinctively different reactivity toward IMe as illustrated in Figure 5.1, where the formers produce simple adducts **5.2** and **5.4**, while the latter generates an unusual species **5.1**, in which the IMe molecule has undergone a rather peculiar transformation involving the cleavage of several bonds within the carbene itself. Given the low Lewis acidity and high stability of compound **4.1** under ambient conditions, the fragmentation of IMe, apparently enabled by **4.1**, is highly unusual and remarkable. Details and mechanistic insight into this interesting double C-N bond activation of an NHC are presented in this chapter.

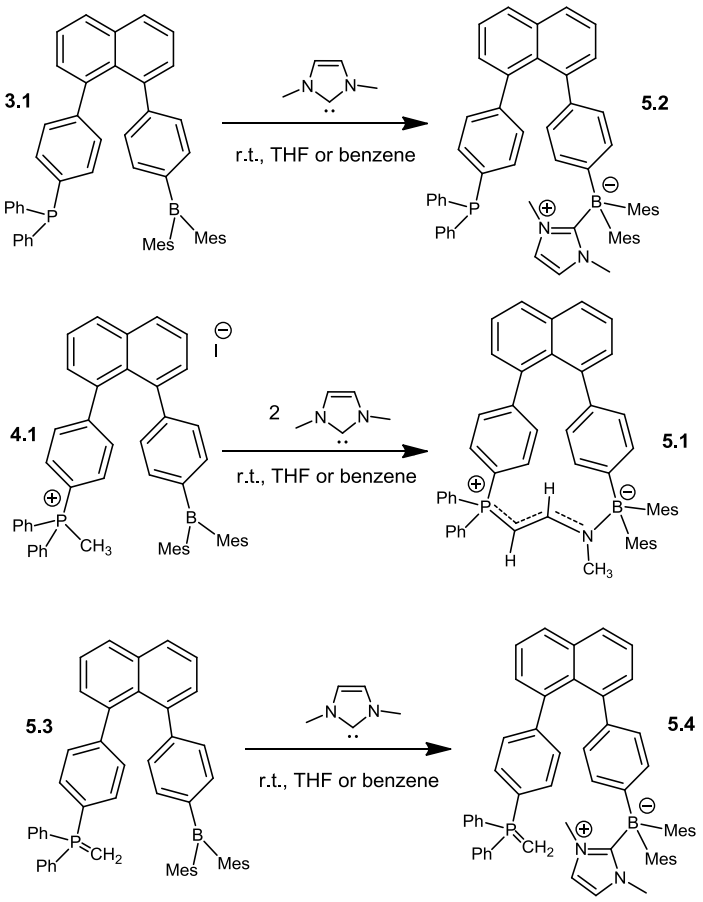

Figure 5.1. Compound **3.1**, **4.1** and **5.3** react with IMe.

5.2 Experimental

5.2.1 General Procedures

All reactions were done under an atmosphere of dry, oxygen-free nitrogen by either employing Schlenk techniques or working inside of an inert atmosphere glove box. Reagents were purchased from Aldrich Chemical Company and used without further purification. Solvents were freshly distilled over appropriate drying reagents. ^{1}H, ^{13}C, ^{31}P and ^{11}B NMR spectra were recorded on Bruker Avance 300, 400, 500 or 600 MHz spectrometers. Deuterated solvents were purchased from Cambridge Isotopes. High-resolution mass spectra (HRMS) were obtained from an Applied Biosystems Qstar XL spectrometer. Elemental analyses were conducted at Laboratoire d'Analyse Élémentaire de l'Université de Montréal. IMe and (*i*Pr)NH_2BH_3 were synthesized by the modified literature procedures.[16, 17]

5.2.2 Synthesis of 5.1

To a solution of **4.1** (124 mg, 0.145 mmol) dissolved in THF (10 mL) was added THF solution of IMe (40 μL, 0.29 mmol) via micro-syringe. The reaction was stirred overnight at room temperature. The product was collected as colorless crystals yielding 8 mg (7.2%) of compound **5.1**, with yielding 35% of the side product **5.6** in solution. ^{1}H NMR (600 MHz, CD_2Cl_2, 240 K, δ) 7.97 (br. d, J = 8.2 Hz, Naph, 1H), 7.89 (br. d, J = 8.1 Hz, Naph, 1H), 7.85 (dd, J = 12.6 Hz, 7.6 Hz, ph, 2H), 7.70 (m, ph, 3H), 7.63 (m, ph, 3H), 7.54 (m, ph, 2H), 7.51 (m, Naph, 2H), 7.43 (br. d, J = 7.8 Hz, ph, 1H), 7.41 (dd, J = 7.1 Hz, 1.1 Hz, Naph, 1H), 7.34 (br. d, J = 7.3 Hz, ph, 1H), 7.28 (d, J = 7.1Hz, Naph, 1H), 7.14 (dd, J = 11.7 Hz, 7.8 Hz, ph, 1H), 7.05 (dd, J = 15.4, 13.3 Hz, =CH-N, 1H), 6.85 (m, ph, 2H), 6.79 (m, ph, 1H), 6.76 (s, Mes, 1H), 6.62 (s, Mes, 2H), 6.33 (s, Mes, 1H), 6.29 (d, J = 7.8 Hz, ph, 1H), 6.25 (d, J = 7.8 Hz, ph, 1H), 3.73 (dd, J = 18.4 Hz, J = 13.2 Hz, P-CH, 1H), 2.61 (s, N-Me, 3H), 2.52 (s, Me, 3H), 2.22 (s, Me, 3H), 2.08(s, Me, 3H), 2.04 (s, Me, 3H), 1.78 (s, Me, 3H), 1.4 (s, Me, 3H) ppm, ^{13}C NMR (126 MHz, CD_2Cl_2, 240 K, δ) 162 (d, $J_{c\text{-}p}$ = 21.4 Hz, =CH-N), 156.6 (Mes), 152.4 (ph), 149.9 (ph), 147.8 (Mes), 144.4 (Mes), 143.6 (Mes), 143.2 (Mes), 141.0 (Naph), 138.7 (Naph), 137.3 (ph, Mes), 136.4 (ph), 135.2 (Naph), 133.6 (ph), 133.1 (ph),

132.9 (Mes, ph), 132.5 (ph), 132.0 (ph), 131.8 (Mes), 131.7 (Naph), 131.4 (Naph), 130.9 (ph), 130.6 (ph), 129.7 (Naph), 129.3 (ph), 129.2 (ph, Mes),. 129.1 (Naph, Mes), 128.9 (Mes), 128.8 (Mes), 128.4 (ph), 127.9 (Naph), 126.4 (ph), 125.7 (ph), 125.6 (Naph), 125.4 (ph), 124.8 (Naph), 117.8 (ph), 47.81 (d, J_{c-p} = 122.4 Hz, P-CH), 39.1 (N-Me), 26.7 (Me), 25. 9 (Me), 24.1 (Me), 23.6 (Me), 20.5 (Me), 20.4 (Me) ppm, $^{31}P\{^{1}H\}$ NMR (162 MHz, CD_2Cl_2, 298 K, δ): 23.4 ppm. $^{11}B\{^{1}H\}$ NMR (128 MHz, CD_2Cl_2, 298 K, δ): 0.22 ppm. HREIMS. Calcd. for $C_{55}H_{51}NBP$: 767.3852. Found: 767.3859. Anal. Calcd for $C_{55}H_{51}NBP \bullet 0.5\ C_4H_{10}O$: C 85.06, H 7.01, N 1.74. Found: C 84.94, H 6.89, N 1.86.

5.2.3 NMR experiment for the formation of 5.2

A sealable J-Young NMR tube was charged with **3.1** (60 mg, 0.084 mmol) and IMe (8 mg, 0.084 mmol) dissolved in C_6D_6 and sealed forming a yellow solution. Compound **5.2** was formed almost quantitatively and recrystallized in THF yielding yellow crystal (94%). ^{1}H NMR (500 MHz, C_6D_6, δ) 7.66 (dd, J = 6.31 Hz, 3.15 Hz, Naph, 1H), 7.63 (d, J = 7.88 Hz, Ph, 1H), 7.38 (m, Ph, 5H), 7.25 (m, Naph, 3H, Ph, 2H), 7.07 (m, Ph, 8H), 6.93 (d, J = 8.2 Hz, Ph, 2H), 6.91 (s, Mes, 4H), 6.84 (d, J = 8.51 Hz, Naph, 2H), 6.07 (br. s, -CH=, 1H), 5.66 (br. s, -CH=, 1H), 3.13 (br. s, N-CH_3, 3H), 2.8 (br. s, N-CH_3, 3H), 2.28 (s, -CH_3, 6H), 1.94 (s, -CH_3, 12H) ppm, ^{13}C NMR (126 MHz, C_6D_6, δ): 145.1 (Ph), 141.9 (Naph, Ph), 140.3 (Ph), 138.8 (Ph), 137.7 (Ph), 136.2 (Ph), 134.3 (Ph), 134.1 (Ph), 133.1 (Mes), 131.9 (Ph), 131.8 (Ph), 131.5 (Naph), 130.1 (Naph, Ph), 130.0 (Mes), 129.7 (Ph), 129.2 (Ph), 128.9 (Ph), 128.6 (Ph), 128.4 (Naph), 127.3 (Mes, Ph), 126.6 (Ph), 125.7 (Naph, Ph), 124.9 (Naph, Ph), 121.9 (carbene, =CH-), 121.5 (carbene, =CH-), 40.7 (carbene, N-Me), 36.8 (carbene, N-Me), 20.9 (Me), 25.5 (Me) ppm, $^{31}P\{^{1}H\}$ NMR (162 MHz, C_6D_6, δ): -3.56 ppm. $^{11}B\{^{1}H\}$ NMR (160 MHz, C_6D_6, δ): -9.7 ppm.

5.2.4 Synthesis of 5.3

In the glovebox, compound **4.1** (200 mg) and NaH (5.6 mg) were charged into a vial with a magnetic stir bar. 10 mL of THF was added into the vial and the mixture was stirred overnight at room temperature.

Solvent was removed and residue was washed with diethyl ether. The yellow solution was filtered over celite and the product was recrystallized of **5.3** with a yield of 65% (110 mg) .^{1}H NMR (500 MHz, C_6D_6, δ) 7.8 (dd, J = 8.04, 11.35 Hz, Ph, 4H), 7.75 (d, J = 7.63 Hz , Ph, 2H), 7.63 (d, J = 7.72 Hz, Naph, 4H), 7.34 (m, Ph, 3H), 7.25 (d, J = 6.99 Hz , Ph, 1H), 7.15 (m, Ph, 6H), 7.06 (d, J = 7.25 Hz, Naph, 2H), 7.03 (d, J = 6.94 Hz, Ph, 2H), 6.93 (s, Mes, 4H), 2.33 (s, Me, 6H), 2.22(s, Me, 12H), 0.84 (d, P=CH_2, 2H) ppm, ^{13}C NMR (126 MHz, C_6D_6, δ): 148 (Ph), 146 (Ph), 142 (Naph, Mes), 141(Naph), 140.7 (Mes), 140.11 (Ph), 138.4 (Naph), 137.2 (Naph, Mes), 135.8 (Ph), 132.4 (Ph), 132 (Ph), 131.2 (Ph), 130.3 (Ph), 129.8 (Ph), 129.2 (Naph, Ph), 128.6 (Mes, Ph), 128.4 (Ph), 128.1 (Ph), 125.4 (Ph), 24.2 (Me), 21.0 (Me), -4.4 (d, $J_{c\text{-}p}$ = 96 Hz, P=CH_2) ppm, ^{31}P{^{1}H} NMR (162 MHz, C_6D_6, δ): 21.0 ppm.

5.2.5 NMR experiment for the formation of 5.4

A sealable J-Young NMR tube was charged with **5.3** (37 mg, 0.051 mmol) and IMe (5 mg, 0.051 mmol) and sealed forming a light orange solution. Compound **5.4** was formed almost quantitatively. ^{1}H NMR (500 MHz, C_6D_6, δ) 7.75 (6H), 7.5 (1H), 7.41 (6H), 7.25 (1H), 7.17 (8H), 7.01 (6H), 6.7 (br. s, -CH=, 1H), 5.82 (br. s, -CH=, 1H), 3.31 (br. s, N-CH_3, 3H), 2.9 (br. s, N-CH_3, 3H), 2.43 (s, -CH_3, 6H), 2.04 (s, -CH_3, 12H), 0.69 (P=CH_2, 2H) ppm. ^{31}P{^{1}H} NMR (162 MHz, C_6D_6, δ): 21.6 ppm. ^{11}B{^{1}H} NMR (160 MHz, C_6D_6, δ): -9.74 ppm.

5.2.6 Synthesis of (*i*Pr)NH_2BH_3

A 50 mL round-bottom flask was charged with 10 mL THF and cooled in an ice water bath for 15 minutes. Borane dimethylsulfide (3 mL, 6 mmol) was added to the flask, followed by the slow addition of isopropylamine (0.51 mL, 6 mmol). The solution was then warmed to room temperature and stirred overnight. After removing the solvent by rotary evaporation the residue washed with hexanes and dried under vacuum yielding 0.35 g of (*i*Pr)NH_2BH_3 (80%) as a white solid. ^{1}H NMR (300 MHz, C_6D_6, δ): 2.95 (2H), 2.59 (1H), 2.05 (3H), 0.71 (6H) ppm, ^{11}B NMR (160 MHz, C_6D_6, δ): -19.7 ppm; ^{13}C NMR (75 MHz, C_6D_6, δ): 49.6 , 21.3 ppm.

5.2.7 Reactivity Study

5.2.7.1 NMR Experiment of H_2 Activation by 3.1

A sealable J-Young NMR tube was charged with **3.1** (10 mg, 0.014 mmol) dissolved in dry C_6D_6 and sealed forming a clear solution. The sample was then subjected to freeze-pump-thaw cycles and exposed to a positive pressure of H_2 gas for 10 minutes at room temperature. The sample was sealed under 1 atm of H_2 over one week at room temperature followed by recording of the ^{1}H, ^{31}P and ^{11}B NMR spectra at different time intervals without any change. The sample was then heated up to 75 °C for one week and still no change was observed.

5.2.7.2 NMR Experiment of CO_2 Activation by 3.1

Experimental techniques and results are the same as described in **5.2.7.1**.

5.2.7.3 NMR Experiment of Phenylacetylene Activation by 3.1

Inside of a glove box, a sealable J-Young NMR tube was charged with **3.1** (10 mg, 0.014 mmol) dissolved in dry degassed C_6D_6 and phenylacetylene (1.5 μL, 0.018 mmol) was added. The sample was sealed for one week at room temperature followed by recording of the ^{1}H, ^{31}P and ^{11}B NMR spectra at different time intervals without any change. The sample was then heated up to 75 °C for one week and still no change was observed.

5.2.7.4 NMR Experiment of Dehydrogenation of (*i*Pr)NH_2BH_3 by 3.1

Experimental techniques and results are the same as described in **5.2.7.3**.

5.2.7.5 NMR Experiment of *N*,*N*'-Bis(2,6-diisopropylphenyl)imidazol-2-ylidene (IPr) Reaction with 3.1

Experimental techniques and results are the same as described in **5.2.3**.

5.2.7.6 NMR Experiment of IPr Reaction with 4.1

Experimental techniques and results are the same as described in **5.2.3**.

5.2.7.7 NMR Experiment of IPr Reaction with 5.3

Experimental techniques and results are the same as described in **5.2.5**.

5.2.7.8 NMR Experiment of H_2 Activation by 5.2

Inside of a glove box, three NMR tubes were charged with freshly prepared **5.2** (10 mg, 0.012 mmol) dissolved in dry degassed C_6D_6 and sealed forming light yellow solutions. Sample **I** was exposed to a positive pressure of normal H_2 gas (5.0) for 10 minutes at room temperature. This sample was sealed under 1 atm of H_2 at room temperature followed by recording of the ^{1}H, ^{31}P and ^{11}B NMR spectra. Sample **II** was exposed to a positive pressure of dried H_2 gas (H_2 gas passed through hexanes solution of *n*-BuLi) for 10 minutes at room temperature and then sealed under 1 atm of H_2 at room temperature followed by recording the ^{1}H, ^{31}P and ^{11}B NMR spectra at different time intervals. Sample **III** was exposed to a positive pressure of argon gas (5.0) for 10 minutes at room temperature. The sample was sealed under 1 atm of argon at room temperature followed by recording of the ^{1}H, ^{31}P and ^{11}B NMR spectra at different time intervals.

5.2.8 TD-DFT Calculation

All calculations were performed using the Guassian 09[18] suite of programs on the High Performance Computing Virtual Laboratory (HPCVL) at Queen's University. Initial Input coordinates were taken from the corresponding crystal structure data where applicable, while others were generated from the optimized geometry of compound **4.1**. Modeling of the reaction pathway was accomplished using the B3LPY[19]/6-31g(d)[20] level of theory. All reactant, intermediate, and product geometries were optimized without constraints and characterized as minima along the potential energy surface through vibrational frequency analysis.

5.2.9 X-Ray Diffraction Analysis

Single crystals of **5.1**, **5.2**, and **5.3** were obtained from either benzene or THF/hexanes by slow evaporation of the solvent mixture in a glove box under nitrogen. The crystals **5.2** are very small and as a result, the crystal data of **5.2** were collected on a Synchrotron X-ray diffraction facility at the Canadian Light Source, Saskatoon, Saskatchwan at 173 K. The crystal data of **5.1** and **5.3** were collected on a

Bruker Apex II single crystal X-ray diffractometer with graphite-monochromated M_o K_α radiation, operating at 50 kV and 30 mA, and at 180 K. Data were processed on a PC with the aid of the Bruker SHELXTL software package (version 6.14) and corrected for absorption effects. All structures were solved using direct methods. The crystals of **5.2** belong to the monoclinic space group P21/c with two independent molecules and 3 THF solvent molecules in the asymmetric unit. The crystals of **5.1** belong to the monoclinic space group P-1 while the crystals of **5.3** belong to the orthorhombic space Pna21 with two independent molecules in the asymmetric unit. All non-hydrogen atoms were refined anisotropically. Complete crystal structural data have been deposited at the Cambridge Crystallographic Data Centre [CCDC No. 1407949-1407951]. These data can be obtained free of charge from The Cambridge Crystallographic Data Centre via www.ccdc.cam.ac.uk/data_request/cif.].The crystal data of **5.1, 5.2** and **5.3** are reported in Table 5.1, Table 5.2 and Table 5.3. The selected bond lengths and angles are given in Table 5.4, Table 5.5 and Table 5.6.

Table 5.1. Crystal data and structure refinement for compound 5.1

Compound	**5.1**
Formula	C55H51B1N1P1
Formula weight	767.75
T, K	180(2)
Wavelength, Å	0.71073
Crystal system	Triclinic
Space group	P-1
a, Å	11.133(3)
α, °	109.811(3)
b, Å	13.275(4)
β, °	99.369(3)
c, Å	17.732(5)
γ, °	103.071(3)
V, $Å^3$	2318.1(11)
Z	2
Density (calculated), Mg/m^3	1.100
Absorption coefficient, mm^{-1}	0.095
Theta range for data collection, °	1.68 to 26.50.
Reflections collected	24440
Independent reflections	9523 [R(int) = 0.0773]
Completeness to theta = 27.04°	99.2 %
Data / restraints / parameters	9523 / 0 / 531
Goodness-of-fit on F^2	0.930
Final R indices [I>2sigma(I)]	
R_1[a]	0.0678
wR_2[b]	0.1447
R indices (all data)	
R_1[a]	0.1324
wR_2[b]	0.1708

[a] $R_1 = \sum [(|F_0| - |F_c|) / \sum|F_0|$

[b] $wR_2 = [\sum w[(F_0^2-F_c^2)^2] / \sum [w(F_0^2)^2]]^{1/2}$

$w = 1 / [\sigma^2(F_0^2) + (0.075P)^2]$, where $P = [Max (F_0^2, 0) + 2F_c^2] / 3$

Table 5.2. Crystal data and structure refinement for compound 5.2

Compound	**5.2**
Formula	C63H66B1N2O1.50P1
Formula weight	916.96
T, K	173(2)
Wavelength, Å	0.68880
Crystal system	Monoclinic
Space group	P2(1)/c
a, Å	25.8016(8)
α, °	90
b, Å	25.2029(7)
β, °	90.4720(7)
c, Å	15.7714(4)
γ, °	90
V, $Å^3$	10255.4(5)
Z	8
Density (calculated), Mg/m^3	1.188
Absorption coefficient, mm^{-1}	0.099
Theta range for data collection, °	0.76 to 25.00
Reflections collected	187947
Independent reflections	19374 [R(int) = 0.0928]
Completeness to theta = 27.04°	97.6 %
Data / restraints / parameters	19374 / 0 / 1251
Goodness-of-fit on F^2	1.098
Final R indices [I>2sigma(I)]	
R_1[a]	0.0664
wR_2[b]	0.1715
R indices (all data)	
R_1[a]	0.0977
wR_2[b]	0.1922

[a] $R_1 = \sum [(|F_0| - |F_c|) / \sum|F_0|$

[b] $wR_2 = [\sum w[(F_0^2-F_c^2)^2] / \sum [w(F_0^2)^2]]^{1/2}$

$w = 1 / [\sigma^2(F_0^2) + (0.075P)^2]$, where $P = [Max (F_0^2, 0) + 2F_c^2] / 3$

Table 5.3. Crystal data and structure refinement for compound 5.3

Compound	**5.3**
Formula	C53H48B1P1
Formula weight	726.69
T, K	180(2)
Wavelength, Å	0.71073
Crystal system	Orthorhombic
Space group	Pna2(1)
a, Å	37.242(2)
α, °	90
b, Å	9.0653(5)
β, °	90
c, Å	24.2757(16)
γ, °	90
V, $Å^3$	8195.7(9)
Z	8
Density (calculated), Mg/m^3	1.178
Absorption coefficient, mm^{-1}	0.103
Theta range for data collection, °	2.00 to 27.15.
Reflections collected	37065
Independent reflections	15980 [R(int) = 0.1559]
Completeness to theta = 27.04°	99.6 %
Data / restraints / parameters	15980 / 1 / 1004
Goodness-of-fit on F^2	0.962
Final R indices [I>2sigma(I)]	
R_1[a]	0.0957
wR_2[b]	0.1981
R indices (all data)	
R_1[a]	0.2099
wR_2[b]	0.2634

[a] $R_1 = \sum [(|F_0| - |F_c|) / \sum |F_0|$

[b] $wR_2 = [\sum w[(F_0^2 - F_c^2)^2] / \sum [w(F_0^2)^2]]^{1/2}$

$w = 1 / [\sigma^2(F_0^2) + (0.075P)^2]$, where $P = [Max (F_0^2, 0) + 2F_c^2] / 3$

Table 5.4. Selected bond lengths (Å) and angles (°) for compound 5.1

P(1)-C(1)	1.704(3)
P(1)-C(4)	1.792(3)
P(1)-C(10)	1.794(3)
P(1)-C(16)	1.797(3)
N(1)-C(2)	1.318(3)
N(1)-C(3)	1.463(3)
N(1)-B(1)	1.596(4)
B(1)-C(22)	1.664(4)
B(1)-C(37)	1.668(4)
B(1)-C(28)	1.675(4)
C(1)-C(2)	1.380(4)
C(1)-P(1)-C(4)	109.52(14)
C(1)-P(1)-C(10)	110.01(14)
C(4)-P(1)-C(10)	111.84(14)
C(1)-P(1)-C(16)	113.49(15)
C(4)-P(1)-C(16)	106.23(14)
C(10)-P(1)-C(16)	105.70(14)
C(2)-N(1)-C(3)	115.5(2)
C(2)-N(1)-B(1)	125.3(2)
C(3)-N(1)-B(1)	118.5(2)
N(1)-B(1)-C(22)	108.8(2)
N(1)-B(1)-C(37)	102.5(2)
C(22)-B(1)-C(37)	113.4(2)
N(1)-B(1)-C(28)	112.3(2)
C(22)-B(1)-C(28)	102.8(2)
C(37)-B(1)-C(28)	117.2(2)
C(2)-C(1)-P(1)	121.2(2)
N(1)-C(2)-C(1)	128.9(3)
C(9)-C(4)-C(5)	118.2(3)
C(9)-C(4)-P(1)	120.0(2)
C(5)-C(4)-P(1)	121.5(2)

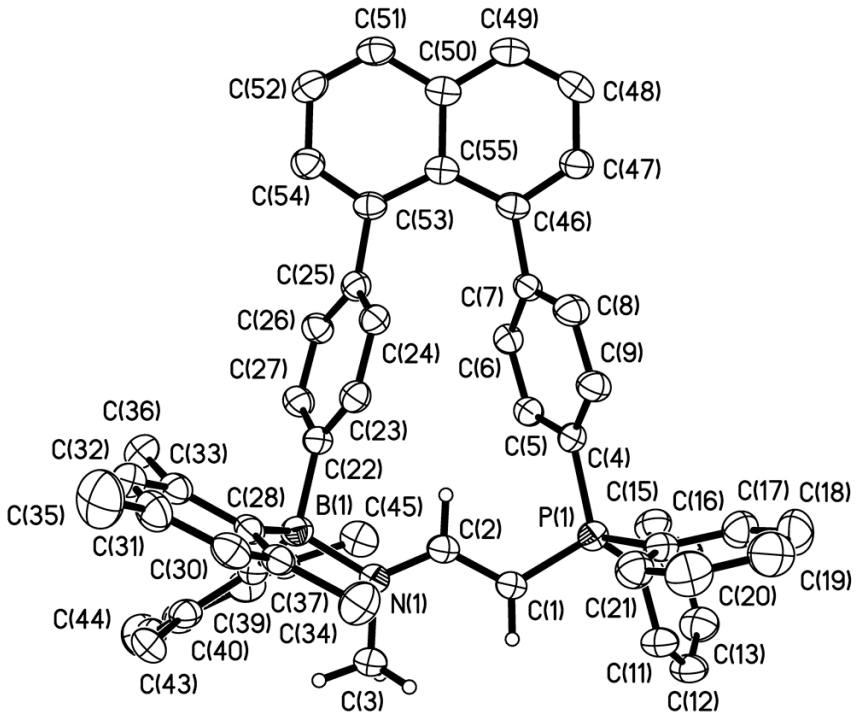

Figure 5.2. Crystal structure of **5.1** with 35% thermal ellipsoids.

Table 5.5. Selected bond lengths (Å) and angles (°) for compound 5.2

P(1)-C(53)	1.824(4)
P(1)-C(47)	1.831(3)
P(1)-C(44)	1.838(3)
P(2)-C(102)	1.826(3)
P(2)-C(105)	1.830(3)
P(2)-C(111)	1.831(3)
B(1)-C(1)	1.652(4)
B(1)-C(6)	1.665(4)
B(1)-C(21)	1.672(4)
B(1)-C(12)	1.692(4)
B(2)-C(60)	1.649(4)
B(2)-C(65)	1.656(4)
B(2)-C(71)	1.688(4)
B(2)-C(80)	1.689(4)
N(1)-C(1)	1.363(3)
N(1)-C(3)	1.381(3)
N(1)-C(4)	1.465(3)
N(2)-C(1)	1.359(3)
N(2)-C(2)	1.378(4)
N(2)-C(5)	1.457(4)
N(3)-C(60)	1.356(3)
N(3)-C(61)	1.384(3)
N(3)-C(63)	1.460(3)
N(4)-C(60)	1.369(3)
N(4)-C(62)	1.380(3)
N(4)-C(64)	1.456(3)
C(53)-P(1)-C(47)	103.48(14)
C(53)-P(1)-C(44)	100.70(14)
C(47)-P(1)-C(44)	101.92(13)
C(102)-P(2)-C(105)	101.80(12)
C(102)-P(2)-C(111)	101.44(12)
C(105)-P(2)-C(111)	101.42(13)
C(1)-B(1)-C(6)	111.7(2)
C(1)-B(1)-C(21)	112.8(2)

C(6)-B(1)-C(21)	102.1(2)
C(1)-B(1)-C(12)	101.5(2)
C(6)-B(1)-C(12)	111.3(2)
C(21)-B(1)-C(12)	117.8(2)
C(60)-B(2)-C(65)	112.3(2)
C(60)-B(2)-C(71)	112.5(2)
C(65)-B(2)-C(71)	102.1(2)
C(60)-B(2)-C(80)	101.7(2)
C(65)-B(2)-C(80)	110.61(19)
C(71)-B(2)-C(80)	118.0(2)
C(1)-N(1)-C(3)	110.8(2)
C(1)-N(1)-C(4)	127.8(2)
C(3)-N(1)-C(4)	121.3(2)
C(1)-N(2)-C(2)	111.1(2)
C(1)-N(2)-C(5)	126.7(2)
C(2)-N(2)-C(5)	122.1(2)
C(60)-N(3)-C(61)	111.2(2)
C(60)-N(3)-C(63)	126.7(2)
C(61)-N(3)-C(63)	122.0(2)
C(60)-N(4)-C(62)	110.2(2)
C(60)-N(4)-C(64)	128.2(2)
C(62)-N(4)-C(64)	121.6(2)
N(2)-C(1)-N(1)	104.1(2)
N(2)-C(1)-B(1)	124.5(2)
N(1)-C(1)-B(1)	131.1(2)
C(3)-C(2)-N(2)	107.0(2)
C(2)-C(3)-N(1)	107.0(3)
C(7)-C(6)-C(11)	114.5(2)
C(7)-C(6)-B(1)	124.7(2)
C(11)-C(6)-B(1)	120.3(2)

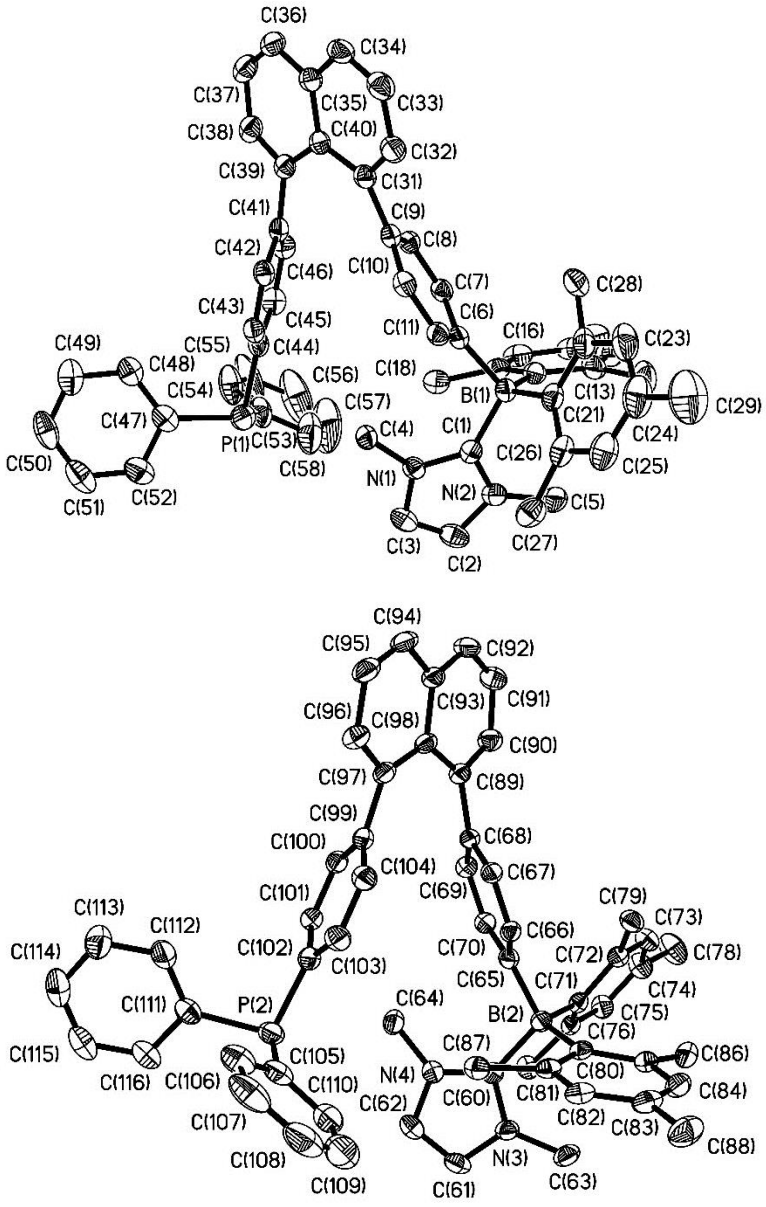

Figure 5.3. The two independent molecules in the crystal lattice of compound **5.2** with 35% thermal ellipsoids. H atoms are omitted for clarity

Table 5.6. Selected bond lengths (Å) and angles (°) for compound 5.3

P(1)-C(1)	1.652(8)
P(1)-C(14)	1.821(7)
P(1)-C(2)	1.820(7)
P(1)-C(8)	1.833(8)
C(20)-B(1)	1.590(12)
C(29)-B(1)	1.590(12)
C(38)-B(1)	1.577(11)
C(1)-P(1)-C(14)	111.6(4)
C(1)-P(1)-C(2)	109.0(4)
C(14)-P(1)-C(2)	109.1(3)
C(1)-P(1)-C(8)	120.6(4)
C(14)-P(1)-C(8)	104.5(3)
C(2)-P(1)-C(8)	101.3(3)
C(3)-C(2)-P(1)	123.4(6)
C(7)-C(2)-P(1)	117.6(6)
C(13)-C(8)-P(1)	121.5(6)
C(9)-C(8)-P(1)	118.0(6)
C(19)-C(14)-P(1)	118.7(6)
C(15)-C(14)-P(1)	123.5(5)
C(25)-C(20)-B(1)	119.5(7)
C(21)-C(20)-B(1)	121.7(7)
C(30)-C(29)-B(1)	122.2(7)
C(34)-C(29)-B(1)	119.7(7)
C(39)-C(38)-B(1)	121.6(7)
C(43)-C(38)-B(1)	122.2(7)

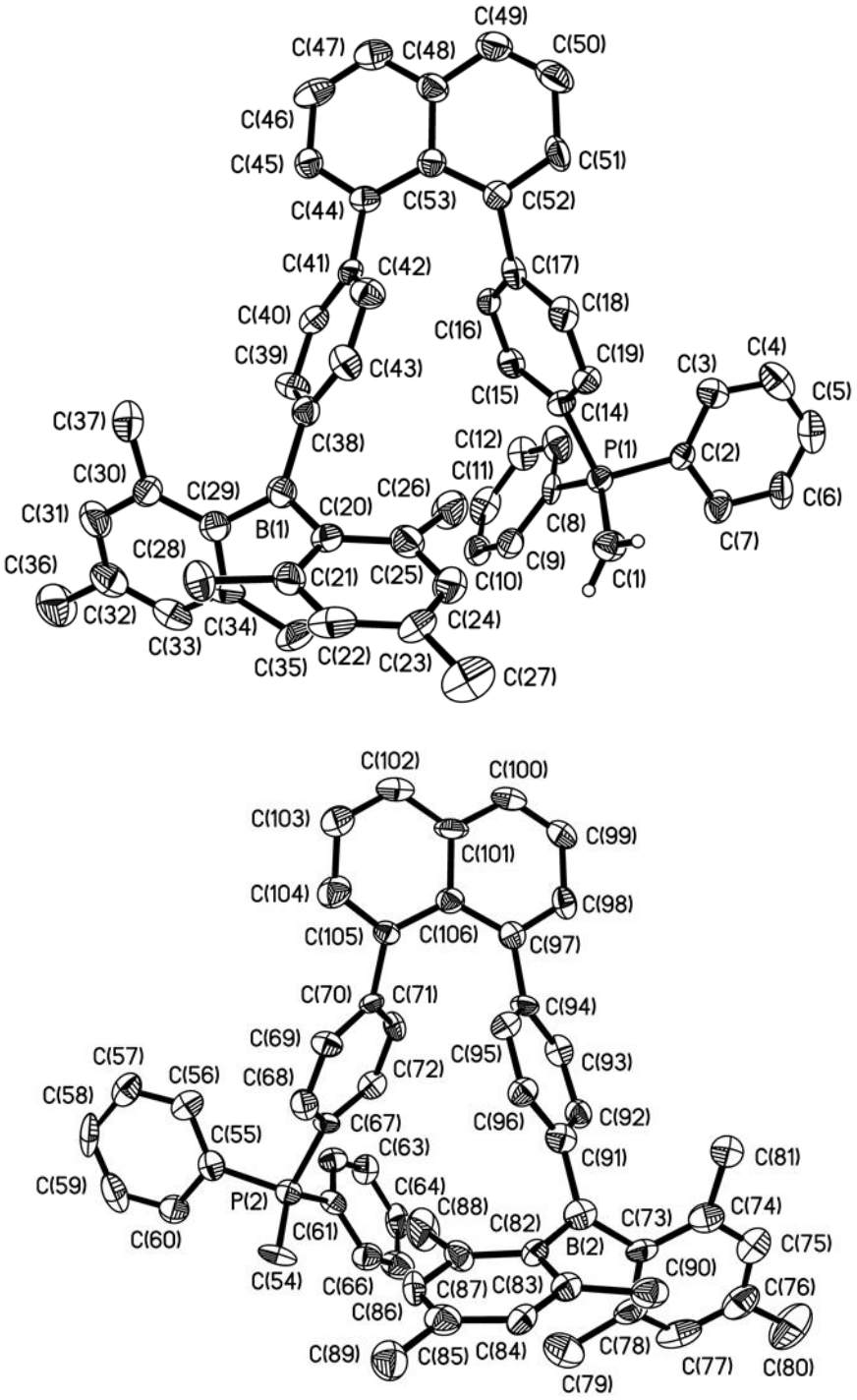

Figure 5.4. The two independent molecules in the crystal lattice of compound **5.3** with 35% thermal ellipsoids. H atoms are omitted for clarity.

5.3 Results and Discussion

5.3.1 Reactivity Studies of 3.1 and Characterizations of 5.2

Beginning with the commonly investigated small molecules, **3.1** displayed no reactivity towards H_2, CO_2, or phenylacetylene both at room and elevated temperatures according to ^1H, ^{11}B and ^{31}P NMR data. Furthermore, it was unable to dehydrogenate (*i*Pr)NH_2BH_3. This lack of reactivity unlike other FLPs is probably due to the boron center which is not as electron deficient as $B(C_6F_5)_2Ar$, a common Lewis acid component in other reactive FLPs.[1] Another reason is that the rigid naphthalene linker forces the phosphine and boron moieties apart at relatively long distance, which likely prevents polarization of small molecules by the system.

The reaction of IMe with **3.1** at room temperature in THF or benzene produced the adduct **5.2** as a light-yellow, air-sensitive solid, quantitatively (Figure 5.5). Compound **5.2** was characterized by NMR spectra and single-crystal X-ray diffraction analyses. Immediately following the addition of IMe to **3.1**, a distinct change in the $^{11}B\{^1H\}$ NMR spectrum was observed where a new peak emerged at -9.7 ppm indicating coordination of IMe to the boron center.[21a] This expected and quantitative formation of **5.2** is further validated in the ^1H NMR spectrum of the reaction, as two new signals appear at 2.9 and 3.2 ppm for the N-CH_3 groups of the coordinated IMe. Compared to the N-CH_3's of free IMe which appear as a sharp singlet at 3.5 ppm, the chemically inequivalent signals for the coordinated IMe display significant broadening indicating steric congestion and an asymmetric environment around this group.

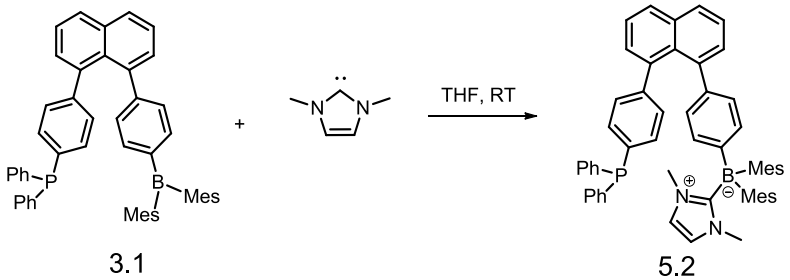

Figure 5.5. Synthesis of compound **5.2**.

This crowding around the boron atom is clearly seen in the X-ray crystal structure of **5.2.** The crystals of **5.2** are very small and not suitable for conventional X-ray diffractometer. Fortunately we succeeded in getting the data of **5.2** collected on a Synchrotron X-ray diffraction facility at the Canadian Light Source. The crystal structure confirmed the binding of IMe to the boron center (Figure 5.6), although the B(1)-C(1) bond is longer than those of the previously reported IMe adducts with boranes due to steric congestion.[22] The P(1) and B(1) atoms in **5.2** are separated by 6.34(1) Å. Interestingly, the IMe ligand is oriented toward the phosphine group with the P(1)···N(1) (4.38 Å) distance being the shortest between P(1) and the IMe ring. The reaction of molecule **3.1** with IMe was monitored at room temperature in C_6D_6 by NMR spectroscopy. Immediately following the addition of IMe to **3.1**, compound **5.2** was produced, which is stable in solution at ambient temperature for days, and does not further react even in the presence of excess IMe.

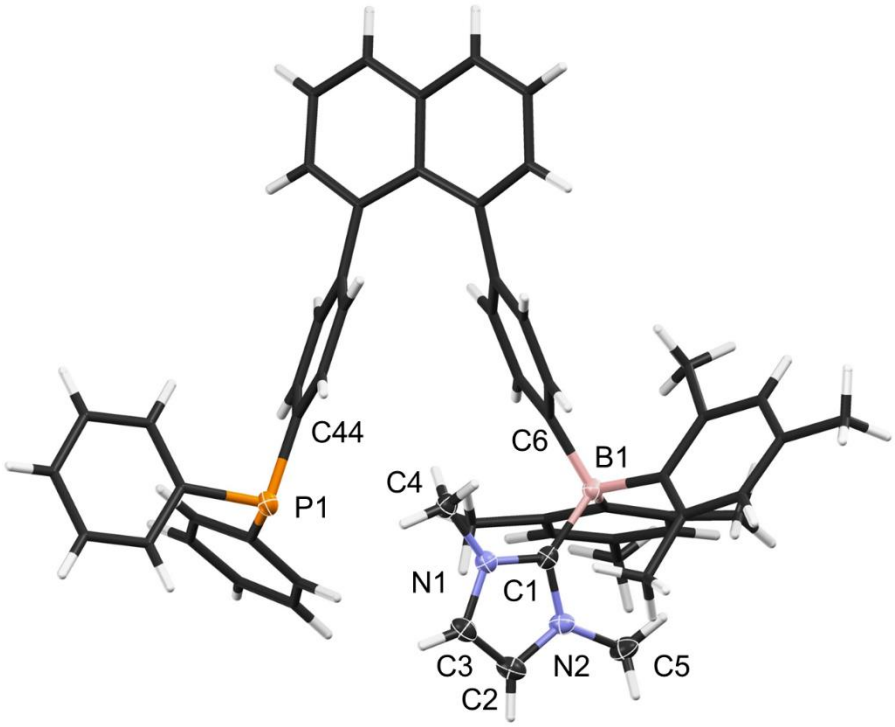

Figure 5.6. X-ray crystal structure of **5.2**.

The reaction between **3.1** and different larger NHCs such as IPr was also performed, however, no coordination between the carbene and borane was observed. This was expected as the longer B-C_{NHC} bond length in **5.2** compared to other carbene-borane adducts already indicates significant steric crowding around the boron center.

Furthermore, H_2 activation by **5.2** was investigated since it possesses two Lewis bases, namely the phosphine and IMe, as well as a bulky Lewis acid. Both ^{11}B and ^{31}P NMR showed distinct changes after the sample of **5.2** was charged with 1 atm of H_2 gas, however, these signals were found to be a result of trace amount of water inserting into the B-C bond of the adduct (as confirmed by the argon gas control experiment). In order to suppress interference from water, compound **5.2** was reacted with a dry H_2 gas that was passed through a solution of butyl lithium before introduced to the solution of **5.2**. In this case, no reactivity was observed.

5.3.2 Reactivity Studies of 4.1 and Characterizations of 5.1

Given the lack of Lewis base in **4.1**, the reactivity studies of **4.1** were focused on IMe reaction. Remarkably, the aforementioned reactivity of **4.1** was found to occur at room temperature in THF after 2 days as outlined below in Figure 5.7, ultimately leading to the unique and unexpected vinyl-amine bridged phosphonium-borane **5.1**. Compound **5.1** is readily purified *via* recrystallization from THF and has been fully characterized by ^{1}H, ^{13}C, ^{31}P, and ^{11}B NMR, HRMS, elemental analysis, and X-ray diffraction. Much to our surprise, **5.1** was found to be relatively stable towards air and moisture likely due to the coordination spheres of the phosphorus and boron atoms now being fully occupied. The $^{11}B\{^{1}H\}$ and $^{31}P\{^{1}H\}$ NMR spectra of **5.1** each possess a single resonance at 0.22 and 23.4 ppm, respectively, indicating a four-coordinated environment around boron[21] and an intermediate coordination mode between phosphonium and ylide for phosphorus.[23]

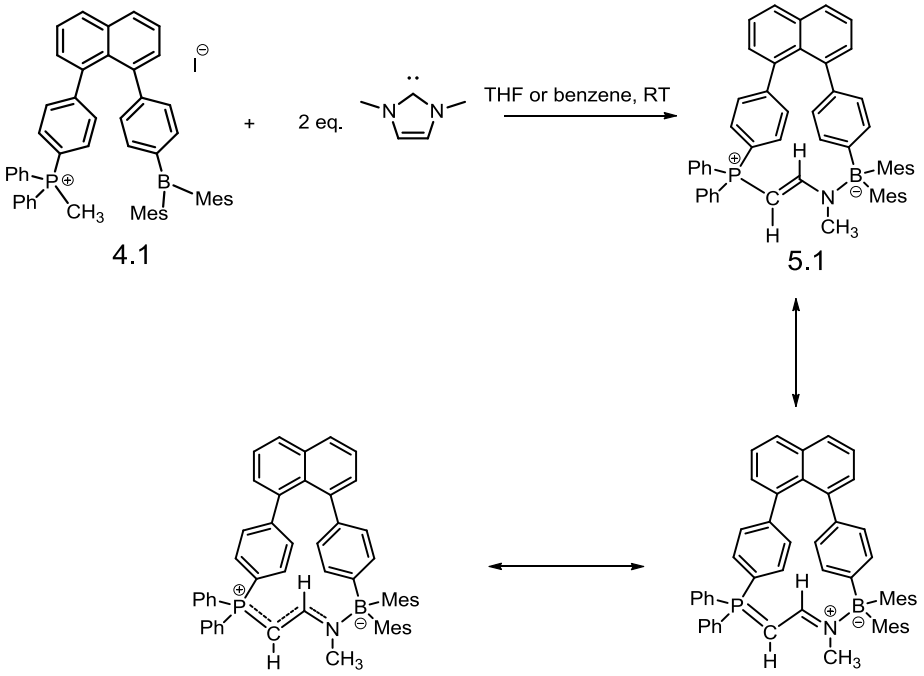

Figure 5.7. Synthesis of compound **5.1**.

The crystal structure of **5.1** shown in Figure 5.8 reveals that a *trans*-vinyl-amido unit is trapped between the phosphorus and the boron atom in the molecule. The C(1)-C(2) (1.380(4) Å) and C(2)-N(1) (1.318(3) Å) bond lengths are consistent with the vinyl-amido linkage. The P(1)-C(1) bond (1.704(3) Å) is about 0.09 Å shorter than the P-phenyl bonds, with a considerable partial P=C double bond character, [24] which is in agreement with the ^{31}P NMR data. As a consequence of the vinyl-amido bridge, the P and B separation distance in **5.1** (5.252(3) Å) is about 1 - 1.2 Å shorter than that in **3.1** and **5.2**. Owing to the crowded nature of molecule **5.1**, the phenyl rings and the mesityl rings display highly restricted rotation around the P-C bond and the B-C bond, respectively, as evidenced by the broad peaks of the protons from these rings in the ^{1}H NMR spectrum at ambient temperature.

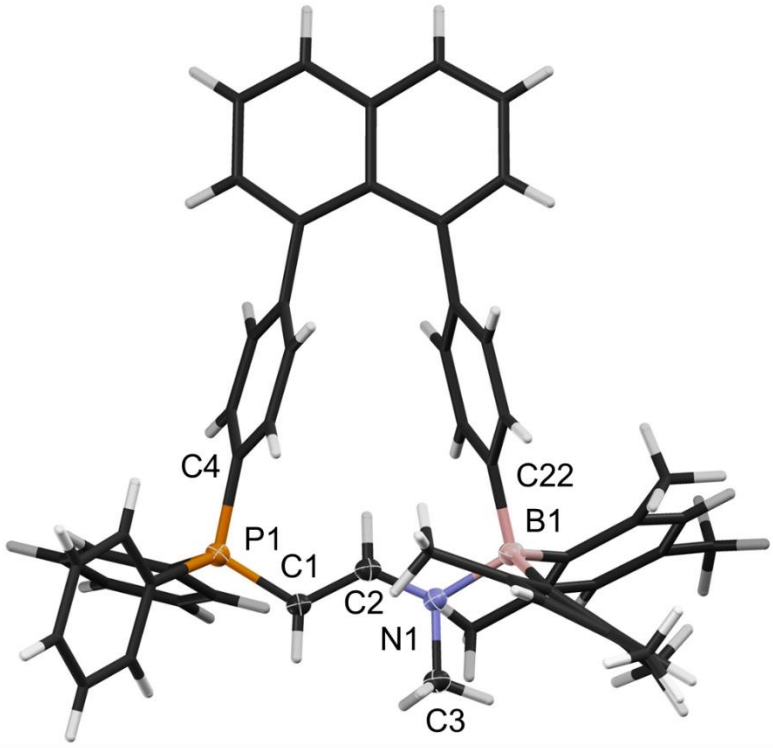

Figure 5.8. X-ray crystal structure of **5.1**.

At 240 K, the ^{1}H NMR spectrum of **5.1** is fully resolved with each proton displaying a distinct chemical shift. The structure of **5.1** in solution is fully established by a series of COSY, HMBC, HSQC and NOESY experiments at various temperatures, which agrees completely with the crystal structure. For example, the protons on the C(1) and C(2) atoms display a doublet-doublet peak at 3.73 ppm and 7.05 ppm, respectively, due to coupling with each other ($^{3}J_{H-H}$ = 13 Hz) and the P atom ($^{2}J_{P-H}$ = 18 Hz for H-C(1), $^{3}J_{P-H}$ = 15 Hz for H-C(2)). Their large $^{1}J_{C-H}$ coupling constants (161 Hz and 164 Hz, for C(1) and C(2), respectively) are consistent with the vinyl structure (Figure 5.9, Figure 5.10). The C(1) and C(2) atoms display distinct coupling to the P atom ($^{1}J_{P-C}$ and $^{2}J_{P-C}$ = 122 Hz and 21 Hz, respectively). Clearly, the vinyl unit in **5.1** is the consequence of the IMe fragmentation, and may be entirely from IMe or the result of a C-C bond coupling between the methyl group on the phosphonium and a portion of the IMe.

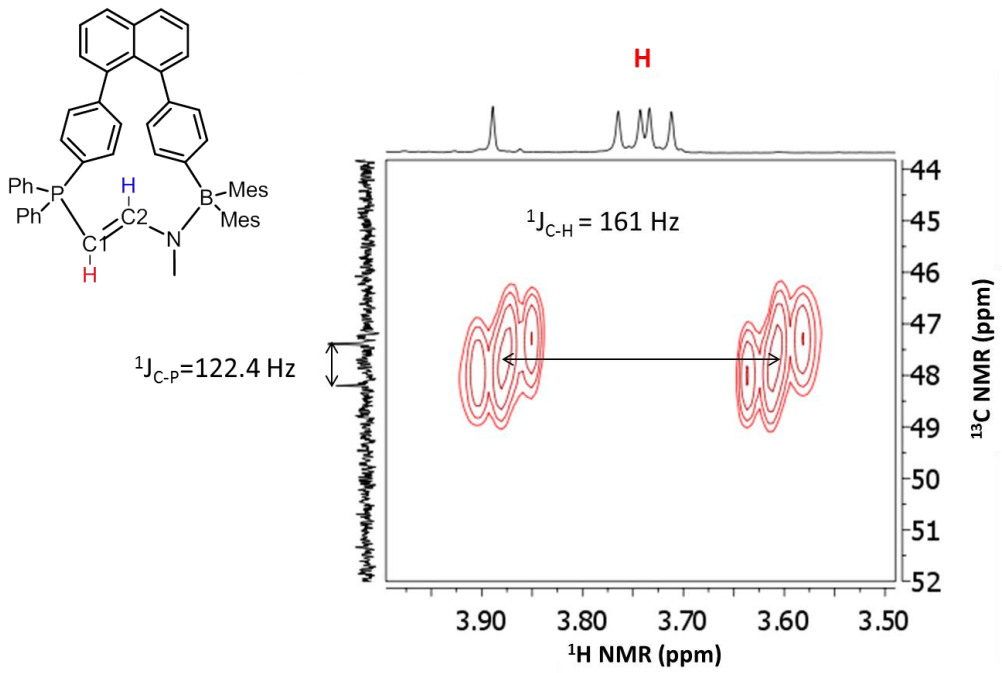

Figure 5.9. Excerpted region of $^1H^{13}C$ HSQC-coupled NMR spectrum of **5.1** at 270 K in CD_2Cl_2.

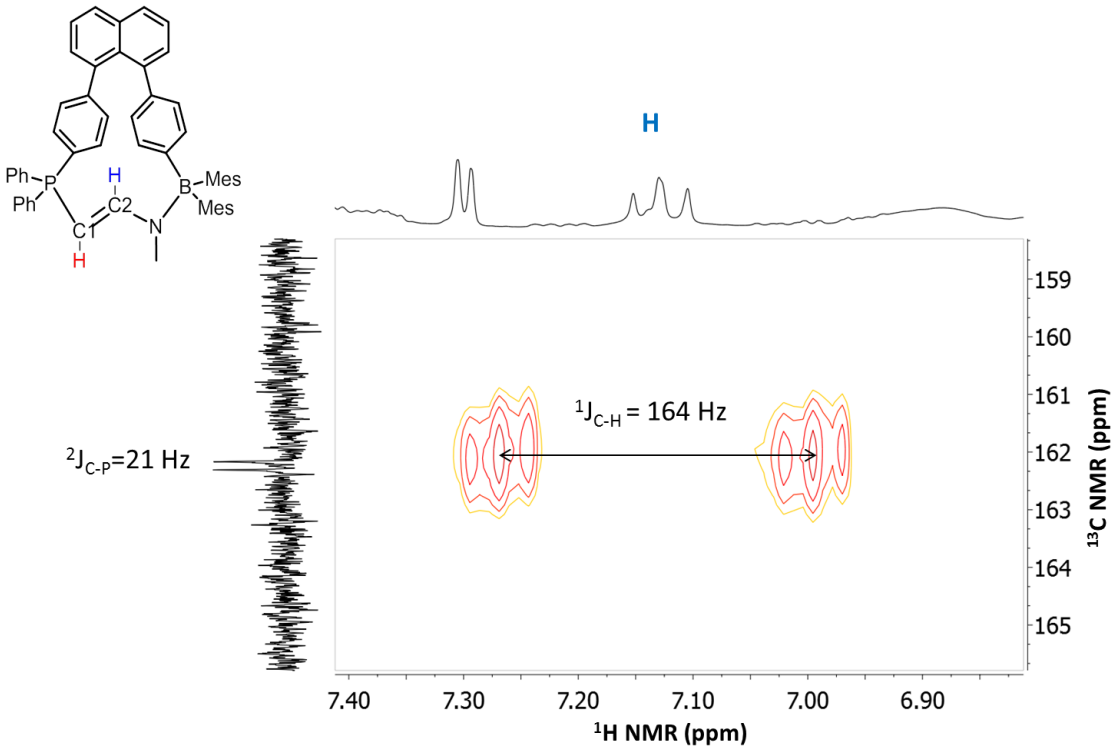

Figure 5.10. Excerpted region of $^1H^{13}C$ HSQC-coupled NMR spectrum of **5.1** at 270 K in CD_2Cl_2.

To gain additional insight into this double C-N bond activation reaction, several control experiments were performed. As mentioned previously, excess IMe to **3.1** will not further activate C-N bond only resulting in IMe adduct. This finding indicates that the phosphonium portion of **4.1** plays a pivotal role in the formation of **5.1**. To determine the possible involvement of the methyl group on the phosphonium, a ^{13}C labeled compound **4.1**-$^{13}CH_3$ was prepared by methylating the phosphine of **3.1** with $^{13}CH_3I$ and examined for the reaction with IMe (Figure 5.11). Compound **5.1**-^{13}CH isolated from the reaction of **4.1**-$^{13}CH_3$ with IMe was found to retain the ^{13}C label at the C(1) atom, as evidenced by the change of the phosphorous peak in the ^{31}P NMR spectrum from a singlet in **5.1** to a doublet in **5.1**-^{13}CH ($^1J_{P\text{-}C}$ = 122 Hz) (Figure 5.12) and the dominant doublet ^{13}C peak of the C(1) atom in the ^{13}C spectrum of **5.1**-^{13}CH (Figure 5.13). In addition, the splitting pattern of the proton on the C(1) atom changed from a doublet-doublet at 3.73 ppm to two distinct sets of doublet-doublet at 3.91 ppm and 3.59 ppm, respectively, in the ^1H NMR spectrum, due to the large ^1J coupling (161 Hz) to the $^{13}C(1)$ atom (Figure 5.14). This confirmed unequivocally that the C(1) atom of the vinyl amido unit in **5.1** originates from the phosphonium methyl group in **4.1**. Much like the observations for **3.1**, the reaction between **4.1** and IPr did not yield adduct formation due to steric congestion.

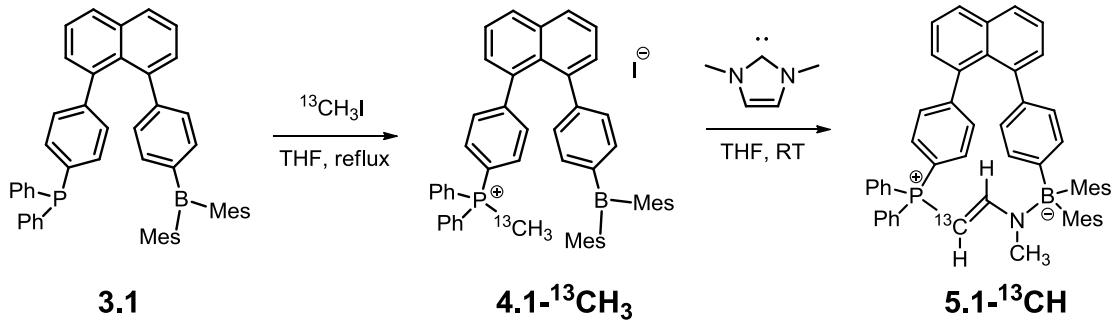

Figure 5.11. Synthesis of compound **5.1**-^{13}CH.

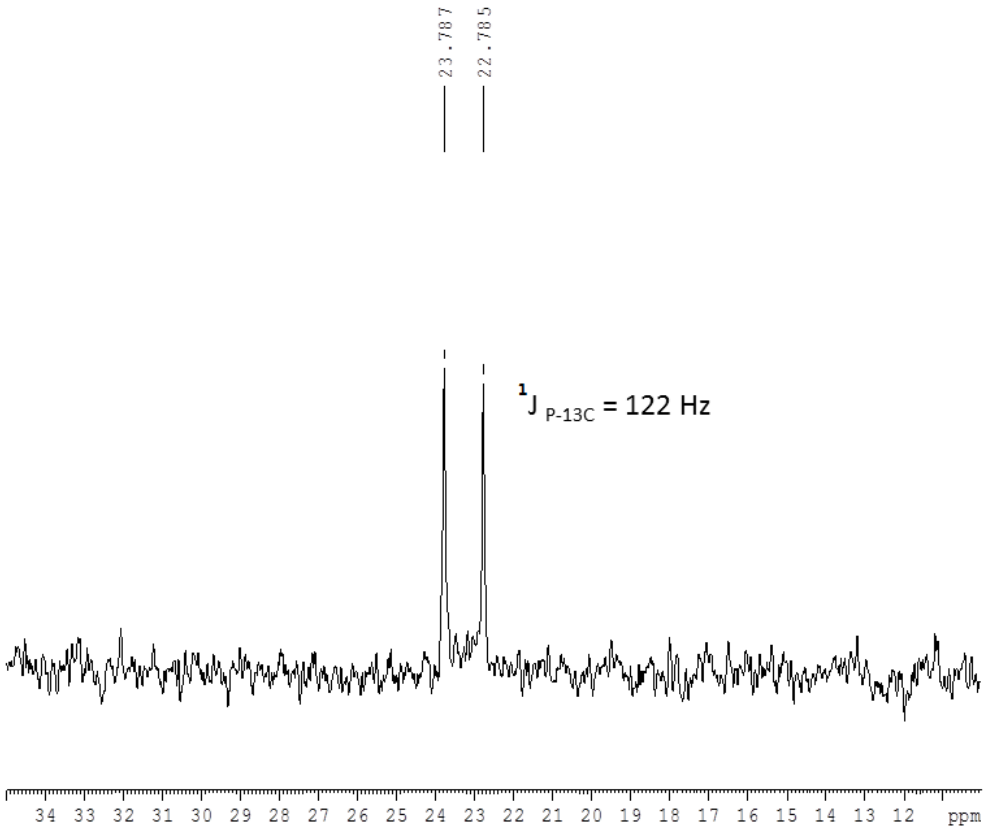

Figure 5.12. $^{31}P\{^{1}H\}$ NMR spectrum of **5.1**-^{13}CH.

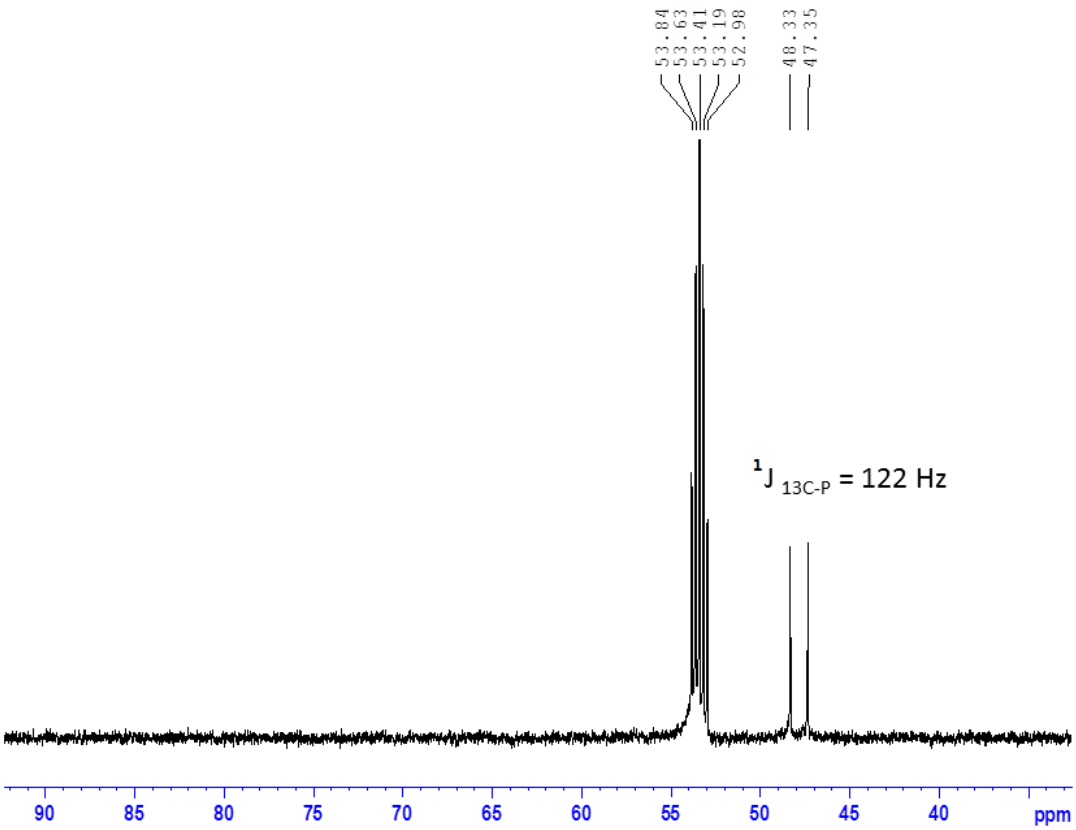

Figure 5.13. ^{13}C NMR spectrum of **5.1**-^{13}CH.

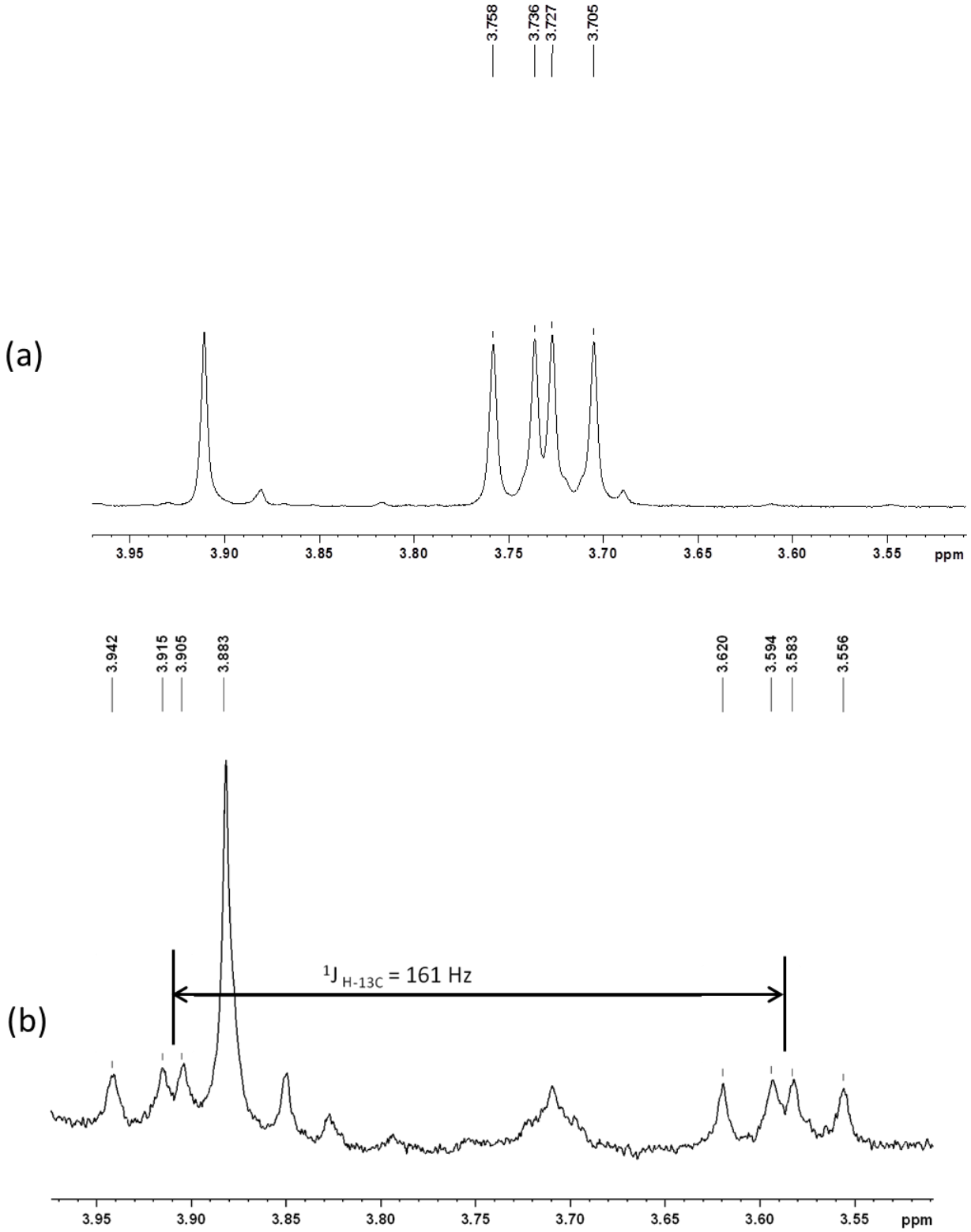

Figure 5.14. ^{1}H NMR spectra (aliphatic region) of **5.1** (a) and **5.1**-^{13}CH (b).

5.3.3 Reactivity Study of 5.3 and Characterizations

The related ylide molecule **5.3** was synthesized by reacting NaH and **4.1** in THF at room temperature for 12 hours, after which it was precipitated as a highly air-sensitive light yellow solid in diethyl ether (Figure 5.15). Ylide **5.3** possesses an alternate electron donating group which, in combination with the Lewis acidic boron, may exhibit interesting reactivity. Molecule **5.3** was characterized by NMR and X-ray diffraction analysis (Figure 5.16). The CH_2 group in **5.3** displays a sharp doublet at 0.83 ppm in the ^{1}H NMR spectrum while the phosphorus atom has a singlet peak at 21.0 ppm in the $^{31}P\{^{1}H\}$ NMR spectrum, comparable to other $Ph_3P{=}CH_2$ species.[25] The $P{=}CH_2$ bond length of **5.3** is 1.652(8) Å/1.649(8) Å (for the two independent molecules), typical of phosphine ylides,[23] and the P and B separation distance (6.91(1) Å) is much longer than those in **5.1** and **5.2**. The CH_2 unit is far away from the B atom (C···B = 6.60 Å). Due to the high sensitivity of **5.3**, the only reactivity study that could be performed was that with IMe. Upon the addition of IMe to **5.3**, a distinct peak at -9.7 ppm was observed in the $^{11}B\{^{1}H\}$ NMR spectrum, which is similar to that of the IMe adduct **5.2**, while the ^{31}P chemical shift experienced little change (21.6 ppm). NMR data indicate the quantitative formation of a 1:1 IMe adduct with **5.3** (designated as compound **5.4**) (Figure 5.15). The crystals of **5.4** are highly air-sensitive and too small for X-ray diffraction study. However compound **5.4** does not convert to **5.1** or show any reactivity in the presence of excess IMe, establishing that the ylide molecule **5.3** and IMe alone are not sufficient for the formation of molecule **5.1**.

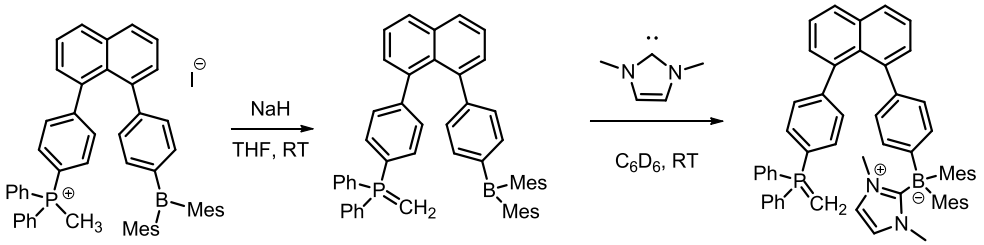

Figure 5.15. Synthesis of ylide **5.3** and compound **5.4**.

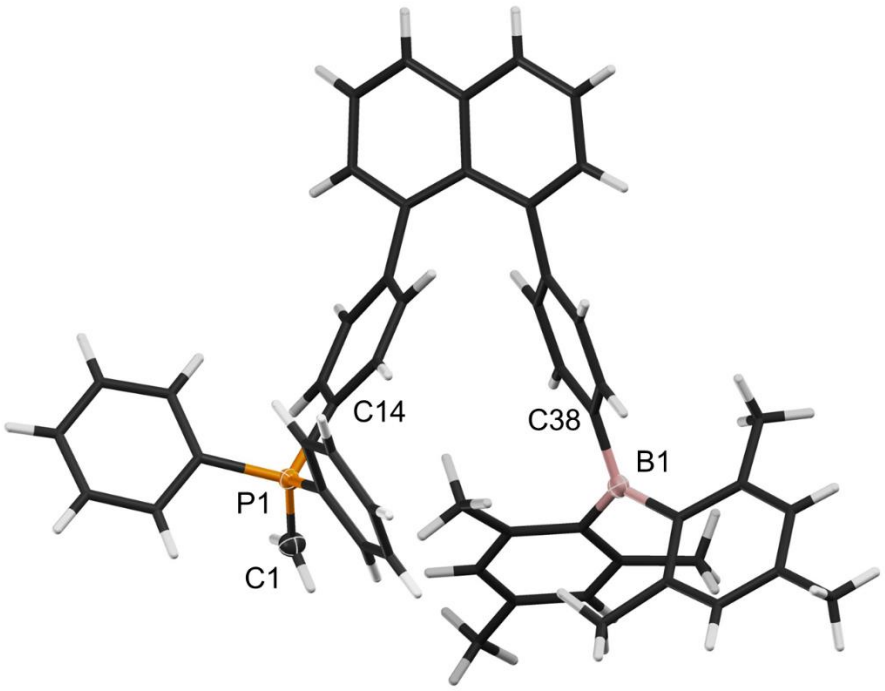

Figure 5.16. X-ray crystal structure of **5.3**.

5.3.4 Mechanism Study of IMe Reaction by 4.1

Now since we have demonstrated the crucial role of the phosphonium group, we set out to determine the role of IMe in this reaction. Given that the pK_a values of triarylphosphonium salts[26] and 1,3-dialkylimidazolium salts[27] are quite similar, we postulated that perhaps the role of IMe is to act as a base, enabling the generation of the ylide species **5.3** which may subsequently act as a nucleophile to activate the second equiv. IMe in conjunction with the nearby borane unit, leading to ultimately the formation of compound **5.1**. As mentioned previously, compound **5.4** cannot further activate IMe and yield **5.1**. It is important to note that this reaction left out one side product formed in the reaction of **4.1** with IMe, namely, the IMe imidazolium salt generated following deprotonation of the phosphonium methyl group. This suggests the imidazolium salt plays a key role in this transformation.

Given the possibility of producing imidazolium salt from the reaction of an IMe with the phosphonium in **4.1**, the possible involvement of the $[IMeH]^+$ salt in the formation of **5.1** was examined. The addition of

one equiv. [IMeH]I to the solution of compound **5.3** resulted in a rapid and complex ^{1}H and ^{31}P NMR spectral change, but the phosphonium compound **4.1** and the vinyl amido bridged compound **5.1** were not observed. The addition of IMe to the reaction mixture of **5.3** and [IMeH]I did however result in the formation of compound **5.1**. Alternatively, adding one equiv. [IMeH]I to a solution of **5.4** also produced the vinyl-amine bridged product **5.1** (Figure 5.17). The ^{31}P NMR spectra of these reactions are in fact very similar to that of **4.1** + 2 IMe (Figure 5.18, Figure 5.19). These experimental observations established that the ylide, the imidazolium salt and the free NHC are all required to produce compound **5.1**.

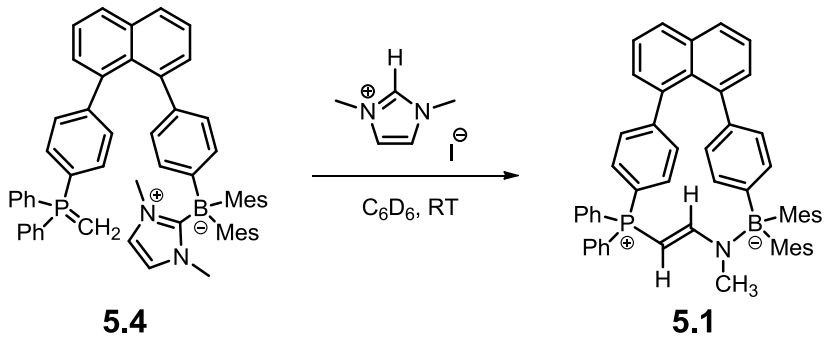

5.4 **5.1**

Figure 5.17. Synthesis of compound **5.1** using **5.4** and [IMeH]I.

After completing these control experiments and the characterization of the key species involved, the ^{31}P NMR spectra of the reaction mixture of compound **4.1** with 2 equiv. of IMe in C_6D_6 was re-examined (Figure 5.18). The ylide compound **5.3** and its IMe adduct **5.4** were not observed in the reaction mixture. A species corresponding to an adduct of IMe with **4.1** (compound **5.5**, ^{31}P, 22.1 ppm; ^{11}B, ~ -9.0 ppm) was identified to be the major species in the early stage of the reaction, which gradually disappeared as compound **5.1** became dominant. A main product **5.6** (~35%) (Figure 5.18 and 5.19) has a ^{31}P peak at 17.6 ppm which has been confirmed by HRESI measurement and a small amount of compound **5.2** (<3%) were also observed in the reaction mixture which indicates the methyl group has been dissociated by IMe from the phosphonium moiety. Furthermore, it was observed that the minimum amount of IMe required

to produce compound **5.1** from **4.1** in good yield is 2 equivalents. The addition of more than 2 equiv. IMe does not change the product distribution significantly.

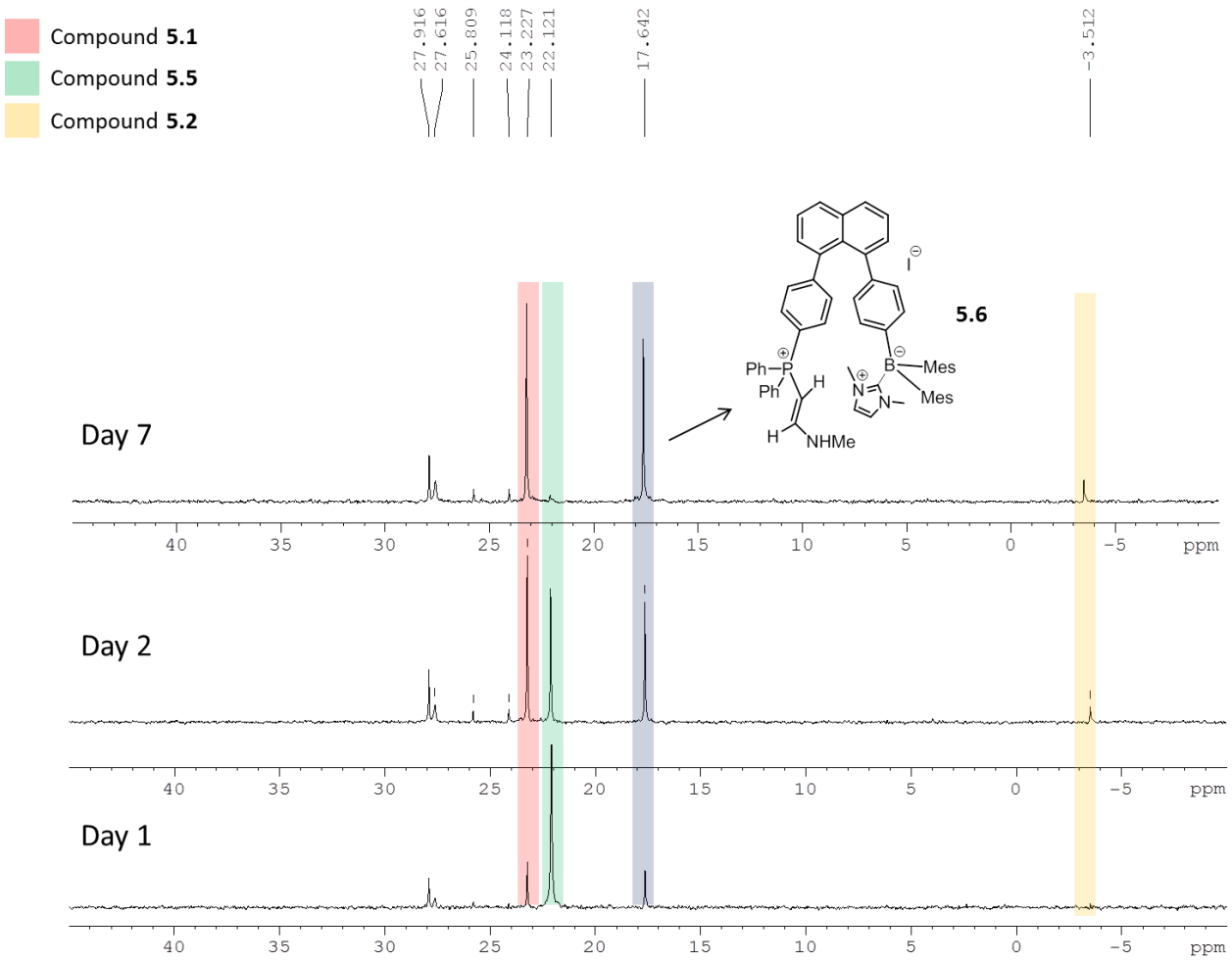

Figure 5.18. $^{31}P\{^{1}H\}$ NMR spectral change of **4.1** + IMe reaction with time.

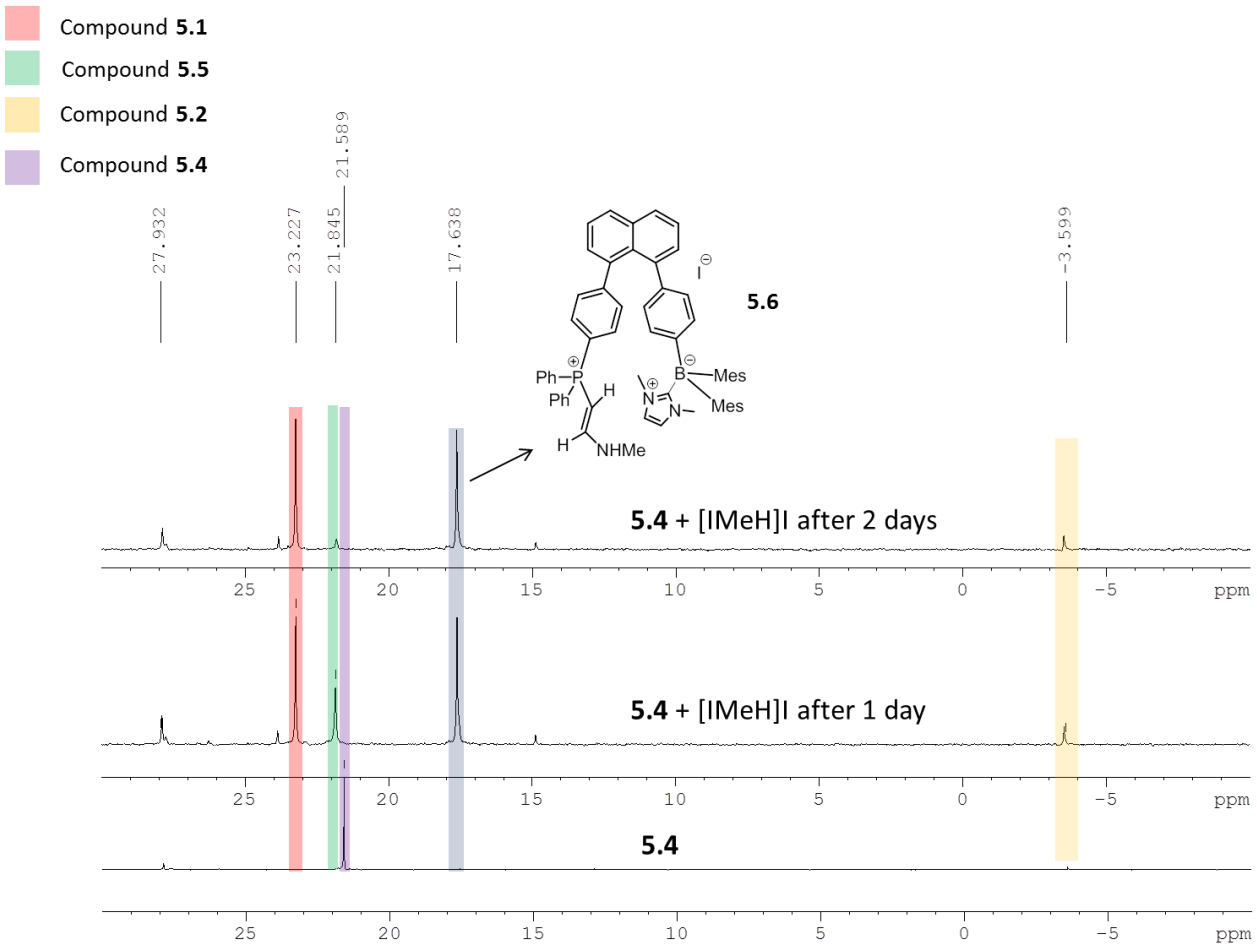

Figure 5.19. $^{31}P\{^{1}H\}$ NMR spectral change of **5.4** + [IMeH]I salt reaction with time.

Based on these data, a plausible reaction mechanism for the formation of **5.1** is shown in Figure 5.20, in which the ylide molecule **5.3** and $[IMeH]^+$ are produced first *via* the reaction of IMe with **4.1**, which are likely in equilibrium with **4.1** and the IMe adducts **5.4** and **5.5**. The ylide **5.3** subsequently reacts with $[IMeH]^+$ *via* nucleophilic attack of the methylene anion to the central carbon atom of $[IMeH]^+$ yielding **Int1**. The 2nd IMe acts as a base to extract a proton from the ylide carbon atom, which ultimately causes the cleavage of the two C-N bonds in **Int1**, releasing an *N*-methylacetylene amine side product **A**, and forming the final vinyl-amine bridged product **5.1**. In fact, compound **A** and a species (designated as **B**) that corresponds to the formula of $[IMeH]^+$ + **A** have been positively detected by HRMS of the reaction mixture. Compound **B** is likely a product of IMe nucleophilic attack at the H-C≡ unit of **A**, followed by the abstraction of a proton, based on the recent work reported by Braunschweig et al.[22a]

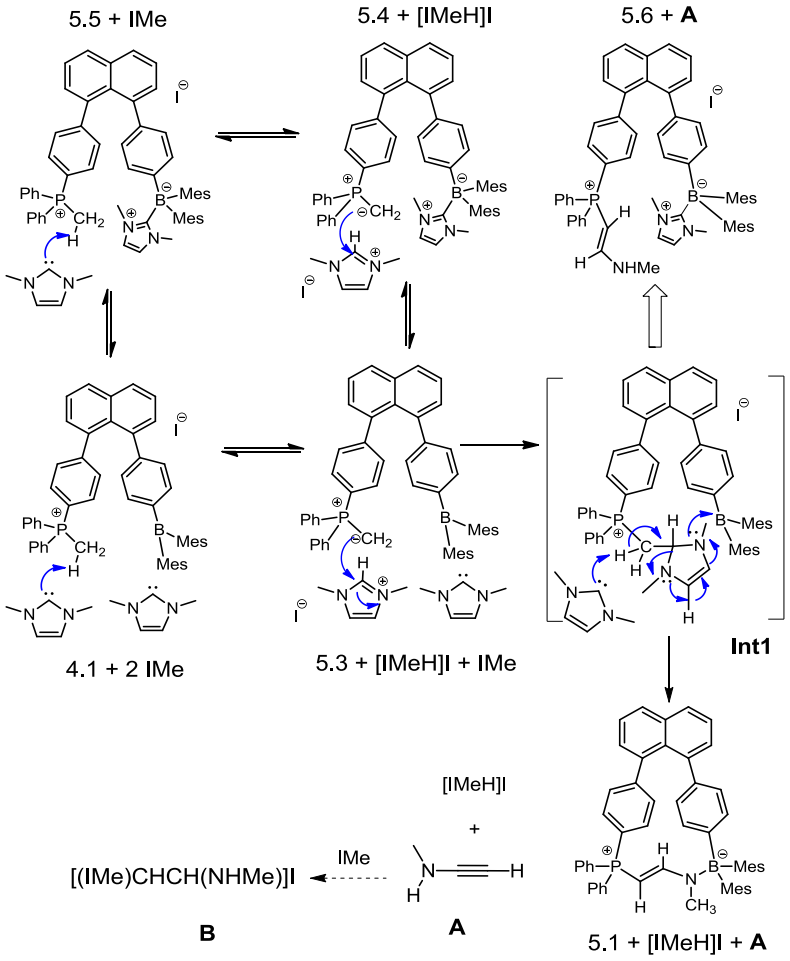

Figure 5.20. Proposed mechanism of formation of compound **5.1**.

The fact that the ylide species **5.3** and **5.4** are not observed in the reaction mixture by NMR is consistent with the control experiments in which both **5.3** and **5.4** were found to react rapidly with $[IMeH]^+$. Calculations performed on the various species involved in the proposed reaction pathway indicate that there are only small energy differences among them (<15 kcal/mol) with the product **5.1** + side products being the thermodynamically most favorable (Figure 5.21). The role of the borane unit in this unusual reaction is likely two folds: (a) it helps to trap and stabilize the reactive vinyl amido product by binding to the nitrogen donor atom, (b) it stabilizes the excess free IMe by forming a weakly bound complex and releases it when needed by the substrate. The binding of IMe by the borane unit certainly slows down the reaction since the phosphonium ion has to compete for the IMe, however, the presence of the intramolecular borane unit likely makes the reaction more selective. A comparison experiment carried out by mixing $[Ph_3PCH_3]^+$ phosphonium with 2 equiv. of IMe demonstrated that the similar NHC fragmentation does not occur without borane moiety. It is conceivable that the combination of $[Ph_3PCH_3]^+$ phosphonium and an appropriate borane may lead to a similar fragmentation phenomenon and reactivity of NHCs. Preliminary test data indicate that such reactions are quite messy compared to the system employing compound **4.1**. However, the isolation of desired product was not successful. Further investigations are underway to establish and understand the reactivity of non-sterically constrained phosphonium-borane systems towards NHCs.

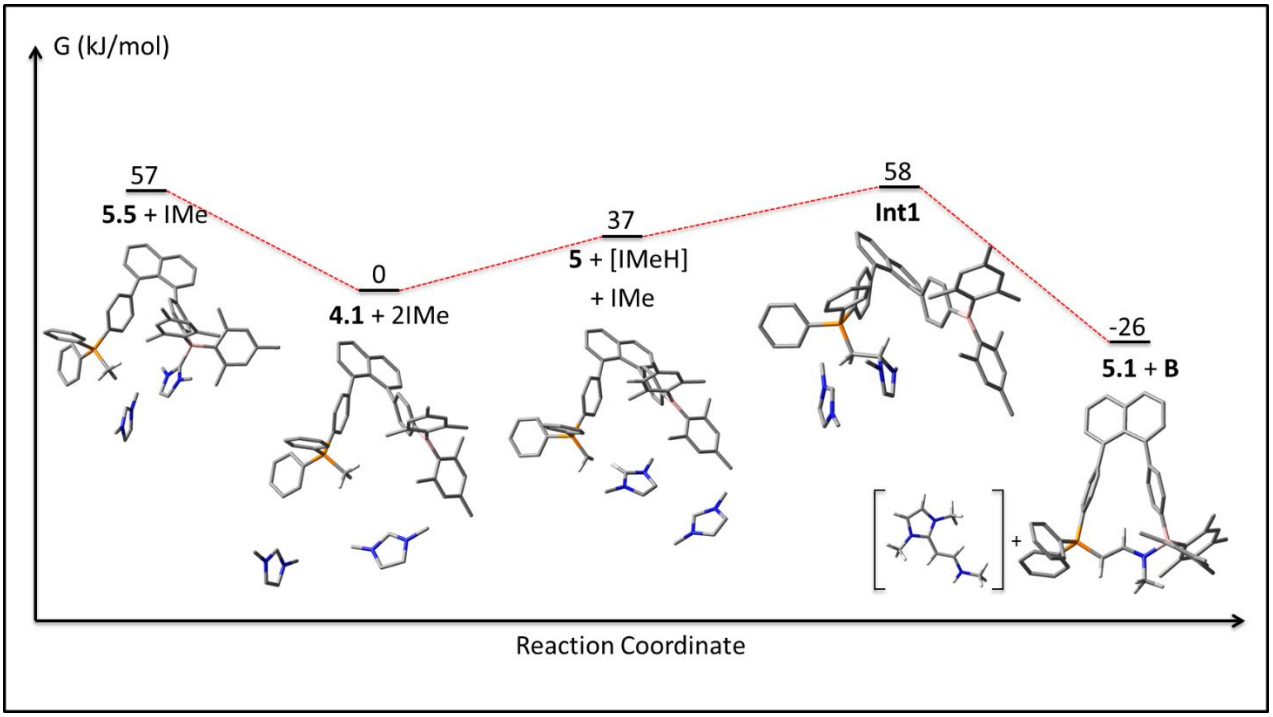

Figure 5.21. Relative ground state energies and structures calculated for the reactant, intermediates, and product involved in the NHC reaction (most H atoms have been omitted for clarity).

5.4 Conclusions

In summary, compounds **3.1** and **4.1** were found to display unique reactivity in the presence of *N,N'*-dimethylimidazol-2-ylidene (IMe), a popular member of the NHCs family, where the former produces a simple adduct and the latter generates an unusual species **5.1**, in which the IMe molecule has undergone a rather peculiar transformation with the cleavage of several bonds. Given the low Lewis acidity and high stability of compound **4.1** under ambient conditions, the fragmentation of IMe, apparently enabled by **4.1**, is highly unusual and remarkable. In order to investigate this reaction, a related ylide compound **5.3** was prepared and only showed coordination with IMe. However, the addition of IMe and imidazoliam salt [HIMe]I leads to the formation of **5.1**. Therefore, in addition to IMe which plays a key role in its self-destruction, the FLP-like ylide-borane **5.3** and imidazolium salt have also been identified as key species

involved in this transformation. The balance of Lewis acidity/basicity and the cooperativity among the phosphonium/ylide, IMe, and borane appear to be critical in this unprecedented fragmentation of IMe.

References:

(1) McCahill, J. S. J.; Welch, G. C.; Stephan, D. W. *Angew. Chem. Int. Ed.* **2007**, *46*, 4968.

(2) a) Welch, G. C.; Juan, R. R. S.; Masuda, J. D.; Stephan, D. W. *Science* **2006**, *314*, 1124; b) Welch, G. C.; Stephan, D. W. *J. Am. Chem. Soc.* **2007**, *129*, 1880.

(3) Spies, P.; Erker, G.; Kehr, G.; Bergander, K.; Fröhlich, R.; Grimme, S.; Stephan, D. W. *Chem. Commun.* **2007**, 5072.

(4) For select examples see: a) Schulz, F.; Sumerin, V.; Heikkinen, S.; Pederson, B.; Wang, C.; Atsumi, M.; Leskela, M.; Repo, T.; Pyykko, P.; Petry, W.; Rieger, B. *J. Am. Chem. Soc.* **2011**, *133*, 20245; b) Zaher, H.; Ashley, A. E.; Irwin, M.; Thompson, A. L.; Gutmann, M. J.; Kramer, T.; O'Hare, D. *Chem. Commun.* **2013**, *49*, 9755; c) Schwendemann, S.; Frohlich, R.; Kehr, G.; Erker, G. *Chem. Sci.* **2011**, *2*, 1842; d) Stute, A.; Kehr, G.; Frohlich, R.; Erker, G. *Chem. Commun.* **2011**, *47*, 4288; e) Geier, S. J.; Stephan, D. W. *J. Am. Chem. Soc.* **2009**, *131*, 3476; f) Dureen, M. A.; Stephan, D. W. *J. Am. Chem. Soc.* **2010**, *132*, 13559.

(5) a) Ashley, A. E.; Thompson, A. L.; O'Hare, D. *Angew. Chem. Int. Ed.* **2009**, *48*, 9839; b) Berkefeld, A.; Piers, W. E.; Parvez, M. *J. Am. Chem. Soc.* **2010**, *132*, 10660; c) Menard, G.; Stephan, D. W. *J. Am. Chem. Soc.* **2010**, *132*, 1796; d) Courtemanche, M. A.; Legare, M. A.; Maron, L.; Fontaine, F. G. *J. Am. Chem. Soc.* **2013**, *135*, 9326.

(6) Sajid, M.; Klose, A.; Birkman, B.; Liang, L.; Schirmer, B.; Wiegand, T.; Eckert, H.; Lough, A. J.; Frohlich, R.; Daniliuc, C. G.; Grimme, S.; Stephan, D. W.; Kehr, G.; Erker, G. *Chem. Sci.* **2013**, *4*, 213.

(7) a) Otten, E.; Neu, R. C.; Stephan, D. W. *J. Am. Chem. Soc.* **2009**, *131*, 9918; b) Menard, G.; Hatnean, J. A.; Cowley, H. J.; Lough, A. J.; Rawson, J. M.; Stephan, D. W. *J. Am. Chem. Soc.* **2013**, *135*, 6446; c) Tskhovrebov, A. G.; Solari, E.; Wodrich, M. D.; Scopelliti, R.; Severin, K. *J. Am. Chem. Soc.* **2012**, *134*, 1471; d) Neu, R. C.; Otten, E.; Lough, A.; Stephan, D. W. *Chem. Sci.* **2011**, *2*, 170.

(8) a) Birkmann, B.; Voss, T.; Geier, S. J.; Ullrich, M.; Kehr, G.; Erker, G.; Stephan, D. W. *Organometallics* **2010**, *29*, 5310; b) Chapman, A. M.; Haddow, M. F.; Wass, D. F. *J. Am. Chem. Soc.* **2011**, *133*, 18463; c) Welch, G. C.; Masuda, J. D.; Stephan, D. W. *Inorg. Chem.* **2006**, *45*, 478.

(9) a) Holschumacher, D.; Bannenberg, T.; Hrib, C. G.; Jones, P. G.; Tamm, M. *Angew. Chem. Int. Ed.* **2008**, *47*, 7428; b) Chase, P. A.; Stephan, D. W. *Angew. Chem. Int. Ed.* **2008**, *47*, 7433.

(10) a) Schuster, O.; Yang, L.; Raubenheimer, H. G.; Albrecht, M. *Chem. Rev.* **2009**, *109*, 3445; b) Diez - Gonzalez, S.; Marion, N.; Nolan, S. P. *Chem. Rev*. **2009**, *109*, 3612; c) Poyatos, M.; Mata, J. A.; Peris, E. *Chem. Rev*. **2009**, *109*, 3677.

(11) a) Ghadwal, R. S.; Azhakar, R.; Roesky, H. W. *Acc. Chem. Res.* **2013**, *46*, 444; b) Roesky, H. W. *J. Organomet. Chem.* **2013**, *730*, 57; c) Wang, Y.; Robinson, G. H. *Dalton Trans*. **2012**, *41*, 337; d) Inoue, S.; Driess, M. *Angew. Chem. Int. Ed.* **2011**, *50*, 5614; e) Wang, Y.; Robinson, G. H. *Inorg. Chem*. **2011**, *50*, 12326; f) Martin, D.; Soleilhavoup, M.; Bertrand, G. *Chem. Sci.* **2011**, *2*, 389; g) Siemeling, U. *Aust. J. Chem.* **2011**, *64*, 1109; h) Fuchter, M. J. *Chem. Eur. J.* **2010**, *16*, 12286; i) Wang, Y.; Robinson, G. H. *Chem. Commun*. **2009**, 5201.

(12) For select examples see: a) Bramananthan, N.; Mas-Marza, E.; Fernandez, F. E.; Ellul, C. E.; Mahon, M. F.; Whittlesey, M. K. *Eur. J. Inorg. Chem*. **2012**, 2213 and references cited therein; b) Wurtemberger, M.; Ott, T.; Doing, C.; Schaub, T.; Radius, U. *Eur. J. Inorg. Chem.* **2011**, 405; c) Wolf, R.; Plois, M.; Hepp, A. *Eur. J. Inorg. Chem*. **2010**, 918; d) Ohki, Y.; Hatanaka, T.; Tatsumi, K. *J. Am. Chem. Soc.* **2008**, *130*, 17174; e) Curran, D. P.; Boussonniere, A.; Geib, S. J.; Lacote, E. *Angew. Chem. Int. Ed*. **2012**, *51*, 1602; f) Xiang, L.; Xiao, J.; Deng, L. *Organometallics*. **2011**, *30*, 2018; g) Hu, Y.-C.; Tsai, C.-C.; Shih, W.-C.; Yap, G. P. A.; Ong, T.-G. *Organometallics*. **2010**, *29*, 516; h) Liu, L.; Wang, F.; Shi, M. *Eur. J. Inorg. Chem*. **2009**, 1723; i) Burling, S.; Mahon, M. F.; Powell, R. E.; Whittlesey, M. K.; Williams, J. M. J. *J. Am. Chem. Soc*. **2006**, *128*, 13702; j) Caddick, S.; Cloke, F. G. N.; Hitchcock, P. B.; Lewis, A. K. de K. *Angew. Chem. Int. Ed*. **2004**, *43*, 5824; k) Galan, B. R.; Gembicky, M.; Dominiak, P. M.; Keister, J. B.; Diver, S. T.; *J. Am. Chem. Soc*. **2005**,

127, 15702; l) Galan, B. R.; Pitak, M.; Gembicky, M.; Keister, J. B.; Diver, S. T. *J. Am. Chem. Soc.* **2009**, *131*, 6822.

(13) a) Waltman, A. W.; Ritter, T.; Grubbs, R. H. *Organometallics*. **2006**, *25*, 4238; b) Bose, S. K.; Fucke, K.; Liu, L.; Steel, P. G.; Marder, T. B. *Angew. Chem. Int. Ed*. **2014**, *53*, 1799.

(14) a) Frey, G. D.; Masuda, J. D.; Donnadieu, B.; Bertrand, G. *122*, 9634; *Angew. Chem. Int. Ed*. **2010**, *49*, 9444; b) Arrowsmith, M.; Hill, M. S.; Kociok-Kohn, G.; MacDougall, D. J.; Mahon, M. F. *Angew. Chem. Int. Ed*. **2012**, *51*, 2098; c) Schmidt, D.; Berthel, J. H. J.; Pietsch, S.; Radius, U. *Angew. Chem. Int. Ed*. **2012**, *51*, 8881; d) Al-Rafia, S. M. I.; McDonald, R.; Ferguson, M. J.; Rivard, E. *Chem. Eur. J*. **2012**, *18*, 13810; e) Franz, D.; Inoue, S. *Chem. Asian J*. **2014**, *9*, 2083; f) Wang, T.; Stephan, D. W. *Chem. Eur. J*. **2014**, *20*, 3036; g) Momeni, M. R.; Rivard, E.; Brown, A. *Organometallics*, **2013**, *32*, 6201; h) Iversen, K. J.; Wilson, D. J. D.; Dutton, J. L. *Organometallics*. **2013**, *32*, 6209; i) Iversen, K. J.; Wilson, D. J. D.; Dutton, J. L. *Dalton Trans*. **2013**, *42*, 11035; j) Iversen, K. J.; Wilson, D. J. D.; Dutton, J. L. *Dalton Trans*. **2014**, *43*, 12820; k) Fang, R.; Yang, L.; Wang, Q. *Organometallics*, **2014**, *33*, 53; l) Iversen, K. J.; Wilson, D. J. D.; Dutton, J. L. *Dalton Trans*. **2015**, *44*, 3318; m) Hemberger, P.; Bodi, A.; Berthel, J. H. J.; Radius, U. *Chem. Eur. J*. **2015**, *21*, 1434; n) Su, M. *Inorg. Chem*. **2014**, *53*, 5080; o) Arrowsmith, M.; Hill, M. S.; Kociok-Kohn, G. *Organometallics*. **2015**, *34*, 653; p) Pietsch, S.; Paul, U.; Cade, I. A.; Ingleson, M. J.; Radius, U.; Marder, T. B. *Chem. Eur. J*. **2015**, *21*, 1.

(15) Li, Y.; Kang, Y.; Lu, J.; Wyman, I.; Ko, S.; Wang, S. *Organometallics*. **2014**, *33*, 964.

(16) Schaub, T.; Backes, M.; Radius, U. *Organometallics*. **2006**, *25*, 4196.

(17) Spielmann, J.; Harder, S. *J. Am. Chem. Soc.* **2009**, *131*, 5064.

(18) Frisch, M. J.; Trucks, G. W.; Schlegel, H. B.; Scuseria, G. E.; Robb, M. A.; Cheeseman, J. R.; Scalmani, G.; Barone, V.; Mennucci, B.; Petersson, G. A.; Nakatsuji, H.; Caricato, M.; Li, X.; Hratchian, H. P.; Izmaylov, A. F.; Bloino, J.; Zheng, G.; Sonnenberg, J. L.; Hada, M.; Ehara, M.; Toyota, K.; Fukuda, R.; Hasegawa, J.; Ishida, M.; Nakajima, T.; Honda, Y.; Kitao, O.; Nakai, H.; Vreven, T.; Montgomery, J. A., Jr.; Peralta, J. E.; Ogliaro, F.; Bearpark, M.; Heyd, J. J.; Brothers, E.;

Kudin, K. N.; Staroverov, V. N.; Keith, T.; Kobayashi, R.; Normand, J.; Raghavachari, K.; Rendell, A.; Burant, J. C.; Iyengar, S. S.; Tomasi, J.; Cossi, M.; Rega, N.; N.; Millam, J. M.; Klene, M.; Knox, J. E.; Cross, J. B.; Bakken, V.; Adamo, C.; Jaramillo, J.; Gomperts, R.; Stratmann, R. E.; Yazyev, O.; Austin, A. J.; Cammi, R.; Pomelli, C.; Ochterski, J. W.; Martin, R. L.; Morokuma, K.; Zakrzewski, V. G.; Voth, G. A.; Salvador, P.; Dannenberg, J. J.; Dapprich, S.; Daniels, A. D.; Farkas, O.; Foresman, J. B.; Ortiz, J. V.; Cioslowski, J.; Fox, D. J. *Gaussian09*; Gaussian, Inc.: Wallingford, CT, 2010.

(19) Yanai, T.; Tew, D.; Handy, N. *Chem. Phys. Lett.* **2004**, *393*, 51.

(20) a) Ditchfield, R.; Hehre, W. J.; Pople, J. A. *J. Chem. Phys.* **1971**, *54*, 724; b) McLean, A. D.; Chandler, G. S. *J. Chem. Phys.* **1980**, *72*, 5639.

(21) a) Rao, Y.; Hörl, C.; Braunschweig, H.; Wang, S. *Angew. Chem. Int. Ed*. **2014**, *34***,** 9086; b) Lu, J.-S.; Ko, S. B.; Walters, N. R.; Kang, Y.; Sauriol, F.; Wang, S. *Angew. Chem. Int. Ed*. **2013**, *52*, 4544.

(22) a) Bertermann, R.; Braunschweig, H.; Brown, C. K. L.; Damme, A.; Dewhurst, R. D.; Hörl, C.; Kramer, T.; Krummenacher, I.; Pfaffinger, B.; Radacki, K. *Chem. Commun.* **2014**, *50*, 97; b) Braunschweig, H.; Damme, A.; Dewhurst, R. D.; Ghosh, S.; Kramer, T.; Pfaffinger, B.; Radacki, K.; Vargas, A. *J. Am. Chem. Soc*. **2013**, *135*, 1903.

(23) a) Fürstner, A.; Alcarazo, M.; Radkowski, K.; Lehmann, C. W. *Angew. Chem. Int. Ed*. **2008**, *47*, 8302; b) Rahm, R.; Espenlaub, S.; Werz, U. R.; Maas, G. *Heteroatom Chemistry*. **2005**, 16, 437.

(24) Bart, J. C. J. *J. Chem. Soc. B.* **1969**, 350.

(25) Crimmin, M. R.; White, A. J. P. *Chem. Commun.* **2012**, *48*, 1745.

(26) Zhang, X. M.; Bordwell, F. G. *J. Am. Chem. Soc.* **1994**, *116*, 968.

(27) Chu, Y.; Deng, H.; Cheng, J. P. *J. Org. Chem.* **2007**, *72*, 7790.

Chapter 6

Summary and Future Work

6.1 Summary

A number of new phosphine-borane donor-acceptor species and their derivatives have been synthesized and fully characterized. The photophysical properties and reactivity of the new compounds have been examined.

Compound **2.1** based on a 1,8-naphthalene linker was synthesized, which possesses a highly congested structure but and contains a typical P-B dative bond even in solution despite the high degree of steric congestion. Compound **2.1** is both thermally and photochemically stable and shows no reactivity towards some common small molecules, except that it reacts with halogen molecules in the presence of water, producing compound **2.2** with a P-O-B fragment. **2.1** is highly stable due to the extremely crowded nature of the molecule and the rigid naphthyl backbone that forces the donor - acceptor dative bond.

Given the low reactivity of compound **2.1**, an unbound phosphine-borane compound **3.1** that has a typical "Frustrated Lewis Pairs" structure with a relatively long P-B separation distance was synthesized. During the investigation of the reactivity of the unbound P-B system, **3.1** and its phosphonium salt **4.1** show different reactivity towards *N,N'*-dimethylimidazol-2-ylidene (IMe). **3.1** forms a simple IMe-**3.1** adduct with the coordination of the IMe molecule to the boron center, while phosphonium-borane **4.1** has been found to effectively activate IMe resulting in a vinyl amine fragment being trapped between the P and B centers. Several reactivity investigation studies indicate that the FLP-like ylide-borane **5.3** and imidazolium salt are also the important components involved in this transformation.

In addition to the remarkable reactivity of the unbound phosphine-borane system, compound **3.1** and its related compounds also exhibit interesting photophysical properties. Compound **3.1** displays intense dual emissions which include a through-space charge-transfer transition from the donor group to the acceptor group. The fluoride sensing ability of **3.1** has been demonstrated, and **3.1** has been found to display a "turn-on" sensor behavior upon the addition of fluoride ions in solution.

By introducing the Coulombic effects to the molecule, phosphonium salt **4.1** was found to significantly improve the binding affinity of the boron center towards fluoride ions by 2 orders of magnitude compared to that of compound **3.1**. Compound **4.1** is a "turn-off" sensor by the observation of the dramatically quenching of the bright deep blue emission colour by the addition of fluoride ions in solution. Au(I) and Pt(II) complexes **4.2** and **4.3** were also prepared based on compound **3.1**. Fluoride titration experiment of complex **4.3** showed a distinctly different response compared with that of **4.1**, in which complex **4.3** behaves as a "turn-on" sensor. Because of the bulky ligand **3.1** and the long distance between the metal and the boron atom, the fluoride affinity of complex **4.3** is not so different, compared to that of **3.1**.

6.2 Future Work

Despite the interesting results of the phosphine-borane donor-acceptor systems described in this thesis, these systems remain mostly inactive towards substrates of interest such as H_2. It is clear that in the case of **2.1**, the compound is simply far too crowded to perform any sort of small molecule activation. Given that similar systems have shown promise in this area,[1] one way to achieve the desired reactivity for this type of phosphine-borane system, a new molecule **6.1** would be interesting since it would have a more flexible biphenyl linker (Figure 6.1), which would not only allow further separation between the P and B atoms, but also give the overall compound much needed flexibility for the desired reactivity. Besides compound **6.1**, another compound **6.2** may also be of interest due to its more congested structure compared with the biphenyl linked species, which should be investigated in future work.

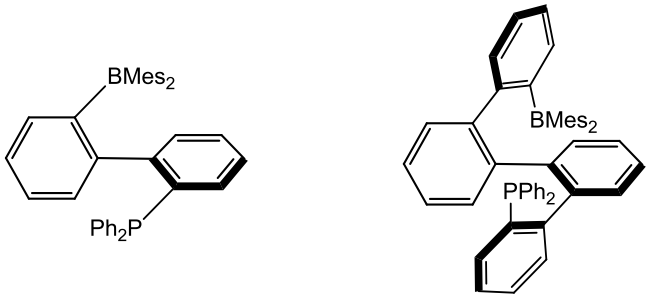

6.1 **6.2**

Figure 6.1. Flexible phosphine-borane systems.

In addition to manipulating the skeleton holding the P and B centers, one could also envision promoting further reactivity by increasing the electron deficiency of the boron center. Although the typical method of doing so is to functionalize the B atom with pentafluorophenyl groups, the $B(C_6F_5)_2$ unit is extremely sensitive to moisture and oxygen which makes it difficult in the preparation and handling of molecules containing this unit. Fortunately, it has been reported recently that by employing 2,4,6-trifluorometylphenyl substituents on boron with same Lewis acidity can be achieved with a dramatic increase in overall stability.[2]

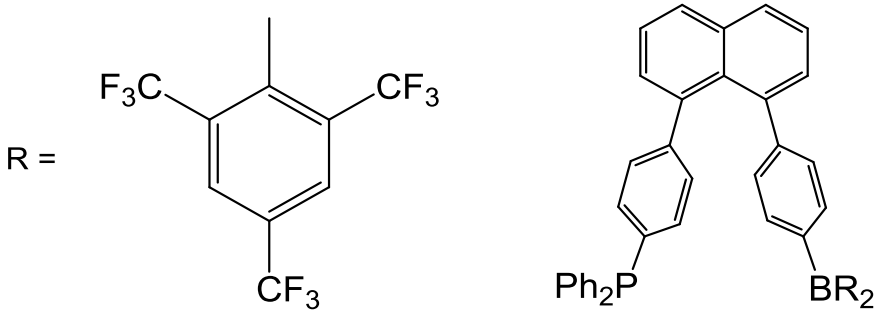

Figure 6.2. Trifluoromethyl substituted mesityl borane containing donor-acceptor compound.

Therefore, the Mes substituent in all compounds described in this thesis should be replaced by 2,4,6-trifluoromethylphenyl (except for **2.1** which would be far too sterically encumbered with the addition of the fluorine atoms) and the resulting new compounds should be investigated for their reactivity towards various substrates. One example shown in Figure 6.2 should be a good target for future work.

References:

(1) Devillard, M.; Brousses, R.; Miqueu, K.; Bouhadir, G.; Bourissou, D. *Angew. Chem. Int. Ed.* **2015**, *54*, 5722.

(2) (a) Yin, X.; Chen, J.; Lalancette, R. A.; Marder,T. B.; Jäkle, F. *Angew. Chem. Int. Ed.* **2014**, *53*, 9761.

(b) Zhang, Z.; Edkins, R. M.; Nitsch, J.; Fucke, K.; Steffen, A.; Longobardi, L. E.; Stephan, D. W.; Lambert, C.; Marder, T. D. *Chem. Sci.* **2015**, *6*, 308.

Appendix 1. Variable Temperature NMR Spectra of 2.1 in C_6D_6. Inset: the ^{31}P and ^{11}B NMR Spectra of 2.1 at 353 K.

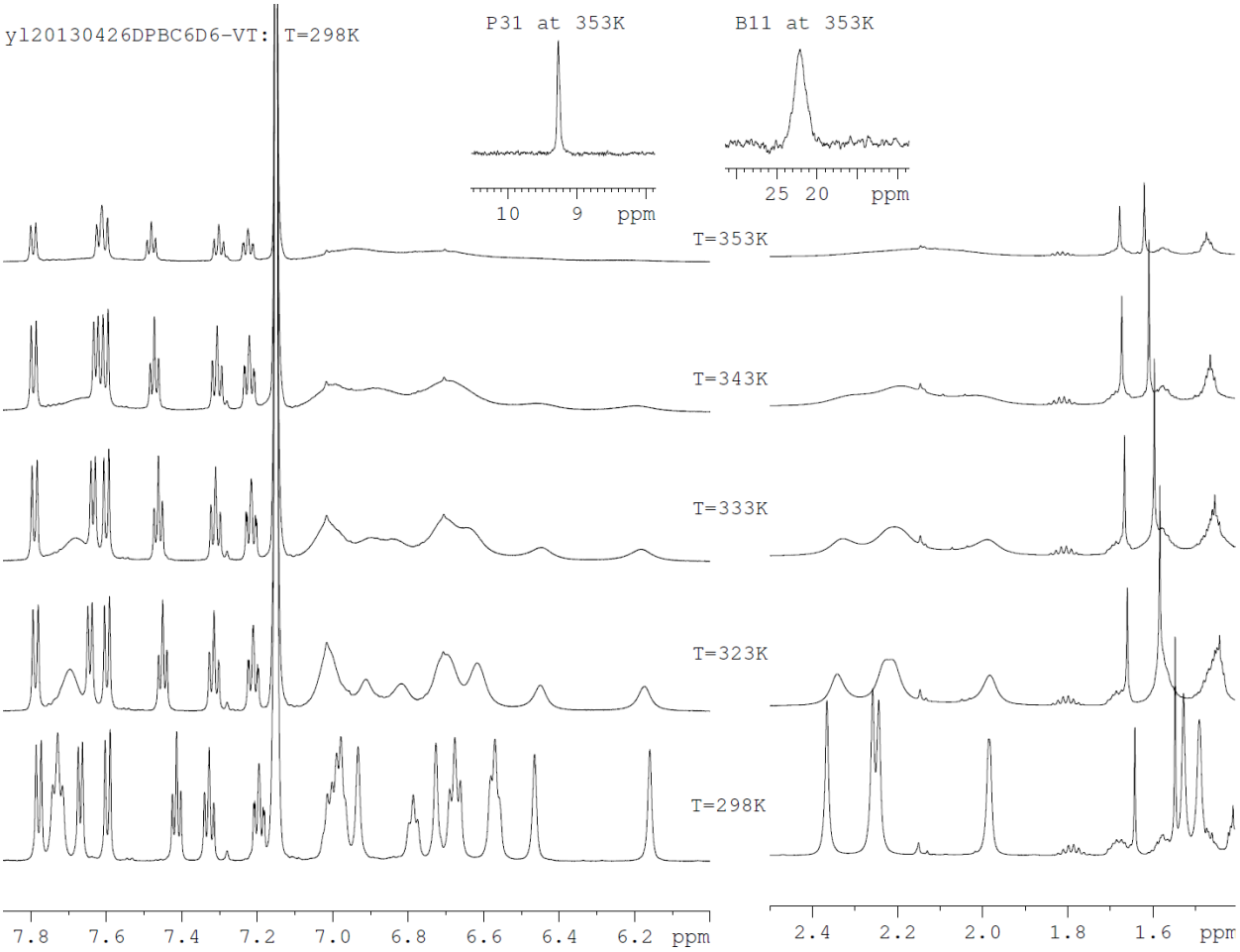

Appendix 2. Summary of Computational Results for 2.1 at the B3PW91/6-31G(d,p) Level of Theory (Top) and at CAM-B3LYP/SVP Level of Theory (Bottom)

	P-B distance (Å)	Total energy (a.u.)	Difference in total energies (kJ/mol)	ZPE-corrected energy (a.u.)	Difference in ZPE-corrected energy (kJ/mol)
Closed form	2.231	-1912.7988	0.96	-1912.1338	4.43
Transition state	2.528	-1912.7979	3.35	-1912.1335	5.29
Open form	2.994	-1912.7992	0	-1912.1355	0

	P-B distance (Å)	Total energy (a.u.)	Difference in total energies (kJ/mol)
Closed form	2.230	-1911.2181	4.81
Open form	3.060	-1911.2200	0

Appendix 3. Plot of the Change in Absorbance Observed at 330 nm Exhibited by 3.1 as a Function of the Fluoride Concentration.

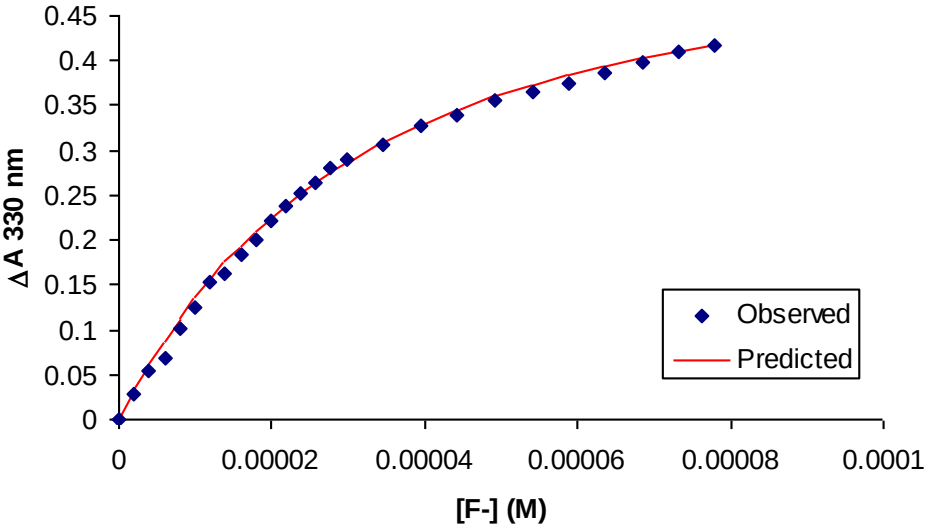

Appendix 4. Plot of the Change in Absorbance Observed at 340 nm Exhibited by 4.1 as a Function of the Fluoride Concentration.

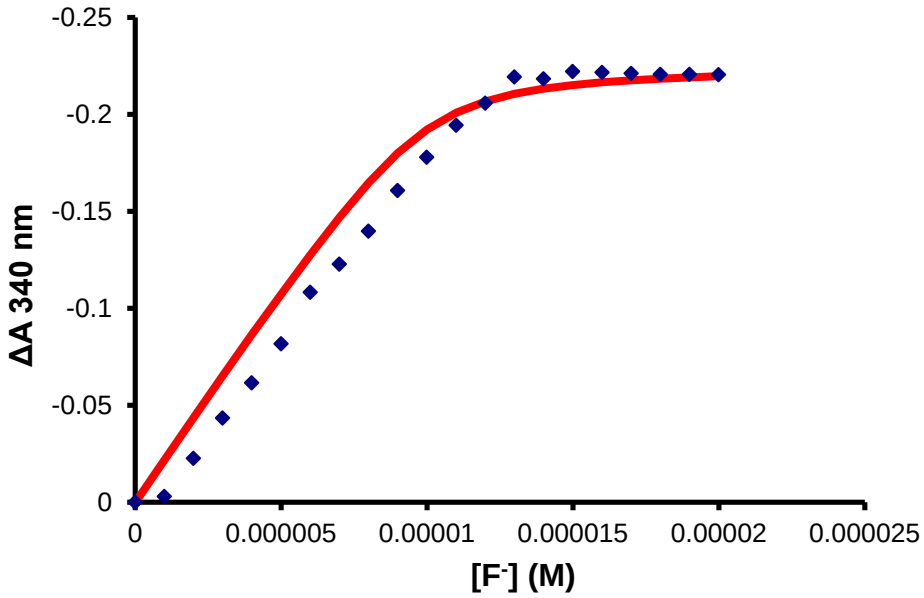

Appendix 5. Plot of 1/A versus 1/[F$^-$] of 4.3 at 330 nm.